Analysis of translational fidelity in cellular proteins

Dissertation

for the award of the degree

"Doctor rerum naturalium"

of the Georg-August-Universität Göttingen

within the doctoral program *Biomolecules: structure-function-dynamics*

of the Georg-August University School of Science (GAUSS)

submitted by

Raffaella Garofalo

from Bari, Italy

Göttingen, 2017

Members of the Examination Board/ Thesis Committee

Prof. Marina V. Rodnina (1st Referee)

Dept. of Physical Biochemistry

Max Planck Institute for Biophysical Chemistry

Göttingen, Germany

Prof. Henning Urlaub (2nd Referee)

Bioanalytical Mass Spectrometry Group

Max Planck Institute for Biophysical Chemistry

Göttingen, Germany

Prof. Peter Rehling (3rd Referee)

Dept. of Cellular Biochemistry

Georg-August University

Göttingen, Germany

Further members of the Examination Board

Prof. Holger Stark

Dept. of Structural Dynamics

Max Planck Institute for Biophysical Chemistry

Göttingen, Germany

Prof. Markus Bohnsack

Dept. of Molecular Biology

University Medical Center

Göttingen

Prof. Ralf Ficner

Dept. of Molecular Structural Biology

Institute for Microbiology and Genetics

Göttingen

Date of oral examination: 03 April 2017

Affidavit

I hereby declare that my thesis „Analysis of translational fidelity in cellular proteins“ has been written independently and with no other sources and aids than quoted.

Raffaella Garofalo

January, 2017

Göttingen, Germany

Related publication

Garofalo, R.[†], Wohlgemuth, I.[†], Pearson, M., Lenz, C., Urlaub, H., & Rodnina, M. V. (2019). Broad range of missense error frequencies in cellular proteins. *Nucleic Acids Research,*.

[†] equal contribution

“Saldi nella furia dei venti

e degli eventi.”

TABLE OF CONTENTS

ABSTRACT

The accuracy of protein biosynthesis determines the quality of the proteome and regulates the fitness of the cell. A comprehensive quantification of miscoding events in the cell is essential to understand the basic mechanisms that ensure fidelity as well as the evolutionary consequences of errors of protein synthesis. Impairment in cellular fidelity is associated with numerous diseases and is, due to the increasing number of protein therapeutics, of central biotechnological importance. However, the systematic analysis of miscoding events *in vivo* is precluded by the limited dynamic range of the available analytical methods. We have developed a method for the quantification of miscoding events such as amino acid misincorporations, which relies on the separation and enrichment of the error-containing peptides from their correct parental ones through multiple rounds of orthogonal chromatography and their absolute quantification by targeted mass spectrometry using isotope-labeled internal standards (AQUA peptides). The dynamic range of the method is linear over more than seven orders of magnitude and it is not restricted to any particular miscoding event, organism, strain or model protein.

The analysis of the model protein EF-Tu revealed that near-cognate missense errors are less frequent than expected (median error frequency 10^{-6}) and that the error frequency varies over three orders of magnitude depending on the type of misincorporation and source of EF-Tu. Among the substitutions tested, histidine misincorporations at arginine codons are the most abundant. Furthermore, error frequency varies depending on the amino acid position in EF-Tu by more than one order of magnitude. Positions at which errors are rare are clustered in the EF-Tu/tRNA interface, indicating either an extensive quality control or an higher encoded fidelity of translation.

We have also analyzed the effect of aminoglycosides on fidelity and stress response. Most aminoglycosides induce significant miscoding which correlates with the induction of proteins from the the heat-shock stress response and growth defects, underlining the central contribution of miscoding to the bactericidal effect of aminoglycosides. In addition to single-position substitutions, aminoglycosides can induce multiple miscoding events leading to peptides with two or three amino acid substitutions. The frequency of multiple consecutive errors is unexpectedly high and because of the detrimental effects on protein stability, such error clusters may contribute substantially to the bactericidal action of aminoglycosides.

1. INTRODUCTION

1.1 Errors of bacterial protein synthesis

1.1.1 Error frequency at different steps of protein synthesis

Protein synthesis is a pivotal cellular process in which the genetic information stored in the DNA is transcribed into RNA by the RNA polymerase and subsequently decoded on the ribosome with the help of transfer RNA (tRNA) molecules into an amino acid sequence and yield functional proteins. Despite the importance of preserving the genetic message, errors might arise at every stage (Parker, 1989) (Table 1). DNA replication is undoubtedly the most accurate step, because the DNA polymerase works with extremely high fidelity and an error frequency that ranges from 10^{-10}- 10^{-6} (Kunkel, 2004; Kunkel and Bebenek, 2000; Schaaper, 1993). Incorporation of errors during the transcription of DNA is, instead, more frequent because the responsible enzyme, RNA polymerase, incorporates incorrect nucleotides with a frequency of 10^{-5} - 10^{-4} (Traverse and Ochman, 2016). The least accurate step is the translation of mRNA, which shows error frequencies of up to 10^{-2} (Table 1). The fidelity of this process, whose average error rate is estimated to be 10^{-4} - 10^{-3} (Ribas de Pouplana et al., 2014; Rodnina and Wintermeyer, 2001b) is the result of a combination of different error-prone events. First, the aminoacyl-tRNAs (aa-tRNAs) delivering the amino acid to the ribosome must be correctly charged by their respective aminoacyl-tRNA synthetases. Second, the ribosome must select the correct aa-tRNA corresponding to the codon exposed in the decoding site of the ribosome and, after peptide bond formation, translocate along the mRNA by exactly three nucleotides at a time. Because tRNA misacylation, ribosome frameshifting and nonsense errors are rather infrequent events, occurring with a frequency of 10^{-6} - 10^{-4}, ~10^{-5} and 10^{-6} - 10^{-3} respectively (Freistroffer et al., 2000; Hopfield et al., 1976; Ibba and Soll, 2000; Jorgensen and Kurland, 1990; Sin et al., 2016; Soll, 1990), most of the errors that occur during translation are mainly attributed to erroneous decoding (Drummond and Wilke, 2009). Cells have evolved sophisticated mechanisms to avoid errors, such as proofreading of DNA and RNA polymerases and editing of aminoacyl-tRNA synthetases (aaRSs) (Jakubowski and Goldman, 1992; Kunkel, 2004; Sydow and Cramer, 2009) or kinetic mechanisms of aa-tRNA selection on the ribosome (Rodnina and Wintermeyer, 2001a). Errors that still arise can be removed by the quality control machinery of the cell, such as chaperones and proteases (Wickner et al., 1999).

Thus, the steady state level of missense errors in proteins reflects the error contributing processes of protein biosynthesis and the correcting processes of the quality control. This steady state level is not static but is modulated by naturally occurring mutations of the translational apparatus such as ribosomes (Rosset and Gorini, 1969; Zaher and Green, 2010a), aaRSs (Li et al., 2011), tRNAs (Bjork et al., 1999; Ranjan and Rodnina, 2016), modifications of translation factors (Van Noort et al., 1986), by the growth and metabolic state of the cell (Meyerovich et al., 2010; Zaborske et al., 2014) or by

external stress factors such as ethanol (Haft et al., 2014), aminoglycosides antibiotics (Davies et al., 1964) and oxidative agents (Ling and Soll, 2010; Netzer et al., 2009).

Table 1. Error frequencies of the individual substeps of protein biosynthesis. The estimated frequencies of error incorporation for every substep of protein synthesis are reported.

Cellular process	Type of errors	Error frequency	Reference
DNA replication	Nucleotide misincorporation	$10^{-10} - 10^{-6}$	(Kunkel, 2004; Kunkel and Bebenek, 2000; Schaaper, 1993)
RNA transcription	Nucleotide misincorporation	$10^{-5} - 10^{-4}$	(Traverse and Ochman, 2016)
tRNA aminoacylation	Incorrect aminoacylation	$10^{-6} - 10^{-4}$	(Ibba and Soll, 2000; Soll, 1990)
mRNA translation	Initiation on non-start codon	10^{-2}	(Milon and Rodnina, 2012)
	Premature termination	$10^{-6} - 10^{-3}$	(Freistroffer et al., 2000; Jorgensen and Kurland, 1990; Sin et al., 2016)
	Stop codon readthrough	$10^{-4} - 10^{-2}$	(Sydow et al., 2014)
	Amino acid misincorporation	$10^{-4} - 10^{-3}$	(Bouadloun et al., 1983; Drummond and Wilke, 2009; Loftfield and Vanderjagt, 1972; Parker, 1989; Parker et al., 1980; Ribas de Pouplana et al., 2014; Rodnina and Wintermeyer, 2001b; Toth et al., 1988)
	Frameshifting	$10^{-5} - 10^{-4}$	(Atkins et al., 1991)

1.1.2 Consequences of translation errors on cellular fitness

Errors of protein synthesis alter the sequence of amino acids in proteins and may cause the production of dysfunctional proteins, the consequences of which can be rather severe not only for the fitness of the single cell but, in case of eukaryotes, for the entire organism e.g., in *Escherichia coli*, ribosome biogenesis and thus translation are limiting the growth of the bacterial cell (Dennis et al., 2004). It requires up to 10 min to synthetize and assemble functional ribosomes, comparable to the time needed for cell duplication, 20 min (Scott et al., 2010). Indeed, translation is by far the most energy consuming phase (Russell and Cook, 1995) and most anabolic processes are devoted to it (Bremer and Dennis, 2008). In prokaryotes, which have rapid cell cycles optimized to outcompete other microorganisms, the synthesis of flawed proteins hijacks the cellular protein synthesis capacity, reduces the absolute levels of active proteins in the cell and directly leads to fitness defects (Andrews and Hegeman, 1976). Eukaryotes, on the other hand, do not exhaust their resources for rapid growth (Kafri et al., 2016); therefore errors of protein synthesis can have less pronounced effects.

The accumulation of random errors into protein is likely to cause loss of function, structural destabilization (Guo et al., 2004) and misfolding (Lee et al., 2006), with an effect which is predicted to increase exponentially with the number of inserted substitutions (Bloom et al., 2005). Accumulation

of errors and protein misfolding may in turn cause abnormal aggregation (Vermulst et al., 2015) or induce protein oxidative damage (Dukan et al., 2000). Additionally, incorrectly folded and unstable proteins seize the working capacity of the chaperones system (Gidalevitz et al., 2006) potentially promoting further cellular damage.

Increased miscoding can be caused by aminogycoside antibiotics and the consequent misfolding and aggregation phenomena have been demonstrated by treating the cells with streptomycin (Ling et al., 2012). Upon antibiotic treatment, mistranslation occurs and more erroneous proteins that favour aggregation are produced. Mass spectrometric analysis of such aggregates has revealed that they mostly consist of heat shock-induced proteases and chaperones (especially IbpA and IbpB) whose response is known to associate with accumulation of errors in proteins (Ruan et al., 2008). Although the proteotoxic stress caused by error accumulation can be alleviated by the concerted action of chaperones and proteases, the clean-up costs – in addition to the energy already spent for their synthesis – impose a energetic burden that can compromise the overall cellular fitness (Drummond and Wilke, 2009). Ultimately, mistranslation can lead to membrane depolarization, radical formation and finally to growth arrest and cell death (Kohanski et al., 2007).

1.2 Cellular mechanisms that ensure the fidelity of protein biosynthesis

1.2.1 General sources of protein synthesis fidelity

The high fitness cost of errors in protein synthesis increases the evolutionary pressure to keep the error frequency low. This led to the development of sophisticated cellular mechanisms that ensure high fidelity of protein biosynthesis or increase the tolerance towards those errors that could not be avoided. An example for this adaptive evolution comes from the study of an error prone *E. coli* strain expressing the TEM1 β-lactamase resistance protein. Under relaxed conditions, where the antibiotic is not present and the resistance protein is not essential, the cells reduce the costs for the synthesis of a superfluous and error-containing protein by lowering its expression level. However, when the antibiotic is present and the protein is required for the cell survival, the cell balances the unavoidable incorporation of errors by promoting the incorporation of amino acids which stabilize the the protein structure (Bratulic et al., 2015). Error-mitigating mechanisms can also be already imprinted in the genetic code. The amino acid sequence of a protein is determined by the sequence of bases in the mRNA and one sequence of nucleotide triplets, a codon, specifies for one amino acid (Crick et al., 1961). However, because the genetic code is degenerate, a particular amino acid may be coded by more that one triplet (Crick et al., 1961) in which the first two positions are strict, but some wobble is accepted at the third base (Crick, 1966). The structure of the genetic code ensures that if a codon is incorrectly translated, this would often lead to the substitution with a similar amino acids, thereby

minimizing the impact on protein stability (Archetti, 2006) as it happens for the frequent third-position mismatches (Woese, 1965). A second mechanism is based on the codon usage optimization. Numerous studies have demonstrated a correlation between the tRNA abundance and the occurrence of the respective codon (Ikemura, 1985), and genes that need to be more efficiently translated display an optimized codon sequence preferentially containing codons decoded by abundant tRNAs. In this regard, the elongation factor Tu (EF-Tu), the most abundant protein in bacteria, contains only abundant codons (Kurland, 1992) whereas rare ones are avoided (Akashi, 1994). In addition, bioinformatics studies revealed that cluster of translationally optimal codons at sites that are important for the function or stability of proteins are highly conserved and that codons whose mistranslation results in less severe amino acid substitutions are preferred at these positions (Lee et al., 2010; Zhou et al., 2009).

1.2.2 Thermodynamic and kinetic sources of accuracy

While the evolution of the genetic template does not bring about significant fitness costs for the cell (Drummond and Wilke, 2009), the accuracy of the enzymes involved in protein biosynthesis cannot improve without a trade-off between speed and accuracy. In general, most enzymes use highly specific binding sides that are complementary to the steric and electronic features of their unique substrates to idiosyncratically recognize them. Kinetically, such tailored binding sites often reflect in dramatically different dissociation constants in the ground state (GS) that almost exclude incorrect substrates in the binding step (Figure 1, A). In contrast, enzymes involved in protein synthesis, such as DNA and RNA polymerases or ribosomes, cannot achieve such high selectivity by evolving idiosyncratic binding sites, because they have to recognize and incorporate with high fidelity different substrates in subsequent cycles of elongation. Different nucleotides or aa-tRNAs are recognized on the basis of only few discriminating interactions, such as for Watson-Crick base pairs. The affinity differences between correct and incorrect substrates are $<10^2$ for single mismatched nucleotides (Grosjean et al., 1978) and can be even lower between cognate and non-cognate triplets (Kurland et al., 1975). Thus, the affinity differences alone fail to explain the high fidelity of all substeps of protein biosynthesis (Rodnina and Wintermeyer, 2001b) (Table 3) and additional sources of fidelity such as induced fit (Gromadski and Rodnina, 2004a; Pape et al., 1999) and proofreading (Ruusala et al., 1982; Thompson and Stone, 1977) apply. First, in the different substeps of protein synthesis, nucleotide mismatches are recognized on the base of their shape through interactions between the minor groove of DNA (or wide shallow groove of tRNA) and the amino acids and rRNA nucleotides of polymerases and ribosome, respectively (reviewed in (Westhof et al., 2014)).

On the ribosome, this recognition leads to conformational changes (Ogle et al., 2002) which then strongly accelerate the productive forward rates for correct aa-tRNAs relative to near and non-cognate tRNAs in terms of an induced-fit mechanism (Gromadski and Rodnina, 2004a; Pape et al., 1999) Second, kinetic proofreading mechanisms are applied in which the same discriminating interactions are energetically and kinetically used several time to amplify the accuracy. This is possible when both selection phases are irreversibly separated by an energy dissipating step (Ruusala et al., 1982; Thompson and Stone, 1977), as happens during decoding where GTP hydrolysis separates two subsequent selection steps which are both based on the same codon-anticodon helix mismatch. However, substrates selection at the ground state can lead to a trade-off between speed and accuracy which are negatively correlated for ground state selection (reviewed in (Tawfik, 2014)). Kinetically, in this scenario, fast forward rates do not allow the substrate binding involved in selection to equilibrate completely and thus the affinity differences between correct and incorrect substrate can be only partially utilized (Gromadski and Rodnina, 2004a). In fast growing *E.coli* cells, ribosomes seem to be optimized for fast translation at the cost of accuracy (Aqvist and Kamerlin, 2015; Wohlgemuth et al., 2010). A concrete example of this trade-off and its reflection on the cellular fitness comes from streptomycin-dependent (SmD) *E. coli* mutants whose viability necessarily depends on the antibiotic (Ruusala et al., 1984). SmD cells, indeed, possess excessively accurate, or hyper-accurate, ribosomes that – in the absence of the drug – slow down the translation process to such an extent that it leads to cells death. Indeed, the presence of streptomycin, which reduces ribosome fidelity (Gromadski and Rodnina, 2004b) and favours a faster translation rate, restores cell viability.

An alternative to GS selection is the transition-state (TS) discrimination where correct and incorrect substrates bind the enzyme with similar affinities but not all interactions of the correct substrate in the TS are realized for the non-cognate ones. Thus, for TS selection, fidelity positively correlates with catalytic efficiency allowing high accuracy at high speed. TS selection is reported for the DNA polymerase Pol1. Upon binding of the correct substrate, the active-site dipoles of the binding sites are organized to maximize TS stabilization, which does not occurs in the presence of a non-cognate substrate (Ram Prasad and Warshel, 2011) allowing for a high synthesis rate ($k_{cat} > 100\ s^{-1}$) and a high accuracy ($<10^{-3}$ even in the absence of proofreading (Caglayan and Bilgin, 2012)) and leads to the predicted positive correlation of speed and accuracy which is determined by a much higher activation entropy for the non-cognate than for the cognate substrate (Caglayan and Bilgin, 2012) (Figure 1, B). In many cases, especially when incorrect substrates differ by only a few atoms, positive GS or TS selection might not be sufficient to guarantee high accuracy. Thus, many enzymes evolved explicit negative selection strategies, termed editing, that remove mistakes that evaded the selection process

as it happens for aminoacyl-synthetases or DNA and RNA polymerases (Fersht, 1977; Reha-Krantz, 2010; Sydow and Cramer, 2009).

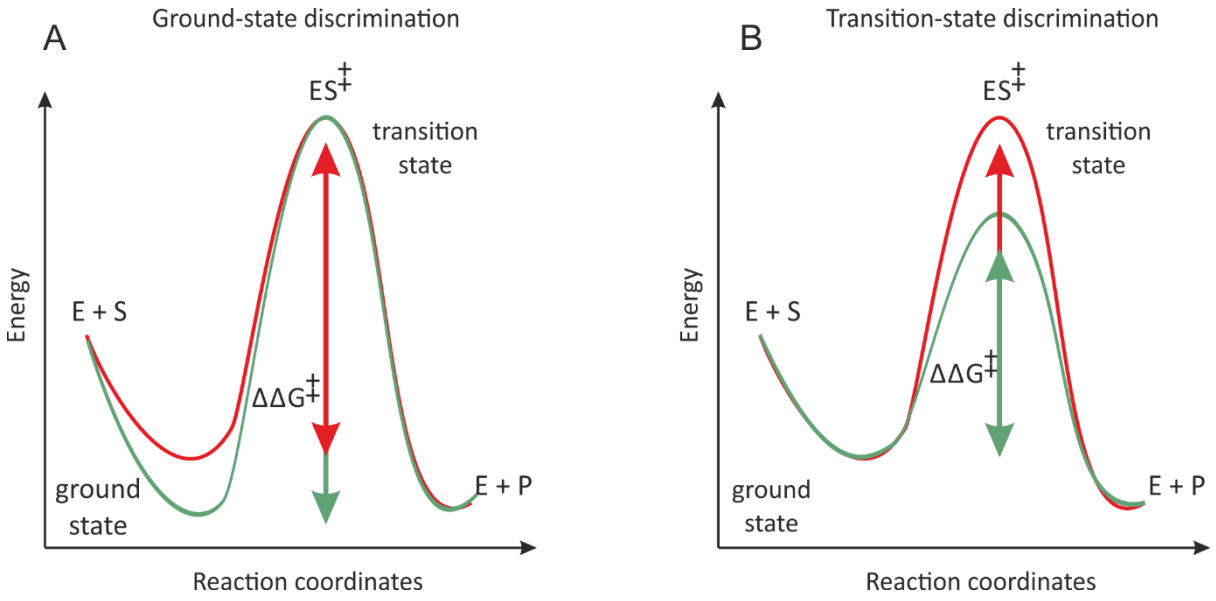

Figure 1. Enzymes ensure their accuracy in different ways. Substrate discrimination can be achieved at the ground state (A) or transition state (B). In red and green are represented the catalytic curves for non-cognate and cognate substrates, respectively.

1.3 Fidelity during mRNA translation and decoding

The most important player of translation is the ribosome. The ribosomes are large macromolecular machines, of approximately 2.5 MDa in bacteria, composed of two unequal subunits, the small 30S and the large 50S, assembled together to form the 70S ribosome. The 30S subunit contains twenty-one proteins and one ribosomal RNA (16S rRNA). It houses the decoding center where mRNA is decoded by tRNA molecules. The 50S subunit is composed of thirthy-six proteins and two rRNAs, 5S and 23S. The 50S subunit harbors the peptidyl transferase center where the peptide bond between two adjacent tRNAs is formed and makes the ribosome a ribozyme (Steitz and Moore, 2003). Each ribosome presents three tRNA binding sites, the A site for binding of aa-tRNA, the P site for binding of peptidyl-tRNA, and the E site from which deacylated tRNA exits the ribosome. The translation process progresses through four consecutive phases of initiation, elongation, termination and recycling, during which the ribosome is assisted by several protein ligands: the translation factors (Figure 2).

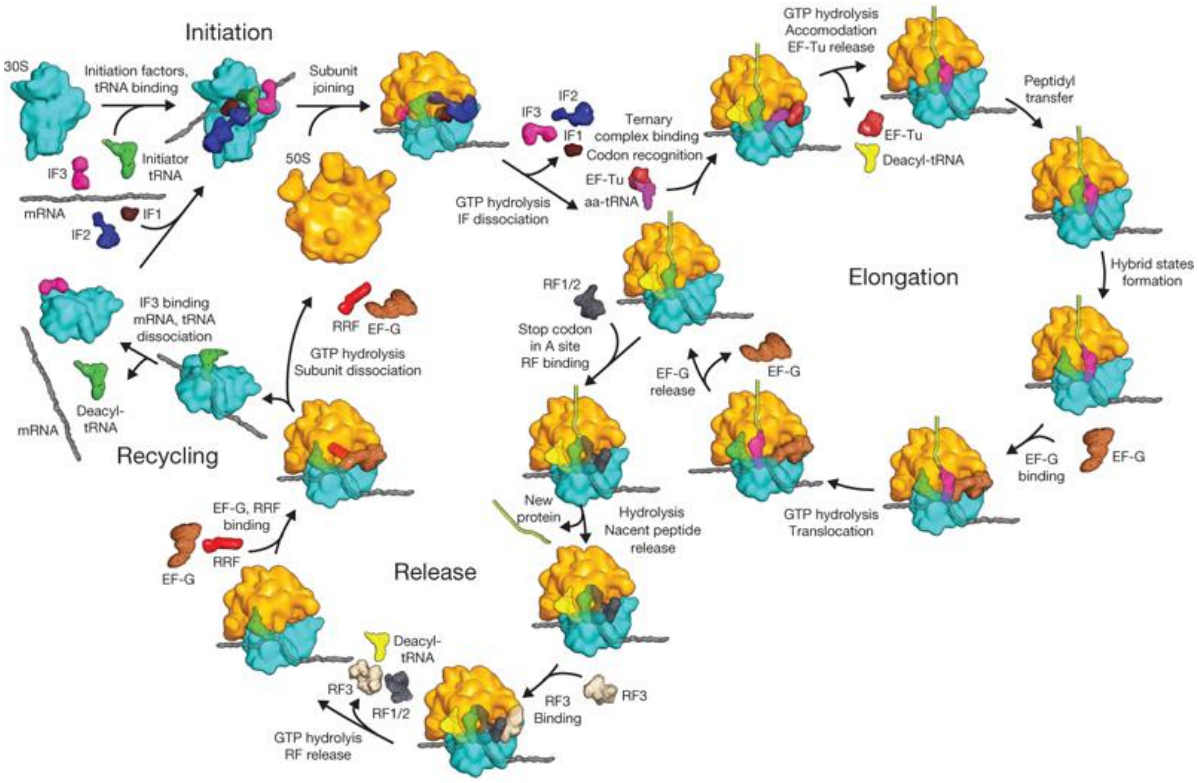

Figure 2. The phases of translation. Synthesis of protein proceeds through consecutive phases of initiation, elongation, termination and recycling. During initiation, the 70S initiation complex assembles on the mRNA starting codon. Upon repetitive elongation rounds, new amino acids are incorporated to form growing polypeptide chain. When a stop codon is read the process terminated and the subunits are recycled for a new round of translation. Figure reproduced from (Schmeing and Ramakrishnan, 2009).

During the initiation phase the 30S subunit, supported by initiation factors (IFs) 1, 2 and 3, stochastically binds the initiation fMet-tRNA^{fMet} and, thanks to its 16S partial complementarity, the mRNA (Shine and Dalgarno, 1974), to form the 30S initiation complex (IC). Correct assembly of the 30S IC allows the joining of the 50S subunit with consequent release of all the IFs. This leaves the newly assembled 70S IC with the fMet-tRNA^{fMet} interacting with the mRNA start codon in the P site (Gualerzi, 2010). During the elongation phase, the mRNA is decoded and amino acids are cyclically added to the growing polypeptide chain. Aa-tRNA is delivered to the ribosome in a ternary complex with EF-Tu and GTP (Figure 3). Upon codon recognition, the geometry of the base pairs at the codon:anticodon helix is recognized by ribosomes to discriminate between base matches and mismatches. Correct codon-anticodon interaction causes the first two bases of codon-anticodon helix to interact with A1492, A1493 and G530 (*E. coli* numbering throughout) of 16S rRNA and induces a series of fast conformational changes (Ogle et al., 2001) which are fundamental for the GTPase activation of EF-Tu and the subsequent GTP hydrolysis and part of the induced-fit rearrangement (Gromadski and Rodnina, 2004a; Pape et al., 1998; Rodnina et al., 1995a). Mismatches at the codon:anticodon helix distort the geometry of the duplex impairing the interactions with the elements of the decoding center

preventing the conformational changes required to trigger GTPase activation (Ogle et al., 2002) and resulting in its reduced rate or complete inhibition. The binding of near-cognate tRNAs, displaying one mismatch, is weaker than that of cognate ones so that they tend to dissociate more easily from the ribosome (Gromadski and Rodnina, 2004a; Pape et al., 1999). While non-cognate tRNAs bearing two or more mismatches are normally rapidly rejected in this initial selection phase, near-cognate aa-tRNAs may escape the selection and are further discriminated at the proofreading phase after the irreversible hydrolysis of GTP. At this stage, the acceptor stem of the aa-tRNA is released from the EF-Tu-GDP complex and accommodates in the peptidyl-transferase center of the ribosome. Also in this case, the accommodation of the cognate substrates is much faster and more efficient than for near-cognates which normally results in their rejection (Pape et al., 1999). Once the tRNA is accommodated into the A site, the complex formed by EF-Tu and GDP dissociates from the ribosome and the new peptide bond can eventually form. The polypeptide chain is then transferred to the aa-tRNA in the A site ready to be translocated back into the P site. Translocation is promoted by another ribosomal GTPase, the elongation factor G (EF-G) and the translating ribosome moves on the mRNA one codon at a time translating 4 - 22 amino acids per second at 37°C (Bhattacharjee et al., 2012; Wohlgemuth et al., 2010)). Translation proceeds until one of the mRNA stop codons (UAA, UAG or UGA) enters the A site and marks the beginning of the termination phase. In the termination phase, the ribosome is assisted by two classes of release factors (RFs). To class I belong RF1 and RF2 that recognize the stop codon (UAG and UAA for RF1 and UAA and UGA for RF2) (Ito et al., 2000) and bind to the ribosome promoting the hydrolysis and release of the peptide chain. The second class includes RF3, another GTPase, that promotes the dissociation of class I factors from the ribosome after the peptide release. After termination, subunits are recycled by the combined action of EF-G, ribosome recycling factor (RRF) and IF3 (Peske et al., 2005).

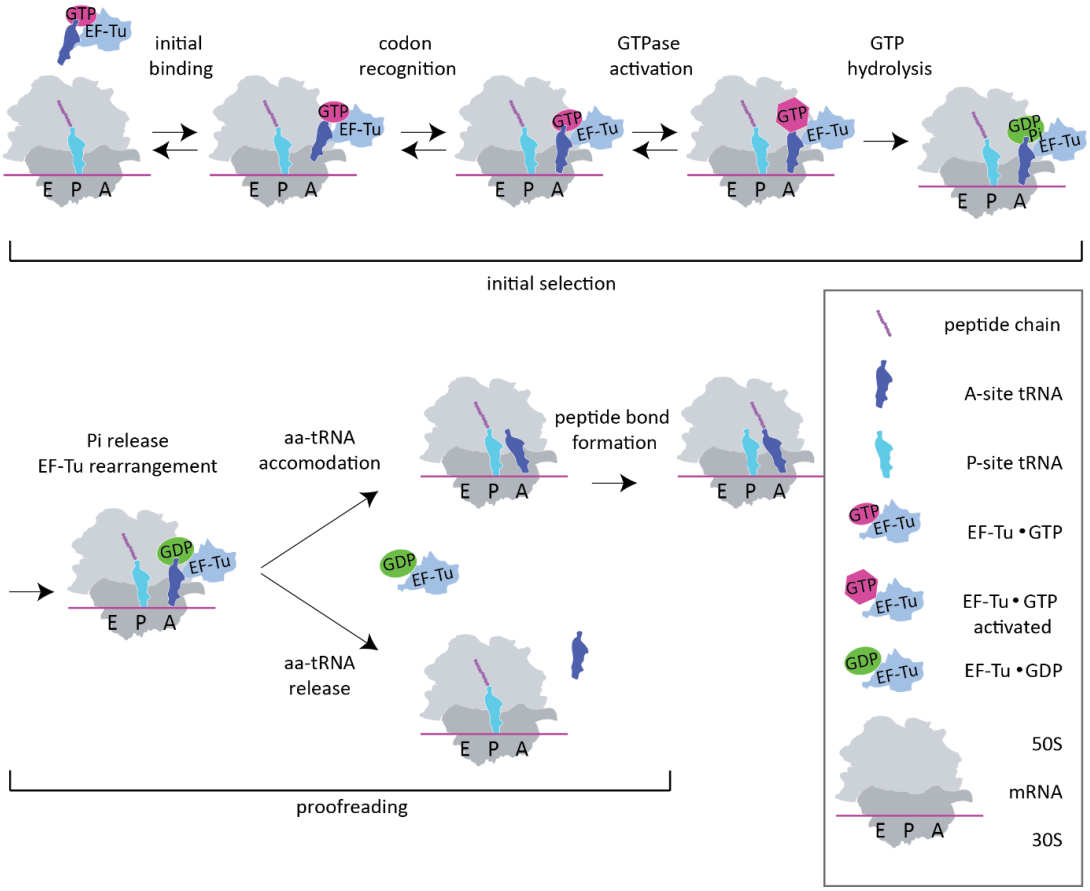

Figure 3. Kinetic scheme of mRNA decoding. Aminoacylated tRNA is delivered to the ribosome in complex with EF-Tu and GTP. The correct codon recognition triggers a series of conformational changes that cause GTPase activation, GTP hydrolysis and inorganic phosphate (Pi) release. The tRNA is released from EF-Tu-GDP complex and accommodates into the A-site of the 50S subunit and peptidyl transfer can occur. Eventually, the presence of one mismatch at codon-anticodon helix might induce the tRNA dissociation before transpeptidylation.

1.3.1 Ribosomal quality control following peptide bond formation

For a long time it was thought that accuracy of mRNA decoding on the ribosome and the selectivity of aminoacyl-tRNA synthetases are the only sources of fidelity in translation. However, an additional step has been discovered recently that acts after the misincorporation of substrates has occurred (Zaher and Green, 2009). Presumably, mismatches in the codon:anticodon interaction of the peptidyl-tRNA in the P site lead to distortions in the ribosome structure and cause a general loss of specificity in the A site promoting in turn repetitive miscoding events (Figure 4) (Zaher and Green, 2009, 2010b). Accummulation of errors in the nascent peptide, which is observed regardless of the type of ribosome used (wild type, error prone *rpsD* or error restricted *rpsL* (Zaher and Green, 2010b)), promotes the termination factor-mediated release of the nascent chain resulting in an abortive termination of the protein synthesis.

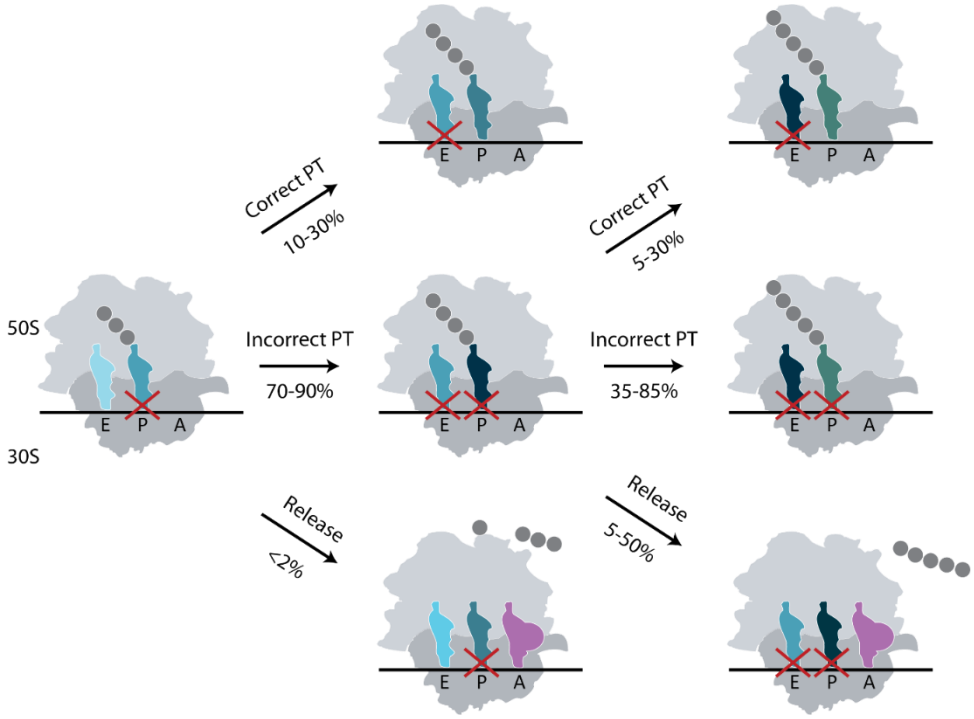

Figure 4. Mechanism of selection triggered by error accumulation. PT, peptidyl transfer. Following the first misincorporation event and translocation of a near-cognate tRNA into the P-site, the probability that the nascent peptide is release by the RFs is less than 2 %, while the probability that a correct aa-tRNA is accepted in the A site is only 10-30 %. In most cases, a second incorrect aa-tRNA is accepted (70-90 %). The second miscoding event reduces the possibility of correct and incorrect PT to 5-30 % and 35-85 %, respectively, but strongly favours the termination of the protein synthesis and the release of the nascent chain (5-50 %). Figure adapted from (Zaher and Green, 2009).

1.3.2 Base pair tautomerization and its effect on decoding

The recognition of Watson-Crick (WC) base pairs is at the core of many processes of gene expression, such as replication, transcription, and translation. In general, complementary Watson-Crick and non-complementary base pairs at the first two positions of the codon-anticodon helix are efficiently discriminated on the ribosome on the basis of their geometry, while the third base pair, i.e the wobble position, is less strictly controlled allowing for non-Watson-Crick interactions and the tRNAs to read synonymous codons.

However, crystal structures showed that some mismatches such as G/U and C/A at the first or second position, can adopt a WC geometry which is isosteric to the canonical WC base pairs and can thus escape this selection (Demeshkina et al., 2013). This occurs because nucleotide bases, although with a low probability of 10^{-5} - 10^{-4}, can adopt alternative tautomeric or anionic forms that cause them to be isosteric with WC bases (Kimsey et al., 2015; Westhof et al., 2014) (Figure 5) and be recognized as cognate by the ribosome. Thus, in these cases the ribosomes lose the ability to discriminate matches against mismatches (Rozov et al., 2015, 2016). This type of loss in fidelity has also been reported in a recent study where mass spectrometric analysis of recombinant and natural proteins

expressed in *E. coli* revealed that a correlation exists between GU mismatches and an increased level of errors (Zhang et al., 2013).

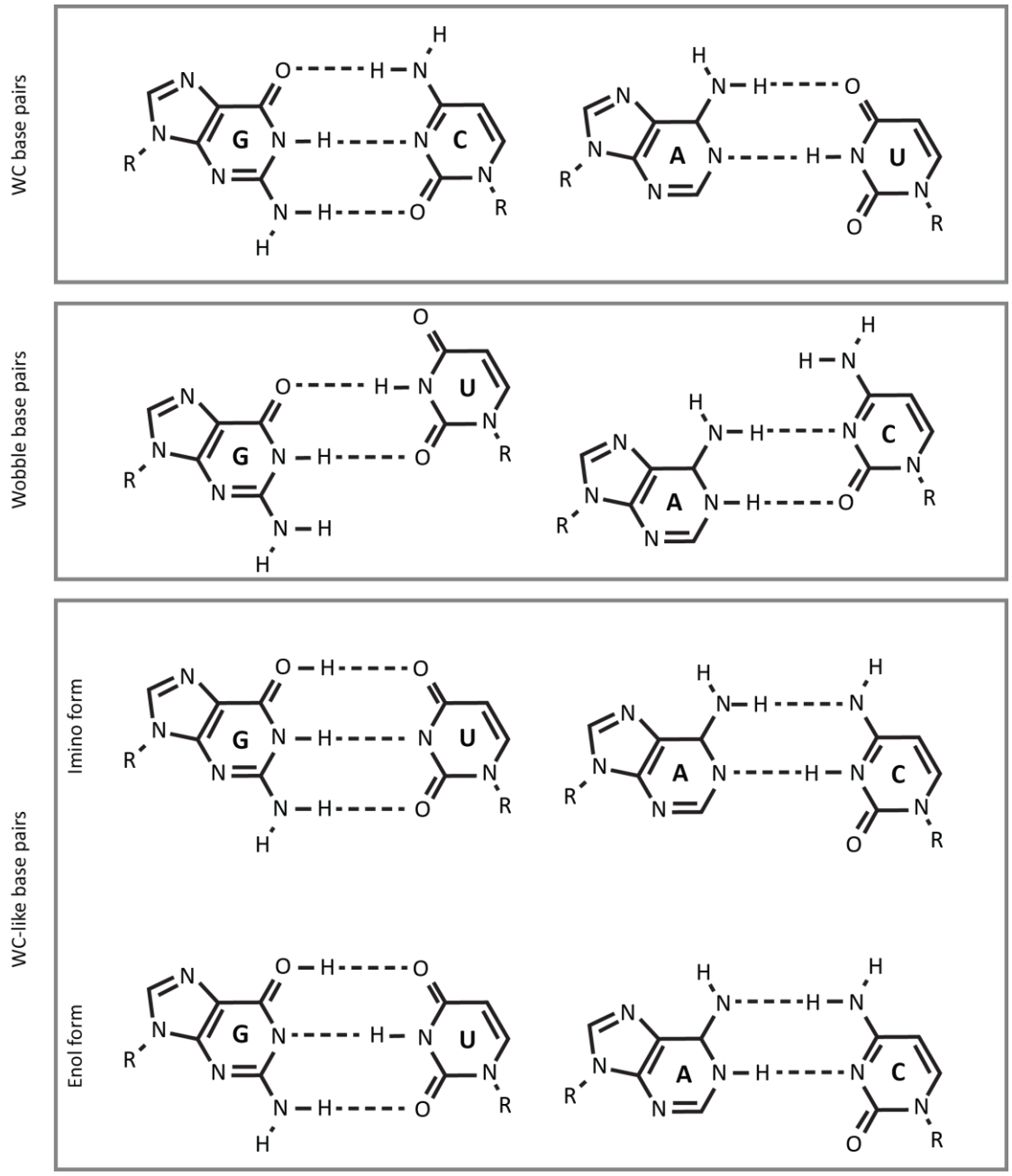

Figure 5. G-U base pair tautomerism. Natural bases of nucleic acids form base pairs with at least two hydrogen bonds between them. Standard complementary base pairs G-C and A-U (upper panel) are compared with Wobble base pair G~U and A~C (center panel) and the isosteric tautomers (bottom panel) imino and enol forms. Wobble pairs present a different geometry which is recognized by the ribosome as a mismatch. However, the Watson-Crick-like geometry of tautomers prevents their discrimination by the decoding site of the ribosome.

1.4 Aminoglycosides and decoding

Reduced fidelity of decoding can be caused by aminoglycosides that target the 16S rRNA of the 30S subunit and affect protein synthesis and decoding. Aminoglyocosides were the first antibiotic class effective against tubercolosis and, despite the fact that their use has helped millions of people, their current clinical application is hampered by their poor bioavailability, the emergence of resistant pathogenic strains and their pronounced nephro- and ototoxicity (Fischel-Ghodsian, 2005) which are likely caused by their interaction with the A site of human mitochondrial ribosomes (Hong et al., 2015). Nevertheless, they remain in use as pivotal tools for the investigation of translation mechanism and ribosome dynamics and as clinically important drugs for the treatment of the symptoms caused by hereditary diseases. In some genetic pathologies, such as the Duchenne muscular dystrophy (Malik et al., 2010a; Malik et al., 2010b), the primary ciliary dyskinesia (Bukowy-Bieryllo et al., 2016) and the phenylketonuria (Ho et al., 2013), the premature insertion of a stop codon in the mRNA causes the generation of shorter, non-functional proteins and the translational readthrough induced by aminoglycosides is used to effectively restore the expression of a functional full-length protein.

Aminoglycosides are positively charged oligosaccharides which usually share a 2-deoxystreptamine ring (also known as 2-DOS or ring II) as a common characteristics, although some exceptions exist such as spectinomycin and streptomycin. Depending on the type of linkages between the 2-DOS ring and the other rings, they can be classified in 4,5-disubstituted, 4,6-disubstituted, 4- and 5-monosubstituted aminoglycosides (Figure 33). To enter the cell, aminoglycosides must first cross the plasma membrane and, in the case of gram-negative bacteria, the outer membrane. Their uptake is an energy-consuming process that is thought to occur in three phases. In the first phase, the positively charged aminoglycosides are adsorbed to the surface of bacteria by electrostatic interactions with the lipopolysaccharides of the outer membrane. The following two steps are dependent on the transmembrane potential generated by the respiratory chain, which is the reason why anaerobic bacteria appear to be impermeable and resistant to aminoglycosides (Bryan and Kwan, 1983; Hancock, 1981; Taber et al., 1987). Once inside the cell, they affect translation by binding to the ribosome. Most aminoglycosides specifically target the 30S ribosomal subunit and bind to the helix 44 (h44) (Carter et al., 2000; Moazed and Noller, 1987), although spectinomycin only binds to helix 34 (h34) (Bilgin et al., 1990; Carter et al., 2000) and some of them such as gentamycin, tobramycin, neomycin and paromomycin have a secondary binding site on the helix 69 (H69) of 50S subunit (Borovinskaya et al., 2007a; Misumi et al., 1978) (Figure 6 and Table 2).

Neamine (Nea) is constituted by the universal two-ring structure which characterizes the base of most aminoglycosides. Its ring I inserts in h44 and causes the two universally conserved A1492 and

A1493 to bulge out in a conformation simar to those induced by codon:anticodon interaction (Francois et al., 2005; Ogle et al., 2001).

Kanamycin (Kan) binds to h44 of the 16S rRNA. It induces a high-affinity conformation of the ribosome for A-site tRNA and promotes the displacement of the 16S rRNA residues A1492 and A1493 affecting both translocation and miscoding (Davies et al., 1965b; Feldman et al., 2010).

Neomycin B (Neo B) has two binding sites, the first on h44 and the second on H69 (Borovinskaya et al., 2007a) affecting decoding fidelity, translocation and also ribosome recycling. It inhibits aa-tRNA translocation and ribosome recycling by stabilizing an intermediate state of subunits rotation and causing a conformational change that negatively effects subunits dissociation (Borovinskaya et al., 2007a; Wang et al., 2012).

Gentamicin (Gen) has two binding sites on h44 and H69. Its effect on the ribosome is similar to those of Neomycin inducing miscoding and affecting translocation (Borovinskaya et al., 2007a; Davies et al., 1965b).

Paromomycin (Par) exerts its main effect on decoding. It displaces A1492 and A1493 of h44 into a position where they could not contact anymore the codon:anticodon helix (Carter et al., 2000; Ogle et al., 2001; Ogle et al., 2003; Ogle et al., 2002) and induces a deformation of the near-cognate codon:antidocon helix and a movement of H69 (Demeshkina et al., 2012). Par specifically increases the GTPase activation for near-cognate ternary complexes, whereas the GTPase activity in the cognate complexes is unaffected (Pape et al., 2000).

Tobramycin (Tob) binds to both h44 and H69 (Borovinskaya et al., 2007a; Scheunemann et al., 2010). It stabilizes the bulged out conformation of the residues A1492 and A1493 (Vicens and Westhof, 2002)

Ribostamycin (Rib) shares the same identical structure of Neo but lacks ring IV. As Nea, it bings to h44 and affects decoding by causing the conformational rearrangement of the the two adenines 1492 and 1493 (Francois et al., 2005).

Apramycin (Apr) binds h44 and is a strong inhibitor of protein synthesis. It inhibits the translocation step but its effect on miscoding is controversial (Matt et al., 2012; Perzynski et al., 1979).

Hygromycin B (Hyg B) binds at the very top of h44 but does not induce any conformational change in the rRNA (Brodersen et al., 2000). However, it might exert its effect as translocation inhibitor (Peske et al., 2004) by blocking the movements of the h44, which are necessary during translocation (Frank and Agrawal, 2000) . In addiction, by increasing the affinity of the A-site tRNA, Hyg B also has a small effect on decoding (Eustice and Wilhelm, 1984a, b; Peske et al., 2004).

Streptomycin (Str) tightly binds to the phosphate backbone of 16S rRNA and makes contact with protein S12 of the small subunit (Carter et al., 2000). Structural works showed that Str shifts the decoding site region of h44 laterally in the direction of S12 protein and h18, without causing the

A1492 and A1493 to flip out from h44 (Demirci et al., 2013a). Str increases the affinity of tRNA binding in the A site (Peske et al., 2004) and acts on the ribosome by reducing the rate of GTPase activation for ternary complexes with cognate aa-tRNAs and accelerating it for those with near cognate aa-tRNAs, thereby reducing ribosomal selectivity (Gromadski and Rodnina, 2004b; Pape et al., 2000). Spectinomycin (Spc) binds in the minor groove at one end of h34, where it contacts C1064 and C1192 (Carter et al., 2000). The antibiotic sterically blocks swiveling of the head domain of the small ribosomal subunit and has a strong inhibitory effect on translocation thereby blocking the translocation cycle (Borovinskaya et al., 2007b; Peske et al., 2004).

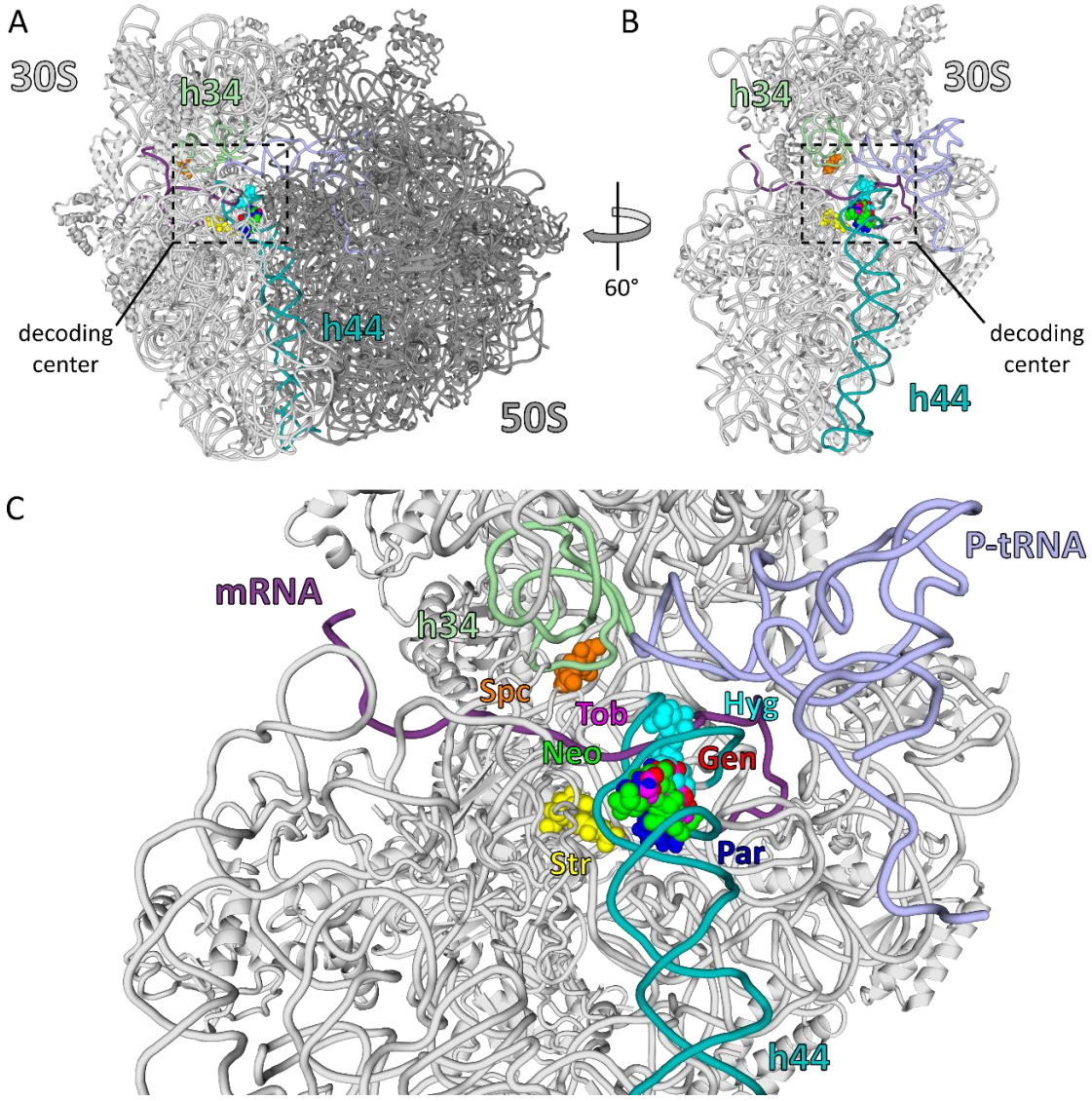

Figure 6. Aminoglycosides binding sites on the ribosome. The binding site of aminoglycosides is shown with respect to the A) 70S and the B) 30S subunit. C) The biding site in h44 of tobramycin (Tob), paromomycin (Par), streptomycin (Str), hygromycin B (Hyg), gentamicin (Gen) and neomicin (Neo). Only the primary sites are shown; Tob, Gen, Neo and Par also have a second binding site in h69. Spectinomycin (Spc) has a binding site in h34. [PDB files: 4ji1 (Demirci et al., 2013b), 4v56 (Borovinskaya et al., 2007b), 4woi (Wasserman et al., 2015), 4lfc , 4w29 (Zhou et al., 2014), 4v64 (Borovinskaya et al., 2008), 4v53 (Borovinskaya et al., 2007a)].

Table 2. Aminoglicosides binding sites and their effects. The binding sites and effects for the most common aminoglycosides are reported.

Aminoglycoside	Binding site	Effect	Reference
Neamine	h44 and H69	Miscoding	(Francois et al., 2005; Pape et al., 2000)
Kanamycin	h44	Miscoding and translocation inhibition	(Feldman et al., 2010; Francois et al., 2005)
Neomycin B	h44 and H69	Ribosome recycling and subunit rotation inhibition	(Borovinskaya et al., 2007a; Wang et al., 2012; Wasserman et al., 2015)
Gentamycin	h44 and H69	Miscoding and ribosome recycling inhibition	(Borovinskaya et al., 2007a)
Paromomycin	h44 and H69	Miscoding and translocation inhibition	(Carter et al., 2000; Demeshkina et al., 2012; Pape et al., 2000; Peske et al., 2004; Wasserman et al., 2015)
Tobramycin	h44 and H69	Miscoding and translocation inhibition	(Cabanas et al., 1978; Fosso et al., 2015; Vicens and Westhof, 2002)
Ribostamycin	h44 and H69	Miscoding	(Francois et al., 2005)
Apramycin	h44	mRNA translocation inhibition	(Matt et al., 2012; Perzynski et al., 1979)
Hygromycin B	h44	Inhibits translocation in both prokaryotes and eukaryotes, by a lesser extent causes misreading	(Brodersen et al., 2000; Eustice and Wilhelm, 1984a, b; Gonzalez et al., 1978; Peske et al., 2004)
Streptomycin	h44	Misreading, h44 distortion, codon-anticodon stabilization, equalization of ribosome selectivity for cognate- and near-cognate ones.	(Carter et al., 2000; Demirci et al., 2013a; Gromadski and Rodnina, 2004b)
Spectinomycin	h34	Translocation inhibition	(Bilgin et al., 1990; Carter et al., 2000; Peske et al., 2004)

1.4.1 Cellular effects of aminoglycosides-induced miscoding

Whereas the primary binding sites of aminoglycosides on the ribosome are well established, the sequence of events that leads to cell death has been under debate for decades. Accumulation of errors in proteins is considered one of the most essential steps contributing to the bactericidal action of aminoglycosides. The insertion of erroneous proteins into the cell membrane is responsible for a membrane damage that, in turn, enhances the antibiotic-mediated killing (Davis et al., 1986). After an initial entry into the cell, aminoglycosides target the ribosomes reducing their fidelity and inducing

miscoding and production of erroneous proteins. The insertion of such proteins into the cell membrane creates abnormal channels that increase the influx and the irreversible entry of more aminoglycoside triggering a positive loop of misreading, membrane damage and antibiotic entrance.

The link between aminoglycosides, miscoding and membrane permeability is also suggested by the following findings: i) when cells containing Str-resistant ribosomes are treated with another aminoglycoside to which they are sensitive, they can then take up more Str (Holtje, 1978, 1979); ii) simultaneous addition of chloramphenicol, a bacteriostatic antibiotic that inhibits protein synthesis, and Str reveals an antagonistic effect of the first on the latter resulting in a decrease Str uptake (Jawetz et al., 1951); iii) the addition of chloramphenicol after the secondary uptake of Str has begun, does not block Str uptake anymore (Holtje, 1978, 1979). These results together suggests that an active, translation-engaged ribosome is necessary for aminoglycosides effect to develop (that is, erroneous proteins must be first synthetized). At the same time, ribosomes that actively synthesize proteins in the presence of an aminoglycoside do not promote its uptake by a direct participation in the process of entry, but rather have an indirect effect involving insertion of erroneous protein into the membrane, which persists even when the ribosome activity is blocked.

In more recent studies, another killing mechanism has been proposed, in which mistranslation of membrane proteins activates a cascade reaction that triggers redox alteration, destabilization of iron-sulfur (Fe-S) clusters (Ezraty et al., 2013) and generation of hydroxyl radicals (Dwyer et al., 2014; Kohanski et al., 2008). Mistranslated proteins are translocated either across the inner membrane into the periplasmic space or are directly inserted into the membrane. As a consequence of the reduced translation fidelity induced by aminoglycosides, many of these proteins are misfolded and activate the two-component stress response sensor consisting of CpxA, which monitors the quality of proteins trafficked through the membrane, and CpxR, which is phosphorylated by CpxA (Dong et al., 1993). This triggers the expression of the envelope stress response proteins, such as degP (Danese et al., 1995; Pogliano et al., 1997), which degrades misfolded proteins and suppresses the toxicity associated with their intracellular accumulation (Isaac et al., 2005).

In addition, CpxA may also activate the redox-responsive two-component transcription factor, ArcA (Iuchi et al., 1989; Ronson et al., 1987). The activation of the envelope stress response system, together with ArcA-regulated changes in metabolic and respiratory systems, leads to the hyperactivation of the respiratory chain and the generation of hydroxyl radicals which cause oxidative stress, generation of 8-oxo-guanine, nucleic acids damage, toxic metabolic perturbations, apoptosis and ultimately cell death (Belenky et al., 2015; Dwyer et al., 2012; Foti et al., 2012). However, the notion that aminoglycosides induce an hydroxyl-radical-mediated killing, has been recently challenged (Keren et al., 2013; Liu and Imlay, 2013), leaving the debate open. Ultimately, the cellular tolerance to

protein errors which accumulate during stress conditions and aminoglyocosides treatment remains elusive and a comprehensive view of aminoglyocosides effects, miscoding and cellular response is still missing.

1.5 Available estimates of error frequencies

A number of estimates for the *in-vivo* abundance of amino acid misincorporations are available in literature (Table 3). Most of the published error frequency values were estimated by biochemical assays that quantified only one specific protein or misincorporation at a time, e.g., incorporation of not naturally encoded amino acids, restoration of the activity of an enzyme variant inactivated by introducing an amino acid replacement at the active site (Kramer and Farabaugh, 2007; Manickam et al., 2014), separation of correct and erroneous proteins by 2D gel electrophoresis. All these techniques share the same common limitations, i.e., use of a reporter system, the choice of the position and type of misincorporation to investigate, and the low sensitivity and the narrow dynamic range associated with the analytical methods being used. Only in recent years mass spectrometry has emerged as a new tool for the evaluation of error frequency (Yu et al., 2009; Zhang et al., 2013), albeit with some constraints due to the wide concentration range between correct and error-containing peptides which often exceeds the dynamic range of the instrument.

Table 3. Estimated *in-vivo* error frequencies. A list of the techniques used so far to determine translation error frequency per codon is reported [adapted from (Ribas de Pouplana et al., 2014)]. Due to the differences which characterize each method, very different frequencies have been determined.

Principle	Error	Error frequency	Assay	References
Detection of aa substitution	I → V	$2x10^{-4} – 6x10^{-4}$	Radioactive Val incorporation	(Loftfield and Vanderjagt, 1972)
	R → C	$1x10^{-4}$	Cys detection in Cys-free protein	(Edelmann and Gallant, 1977)
	R → C; W → C	$4x10^{-3}$	Radioactive Cys incorporation, interference with protease digestion	(Bouadloun et al., 1983)
	N → K	$2x10^{-4} – 2x10^{-3}$	Isoelectric focusing	(Parker et al., 1980)
Reporter systems	G → S	$1x10^{-3}$	lacZ activity restoration	(Toth et al., 1988)
	Y → H	$5x10^{-6}$	CAT activity restoration	(Stansfield et al., 1998)
	± frameshift	$2x10^{-5}$	lacZ activity restoration	(Curran and Yarus, 1986)
	Frameshift, stop codon readthrough	2-10 %	GFP fluorescence	Meyerovich et al. 2010
	24 codons to K	$3x10^{-4}$	Firefly luciferase	(Kramer and Farabaugh, 2007)
	N → D; Q → E	$2x10^{-3} – 8x10^{-3}$	*Renilla* luciferase	(Javid et al., 2014)
tRNA misacylation	Mismethionylated tRNA	$1x10^{-2} – 1x10^{-1}$	Radioactive Met on tRNA microarray	(Netzer et al., 2009)
Mass spectrometry	N → D	$1x10^{-1}$	MS/MS	(Ruan et al., 2008)
	S → N	$2x10^{-2}$	Modified database algorithm and MS/MS	(Yu et al., 2009)
	G ↔ D, G → Q, D → E, E → K; M → I, M → N; S → N; S → R; V → I; D → N; A → T; H ↔ Q; P → L; P → S; R → Q, Y → N.	$10^{-5} – 10^{-3}$	High resolution mass spectrometry	(Zhang et al., 2013)

1.6 Mass spectrometry: an emerging tool for the quantification of miscoded translation products

Mass spectrometry is one of the most efficient ways to identify and quantify proteins. It relies on the separation of ions based on their mass-to-charge ratio and, in association with continuously improved techniques for the ionization of samples (e.g., electrospray ionization (ESI)), has rapidly become the method of choice for the analysis of peptides, single proteins and protein complexes. The advantages of mass spectrometry arise not only from the possibility of a fast and sensitive peptides identification, but also from the low amounts of sample required for the analysis. The identification of a protein can be attained by the direct mass spectrometric anaylsis of the intact protein (top down characterization), or alternatively, due to the ionization and fragmentation limitations associated with this technique, on the base of the peptides generated from protein hydrolysis (bottom up or shotgun proteomics). Peptides, which are easier to fractionate and fragment than the intact protein, are then analysed by tandem mass spectrometry and their spectra compared with databases and spectral libraries which allow their identification and their assignation to the corresponding protein (Lin et al., 2003; Meng et al., 2002; Yates, 2004).

Mass spectrometry has been recently used also for the identification of amino acid misincorporation. The identification of misincorporation-containing peptides is performed on the basis of the mass shift caused by the amino acid substitution, as it happens for the identification of post-translational modifications (PTMs). Hovewer, the extremely low abundance of error-containing peptides, the limited dynamic range of current mass spectrometers (3 - 5 orders of magnitude depending on the sample and the type of mass analyzer (Domon and Aebersold, 2010; Gallien et al., 2012; Gillet et al., 2012; Stahl-Zeng et al., 2007)) and the limited amount of sample that can be tolerated by both chromatographic system and mass spectrometer, makes the identification of rare error-containing peptides often impossible in a sample which also contains high abundance correct peptides and poses a big challenge to their quantification. Indeed, recent fluorescence based *in-vivo* studies (Manickam et al., 2014) and kinetic *in-vitro* studies (Zhang et al., 2015) indicate that many misincorporations might be far less abundant ($<10^{-5}$) than previously expected. This is further complicated by the fact that misincorporation-containg peptides are suppressed by the high abundant co-eluting correct tryptic peptides. To the best of our knowledge, no mass spectrometric study detected more than 5 % of all possible near-cognate misincorporations, presumably due to their low abudance.

After the mass spectrometric analysis, erroneous peptides can be identified by several approaches. Erroneous peptides can be found using the database search algorythms that compare the MS/MS data to *in-silico* predicted fragmentation pattern of all possible peptides in the database e.g., MASCOT (Perkins et al., 1999), Andromeda (Cox et al., 2011), Sequest (Eng et al., 1994), Paragon (Shilov et al.,

2007) or MassAnalyzer (Zhang, 2009). However, because the search space exponentially expands with the number of subsitutitions allowed per peptide, different strategies exists to overcome this limitation while applying traditional search engines. First, the search space can be restricted only to proteins or peptides whose unmodified parental peptide has been observed in the sample and the number of variable misincorporations per peptide can be restricted (Creasy and Cottrell, 2002). Database searches can also identify parental peptides and so called "dependent" peptides that derive from the repective parental peptide but differ by a delta mass (Cox and Mann, 2008). In this case the search space does not expand, because the delta masses are not interpreted in terms of defined PTMs or amino acid substitutions and thus could reflect different deviations from the parental peptide. In this approach the indentification and validation of amino acid substitutions has to occur after the database search. A similar peptides-dependent approach has been recently applied to study the proteome-wide incorporation of norvaline (Cvetesic et al., 2016). When the database search time needs to be reduced, tag-based hybrid methods can be applied in which a sequence tag of 2 - 4 amino acids is derived from a MS/MS spectrum and only tag-containing peptides are searched in the database (Mann and Wilm, 1994; Shilov et al., 2007; Valledor et al., 2008). Spectral library searching can also be used as alternative method to reduce the search space and perform a fast and accurate analysis in which the query MS/MS spectra are searched against a large collection of experimental MS/MS spectra (Frewen et al., 2006), although this method finds its biggest limitation in the fact that the identification of the peptide can be performed only if it is already included in the library. Another approach to adapt classical search engines without restricting it to the prior identification of parental peptides, consists in the increase of the mass tolerance in the delta mass comparison with respect to the parental peptide from the database and in the interpretation of the resulting delta masses only subsequently. This approach was recently used to systematically analyze unassigned spectra from shotgun analysis of HEK cells (Chick et al., 2015). Apart from single missense errors, the algorythm was also able to identify more complex alterations in the amino acid sequence *de novo* such as polyalanine insertions in the ribosomal protein L14. Alternatively, when all amino acid substitutions are included in the database, classical database search engines can be applied (Muhlhausen et al., 2016).

However, in specific cases as for the identification of modified peptides whose sequence is not included in any database, the use of alternative approaches such as d*e novo* sequencing can be favourable. This method, based on software packages such as PEAKS (Ma et al., 2003) and PepNovo (Frank and Pevzner, 2005), directly infers the peptide sequence from MS/MS spectra and bypass the need for spectra comparison with the database. With this approach, many substitutions and modifications can be identified; on the other hand, the high frequency of false positive results and the requirement for high quality spectra limit the applicability of the approach, especially when the

resulting mass shift is not unique or for very low-abundance peptides whose spectra is difficult to obtain with good quality.

Another drawback of current PTM identification and quantification procedures concerns the data interpretation and is associated with the underestimated chemical complexity of tryptic digests. Similar or identical delta masses might be introduced *in vivo* by enzymatic- (e.g., methylations or acetylations) or non-enzymatic posttranslational modifications (e.g., carbon, oxidative or nitrosative stress) (Wagner and Hirschey, 2014; Weinert et al., 2013) which could lead to false positive identifications. Subsequently, modifications might be introduced upon cell opening and sample preparation (e.g., oxidation, iodoacetamide (IAA) labelling, atryptic cleavage (Picotti et al., 2007) and transpeptidation (Fodor and Zhang, 2006; Schaefer et al., 2005)). Moreover, such peptide decay reactions are often accelerated when the individual residues of trypytic peptides are not protected by the protein environment (Manning et al., 2010). In the mass spectrometric workflow, co-ionizing adducts (e.g., sodium ions) and gas phase reactions (e.g., cyclizations, deamidations or water loss) can further lead to modifications that are isobaric to amino acid misincorporations. For example, a +14 Da Δmass might be explained by replacements D → E, G → A, N → Q, V → I, V → L, S → T, as well as by methylations at K, R, H, Q, N, E, D (Jung et al., 2008) that can be either introduced *in vivo* or artificially during sample processing using methanol (Chen et al., 2010), e.g., upon Coomassie staining (Sumpton and Bienvenut, 2009). A +14 Da Δmass can also arise by misincorporations of β-methylnorleucine (Muramatsu et al., 2003) in place of I or oxidations of Y and W. Cysteinyl-S-β-propionamide, a by-product of acrylamide adduct formation in SDS-PAGE, can produce the same mass associated with cysteine alkylation plus monomethylation on a proximal amino acid (Hart-Smith et al., 2016) and methylations which are difficult to reliably identify by conventional scoring algorythms due to high false discovery rates (Bogdanow et al., 2016). Incidentally, the identification of those errors that are expected to be highly abundant, because they are introduced by third position codon-anticodon mismatches, is particularly difficult, because they often lead to common delta masses (i.e., -16, -14, +14, +16 Da). These identification problems are aggravated by the fact that low-abundance erroneous peptides often have incomplete fragmentation patterns precluding the exact identification of the position of the delta mass in the peptide sequence. In addition, isobaric peptides often co-elute during chromatography and thus hamper the correct quantification on the MS1 level, and lead to chimeric MS/MS spectra that are often hard to correctly assign to the respective sequences. Finally, the correct parental and erroneous peptides might differ in their ionizability which is especially relevant for peptide pairs with very different physicochemical properties which reflect in deviating retention times and large delta masses e.g., when the amino acid substitution introduces or eliminates a tryptic cleavage site generating error-containing peptides which are shorter or longer than the correct ones.

Overall, this leads to the unfortunate situation in which most misincorporations might escape detection and prompted us to develop an alternative experimental approach that would allow the reliable and systematic identification and quantification of erroneous peptides with high sensitivity and over a wide dynamic range.

1.7 Selected reaction monitoring (SRM) and triple quadrupoles mass spectrometer

Selected reaction monitoring (SRM) is an attractive method for the accurate quantification of peptides, not only for its high sensitivity (to attomole concentration levels), but also for its broad dynamic range – up to five orders of magnitude – and excellent analytical reproducibility (Domon and Aebersold, 2010).

During a typical LC-MS/MS analysis, the peptides of the sample are separated by reversed phase chromatography performed using a low-flow nano-LC system. Upon elution peptides are directly sprayed into the mass spectrometer from a needle which is kept at high potential (see Materials and Methods). The ejection of liquid from the needle in the presence of voltage gives raise to the formation of a cone, known as the Taylor cone (Taylor, 1964) and the sample is ionized for the mass spectrometric analysis using ESI (electrospray ionization) technique. At high temperature, the solvent evaporation and the droplet shrinking increases the charge density until ions are kinetically and energetically ejected from the droplet, to then pass through a transfer ion capillary and enter the vacuum region of the mass spectrometer for the analysis (Ho et al., 2003). For SRM analysis, a triple quadrupole mass spectrometer is used. The instrument consists of three consecutive quadrupoles, named Q1, Q2 and Q3, each constituted by an assembly of four parallel metal rods, where two opposite rods are electrically connected, but offset relative to one another giving two sets of rods pairs per quadrupole. Although a triple quadrupoles mass spectrometer can operate in a variety of scan types, when in SRM mode, it performes two stages of mass selection, referred to as tandem MS or MS/MS. At every time point, a variable combination of radio frequency (rf) and direct current (dc) voltages of the same amplitude and sign is applied in the Q1 and Q3 for each set of rods. This causes ions to oscillate and guides them through the rod assemblies. The oscillation stabilizes only selected ions with a specific mass-to-charge ratio (*m/z*) and allows them to pass, while all other ions crash on the rods and are eventually eliminated. Q1 and Q3 act as mass analyzers. After the Q1, only selected precursors will be allowed to enter the Q2. On this quadrupole, only rf voltage is applied and because selection of ions is not possible with the rf alone, this quadrupole only acts as transmission device instead of a mass analyzer. Q2 is a collision cell, where the ions that have been selected in the Q1 collide with gas molecules (e.g., nitrogen or argon) at a defined gas pressure and electrostatic energy potential and fragment to yield a second type of ions, the fragment ions, that will be then selected in

Q3 during the last stage of selection and ultimately recorded by the ion detection system (Figure 7). After a certain time, the dwell time, the rf and dc ratio are changed, and a new pair of ions are selected. The settings used for the selection of a precursor ion in the first quadrupole and the selection of its fragment ions in the third, are called transition. Usually 2 - 3 transitions are monitored for each peptide. The type of fragment ions which can be observed at the MS/MS level depends on various factors such as the sequence of the peptide and the charge state, and can be detected only if they retain a positive charge at their N terminal (a, b and c ions) or at their C terminal (x, y, z) (Roepstorff and Fohlman, 1984). The narrow selection windows of the first and third quadrupoles, between 0.2 and 0.7 Da, allow the transitions of a very small set of ions, contributing to a high degree of selectivity and reducing the chemical noise. In this way, SRM analysis permits an instrument linearity which can easily span 5 orders of magnitude (Worboys et al., 2014). High degree of selectivity and sensitivity constitute the pivotal charachteristics that make this approach particularly suitable for biomarker discovery, where very low abundant marker peptides need to be found in extremely complex mixtures like, for example, blood sample (Stahl-Zeng et al., 2007).

However, mass spectrometry is not quantitative *per se,* because the variation in the stability of ESI spray and the different intrinsic ionization properties of each peptide, hamper the direct comparison of peaks intensities. For this reason, to obtain an accurate quantification, the insertion of a mass tag by metabolic, enyzymatic and chemical labeling of peptides or proteins, or by spike of synthetic peptide standards into the sample is commonly employed (Ong and Mann, 2005). Stable isotope-labelled peptides are chemically identical to the native light counterparts and they behave identically during liquid chromatography separation and mass spectrometric analysis. Nonetheless, the mass tag is detected by the mass spectrometer and the quantification can be performed by comparison of the signal intensity of light and heavy-labeled peptides (Bantscheff and Kuster, 2012). One optimized application of this strategy is the so called AQUA (Absolute QUAntification) approach, based on the use of custom designed and chemically synthetized peptide standards which contain C-terminal heavy amino acids labeled with carbon and nitrogen stable isotopes i.e., ^{13}C- and ^{15}N-, and that are spiked in the samples in known amount prior to the analysis (Gerber et al., 2003). Once the target peptides are analyzed in the sample by mass spectrometry, the area under the peptides peak is integrated, the peptides are detected and the ratio between the internal standard and the analyte is determined (Figure 7). Finally, because the amount of internal standard in the sample is known, also the amount of the analyte can be easily calculated. The first step in the development of the AQUA strategy is the selection of the peptides to be monitored during the SRM experiment. In our case, the selection is performed on the base of pre-existing data obtained from data-dependent acquisition, but in general, their selection can also be performed on empirical observations around their stability and ionization

performances. Furthermore, some general features can be used to predict if a peptide is suitable or not for this analysis. Tryptic peptides length is between 5 and 20 amino acids and their sequence should lack reactive amino acid that could undergo modifications, e.g., methionine, or residues that could make the synthesis and purification of the synthetic peptides difficult, e.g., multiple serine or proline residues should be avoided because they cause deletion during the synthesis process (Lange et al., 2008; Picotti and Aebersold, 2012). Target peptides must be unique for the target protein and their sequence should not be shared by any other tryptic peptide from other proteins in the organism of choice ("proteotypic peptides" (Mallick et al., 2007)). It is also important that the peptides accurately represent the level of the protein ("quantotypic peptides" (Brownridge and Beynon, 2011)), which means that several factors that could affect their concentration – the completeness of proteolytic reaction, peptide stability, and the absence of post-translational modification – should be taken into consideration.

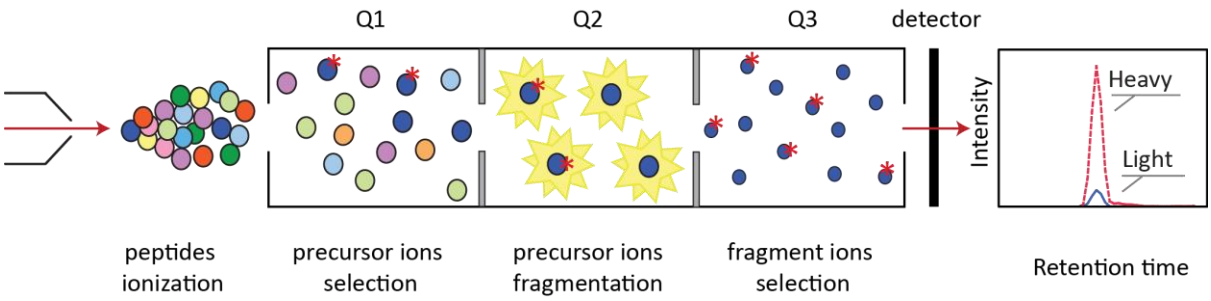

Figure 7. SRM analysis on a triple quadrupole mass spectrometer. Peptides are eluted from the nano-LC system and ionized before entering the instrument. Isotope-labeled peptides are indicated with the asterisk. Precursor ions are selected in the Q1, fragmented in Q2 and resulting fragment ions are ultimately selected for detection in Q3. Comparison of the peak area of light peptides and stable-isotope labeled peptides provides precise quantification of the endogenous analyte.

1.8 Parallel reaction monitoring (PRM) to confirm the identitity of enriched peptides

Although SRM is highly selective, some limitations arise from the resolution and mass accuracy of the quadrupoles mass analyzer used in triple quadrupole instruments, especially when near-isobaric fragment ions are analyzed (Abbatiello et al., 2010; Gallien et al., 2013; Sherman et al., 2009). Parallel reaction monitoring (PRM) can be an attractive alternative method for targeted quantification, especially when a higher degree of selectivity is required (Gallien et al., 2012; Peterson et al., 2012). As for SRM, peptides are separated by reversed phase chromatography on a nano-LC system and directly sprayed into the instrument, e.g., quadrupole-Orbitrap mass spectrometers (Gallien et al., 2012). This instrument type consists of an Orbitrap mass analyzer (Hu et al., 2005) preceded by a quadrupole mass filter which is used for the selection of only specific precursor ions. When PRM is performed on a quadrupole-orbitrap instrument, a defined precursor ion is selected in the quadrupole

mass filter and transferred via the C-trap into the higher-energy collisional dissociation (HCD) cell, where it is fragmented. In contrast to the triple quadrupoles mass spectrometers, the quadrupole-orbitrab mass spectrometers have a discontinuous data acquisition regime in which ions with target *m/z* values are selected by the quadrupole and collected in the C-trap while, in parallel, fragments of the previous measurement are still anaylzed in the Orbitrap. When enough ions are collected or the maximal fill time is reached, precursor peptides are transferred to the HCD cell for fragmentation. After fragmentation, the product ions are transferred via the C-trap to the Orbitrap and analysed simultenaously (Figure 8). In the Orbitrap the attraction to the central electrode is compensated by the initial tangential velocity of the ions. Upon measurement, the axial component of the circulation around the central electrode is detected as image current on the electrode encapsulating the orbitrap. The transient of all ions that is monitored over time is deconvoluted by Fourier transformation resulting in high resolution mass spectra. Longer fill times potentially increase the signal and, in parallel, longer analysis times allow for higher resolution spectra. On the other hand, the same factors limit the number of precursor masses that can be analyzed in a given time window, which results in a trade-off between resolution, sensitivity and the number of analytes. Because all fragments ions of a selected precursor can be monitored in parallel, PRM does not require the selection of only few of them, but all the pseudo transitions that have been recorded during the mass spectrometry run can be easily extracted post-acquisition, during data analysis. This translates into a simplification of the protocol with respect to SRM, in which less method optimization is required, with only the precursor *m/z* ratio that has to be selected in the quadrupole and the elution time of the peptide.

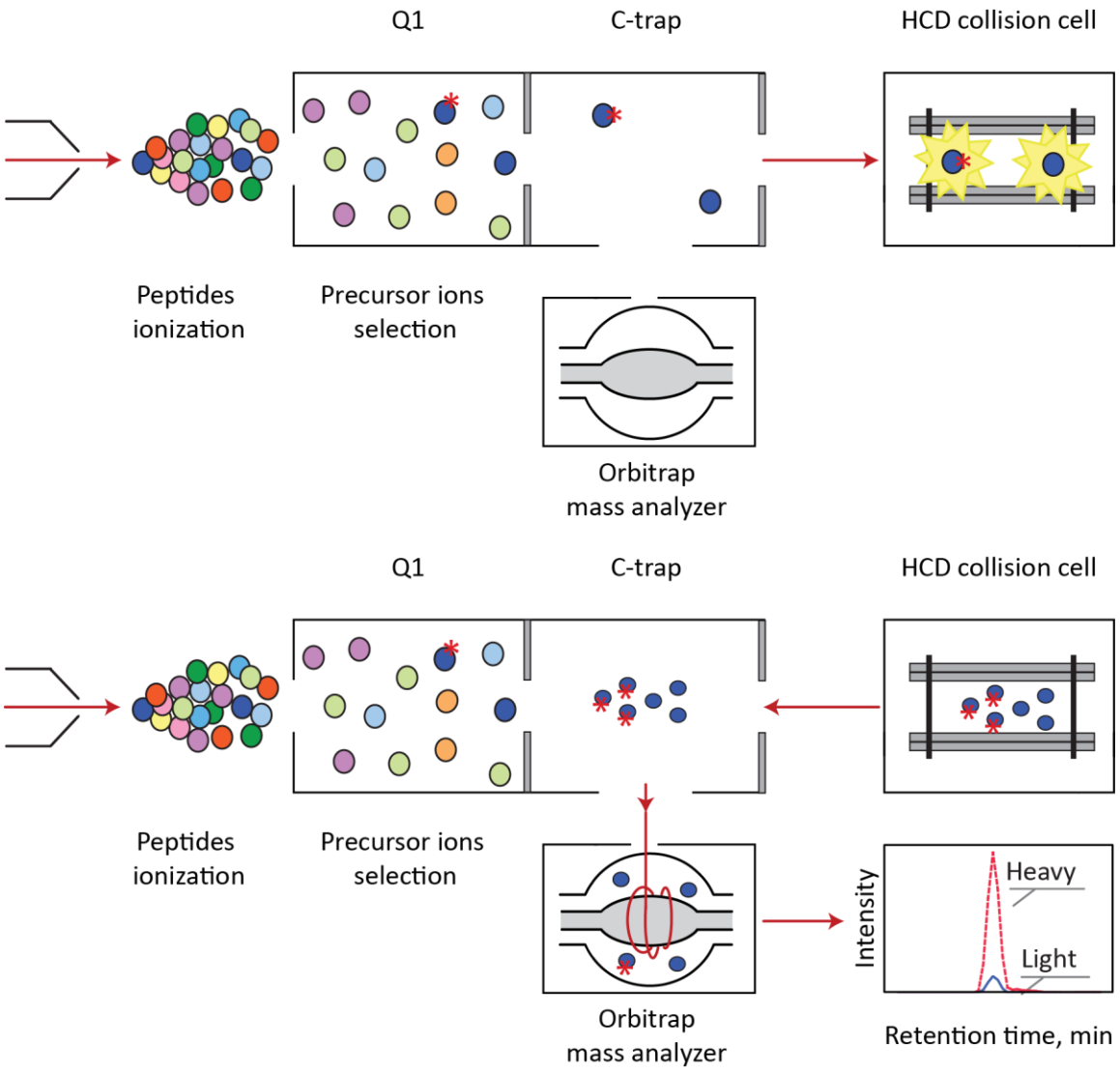

Figure 8. PRM analysis on a hybrid quadrupole/Orbitrap mass spectrometer. Peptides are eluted from the nano-LC system and ionized before entering the instrument. Isotope-labeled peptides are indicated with the asterisk. Precursor ion are selected in the Q1 and move via the C-trap to the HDC cell for fragmentation. All fragment ions are then transmitted back into the C-trap and injected into the Orbitrap for analysis. Comparison of the peak area of light peptides and stable-isotope labeled peptides provides precise quantification of the endogenous analyte.

1.9 EF-Tu as a model protein

Although a proteome-wide quantification of misincorporations would be desiderable, such large-scale quantification is hampered by the large difference in the abundance of many error-containing peptides and their cognate counterparts, whose concentration ranges often exceed the linearity of the instrument. Because there is no evidence that misincorporations in endogenous proteins can be more adundant than 10^{-3} (Table 1 and Table 3), the vast majority of proteins comprising the *E. coli* proteome cannot be studied in the lysate. In addition, the mechanisms that ensure the fidelity of protein synthesis are expected to be the same regardless of the protein choosen, because the same type of errors that occur during DNA replication, transcription or translation affect every synthetized

protein. These considerations prompted us to select a model protein that could be investigated without limitations in terms of source, strain, construct, tag or stress condition and that could be easily purified by affinity protocols as well as traditional tag-free chromatographic strategies (to minimize external interferences coming from other proteins), but that would also be abundant enough to be directly investigated in lysates without any enrichment. Among the high-abundance proteins in *E. coli*, EF-Tu emerged as the best candidate for our analysis. It is by far the most abundant protein of the *E. coli* proteome (Figure 9), 10-times more abundant than ribosomes (Furano, 1975; Schmidt et al., 2016). EF-Tu is directly involved in decoding and thus manipulations such as the addition of a tag for affinity purifications might effect the levels of misincorporations in the cell. However, the protein is functional when fused to a His-tag at the C-terminus *in vitro* and *in vivo* and supports the wild type accuracy levels (Boon et al., 1992).

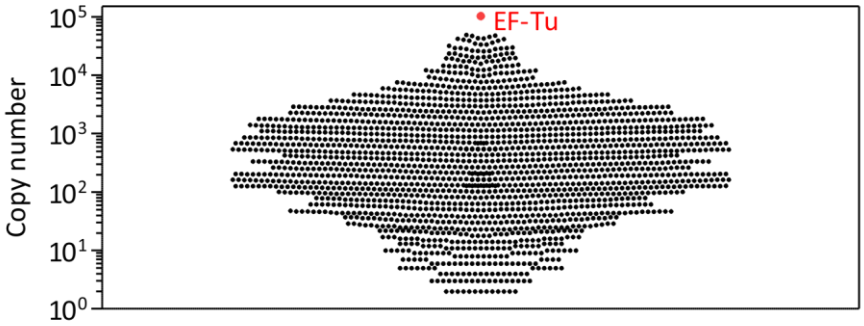

Figure 9. Abundance of proteins in *E.coli*. Mass spectrometry analysis of the proteome of *E. coli* cells grown in LB medium. Figure based on the data from (Schmidt et al., 2016).

EF-Tu is a monomeric protein of 393 amino acids and consists of three domains (Kjeldgaard and Nyborg, 1992). Domain I is composed of a central sheet formed by five parallel β-strands plus one which is antiparallel and which is in turn surrounded by α-helices and contains the GDP/GTP binding pocket (Figure 10). Domains II and III constist of antiparallel β-barrel structures. EF-Tu is encoded by two genes, *tufA* and *tufB* (Lindahl et al., 1975), which have almost the same sequence, except for 13 nucleotides that result in synonymous codon substitutions. The products of the two genes share the same structure, almost identical molecular weight (43314 Da and 43284 for the product of *tufB* and *tufA,* respectively) and their amino acid sequence is identical, except for one amino acid at the C-terminus for *E. coli* MRE600 (glycine in *tufA* and serine in *tufB*) (Arai et al., 1980). Sequence variations can be observed in different *E. coli* strains. The amino acid sequence for the EF-Tu used in this project can be found in the Appendix (Section A) of this thesis.

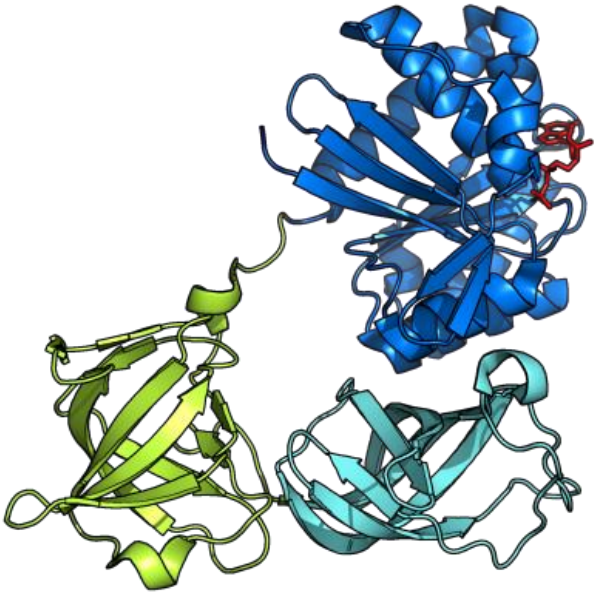

Figure 10. EF-Tu crystal structure. The three domains are highlighted in different colors: GTP/GDP-binding domain I (1-200 aa) in dark blue, domain II (209-299 aa) in lime , domain III (300-393 aa) in aquamarine. The structure of GDP molecule bound to domain I is highlighted in red. [PDB file 1dg1 (Abel et al., 1996)].

1.10 Aim of the study

The aim of this project is to develop a mass spectrometric assay to systematically quantify the error frequency of amino acid misincorporation *in vivo* and to overcome the limitations inherent in other published approaches e.g., codon-specific reported systems, amino acids or positions in the protein sequence, narrow instrument dynamic range and sensitivity. The second aim is to apply this assay in order to characterize the basic features and dimensions of the fidelity landscape *in vivo* determining i) the accuracy of the proteome; ii) the range in which misincorporations occur; iii) the fidelity of translation at different position of the protein; iv) the potential effect of the quality control machinery. The third aim is to characterize the error-inducing signatures of aminoglycosides and to correlate them with the impact on the cell physiology, such us growth defects and induction of stress response, and to ultimately dissect the complex mechanisms underlying the bactericidal effects of miscoding-inducing antibiotics.

2. RESULTS

2.1 Multidimensional chromatography for peptides enrichment

2.1.1 An overview of the method

Quantification of misincorporations and estimation of translational error rate are often affected by limitations in the type of misincorporation to be selected for the study, by poor sensitivity of the method or its restriction to *in-vitro* assays or fixed model systems. Here we describe a novel method to quantify amino acid misincorporations *in vivo.* The advantage of the method is its sensitivity and broad applicability to unrestricted types of substitutions and reference systems. The protocol relies on the separation of error-containing peptides and their enrichment against the more abundant correct peptides through consecutives rounds of orthogonal chromatographies including alternating rounds of size-exclusion and reversed phase separation. This is combined with final quantification by targeted mass spectrometry and SRM analysis (Figure 11). This approach has some similarities with the methods employed for the detection of low-abundance protein biomarkers from complex biological fluids, like blood plasma or urine, in which high-abundance proteins are depleted prior to the analysis (Surinova et al., 2011).

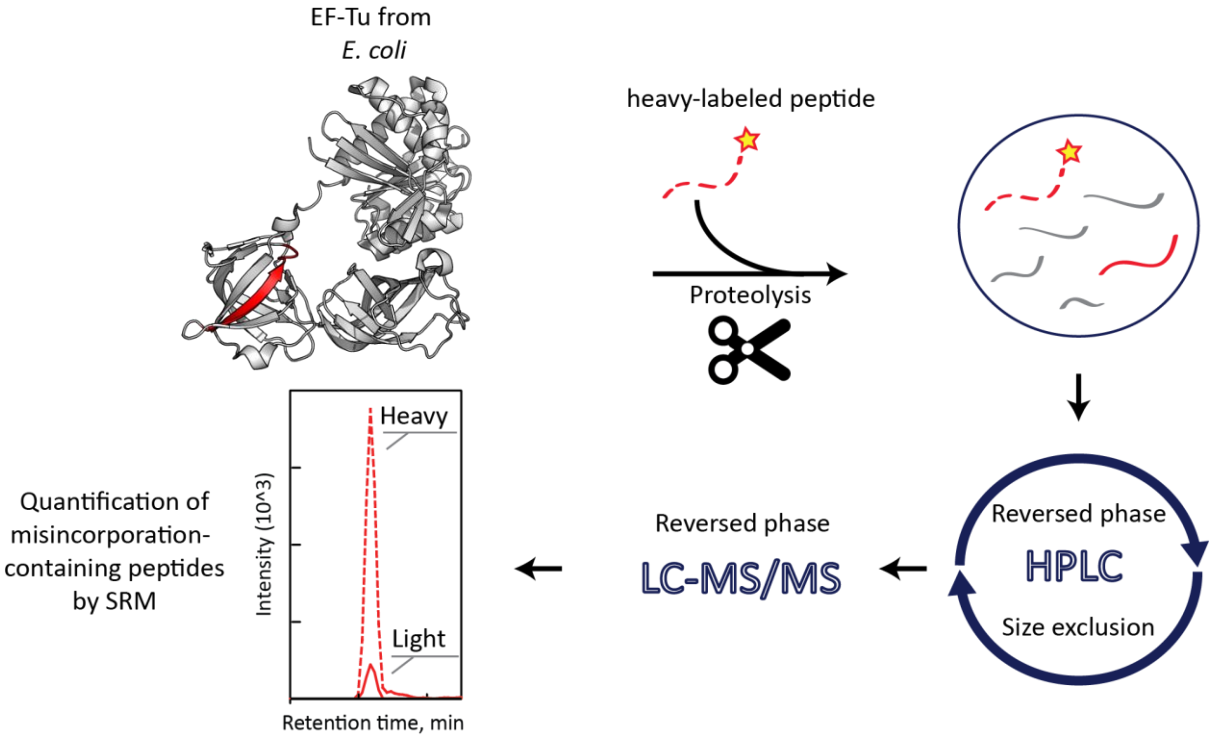

Figure 11. Schematic of the workflow for the enrichment of error-containing peptides. A model protein, EF-Tu, is proteolyzed. The peptide of interest (red) is selected and the corresponding isotope-labeled reference peptide (dashed red), is spiked in the sample. The sample is subjected to multiple rounds of HPLC chromatography. Ultimately, peptides are separated on the nano-LC on-line with the mass spectrometer (LC-MS/MS). Quantification of misincorporations is performed on triple quadrupole mass spectrometer operated in Selected Reaction Monitoring (SRM) mode and the ratio of light/heavy peptides is used to calculate the error frequency.

2.1.2 Sample preparation

The performance of the protocol depends on the accurate preparation of the sample, which in our case starts with proteolysis by trypsin, a protease that cleaves polypeptide chains after lysine and arginine residues. To optimize protein digestion, we selected four tryptic peptides from the model protein EF-Tu, i.e., FESEVYILSK, VGEEVEIVGIK, ELLSQYDFPGDDTPIVR and TVGAGVVAK (Figure 12, A), which are proteotypic within the *E. coli* proteome and we monitored their formation over time. At selected time points, an aliquot from the digestion mix is withdrawn, mixed with the heavy-labeled counterparts of the four reference peptides and the sample analyzed by mass spectrometry. The area under the peak of light and heavy peptides is integrated and their ratio is calculated (Figure 12, B).

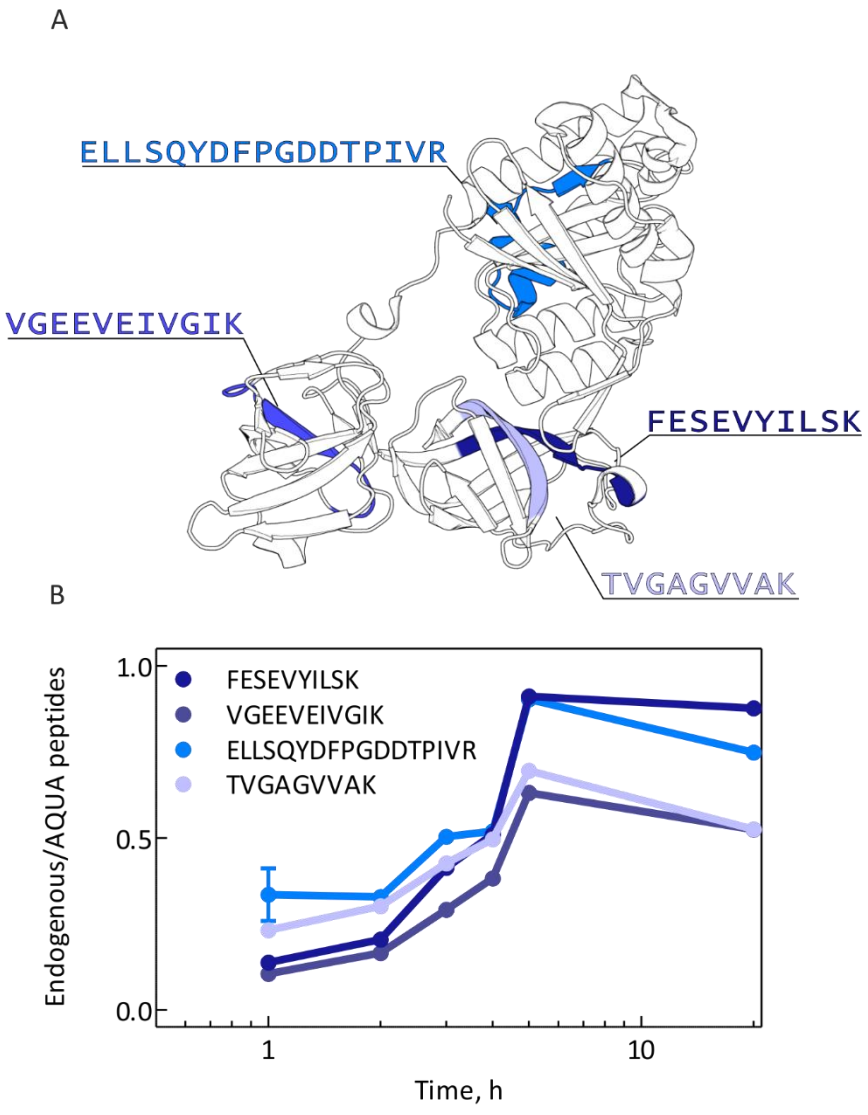

Figure 12. Proteolysis time courses. A) Four proteotypic peptides are selected from the EF-Tu sequence [PDB file 1dg1]. B) The progress of the proteolysis is assessed by monitoring four quantotypic peptides. Error bars represent the standard deviation of 3 technical replicates.

The relative concentration of the endogenous peptides increases with reaction time and reaches a plateau after 5 hrs of incubation at 37 °C. At this point the digestion is complete and the peptides remain stable in the reaction tube for the next 20 hrs. The stability of the peptides indicates that they are potentially quantotypic for the protein, which means that an any point their concentration exactly reflects the amount of protein in the sample, and that their quantification is reliable and not affected by decay due to instability, which could lead to an underestimation of the amount of proteins (Shuford et al., 2012).

After proteolysis is completed, the total amount of digested EF-Tu is quantified by mass spectrometry using the same four peptides employed to monitor the digestion. A small aliquot of the digested protein is spiked in with a known concentration of AQUA peptides containing identical amounts of the four reference peptides and the mixture is then analyzed by mass spectrometry. The ratio of endogenous and heavy peptides is determined (Figure 13) and because the concentration of the latter is known, the amount of EF-Tu can be easily calculated. Once the concentration of the correct tryptic peptides is determined, we spike in the isotope-labeled reference peptides containing misincorporations of interest and assess the error frequency, e.g., for the quantification of R to H substitution in the GTVTTGRVER peptide, the AQUA peptide GTVVTGHVER is used.

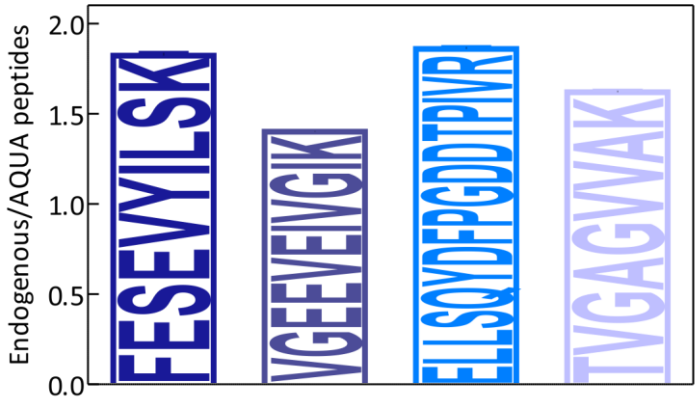

Figure 13. Quantification of proteolysed EF-Tu. The ratio of endogenous/AQUA peptides for the reference peptides is calculated and used to quantify the concentration of correct tryptic peptides obtained from EF-Tu proteolysis. Digested peptides and AQUA peptides are not mixed in a 1:1 ratio so that the calculated endogenous/AQUA ratio does not need to be necessarily 1. However, comparable ratios among the four reference peptides indicate that they are are stable in the reaction tube. Error bars represent the standard deviation of 3 technical replicates.

2.1.3 Chromatographic separation and enrichment of target peptides

In the first chromatographic dimension, the peptides are separated based on their hydrodynamic radius by size-exclusion chromatography, whereas in the second dimension they are separated depending on their hydrophobicity by reversed phase chromatography at neutral pH (Figure 14). At

both steps, all the fractions obtained are screened by mass spectrometry, and only the ones containing the target peptides are processed further. At this stage, the signal from the error-containing peptides is still too low to be detected, so that only the respective heavy-labeled standards are monitored. For the subsequent quantification the peptides are loaded onto a nanoflow chromatographic system and separated by reverse phase at acidic pH prior to their detection in the mass spectrometer. Although the last two dimensions both rely on reversed phase chromatography, the different pH at which they are performed confer separation power, especially for those peptides which contain residues whose protonation status changes upon pH shift – i.e., aspartate and glutamate – and whose separation can be altered by using different pH range. Because our peptides normally contain one of these amino acids, their chromatographic behavior changes from neutral to acidic pH ensuring their efficient separation. For an initial screening of error frequencies, we have chosen to follow the Arg to His substitutions (Table 4), known to be relatively abundant (Zhang et al., 2013). In addition, this type of amino acid misincorporation is particularly favourable to be investigated using our enrichment protocols because it changes the tryptic pattern of the protein which we proteolyzed using trypsin (which cleaves at R and K residues). The proteolysis of the error-containing protein yields longer peptides that elute earlier from the size-exclusion column than the products of digestion of the correct protein which are shorter. Thereby, the complexity of the sample and the background noise are efficiently reduced. Low-abundance erroneous peptides are enriched, separated within each other and from the more abundant cognates allowing us to increase the column load, pulling low abundance-peptides in the dynamic range of the instrument so that their signal can be detected.

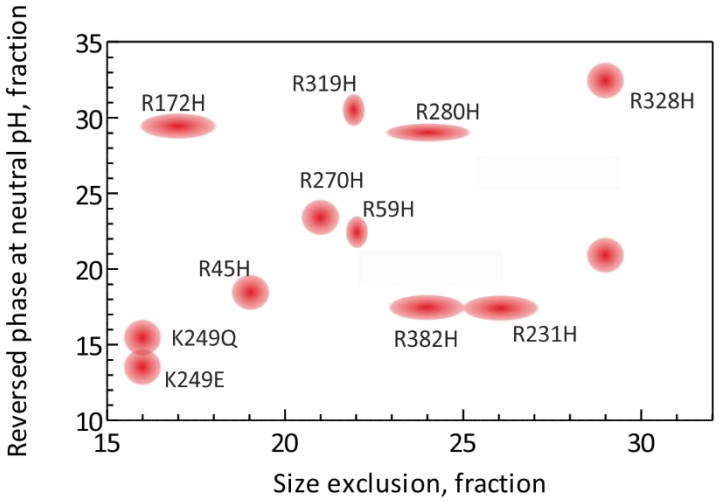

Figure 14. Distribution of peptide elution intervals in the first two chromatographic dimensions. EF-Tu peptides displaying different chemical property can be efficiently separated according to their size and hydrophobicity. Separated peptides are represented by the red dots. The size of each dot reflects the number of fractions in which the respective peptide is eluting.

Table 4. General properties of R to H substituted peptides. Distinct physicochemical characteristics allow for efficient separation and correct identification of error-containing peptides. Hydrophobicity factors are estimated using the peptide analyzer tool https://www.thermofisher.com/de/de/home/life-science/protein-biology/peptides-proteins/custom-peptide-synthesis-services/peptide-analyzing-tool.html.

Misincorporation	Peptide	Length	Hydrophobicity
R45H	TYGGAAHAFDQIDNAPEEK	19	28.03
R59H	AHGITINTSHVEYDTPTR	18	24.83
R231H	GTVVTGHVER	10	13.43
R234H	VEHGIIK	7	13.53
R270H	LLDEGHAGENVGVLLR	16	32.49
R280H	AGENVGVLLHGIK	13	27.51
R284H	HEEIER	6	5.86
R319H	DEGGHHTPFFK	11	19.94
R328H	GYHPQFYFR	9	28.31
R378H	FAIHEGGR	8	13.16
R382H	EGGHTVGAGVVAK	13	15.52

In some cases, enrichment and analysis of error-containing peptides which have very similar physicochemical characteristics to their cognate peptides (e.g., FESEVYILSK peptide (Table 5)) might not be achieved in the first two dimensions (Figure 15). However, the separation of target peptides from the highly abundant cognate peptide is essential, as without their separation the sample complexity cannot be reduced. To improve the separation, further chromatographic steps are required which are tailored to the characteristics of specific peptides. We chose to add the third chromatographic step, reversed phase at acidic pH prior to the reversed phase performed on the nanoflow system. Although three rounds of reversed phase might not be fully orthogonal, they synergistically provide not only a further reduction of sample complexity, but also improve the separation of histidine-containing peptides due to the different pH. The second reversed phase chromatography, therefore, enhances the separation of error-containing peptides from the correct FESEVYILSK, before that the sample is loaded on the LC-MS/MS system (Figure 16). This reduces local interferences in SRM quantification and allows to load more target peptide without saturating the LC system, both improving the signal to noise ratio and signal intensity.

Table 5. Physicochemical characteristics of peptides differing by a few amino acids may be very similar. When compared to the cognate peptide FESEVYILSK, peptide variants with one, two or three amino acid difference have very similar charachteristics in terms of both length and hydrophobicity. Hydrophobicity factor has been estimated using the peptide analyzer tool available on the website of Thermo Fischer Scientific at the link https://www.thermofisher.com/de/de/home/life-science/protein-biology/peptides-proteins/custom-peptide-synthesis-services/peptide-analyzing-tool.html

Errors	Peptide	Length	Hydrophobicity
Cognate	FESEVYILSK	10	28.2
F305L	LESEVYILSK	10	26.41
E306D	FDSEVYILSK	10	28.51
E308D	FESDVYILSK	10	27.45
Y310H	FESEVHILSK	10	23.69
Y310N	FESEVNILSK	10	25.23
E306D-E308D	FDSDVYILSK	10	27.83
E306D-Y310H	FDSEVHILSK	10	24.00
E308D-Y310H	FESDVHILSK	10	23.10
E306D-Y310N	FDSEVNILSK	10	25.56
E308D-Y310N	FESDVNILSK	10	24.64
E306D-E308D-Y310H	FDSDVHILSK	10	23.41

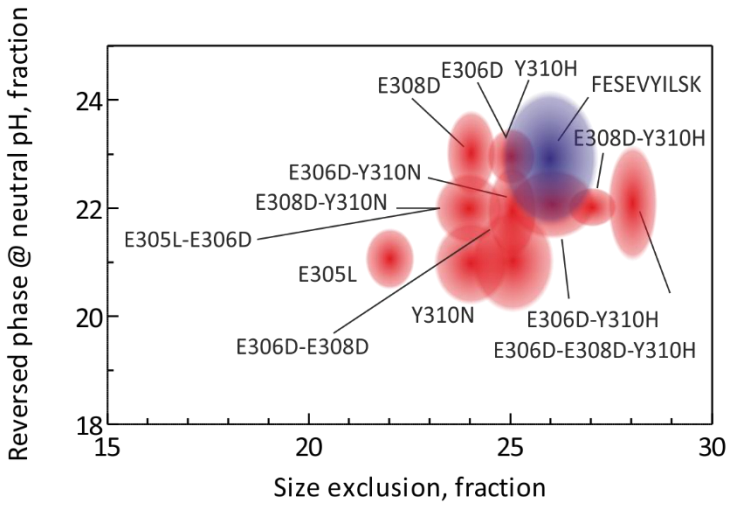

Figure 15. Poor separation of similar peptides in the first two chromatographic dimensions.The two-dimensional separation of peptides that differ in only few amino acids with respect to the correct peptide is poor. Separated peptides are represented by dots (error-containing peptides in red, correct FESEVYILSK in blue). The size of each dot reflects the number of fractions in which they are eluting.

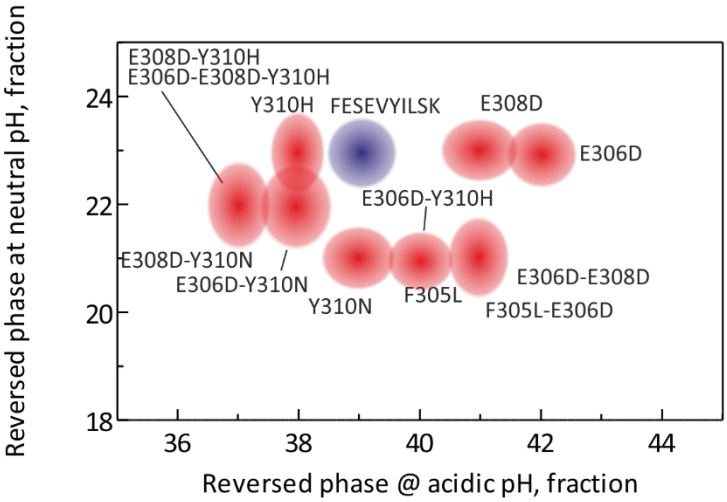

Figure 16. Elution pattern of similar peptides in reversed phase chromatography runs at neutral and acidic pH. The different pH of the mobile phase changes the separation profiles of peptides which contain ionizing amino acids. Separated peptides are represented by dots (error-containing peptides in red, correct FESEVYILSK in blue). The size of each dot reflects the number of fractions in which peptides elute.

2.2 Identification of enriched error-containing peptides

2.2.1 Identification of peptides by SRM analysis

Data obtained by SRM analysis are processed using Skyline software (MacLean et al., 2010b) which integrates the area under peptides peak and calculates the L/H ratio between light (L) and heavy (H) peptides. Each peptide, both in its light and heavy forms, is identified by the precursor mass-to-charge ration (*m/z*) selected in the first quadruple of the mass spectrometer (527.7865 and 532.7856, respectively for the example shown in figure 17) and the *m/z* of 3 – 5 fragment ions which are selected in the third quadrupole. The same intensity pattern for light and heavy peptides transitions, together with the identical elution time, allow us to identify the endogenous target peptide (Figure 17). A quantitative expression for this identification is the ratio dot product (rdotp) (Sherwood et al., 2009), for which the maximum value 1 indicates a perfect identification, whereas a value of 0 suggests complete orthogonality.

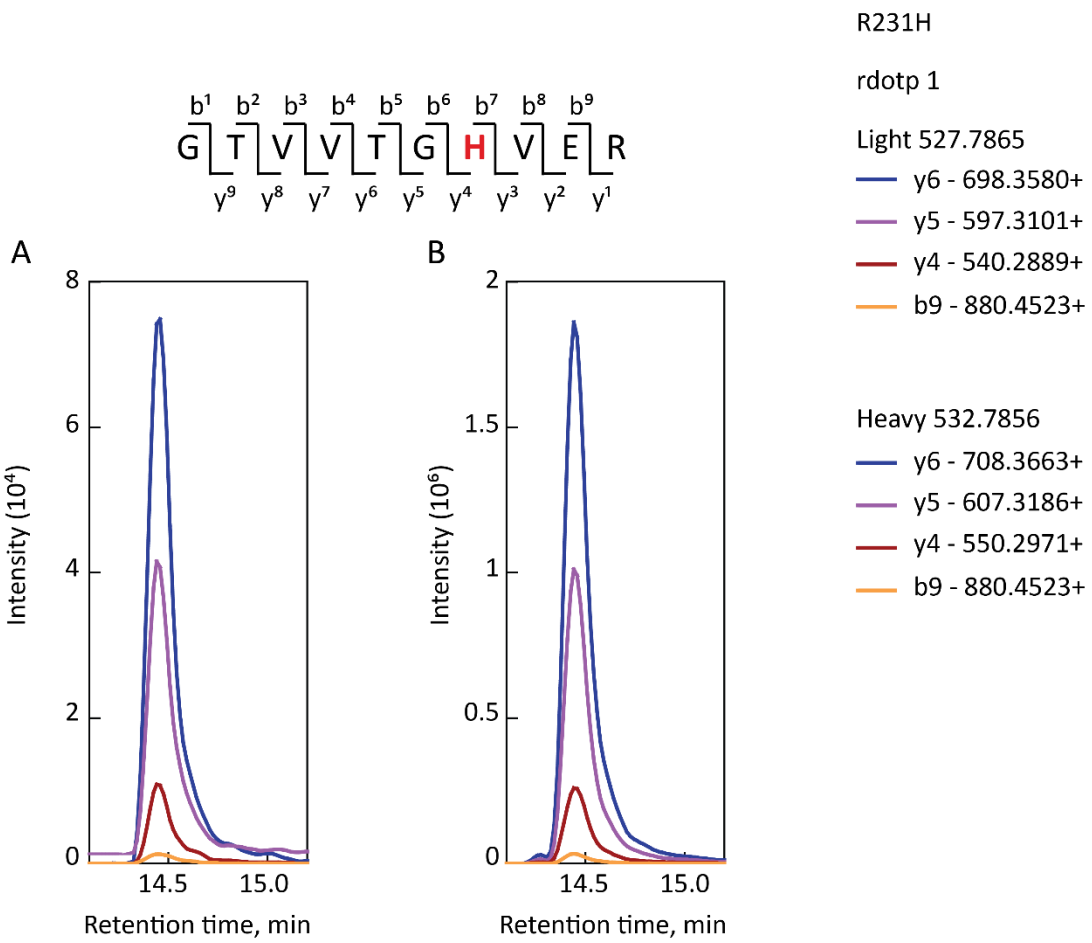

Figure 17. Detection of error-containing peptides. Top panel, the sequence of the peptide and its fragmentation pattern. Co-eluting light (A) and heavy [Arg (^{13}C6; ^{15}N4)] (B) versions of the R231H peptide are detected. Four transitions y6, y5, y4 and b9 are selected, whose intensity order is identical between the light and heavy peptide. A rodtp value of 1 confirms the confidence of the identification.

2.2.2 Identity validation by manual annotation of MS1 and MS/MS spectra

Even though the co-elution of light and heavy peptides and the transitions pattern alone are generally accepted as a proof of the peptide identity, we decided to further validate our identifications using high resolution MS1 and MS/MS spectra. Precursor and the fragment ions spectra are compared with the fragmentation pattern predicted for the peptide (Figure 18). In cases where a clear MS1 and MS/MS could not be acquired due to the limited dynamic range of the mass spectrometer or to signal interference, for example for non-cognate misincorporations, the identity of the peptides detected by SRM was substantiated by parallel reaction monitoring (PRM) (Figure 19).

A

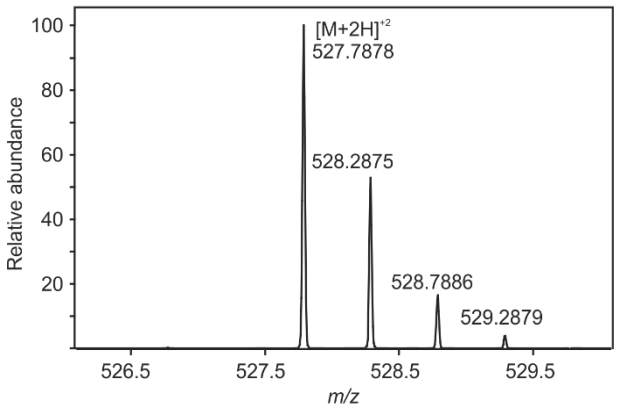

B

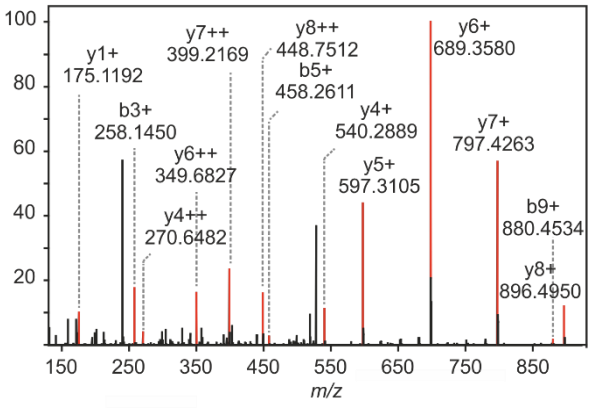

C

MH^{+1}	**MH^{+2}**	MH^{+3}
1045.5640	**527.7856**	352.1928

b	b^{+2}				y	y^{+2}
-	-	1	G	10	-	-
159.0764	-	2	T	9	977.5425	499.2749
258.1448	-	3	V	8	**896.4948**	**448.7511**
357.2132	-	4	V	7	**797.4264**	**399.2169**
458.2609	-	5	T	6	**698.3580**	**349.6826**
515.2824	-	6	G	5	**597.3103**	299.1588
652.3431	326.6743	7	H	4	**540.2889**	**270.6481**
751.4097	376.2085	8	V	3	403.2300	202.1186
880.4523	440.7298	9	E	2	304.1615	152.5844
-	-	10	R	1	**175.1190**	88.0631

Figure 18. Identification of error-containing peptides by high resolution MS1 and MS2 spectra. The precursor (A) and the fragment (B) spectra are compared with the predicted fragmentation pattern (C). Their identification in the sample is essential to confirm the identity of the enriched peptide. The peak of the doubly charged precursor is indicated in bold in both A and in the predicted fragmentation pattern. The spectra of the freagment ions are indicated in bold in the fragmentation pattern and annotated on the MS/MS spectra.

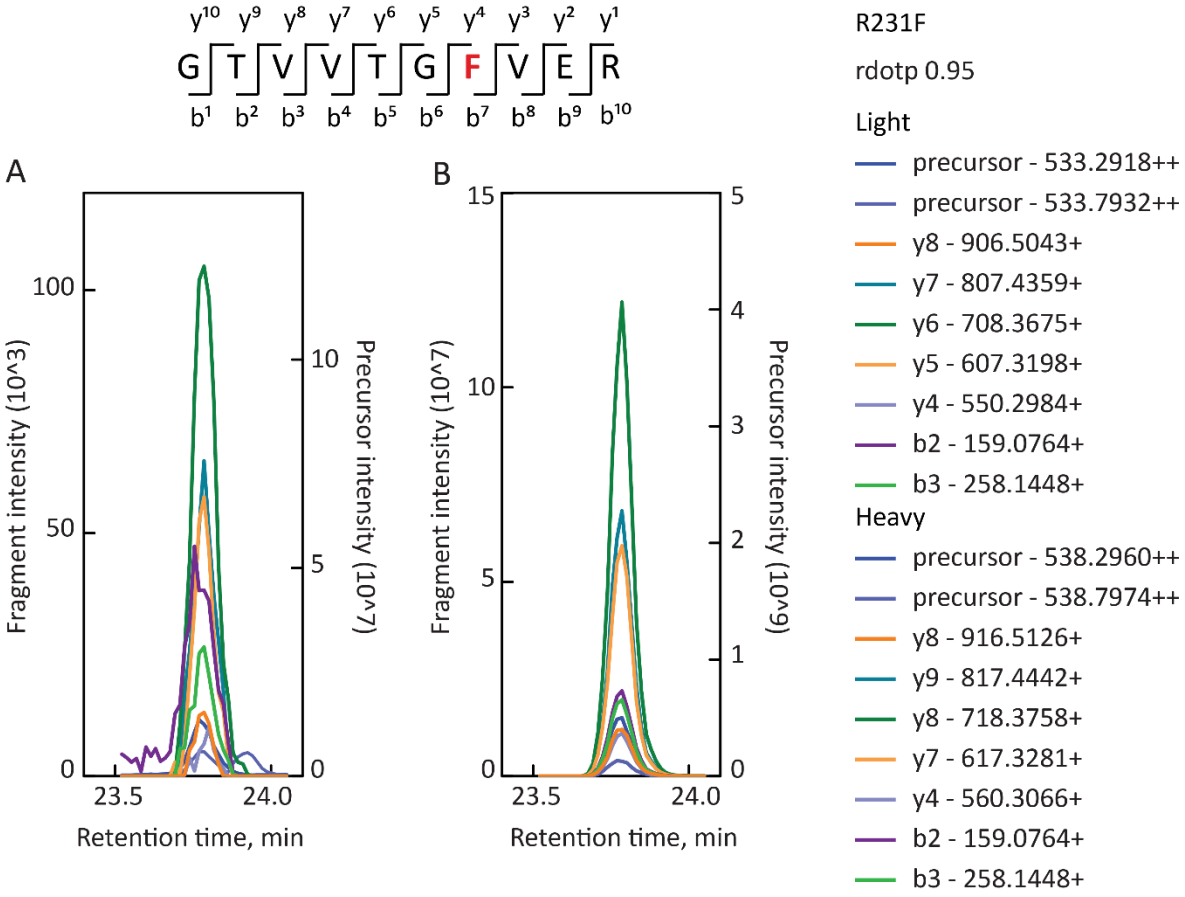

Figure 19. Identification of misincorporation-containing peptides by parallel reaction monitoring (PRM). Top panel, the sequence of the peptide and its fragmentation pattern. For peptides including non-cognate misincorporations, the validation is performed by PRM. In the example, the peak obtained for the light (A) and heavy (B) R231F peptide is shown. The mass of precursor and fragments ions are indicated, and the rodtp for the identification is reported**.**

2.3 Quantification of enriched error-containing peptides

2.3.1 Quantification of peptides by SRM analysis

When the identity of the enriched error-containing peptides is confirmed and quantified using their L/H ratios in Skyline, the concentrations of the correct peptides is used to calculate the error rate according to the equation:

$$Error\ frequency = \frac{pmol\ AQUA}{pmol\ EF-Tu} \times \frac{L}{H} \quad (1)$$

The purity and the labeling efficiency of the isotopic labeled AQUA peptide can alter the calculated L/H ratio. Therefore, prior to the quantification, we ran a blank sample with only the heavy peptide (Figure 20) to ensure that is free from any light counterpart contamination.

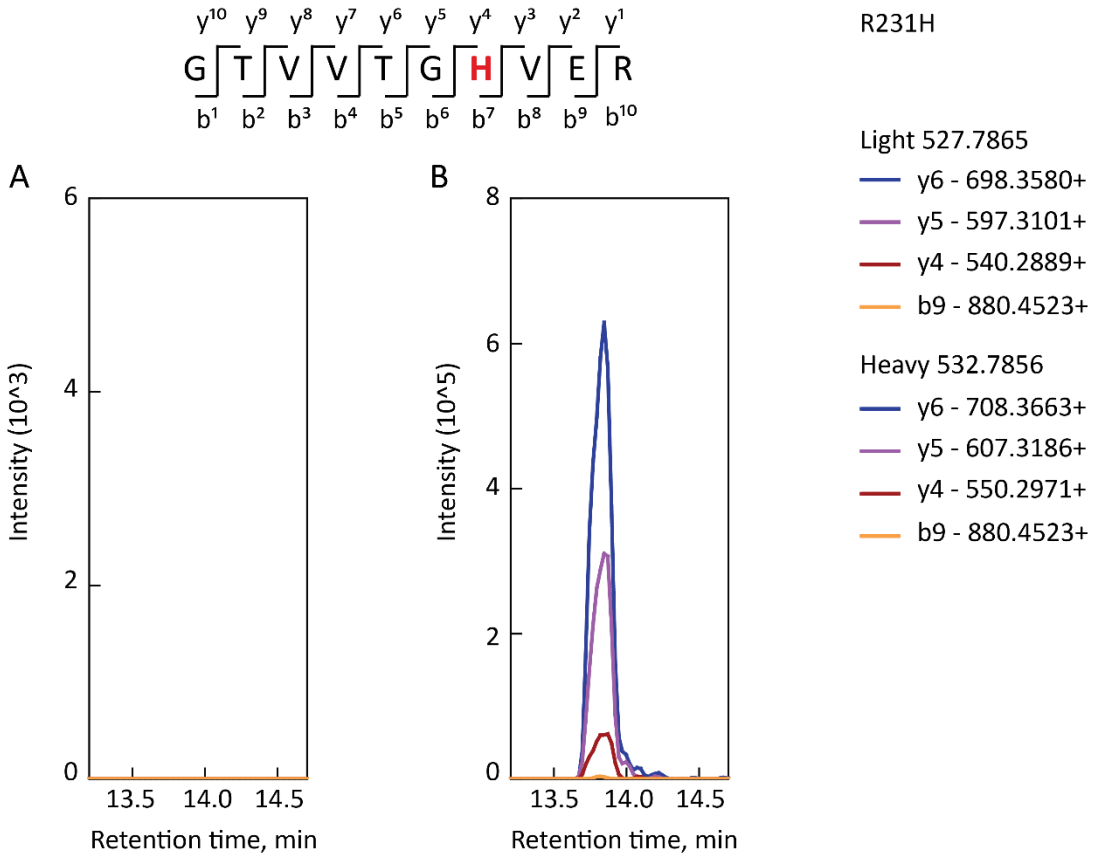

Figure 20. Assessment of AQUA peptides purity. To assess the purity of the purchased AQUA peptides and to exclude any light-peptide contaminations, each AQUA peptide (in the reported example, R231H peptide) is analysed by SRM and the signal for both light (A) and heavy (B) counterpart is recorded.

2.3.2 Pseudo-linear quantification assessment

To assess the linear dynamic range of our assay, the enriched peptide, which is already mixed with the identifier AQUA peptide used for the identification and quantification, is titrated with increasing concentrations of a second quantifier AQUA peptide which has identical amino acid sequence and contains a second isotope-labeled residues. These features allow us to distinguish the quantifier AQUA peptide from both the endogenous and the first identifier AQUA peptide and to assess the linearity of the quantification which extends over 7 orders of magnitude, with respect to the original dynamic range of the instrument, spanning 3 - 5 orders of magnitude (data provided by Dr. Ingo Wohlgemuth) (Figure 21).

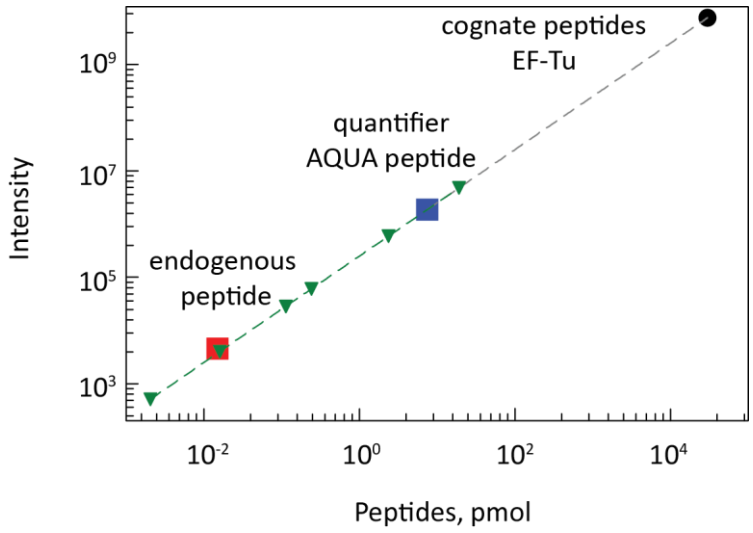

Figure 21. Pseudo-linear dynamic range of correct and erroneous peptides quantification. Quantification of correct peptides (black) is performed independently of the error-containing peptides (red). This allows to extend the dynamic range over 7 orders of magnitude. The linearity of the measurement is then assessed by titrating the enriched sample with a second quantifier AQUA peptide (blue). In the example is reported the titration for the peptide K249N (Appendix, Section B).

2.3.3 Post translational modifications and peptide degradation

Whereas the absolute quantification of a protein by mass spectrometry is based on the averaged quantification of 3 or more of its peptides, the quantification of misincorporations has to rely on the singular quantification of the respective unique peptide. Thus, their quantification must necessarily be as accurate as possible to truly reflect the error frequency and any potential sources of misquantification such as incomplete trypsination, peptide instability, inaccurate AQUA peptide concentrations or post-translational modifications must be excluded. To confirm the quality of the quantification by SRM, we generated EF-Tu mutants for each of the R → X and K → X amino acid misincorporations under analysis and analyzed the stoichiometry of the peptide carrying the mutation in relation to the four tryptic reference peptides used for EF-Tu quantification (Figure 22). A stoichiometry close to 1 for each of the peptides indicated that no modification or degradation occurs on the mutated peptides and, therefore, that the error frequency quantification can be considered reliable. Little variations for in the ratio obtained from peptide to peptide should be acceptable considering that i) the quantification of the AQUA peptides is perfomed by the supplier with an accuracy of ± 25 %; ii) peptides with different sequence might have different ionization properties and might not be equally represented during the mass spectrometric analysis.

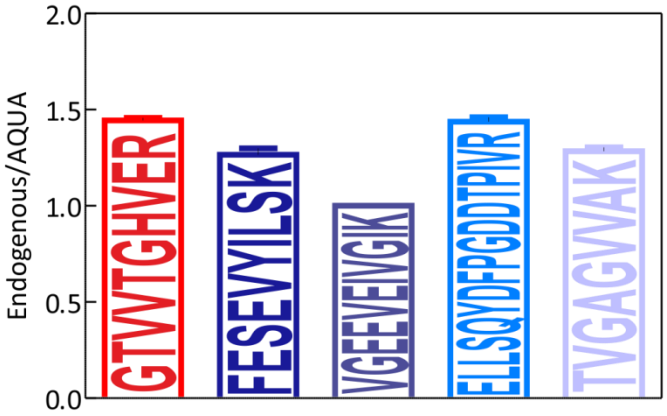

Figure 22. Validation of error quantification with EF-Tu mutants. The endogenous/AQUA peptides ratio for the error-containing peptide (R231H shown in red) and four tryptic reference peptides is calculated by SRM analysis. Error bars represent the standard deviation of 3 technical replicates.

2.4 The steady-state error level of misincorporations *in vivo*

As described in the introduction, the limitations in the available biophysical and mass spectrometric methods have precluded the systematic analysis of the *in-vivo* steady-state error frequencies. Albeit the strong analytical advantages of our method, the use of the internal standards and the targeted method used for the mass spectrometric analysis do not allow a complete analysis of all possible misinicorporations occurring in the protein. Therefore, to achieve a comprehensive and representative analysis of the cellular error frequency landscape we decided to split it into two steps and first focus on the quantification af all possible misincorporations at individual residues of EF-Tu, and subsequently on the error quantification for one particular amino acid susbstitution and monitor its frequency at various positions of the protein. In the last part we correlated the changes of the steady-state error frequencies in response to external stimuli as antibiotics, with the cellular stress response of the proteome. Moreover, we discovered that aminoglycosides induce highly abundant strings of errors that are likely to be relevant for their bactericidal effect.

2.4.1 Amino acid substitutions at selected positions in EF-Tu

To get the first insights into the relative abundance of different types of errors, we selected three positions in the EF-Tu sequence, R231, K249 and K314, for which we already identified individual error-containg peptides in previous data-dependent acquisition analysis (DDA). For each position, we were able to enrich and quantify all peptides resulting from an incorporation of a near-cognate aa-tRNA, displaying one mismatch in the codon-anticodon complex. To validate the significance of the results, we analysed errors in EF-Tu from three different *E. coli* sources: i) endogenous EF-Tu from MRE600

purified by conventional chromatography (Rodnina and Wintermeyer, 1995); ii) chromosomally-encoded EF-Tu from *E. coli* K12 strain, engineered to contain a His-tag and purified by affinity chromatography; iii) plasmid-encoded EF-Tu with a His-tag, overexpressed in BL21 (DE3) upon IPTG induction and purified by affinity chomatography.

The error frequencies span over 3 orders of magnitude depending on the position of the mismatch in the codon:anticodon helix. With an error frequency of 10^{-4}, the arginine-to-histidine substitution at position 231 (Figure 23, A), referred to as R231H, is much more abundant than any other substitution. Notably, different error rates are obtained for EF-Tu purified from different sources. The source of EF-Tu seems to play an important role in the fidelity of amino acids incorporation. In fact, independently of the position of mismatch and position in the protein sequence, the errors quantified in the overexpressed EF-Tu are always more abundant than the ones in the wild type protein (median values 5.8×10^{-6} and 1.5×10^{-6}, respectively), with a difference that reaches 1 order of magnitude for some substitutions at positions K314 (e.g., K314E with an average frequency of 1.7×10^{-5} for overexpressed and 1.3×10^{-6} for the wild type) and even 2 orders of magnitudes for some substitutions at position K249 (e.g., K249Q with an average frequency of 3.4×10^{-5} for overexpressed and 3.7×10^{-7} for the wild type) (Figure 23). Chromosomally-encoded EF-Tu with the His-tag has an error frequency which is intermediate between the overexpressed and the native EF-Tu obtained from the wild type stain. The results show that not only our separation and enrichment method achieves a very high sensitivity ($< 10^{-7}$), but also that the overall frequency of near-cognate misincorporation varies over orders of magnitude and is, in many cases, rather low and much less abundant than reported so far (Edelmann and Gallant, 1977; Ellis and Gallant, 1982; Kramer and Farabaugh, 2007; Loftfield and Vanderjagt, 1972; Parker et al., 1983). The SRM peaks for R231L (Figure 24, A), K249Q (Figure 24, B) and K314Q (Figure 24, C) are shown as example. For a more comprehensive list of the spectra refer to the Appendix (Section C).

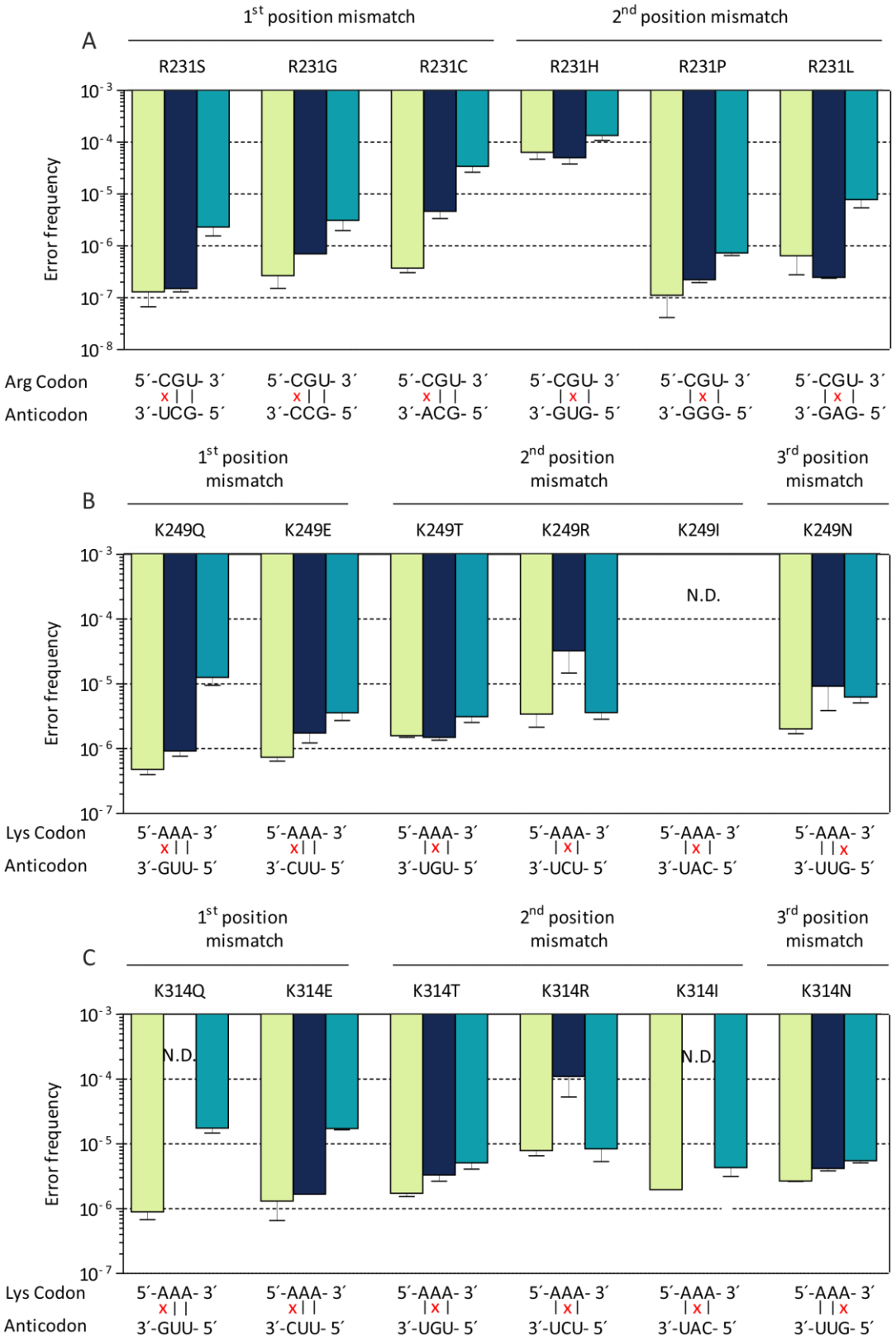

Figure 23. Error frequencies of near-cognate substitutions at three positions in EF-Tu. R231(A), K314 (B) and K249 (C). The results obtained from three types of EF-Tu are reported: wild type chromosomally-encoded EF-Tu from MRE600 (green), chromosomally-encoded EF-Tu with a His-tag isolated from K12 (blue), or plasmid-encoded overexpressed in BL21 (DE3) (teal). Error bars represent the standard deviation of 3 biological replicates.

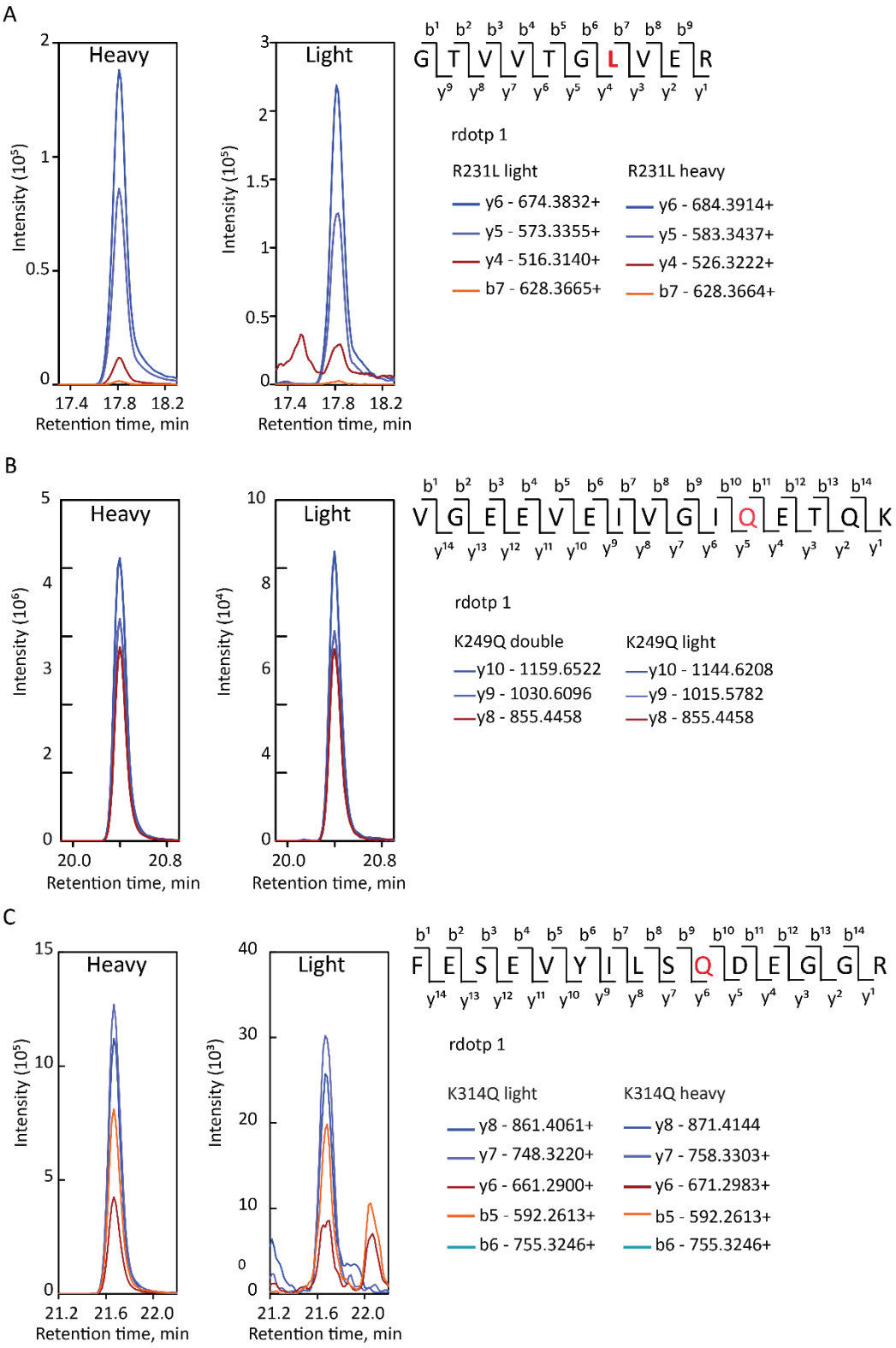

Figure 24. SRM peaks for enriched peptides. The peaks for the enriched peptides R231L (A), K249Q (B) and K314Q (C) are reported. Co-eluting light and heavy versions of the peptides R231L, K249 and K314Q are identified by SRM. The monitored transition for each peptides are reported and the sequence of the peptides, with their fragmentation pattern is shown. A rodtp value of 1 confirms the confidence of the identification.

2.4.2 Misincorporations involving non-cognate aa-tRNAs

Given the high sensitivity and dynamic range of the method and the success in the analysis of errors resulting from the near-cognate decoding, we expanded our analysis to misincorporations that arise at position R231 of EF-Tu when arginine is replaced as a results of all the possible non-cognate misincorporations i.e., tyrosine, glutamic acid, aspartic acid, alanine, threonine, tryptophan, glutamine, valine, isoleucine and phenylalanine. In some cases, non-cognate substitutions are very rare and thus below the detection limit of our method. Some errors could be only quantified in the overexpressed EF-Tu, which confirms that its translation is error prone (Figure 25). For the overexpressed EF-Tu, the error frequency resulting from non-cognate decoding is comparable to that of near-cognate ones ($10^{-5} – 10^{-7}$). It must be noted that for R231E, the observed frequency might arise not only from the amino acid substitution, but also from an oxidation of arginine to glutamic acid. The PRM traces for R231Q peptide are shown as example (Figure 26), for the other peptides refer to Appendix (Section D).

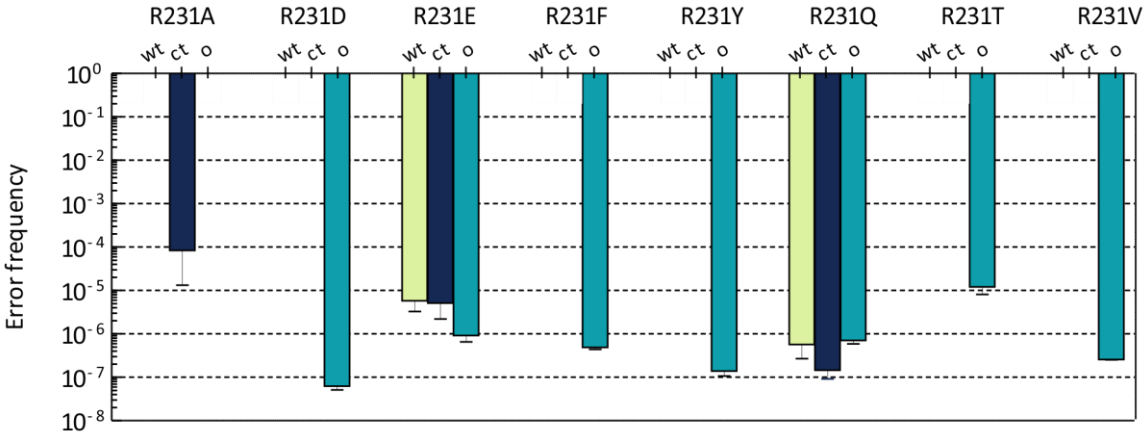

Figure 25. Non-cognate amino acid substitutions. Misincorporations involving non-cognate amino acids were investigated at position R231 of EF-Tu. The results obtained from three types of EF-Tu are reported: wild type chromosomally-encoded EF-Tu from MRE600 (green), chromosomally-encoded EF-Tu with a His-tag isolated from K12 (blue), or plasmid-encoded overexpressed in BL21 (DE3) (teal). Error bars represent the standard deviation of 3 biological replicates.

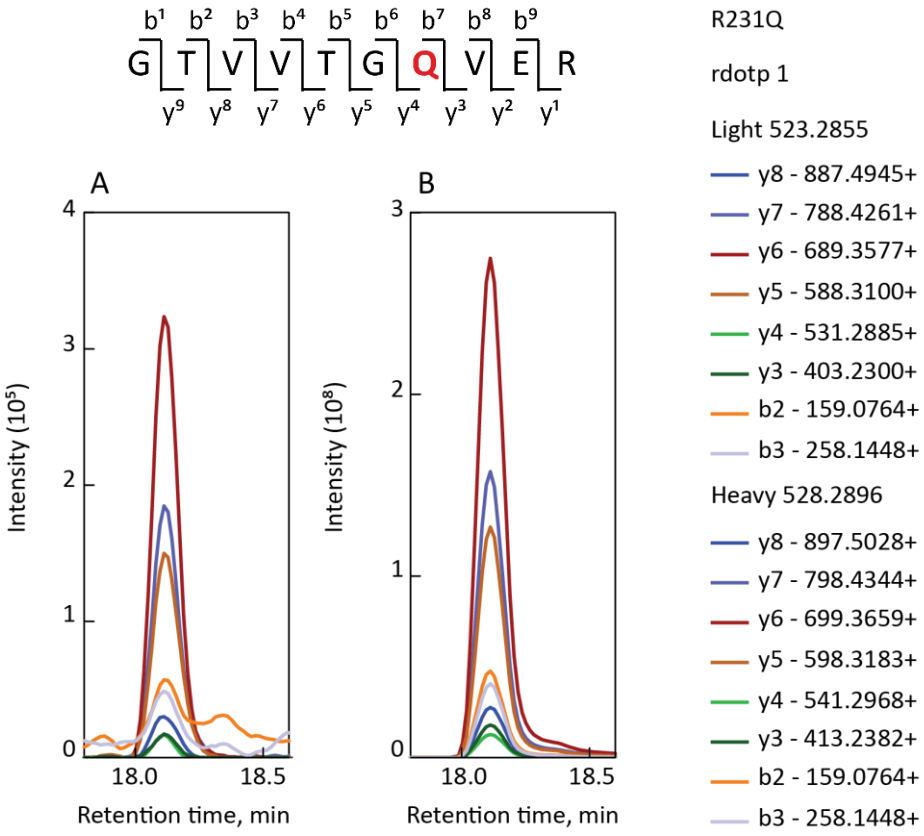

Figure 26. PRM analysis of enriched R213Q peptide. Top panel, the sequence of the target peptide. Co-eluting light (left) and heavy (B) versions of the R231Q peptide are detected. The list of fragment ions used for the analysis is indicated on the right. A rodtp value of 1 confirms the confidence of the detection.

2.4.3 Distribution of misincorporations over the EF-Tu sequence

The reported error frequencies reflect the intracellular steady-state error level, which is the result of the accumulation of errors through the different phases of protein synthesis and their removal by cellular quality control mechanisms. We next tested whether the observed errors arise during the translation phase. The comparison of the error frequencies in *E. coli* strains harboring hyperaccurate and error prone mutants of the ribosome (with mutations on S12 and S4 protein of the small subunit, respectively) and the parental wild type strain (Zaher and Green, 2010a) confirmes that R → H errors are introduced by the ribosome (Figure 27). When this type of substitution was investigated at three positions of EF-Tu i.e R59H, R231H and R234H, the error- prone strain, which bears less accurate ribosomes, showed an increased error rate with a frequency which is almost one order of magnitude higher than the wild type, whereas the hyperaccurate strain, whose ribosomes have a higher fidelity, shows a lower error frequency. The fact that the error rate is modulated by the ribosome suggests a ribosomal origin for their incorporation.

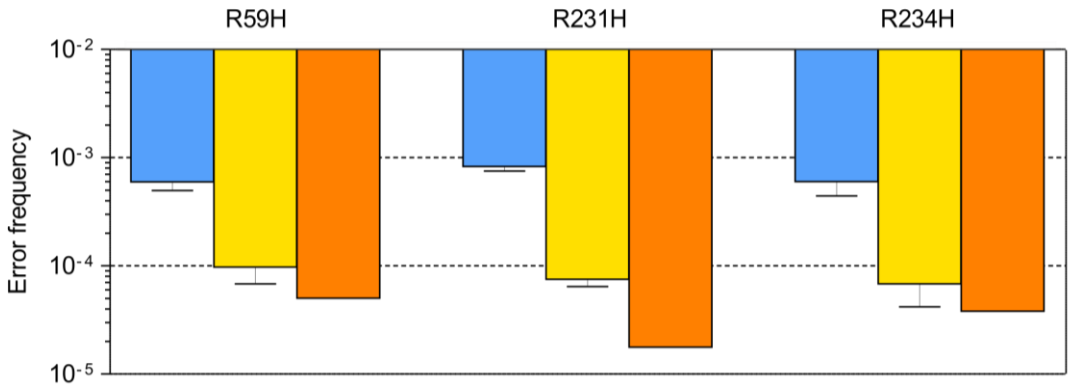

Figure 27. R to H misincorporation measured in error prone, hyperaccurate, and the parental wild type strains. Analysis of R to H substitutions in error prone (light blue), wild type (yellow) and hyperaccurate (orange). Error bars represent the standard deviation of 3 technical replicates.

Quantification of near-cognate amino acid substitutions at specific positions of EF-Tu allowed us to investigate the link between fidelity, type of substitution and codon:anticodon mismatch position. However, to understand how errors are distributed along the protein, we expanded our error profile analysis to the investigation of R → H substitutions at several positions of the protein sequence (Figure 28). Out of 21 arginine residues in the EF-Tu sequence, we selected 12 positions for the error quantification, while the others had to be excluded from the analysis due to an unsuitable peptide length or presence of reactive amino acids which preclude an accurate determination of the error (e.g., methionine). For the chosen type of replacement, the error frequency varied over 2 orders of magnitude (10^{-6} – 10^{-4}) depending on the position along the sequence. At most positions, arginine is coded by the CGT codon, except for two cases, i.e., R45H and R234H, where the codon is CGC. However, codon choice does not appear to correlate with a specific effect on the error rate.

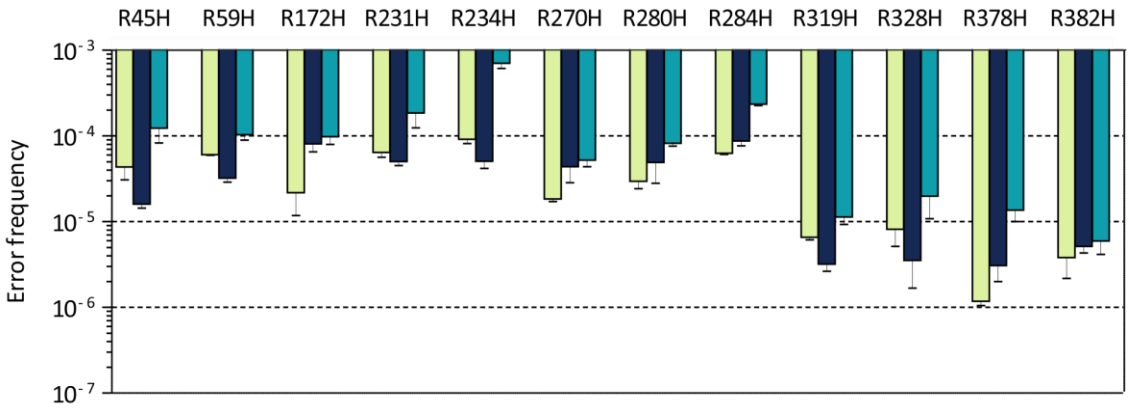

Figure 28. R to H misincorporations at several positions of EF-Tu sequence. Distributionof R to H substitutions reveals that the errors are unevenly distributed along the sequence independently from the type of EF-Tu used for the analysis: wild type chromosomally-encoded EF-Tu from MRE600 (green), chromosomally-encoded EF-Tu with a His-tag isolated from K12 (blue), or plasmid-encoded overexpressed in BL21 (DE3) (teal). Error bars represent the standard deviation of 3 biological replicates.

The analysis of the distribution of R to H substitutions reveals that at four positions of the domain III of EF-Tu, R319, R328, R378 and R382 (Van Noort et al., 1986), the error frequency is between 1 and 2 orders of magnitude lower than at other positions, regardless of the source of EF-Tu. As these positions are important for the binding of tRNA, being near the EF-Tu/tRNA interface (Yikilmaz et al., 2014) (Figure 29), we hypothesized that errors at these positions may be more rigorously controlled than elsewhere in the protein. This may be achieved by a more accurate translation to ensure a low steady-state error level, or by applying a more strict quality control to degrade with a higher frequency EF-Tu molecules that present these misincorporations and whose functionality might be impaired.
For the SRM traces and peptides validation for R → H errors, refer to Appendix (Section C).

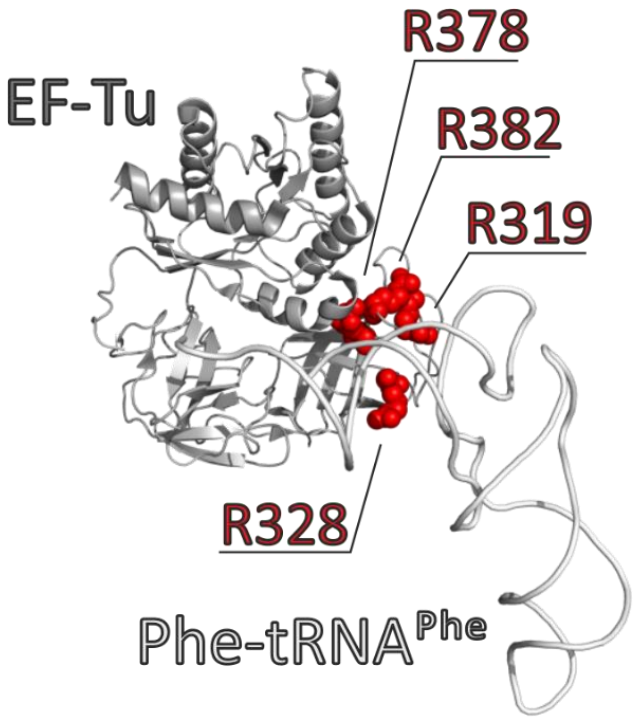

Figure 29. Position of low-abundance R → H substitution with respect to EF-Tu/tRNA interface. R319, R328, R378 and R382 residues are indicated in red and are localized near the interface between the protein (dark grey) and the Phe-tRNA^{Phe} (light grey) [PDB file 5AFI (Fischer et al., 2015)].

2.4.4 Contribution of quality control machinery to the steady-state error levels

To investigate whether the differences in error frequencies are caused by translation or by the subsequent quality control steps which may selectively degrade some of the peptides, we thought to decouple these processes by using an *in-vitro* translation system that lacks all potential proteases that might degrade misincorporation-containing EF-Tu. Because *in-vitro* translation kits can only provide a

limited amount of protein (~100 pmol/kit), which is far from the amount we use for the chromatographic enrichment protocol (4000 - 40000 pmol), we decided to digest the purified *in-vitro* translated EF-Tu after the SDS-PAGE run, and to directly determine the frequency of misincorporations without prior fractionation (Figure 30). Because misincorporation-containing peptides are not separated from their cognates, and only a modest amount of EF-Tu can be injected for LC-MS/MS analysis, only a limited number of positions can be investigated using this procedure, i.e., the ones which appear to have the highest error rates. For these errors, the frequencies are ~10^{-4} and are thus comparable with the ones determined *in vivo*. The similarity of error frequencies *in vivo* and *in vitro* suggests that misincorporations at some positions are indeed well tolerated and are not removed by the cellular quality control mechanisms. Unfortunately, the error frequencies for the positions located in domain III remain below the detection limit. Therefore, for these positions the contribution of the quality control machinery cannot be directly assessed, but the error frequency remains low even in a protease-free environment, suggesting that these errors are rare already at the translation level.

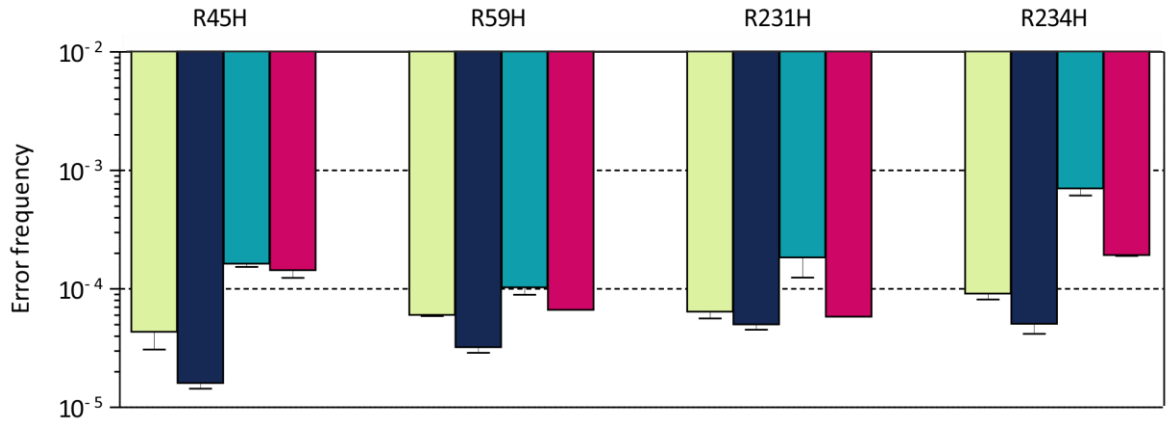

Figure 30. Error frequency in EF-Tu translated *in vitro*. The error frequency of R → H errors at positions R45, R59, R231 and R234 of EF-Tu wild type MRE600 (green), K12 chromosomal his-tag (blue), BL21 (DE3) overexpressed (teal) are compared with the EF-Tu synthesized *in vitro* (magenta). Error bars represent the standard deviation of 3 biological replicates.

To provide a more comprehensive explanation to the high accuracy detected for some positions, we tried a further approach where the activity of the quality control machinery is eliminated. We cloned the nucleic acid sequences of each one of our low-abundance erroneous peptides into a pSUMO vector and overexpressed it to generate a polypeptide product consisting of an N-terminal 11 kDa SUMO-tag followed by the EF-Tu FESEVYILSK cognate peptide necessary for the quantification and the EF-Tu peptide of interest (Figure 31).

Figure 31. Schematic view of the pSUMO constructs. The N-terminal SUMO-tag is followed by the cognate FESEVYILSK peptide used for the quantification. At the C terminus the specific peptide in which we want to test the misincorporation is added (in the reported example the tryptic peptide comprising the amino acid position R231).

The SUMO-tag approach is a common technique used in molecular biology to increase protein solubility, especially for overexpression procedures (Wang et al., 2010). Our hypothesis is that the SUMO-tag might prevent the aggregation and degradation of the EF-Tu peptide attached. A further advantage of this approach is that the errors can be studied out of the EF-Tu context, which circumvents a potential effect of the nascent chain on the peptidyl transferase activity of the ribosome (Ramu et al., 2011). When cloned in the SUMO-constructs, the peptides with the R to H substitutions at positions R378, R382 and R328 have up to 10-fold higher error frequency than the peptides obtained by overexpression of EF-Tu (Figure 32). Little or no difference is observed at position R319 and R280, respectively. Surprisingly, translation of pSUMO-R231H peptide is 10-times more accurate than overexpressed EF-Tu. While these results suggest that the quality control machinery may acts on some of the positions tested, in some cases the effects cannot be unambiguously assigned.

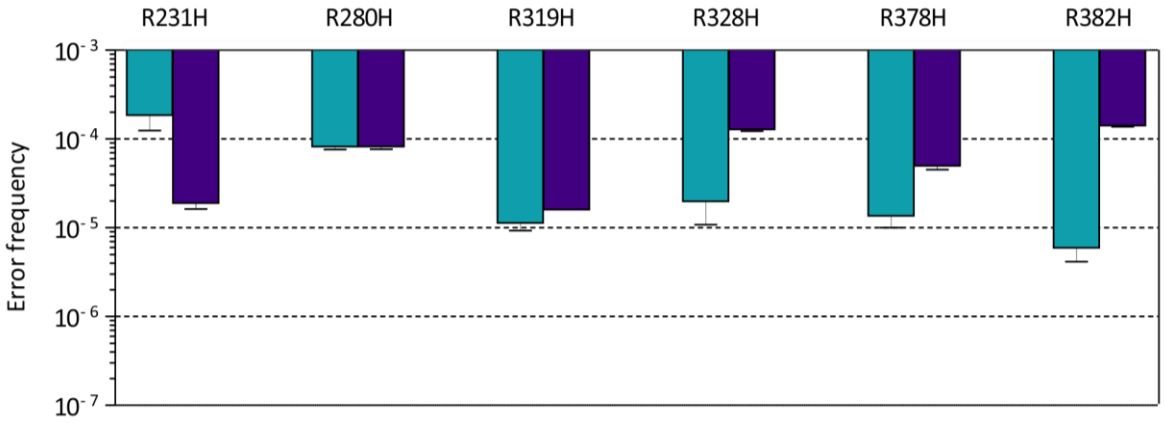

Figure 32. Misincorporation frequency in and out the EF-Tu context. R → H error frequency is compared in BL21 (DE3) overexpressed EF-Tu (teal) and in pSUMO construct (dark blue). Error bars represent the standard deviation of 3 biological replicates.

2.5 Aminoglycosides as a tool to study cellular response and misincorporations

Aminoglycosides are antibiotics that affect protein synthesis by inhibiting translation and decreasing the fidelity of ribosomes. We first examined the proteome response to aminoglycosides by systematically investigating the effect of antibiotics on the cellular stress response (Figure 33, A). We

treated *E. coli* MG1655 with increasing concentrations of aminoglycosides and monitored the expression of three proteins that were reported to be significantly induced by misfolded proteins and aminoglycoside treatment, i.e., heat shock response chaperones IbpA and IbpB, and their transcription sigma factor rpoH (Kohanski et al., 2008; Wu et al., 2015). EF-Tu was used as a reference and L10 was used to normalize the total amount of protein. For each protein, 2 - 3 peptides are selected and the corresponding isotope-labeled standards are spiked in the sample before SRM analysis. For the list of peptides used refer to Appendix (Section B). For each antibiotic, the proteome response is plotted together with the final optical cell density after 120 min treatment expressed as OD_{600}/ml. In each case, the growth inhibition due to the antibiotic activity increases with its concentration. Surprisingly, cells grow even at antibiotic concentrations which correspond to the minimal inhibitory concentration (MIC) (Gualerzi, 2013; McGaha and Champney, 2007). Conversely to what happens for the determination of MIC where the growth inhibition is assessed by an over-night incubation with the antibiotic, in our experiment the incubation is much shorter, i.e., 2 hrs, and might be not enough to allow the antibiotic to fully enter the cell and lead to its death. Hyg B and Spec, both known to affect tRNA translocation rather than decoding fidelity, show the lowest growth inhibition efficacy and no stress response stimulation. This is consistent with the notion that error induction is a primary cause of the bactericidal effects of aminoglycosides. For other antibiotics a clear induction of the stress response is observed and associated with a growth defect. Str and Tob show the strongest induction of IbpA and IbpB by approximately 20-fold. Surprisingly, the synthesis of the monitored proteins does not reflect the growth defects induced by the antibiotic but their concentration continues to raise even after the cell growth is blocked, indicating that it is not an arrest in the protein synthesis that interfers with the growth.

A

4,6-Disubstituted aminoglycosides

Kanamycin A
MIC 0.5-1 µg/ml
MW 582.58

Kanamycin B
MIC 2-4 µg/ml
MW 483.51

Gentamicin
MIC 1 µg/ml
MW 449.5
(Gentamycin C1A)

Tobramycin
MIC 2 µg/ml
MW 467.51

4,5-Disubstituted aminoglycosides

Neomycin B
MIC 1-2 µg/ml
MW 908.88

Paromomycin
MIC 1 µg/ml
MW 713.7

Ribostamycin
MIC 8 µg/ml
MW 454.47

4-Monosubstituted aminoglycosides

Neamine
MIC 64 µg/ml
MW 468.2

Apramycin
MIC 5 µg/ml
MW 509.58

5-Monosubstituted aminoglycosides

Hygromycin B
MIC 150 µg/ml
MW 527.52

Atypical aminoglycosides

Streptomycin
MIC 2-4 µg/ml
MW 728.69

Spectinomycin
MIC 7-15 µg/ml
MW 495.35

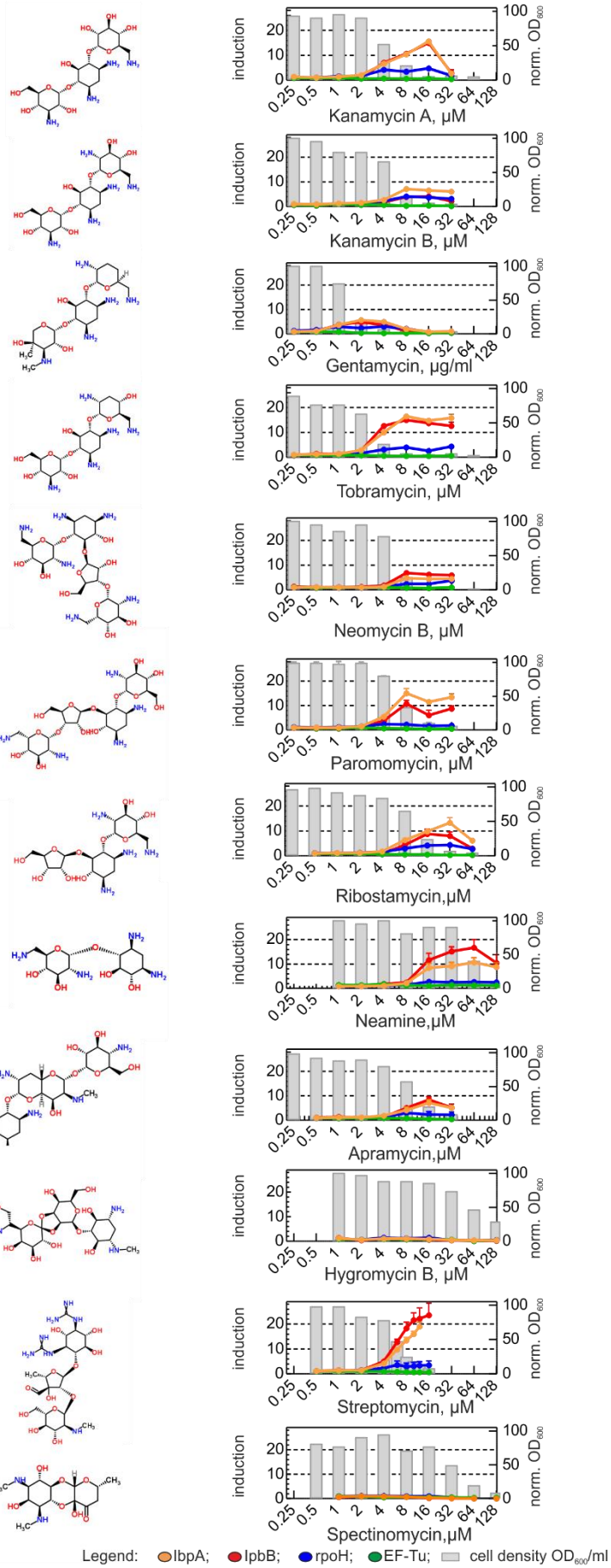

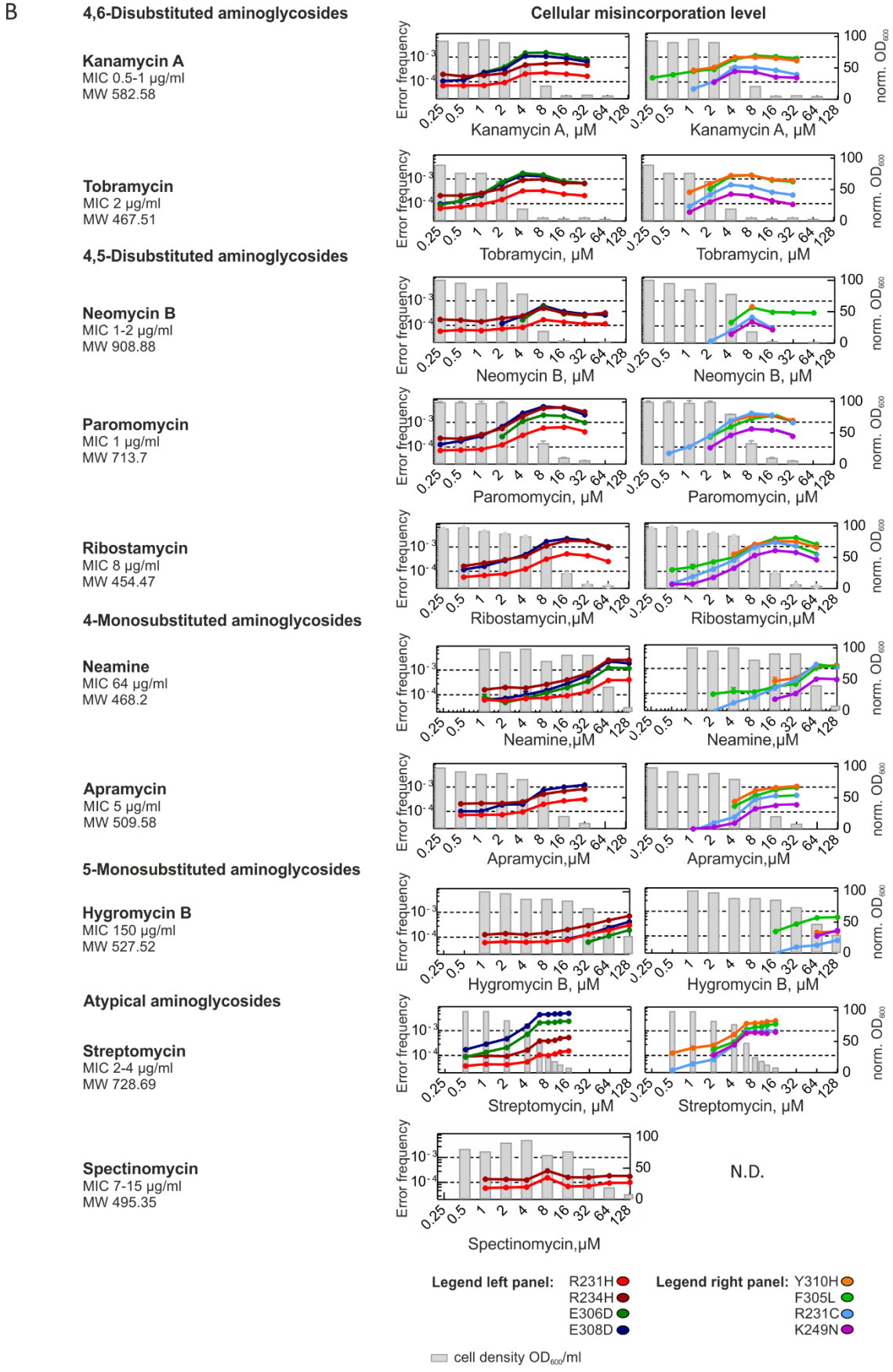

Figure 33. Effect of aminoglycosides on the cellular response and the steady-state error level. A) Changes in the concentrations of stress response proteins. B) Error frequency at increasing concentration of antibiotic. Error bars represent the standard deviation of 3 technical replicates.

In order to correlate the cellular stress response with the increase of error frequencies, we then selected seven EF-Tu peptides based on our data-dependent results and determined their error frequencies in the same samples used for the proteome change analysis (Figure 33, B). The high abundance of EF-Tu in the lysate allows for the direct quantification of the more abundant errors in the protein without requiring the enrichment procedure. The error frequencies induced by most aminoglycosides, exception made for Spc, depend on the antibiotics concentration and increase by one order of magnitude in the presence of the antibiotic from 10^{-4} to > 10^{-3}. However, the error induction does not affect all amino acid substitutions in the same way and some misincorporations appear to be more enhanced than others. With Str, which induces the highest levels of misincorporations, the frequency of E → D substitutions increases by almost 100-fold, whereas the induction of R → H errors is much milder, barely 10-fold. Surprisingly, in some cases the induction of errors does not reach a stable plateau but rather reaches a maximum to then decrease as if, during the antibiotic treatment, some cells are able to adapt to the increasing level of errors, e.g., by producing more chaperones, already observed to be induced during the treatment, or proteases. In this scenario, these cells would be able to remove error-containing proteins and this could explain the decreased error frequency observed. However, also with this kind of adaptive behavior, only a certain error threshold can be tolerated and a growth defect is observed. Overall, our analysis demostrates that the imprint of aminoglycosides on the proteome accuracy is far more complex than expected and that their phyisiological and biochemical effects depend on the type of aminoglycoside used.

To gain a deeper understanding of aminoglycosides effect, we compared the errors induced by different antibiotics. The error profile induced by the treatment appears to vary depending on the type of antibiotic used (Figure 34, A) and in some cases aminoglycosides which belong to the same class are found to induce the same set of errors. The most evident example comes from the comparison of the structurally related Tob and Kan A, both belonging to the class of 4,6-disubstituted aminoglycosides, for which the error induction pattern is almost identical (Figure 34, B). On the other hand, the comparison of the structurally different Hyg B and Str shows that their effects are different (Figure 34, C), suggesting that the stimulation of specific misincorporations can then be seen as a fingerprint specific for each type of antibiotic.

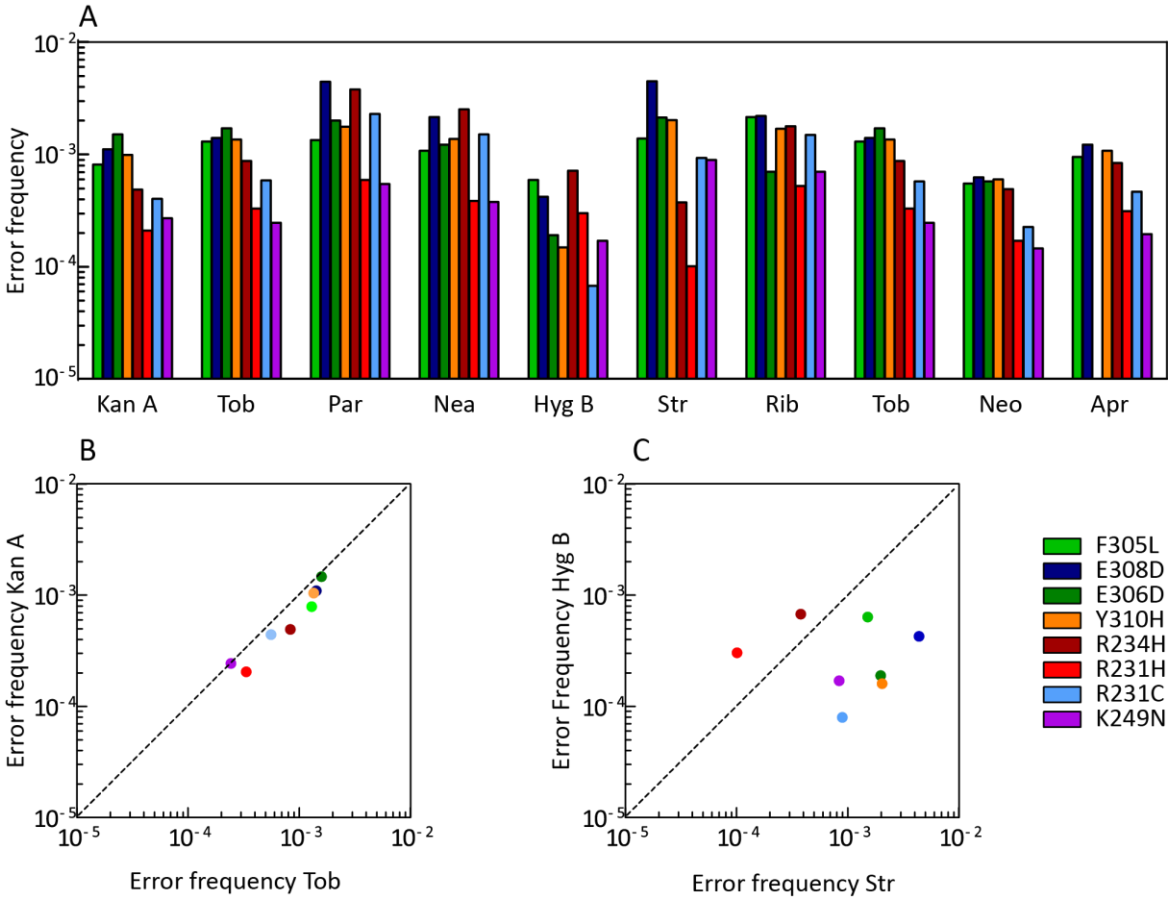

Figure 34. Comparison of error profiles induced by different aminoglycosides. Different errors are stimulated to a different extent depending on the type of aminoglycoside used (A). Structurally related aminoglycosides such as tobramycin and kanamycin A (B) share similar error pattern (Pearson r= 0.9535, P value= 0.0002) while structurally distant aminoglycosides such as streptomycin vs Hygromycin B show a weaker correlation (Pearson r= 0.01297, P value= 0.9757) (C).

2.5.1 The complex error signature of aminoglycosides

2.5.2 Validation of doubly-substituted peptides by PRM analysis

After we determined the conditions of maximal error induction for all aminoglycosides, we collected the data on the individual error profiles for a given antibiotic in a more comprehensive way by data-dependent acquisition (DDA) (data not shown, courtesy of Dr. Ingo Wohlgemuth). In order to maximize the dynamic range at the MS1 level and reduce the interference by other proteins, we decided to analyse affinity-purified endogenous EF-Tu. Surprisingly, some of the misincorporation-containing peptides identified by DDA contained more than one amino acid substitution. This is remarkable because the theoretical error frequencies calculated on the basis of the individual error frequencies are so low that peptides with more than one misincorporation are unlikely to be detected in the linear dynamic range of current mass spectrometers. In addition, the identification of amino acid substitutions in DDA is usually affected by false positive results, and the presence of multiple substitutions can further increase the false discovery rate. Thus, to exemplarily verify our identifications we monitored the induction of the double error E308D-Y310H (FESEVYILSK) by parallel

reaction monitoring (PRM) (Figure 35). To exclude a potential impact of the C-terminal His-tag used to enrich EF-Tu for data-dependent analysis, we analysed EF-Tu in the lysate of wild type strain MG1655. While the double error was not detectable in the absence of Str, the abundance of the E308-Y310H peptide increased with the increasing Str concentration. This allowed us to unambiguously identify the double misincorporation based on its ratio dot product of 0.99. In order to test whether double misincorporations are common in the aminoglycoside treated samples, we studied EF-Tu in MG1655 cells treated with three different aminoglycosides from different classes. Consistently, the double misincorporation was detected with high confidence (rdotp 0.98 - 1) after treatment with Apr, Tob and Par.

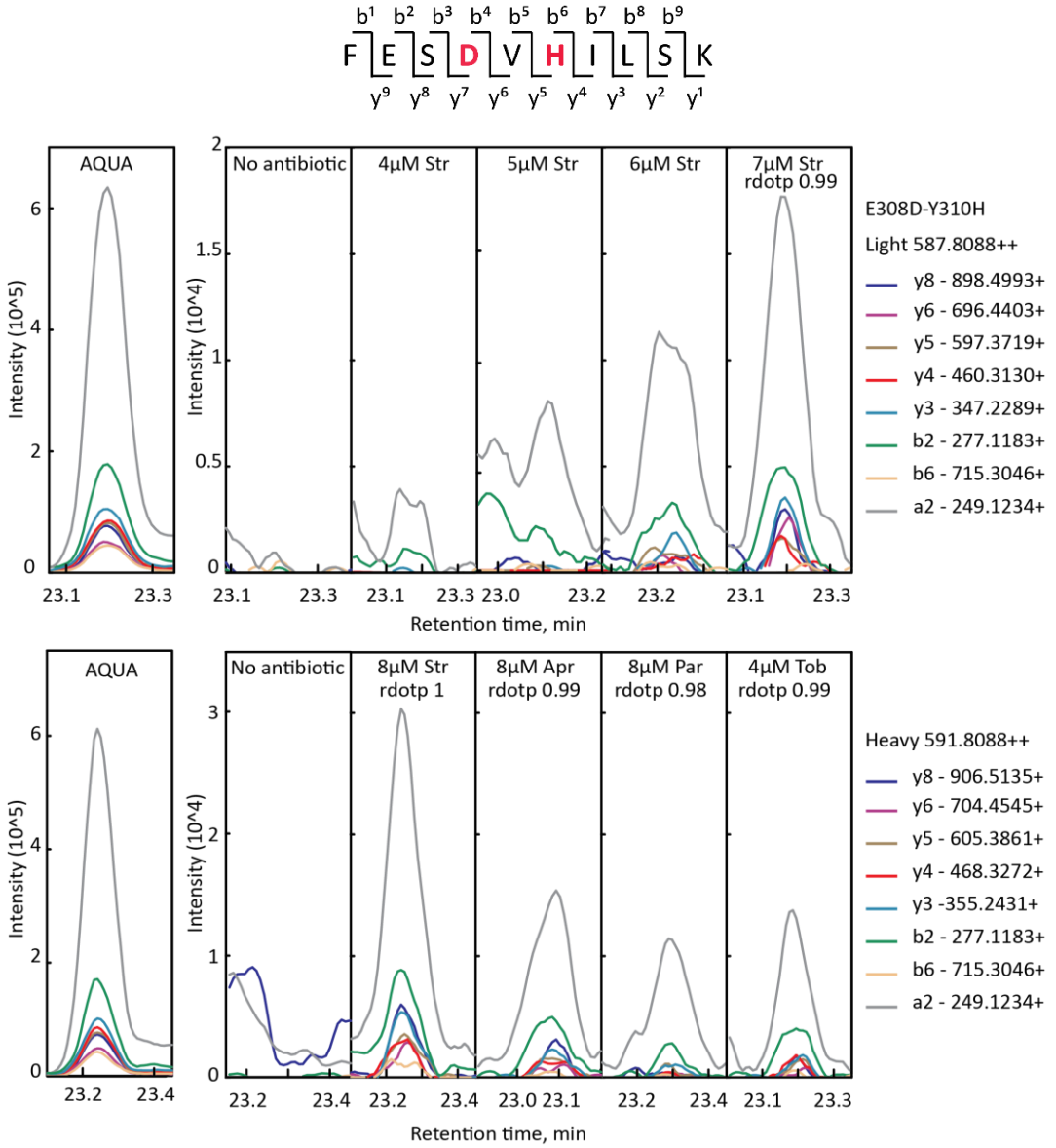

Figure 35. Verification of double-substituted peptide E308D-Y310H by PRM. The sequence of the peptide and its fragmentation patter. The presence of the peptide was determined in the wild type MG1655 cells treated with increasing concentration of Str (upper panel) or various amingoglycosides (bottom panel). For each reported condition, the same amount of sample is injected into the instrument. The elution profile of the isotope-labeled reference peptide (AQUA) is shown on the left. The observed precursors for both heavy and light peptides are indicated.

Once we assessed the presence of doubly-substituted peptides by PRM, we systematically analysed and quantified their pattern. We selected the model peptide FESEVYILSK for analysis because it has an optimal peptide stability, chromatographic behaviour, amino acid composition and ionization properties. Chromosomally-encoded His-tag EF-Tu was purified from cells grown with and without Str, and the error-containing peptides were enriched and ultimately identified and quantified by SRM (Figure 36). Double errors could not be found in the cells grown without Str suggesting that they are rare events. The signal for the respective peptide is under the detection limit of the assay and was calculated by peak integration on a high noise background. Thus, the reported values represent the upper limit of the error frequency rather then a defined error frequency. Incorporation of double errors become more frequent after Str treatment and their frequency, about 10^{-5}, is comparable with the rate of the respective single errors (Figure 37). In addition, when we extended our measurements to other positions of the peptide we managed to quantify all the double errors included in the analysis (Figure 38). This suggests that the incorporation of multiple errors is not restricted to specific positions but is rather a generalized phenomenon. The high abundance of the double errors prompted us to also test a peptide that contained three misincorporations (E306D-E308D-Y310H). As expected, the peptide could not be detected in the untreated sample but could be easily quantified in the streptomycin-treated sample.

Once the mono-substituted peptides are quantified, the estimated frequency of the independent incorporation of double and triple erros can be calculated in the following way:

$$P(E_{multiple}) = P(E_{first}) \times P(E_{second}) \times P(E_{third}) \quad (2)$$

Where $E_{multiple}$ is the frequency of conseutive errors and E_{first}, E_{second} and E_{third} the frequencies of the first, second and third error, respectively. Comparison between the error frequency obtained by SRM analysis and the predicted error frequencies, assuming that each misincorporation event is independent, revealed that the double errors are remarkably more abundant (10 - 1000-fold) than expected. This strikingly higher abundance can be explained as if double and triple errors do not occur independently; rather, their incorporation is synergistic.

Several mechanism for the synergistic appearance of errors exist. The first misreading event and the presence of errors in the protein nascent chain might alter the A site and induce further errors. Alternatively, the codon-anticodon mismatch in the P site, which results from the miscoding event, could distort or displace the peptidyl-tRNA in the P site rendering the ribosomal A more prone to accept incorrect tRNAs. A similar mechanism was proposed as a mechanism of post-transfer editing on the ribosome (Zaher and Green, 2009). Eventually, the propagation of misincorporation could be

due to stable binding of the aminoglycoside to the ribosome which, persisting for several rounds of elongation, would perpetrate its fidelity-reducing effect.

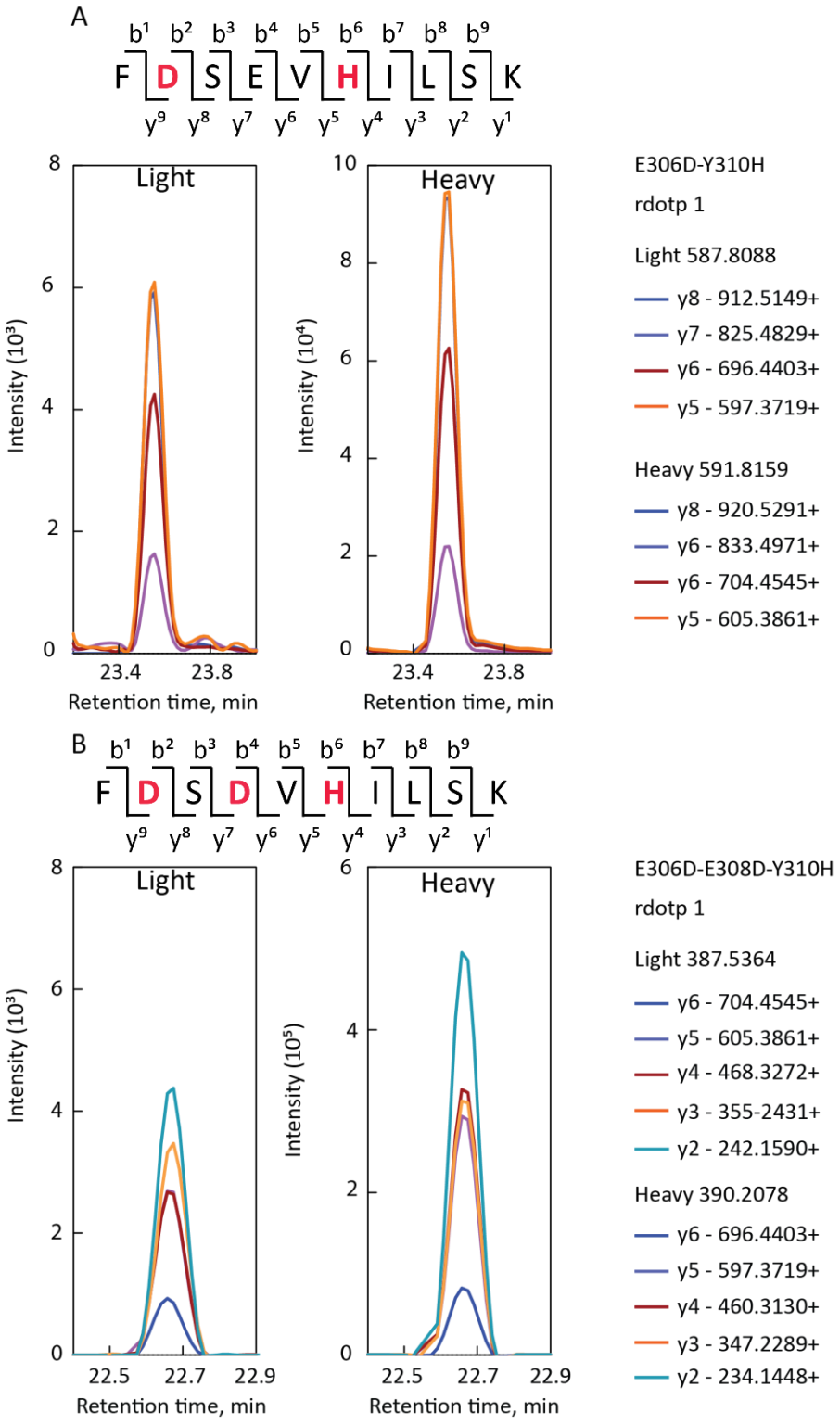

Figure 36. SRM quantification of double and triple errors. The peaks for the enriched peptides E306D-Y310H (A) and E306D-E308D-Y310H (B) are reported. The SRM signals for both light and heavy-labeled are reported. The monitored transition are indicated the fragmentation pattern is shown. A rodtp value of 1 confirms the confidence of the identification.

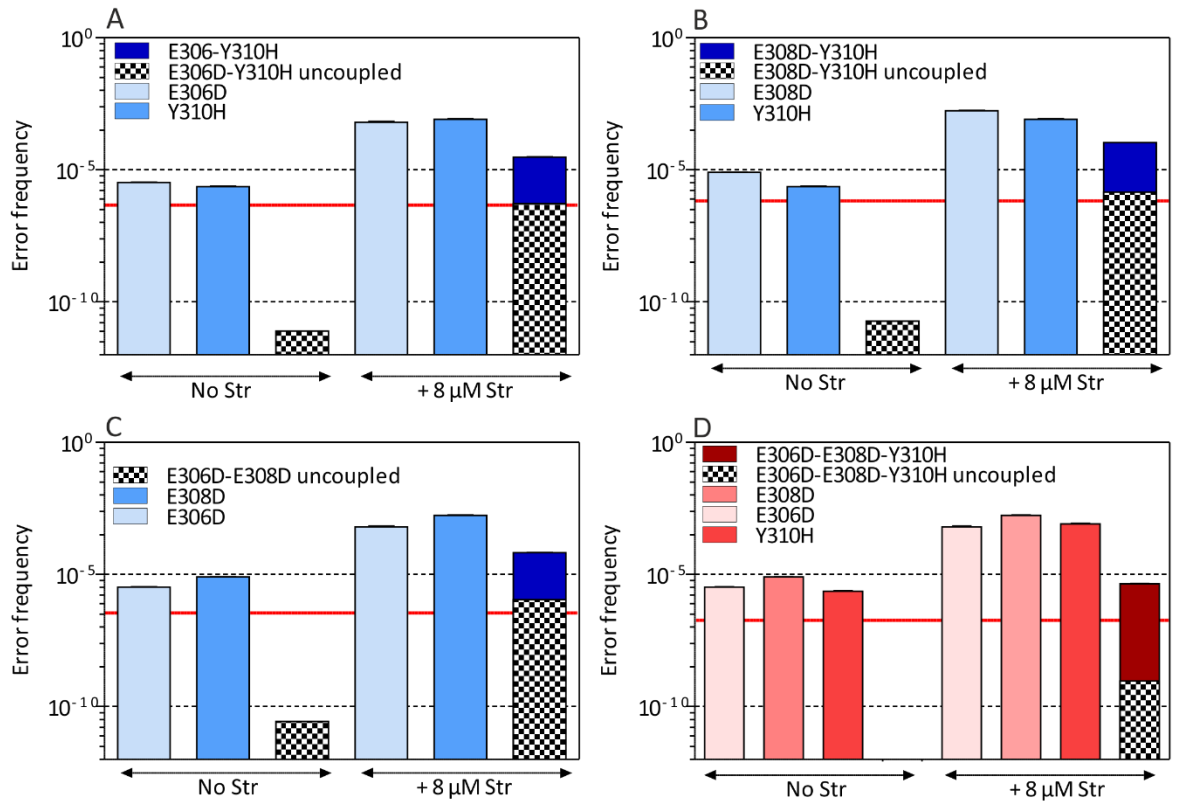

Figure 37. Example of quantification of double and triple errors. SRM analysis of error frequencies for E306D-Y310H (A), E308D-Y310H (B), E306D-E308D (C) and triple error E306D-E308D-Y310H (D). Each plot shows the frequency of the single, double, and where indicated triple errors for the purified chromosomally-encoded EF-Tu with a His-tag from K12 cells grown with and without Str. The theoretical error frequency of independent double and triple errors is indicated in the chequered bars. The red line represents the detection limit of the measurement. Error bars represent the standard deviation of 3 technical replicates.

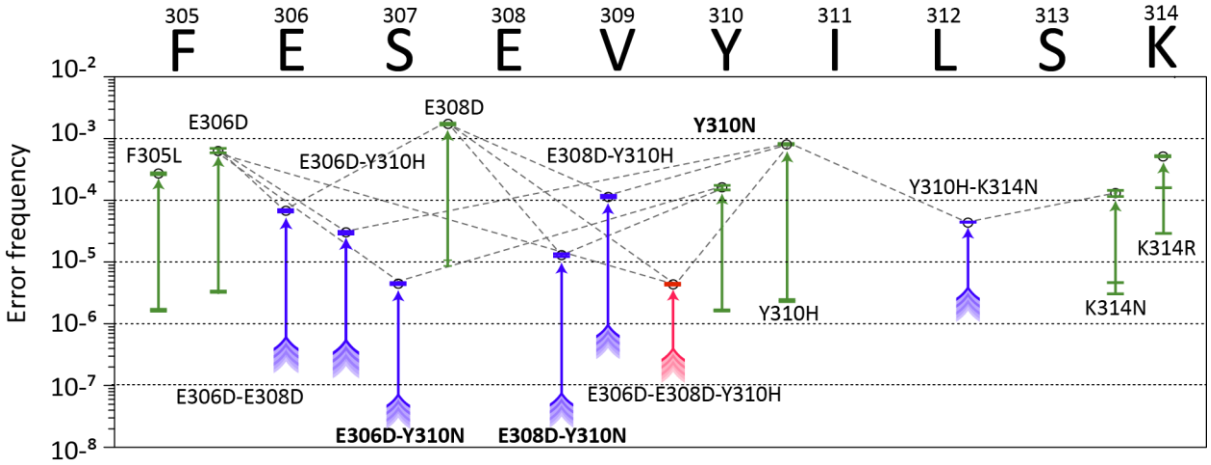

Figure 38. Abundance of the single, double and triple errors in one peptide. Frequency of single (green), double (blue) and triple (red) misincorporations. The sequence of the peptide togheter with the residue positions is indicated on top. Arrows indicate the increase in the error frequency in the absence (arrow´s tail) and in the presence of 8 µM streptomycin (arrow´s head). In some cases, the error frequency for the wild type strain is below the detection limit, and the reported value is an estimation of the upper limit of the peptide´s concentration ( ). JPT peptides are indicated in bold. Dashed lines connect single-substituted peptides with their respective double-substituted peptide. Error bars represent the standard deviation of 3 technical replicates.

To test whether misincorporations in the nascent chain, mismatches in the codon-anticodon interaction or the presence of the aminoglycoside lead to double misincorporations, we tested error incorporations in an aminoglycoside-independent system. We purified wildtype EF-Tu from the *rpsD* strain containing error-prone ribosomes. These ribosomes harbour a mutation in the ribosomal protein S4 which affects the initial selection phase of decoding reducing the stability of the codon:anticodon complex with a near-cognate aa-tRNA and accelerating the subsequent step of GTPase activation (Zaher and Green, 2010a). For comparison, we prepared EF-Tu from the respective wild type strain in the presence of Str (Figure 39). Str was titrated to match the level of single misincorporations found in EF-Tu from the error-prone strain, which was achieved at 4 µM Str. We selected three double misincorporations for the enrichment, E306-Y310H, E308D-Y310H and E306D-E308D. The experimentally determined rate for double-substituted peptides in the wild type strain shows that, in all cases, the calculated frequency ranges between 10^{-5} - 10^{-4} and is about 2 orders of magnitude higher than the theoretically estimated value, suggesting the existence of a mechanism that promotes the incorporation of the second error. In the error-prone strain, the error frequency of double-substituted peptides remains below the detection limit of the instrument and, as for the wild type strain in the previous experiment, their determination is rather an estimation of the upper limit of their concentration based solely on the background noise detected, rather than an accurately measured value.

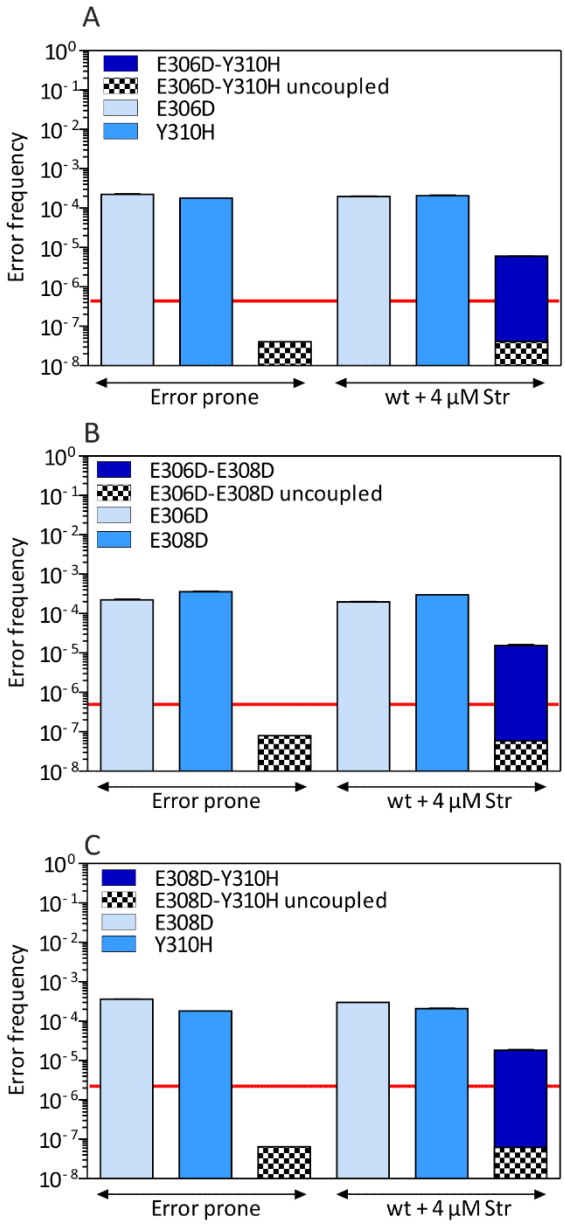

Figure 39. Quantification of single and double errors. Incorporation of E306D, E308D, and Y310H is measured in wild type in the presence of 4 µM Str in error prone strains. In each plot the error rate for the single error is shown (light blue and brilliant blue). The incorporation of their respective double error is monitored and indicated as follows: E306D-E308D (A), E360D-Y310H (B) and E308D-Y310H (C). Estimated (chequered) and calculated (dark blue solid) error frequencies. Detection limit is indicated by a red line. Error bars represent the standard deviation of 3 technical replicates.

3. DISCUSSION

3.1 Method development to study rare translation errors

Incorrect mRNA decoding is a rare event, occuring with an estimated frequency of 1 error every 10000-100000 decoded codons (Table 1 and Table 3) and misincorporation-containing peptides are present in the cell in an extremely low abundance with respect to the correct ones. For this reason, their detection is challenging and their comprehensive investigation requires the development of a high-sensitivity detection method. All the mass spectrometric data obtained so far on amino-acid misincorporations rely on data acquired by DDA analysis. Although DDA can provide a wider set of results than targeted mass spectrometric approaches, it is limited not only by the intrinsic lower sensitivity (Michalski et al., 2011; Sandhu et al., 2008) but also by the necessity to interpret the data by spectral matching algorithms (Cox et al., 2011; Eng et al., 1994; Perkins et al., 1999; Shilov et al., 2007; Zhang, 2009), which might not be optimal for the analysis of isobaric amino acid misincorporations (see Introduction).

Analogous challenges can be found in the protein biomarker discovery, where the low-abundance of the target protein and the high complexity of the sample i.e., body fluids, make the identification of the biomarkers extremely difficult (Surinova et al., 2011). In this field, targeted mass spectrometry finds large application and SRM is often applied due its high selectivity and reproducibility. However, because the dynamic range required for the detection often exceeds the dynamic range of currents mass detectors, SRM is often combined with separation techniques, e.g., immunodepletion, size-exclusion chromatography (Liao et al., 2004), gel electrophoresis (Ang and Nice, 2010), aimed to reduce the complexity of the sample and eliminate high-abundance proteins that would otherwise hinder the efficient identification of the low-abundance biomarkers. The combination of these techniques with the use of heavy-labeled standards (AQUA peptides) have led to further advance of mass-spectroscopy in this field (Shi et al., 2012).

Given the robustness, sensitivity and reproducibility of biomarker-oriented approaches for the quantification of proteins, we have adapted its strategy of target separation and mass spectrometry to develop an assay for the systematic investigation of peptides which contain amino-acid substitutions. As biomarker quantification approaches, our assay relies on the enrichment of target peptides by separating the error-containing peptides from the more abundant correct ones. The peptides enrichment and reduction of the sample complexity allows to load more target peptides on the LC-MS/MS system leading to higher signal intensities. Moreover, endogenous and AQUA peptides co-elute during several subsequent chromatographic rounds of separation and co-fragment, yielding a high confidence assignment. Thus, together with the validation of our results by high resolution mass spectrometry, the identification of peptides is based on more – and partially orthogonal – evidence

than the traditional DDA data. In addition, the use of AQUA peptides as internal standards solves quantification problems of data-dependent approaches which are related to the performance variations of ESI stability or to the different ionization properties of cognate and misincorporation-containing peptides.

The disadvantages of the method are the laborious peptide enrichments, the necessity for assay optimization for each peptide to enrich, and the high costs of commercial peptide synthesis which limit the number of peptides that can be analyzed and preclude a broad or even proteome-wide analysis. These problems are especially aggravated when peptides of interest cannot be selected on the basis of previous experiments or published data. In such cases, after AQUA synthesis and enrichment procedures, the target peptides may turn out to have poor ionization properties, being undetectable in both their light and heavy forms or simply not informative, being the light counterpart too rare to be detected.

Our assay provides an unprecedented flexibility in the choice of misincorporations to study because it allows to study most of the miscoding events which are imprinted in the amino acid sequence of the protein of choice, independently from reporter systems and types of substitution, as demonstrated for the quantification of several consecutive miscoding events (Figure 38). In this scenario proteomics can be considered as single molecule technique in which the translation process carried out by individual ribosomes can be studied, although this single molecule character is clearly only conserved within the individual tryptic peptide. In addition, the present approach allows to quantify different miscoding and misincorporation events in parallel or even correlate miscoding events with the cellular response, e.g., changes in the expression of proteins involved in the stress response. One other important advantage of the mass spectrometry-based assay is that, the sensitivity is significantly increased with respect to the other approaches and that the noise is extremely low and can be distinguished from the signals of the target peptides, even when the latter are present at very low concentrations (10^{-7}). In contrast, in fluorescence-based assays which are commonly used to study amino acid substitutions (Kramer and Farabaugh, 2007; Kramer et al., 2010), there is often a background fluorescence (10^{-4}) either due to the experimental setup or to a residual fluorescence of the mutated reporter proteins which cannot be avoided and which inevitably limits the dynamic range of the method. The pseudo-linear quantification of the biomarker approach presented here has, at least theoretically, no limit in the dynamic range, because, more starting material could be used for the analysis and the peptides could be separated by several orthogonal chromatographic steps for a better enrichment. However, the high sample losses which occurs at individual chromatographic dimensions and the limited numbers of truly orthogonal chromatographic separation strategies hamper the quantification of misincorporations with error frequencies < 10^{-8},

although this limit strongly depends on the individual peptide sequences. Finally, peptides with almost identical physicochemical properties to the cognate ones could be difficult to separate by any chromatographic step and might require additional rounds of chromatography (Figure 16) or even remain undetected, independently of their frequency.

3.2 Misincorporations are rare and occur less frequently than expected

The systematic investigation of misincorporations has revealed that on average errors of translation can be much less frequent than currently described in literature. We could quantify errors occurring with a frequency as low as 10^{-7}, reaching a level of sensitivity which is not achievable by other methods. The calculated median for the error frequency of near-cognate substitutions at three positions of EF-Tu (Figure 23) was 10^{-6}. Thus, the expected higher error frequency introduced by translation is not reflected in the cellular steady state error level, and even R → H substitutions, the most abundant type of misincorporation (Manickam et al., 2014; Zhang et al., 2013), occur with a frequency between 10^{-6} - 10^{-4} in wild type EF-Tu (Figure 28), a result which matches the error frequency estimated for transcription (Table 2). Most likely, this discrepancy between the different estimations of error frequencies is the consequence of a lower sensitivity of the methods employed so far, which enabled the identification of only the most abundant errors, leading to an incomplete and biased picture of the translational error frequency landscape. This is supported by the results we obtained from the analysis of error incorporation during aminoglycosides titration. After the addition of the antibiotic to the growing cells, the studied misincorporations approach a range between 10^{-5} - 10^{-3} (Figure 33, B) which matches the range of errors reported for cells under optimal growth conditions (Table 1) and supports the scenario in which the error frequency of translation is lower than previously estimated, but its accurate detection was hampered by the limited sensitivity of the methods used.

3.3 Error rate depends on the protein source

Strikingly, regardless of the type of amino acid substitution, codon involved, mismatch and amino acid position, overexpressed EF-Tu always displayed a higher frequency of error incorporation. In contrast, wild type and chromosomally-encoded His-tag proteins showed a comparable error frequency confirming that the His-tag we inserted in the chromosome is well tolerated (Figure . The reduced accuracy of translation during recombinant-protein production is a known phenomenon (Scorer et al., 1991) and different explanations might be envisioned. The presence of the plasmid already constitutes a significant metabolic burden for the organism which, to maintain it, is usually grown in the presence of an antibiotic and faces the energy costs of the synthesis of the protein conferring antibiotic resistence. Such stress phenotypically manifests as a slower growth rate (Bentley

et al., 1990) and might originate from a combination of nutritional imbalance and competition for the expression machinery, which in turn could increase the frequency of random translational errors. The type of plasmid used for the overexpression may also play a role. The pET vectors we used for the overexpression are commonly utilized in molecular biology for the expression of recombinant proteins. However, their use is also associated with the cellular proteome imbalance caused by the very high amount of mRNA that accumulates in the cells and the resulting very high yield of the encoded overexpressed protein, which can reach as high 40 - 50 % of the total cell protein content. The presence of the pET plasmid alone (i.e without the cloned gene to be overexpressed) can be toxic in *E. coli* in the presence of IPTG (Miroux and Walker, 1996). IPTG itself has been demonstrated to be harmful for *E. coli* BL21 (DE3), the host strain which is often employed for protein overexpression (Dvorak et al., 2015). In addition, pET vectors are transcribed by T7 RNA polymerase. Although this polymerase has an estimated error frequency comparable to the bacterial one (10^{-4} and 10^{-4} - $10^{-5,}$ respectively (Huang et al., 2000)), it cannot be excluded that an increased error rate generated by the overexpression stress affects T7 polymerase fidelity leading to an increase of transcriptional errors which are then manifested in translation. A plausible alternative explanation includes a depletion of the aa-tRNA pools caused by the high demand of substrates for the protein synthesis.

Protein overexpression is known to induce the cellular stress response and the expression of proteases and chaperones as well as many proteins involved in the SOS regulatory system for nucleic acid damage repair (Gill et al., 2000). A limited capacity of the chaperone system to mediate the proper folding as the protein copy number dramatically increases could also induce the accumulation of more erroneous proteins.

In our setup, another source of error incorporation might stem from the type of antibiotic used to select the plasmid-containing cells (i.e., Kan), which is long known to induce miscoding (Davies et al., 1965b; Tanaka et al., 1967) and which could contribute to an overall decrease of the ribosomal fidelity, as observed during Kan treatment (Figure 33, B). In pET vector-containing cells, the Kan resistance is conferred by the expression of aminoglycoside phosphotransferase which modifies and inactivates the antibiotic after it enters the cell (Wright, 1999), so that a residual miscoding activity of Kan cannot be excluded.

Our results revealed that overexpressed EF-Tu is also more prone to non-cognate amino acid substitutions (Figure 25), which are for the first time quantified *in vivo*. Surprisingly, the frequency of errors due to non-cognate decoding ranges between 10^{-7} - 10^{-4}, and is similar to that of the near-cognate one. This may be a result of the strongly depleted pool of cognate tRNAs caused by the overexpression. However, not every possible non-cognate substitution are frequent enough to be quantified, suggesting that overall they remain rare events even during overexpression.

3.4 Error variation and distribution

Among the missense errors studied here, R → H substitutions are the most frequent types of errors. This results can be explained by the nature of the codon-anticodon mismatch that generates this replacement, the G-U mismatch that is reported to increase the error frequency (Westhof et al., 2014).

Whereas in literature it is reported that different error frequencies are associated to the position of the mismatch at the codon:anticodon duplex, (Gromadski et al., 2006; Manickam et al., 2014; Zhang et al., 2016), our results reveal that no correlation between the error frequency of amino acid incorporation and the mismatch can be observed. When we compare our results to *in-vitro* data, the difference might be explained by the activity of the cellular quality control activity *in vivo* which is obviously not present in the *in-vitro* experiment and which might acts on erroneous peptides equalizing them. The difference to the *in-vivo* results can be also easily explained. The difference with the error frequency levels reported by Farabaugh and collegues (Kramer and Farabaugh, 2007; Manickam et al., 2014) can be caused by the specific experimental setup used in their work. Their system is based on the use of β-galactosidase, in which the catalytic glutamic acid residue (E537) is mutated to a set of possible near-cognate codons, causing a reduced activity of the protein. Amino acid substitutions are then investigated by monitoring the gain in activity caused by the replacement of the near-cognate mutated amino acid back to the wild type glutamic acid. This means that their quantification considers the wild-type protein, whereas in our case we quantify the errors on the base of the abundance of a mutated protein, which may be partially degraded due to the quality control activity. In addition, we have to consider that, Manickam´s results for first-, second- and third-position mismatch errors are based on amino acid substitution at only one position of the protein and our data extend to only 3 amino acids positions (R231, K314 and K249). In both cases the results may be not completely representative of the general error rate frequency for various mismatches. In other cases e.g., (Manickam et al., 2014; Zhang et al., 2013), discrepancies might be explained by their choice of monitoring the accuracy of heterologous proteins which are normally not expressed in *E. coli* and which might be encoded by codons which are not optimal for the bacterial translation system, leading to an increased error frequency.

Analysis of the distribution of R → H substitution at 12 different positions suggests that the location in the protein and the context have a strong influence on the error frequency and the synthesis at some region of the protein, e.g., between residues 319 and 382, can be more accurate than at others (Figure 28). In EF-Tu, the least frequent substitutions are localized in a region which is important for the binding aa-tRNA (Yikilmaz et al., 2014) and might suggest that the proteins bearing amino acid replacements at these positions are unstable and are preferentially removed by the quality control machinery. Notably, frequent errors are also detectable in the protease-free environment of *in-vitro*

translation system (Figure 30). Unfortunately, low-abundance error containing peptides could not be detected *in vitro* due to the low yield of *in-vitro* translation. When a general effect of the nascent chain and sequence context on the translation was studied (Figure 32) a general reduction of accuracy was observed at these positions but whether the lower error frequency observed in figure 28 is an effect caused by the quality control activity or an intrinsic higher accuracy of the ribosome, remains difficult to discriminate.

3.5 Stress response and error profiles induced by aminoglycosides

The effect of aminoglycosides on translation is well established (Anderson et al., 1967; Davies et al., 1965a), and consistent with previous reports, all the aminoglycosides we tested, except Spc, induce miscoding (Figure 33,B) (Bilgin et al., 1990; Borovinskaya et al., 2007b; Carter et al., 2000; Peske et al., 2004). Among the miscoding-inducing aminoglycosides, Apr merits a special comment. At the time of its discovery in 1978 (Walton, 1978) a concentration-dependent miscoding effect was demonstrated (Perzynski et al., 1979). However, a recent study of its effect on the frequency of R → H substitutions *in vivo* suggested that Apr has no effect on the fidelity of either bacterial or mitochondrial ribosomes and that the lack of the miscoding activity may be the reason for its reduced ototoxicity (Matt et al., 2012). These findings were recently confirmed *in vitro* by a combination of single molecule fluorescence, NMR and bulk kinetics approaches (Tsai et al., 2013). Puglisi and colleagues concluded that Apr does not induce miscoding but it rather inhibits cell growth by blocking translocation. Instead, our data clearly show that Apr induces a significant level of miscoding, including errors of R → H substitutions. Apr also induces a concerted expression of IbpA and IbpB, whose expression is associated with erroneous proteins synthesis (Ruan et al., 2008) (Figure 33, A). Moreover, although for Apr the error frequency of single misreading events was lower than with Par, Tob, or Str (Figure 33, B), the level of consecutive miscoding events was comparable (Figure 35), indicating that the contribution to the incorporation of multiple errors of Apr might be higher than those of Par, Tob and Str. The disagreement with the results by Matt et al. can be explained by the narrow range of Apr concentrations used in their experiments (0 - 10 μM) and the combination with an assay which has a limited dynamic range and a low sensitivity, as the detection of fluorescence of Luciferase protein.

Overall, our data also revealed that as a result of the antibiotic treatment, the induction of intracellular error levels is also associated with a cell growth defect. The antibiotic-induced error frequency ranges between 10^{-5} - 10^{-3} (Figure 33, B). Interestingly, each aminoglycoside has a unique pattern of induced error frequencies for different types of amino acid substitutions, which constitutes a miscoding-fingerprint of the antibiotic (Figure 33, A) and supports the notion that the mechanism of aminoglycosides action cannot be generalized (Figure 33, B and C). Rather, for each antibiotic the

cellular outcome in terms of error frequency depends on the effect of the antibiotic on the elemental rates of decoding (Gromadski and Rodnina, 2004b; Pape et al., 2000) and on structural and dynamic changes of the ribosome induced by the antibiotic binding (Carter et al., 2000; Demirci et al., 2013a). Surprisingly, the error frequencies observed in response to the antibiotic treatment are remarkably similar to those observed in the error prone strain (Figure 39). However, the growth defects of wild type cells observed in the presence of antibiotics are not found in the error prone strain.

Aminoglycosides treatment induces the incorporation of consecutive errors, which are detected in aminoglycosides-treated cells but not in the error-prone strain. These multiple replacement in a single polypeptide chain may have a stronger toxic effect on the cell than single substitutions. Not surprisingly, the increased level of errors is associated with an increased expression of the proteins involved in the cellular stress response, such as IbpA and IbpB, whose induction is usually associated with the presence of aggregated misfolded proteins that accumulate as a consequence of the antibiotic treatment (Laskowska et al., 1996), although this effect is not observed in Spc-treated cells, where no fidelity defect is observed. In contrast to what happens for IbpA and IbpB, the concentration of the transcription factor rpoH, which regulates the expression of IbpA and IbpB, remains constant upon aminoglycoside treatment, consistent with the notion that rpoH expression increases only after a temperature shift (Erickson et al., 1987) and that the expression of heat-shock proteins may be also mediated by other transcription factors or other metabolic signals, as proposed in literature (Kuczynska-Wisnik et al., 2001). Surprisingly, although Gen is known to induce significant miscoding (Tsai et al., 2013), only a minimum effect on the stress response is observed in Gen-treated cells (Figure 33, A). Although the error profile for Gen is not available yet, the lack of stress response induction could be explained by the high efficiency of Gen cellular uptake which might lead to a fast cell death which leaves no time for the stimulation of IbpA and IbpB expression.

Notably, for many aminoglycosides such as Kan A, Tob, Par, Rib and Str, the expression levels of chaperones increase even when cells already display a strong growth impairment (Figure 33, A), suggesting that even when the cell growth is reduced, cells continue to actively translate the stress response proteins necessary to mediate correct protein folding and reduce their aggregation. In those cases where a stress response is observed, this increase reaches a maximum and then decreases with the error level. We hypothesize that as soon as aminoglycosides are added in the medium, the small amount of antibiotic which is able to enter the cells acts on the ribosome inducing miscoding and stimulating the expression of stress response proteins. When the intracellular concentration of aminoglycoside has reached a critical point, translation is completely inhibited (Tsai et al., 2013) and the cell can temporarily eliminate erroneous proteins up to the point where the cellular damage is too high.

In our experiments with aminoglycosides, cells grow even at antibiotic concentrations which exceed the estimated MIC values (Figure 33, A). Such discrepancy might be explained by differences in the experimental setup. To determine the MIC values, bacteria are inoculated at low cell densities into a medium which is already supplemented with different concentrations of antibiotic and their growth is assessed after a very long incubation time (usually 16 - 20 hrs) (Wiegand et al., 2008). In our assay, exponentially growing cells at high cell density are monitored for a shorter time window (2h). Because the uptake of aminoglycosides is slow, the external and cellular aminoglycoside concentrations might not be equilibrated. Thus, higher concentrations may be necessary to completely suppress cell growth, far above the MIC values. Because the efficient uptake of the antibiotic increases with the incorporation of error-containing proteins into the membrane, aminoglycosides which do no induce significant miscoding (e.g., Spc, Hyg B) become inhibitory only at very high concentrations.

3.6 Quantification and induction of miscoding pattern

The aminoglycosides treatment has allowed us to identify a pattern of multiple miscoding events in EF-Tu. These consecutive misincorporations remain below the detection limit in the wild type cells but become more frequent after aminoglycoside-treatment (Figure 37, 38, 39). Their frequency is higher than expected for uncoupled independent events (Equation 2). We note that at the conditions of error accumulation, prediction of error frequencies may become a problem, unless the peptides with single substitutions are less abundant than the correct peptides (Equation 1). If the error frequencies of the individual errors would be higher, and comparable to the cognate peptide, the frequencies of the cognate peptides and all its derivatives would have to be summed up to properly reflect the protein concentration. This would be particularly important when these values are used to predict the probability of two independent errors in a single peptide. However, even when cells are treated with high concentrations of aminoglycosides, the frequency of single errors never exceeds 10^{-3} (Figure 33, B) and the stochastic occurrence of consecutive errors can be considered negligible. Notably, consecutive errors are not detectable in the absence of aminoglycosides and thus can be attributed to the action of the antibiotics. Due to the vectorial nature of protein synthesis, the incorporation of consecutive C-terminal errors must depend on the first N-terminal miscoding event.

To explain the observed effect of antibiotics on error propagation, different mechanisms can be envisioned. First, the first miscoding event itself might induce subsequent errors and the error propagation could be mediated by misincorporations in the nascent chain or by distortion of the P-site tRNA introduced by codon:anticodon mismatches (Zaher and Green, 2009). Stalling peptides such as ermA can alter the catalytic proficiency for certain aa-tRNAs in the A site in the presence of their

regulator, i.e., erythromycin (Ramu et al., 2011). If an incorrect aa-tRNA binds to the A site and is translocated to the P site after peptide bond formation, the misalignment of the P-site tRNA due to mismatches in its codon:anticodon interaction can elicit error-prone decoding (Zaher and Green, 2009, 2010b, 2011). This, in turn, promotes a rescue mechanism of sense codon reading by a translation termination factor, which stops translation of a peptide in which several consecutive error have already occurred. Importantly, this mechanism is supposed to increase fidelity by the preferential release of the highly erroneous peptides from the ribosome. Alternatively, consecutive misincorporations could be introduced by the presence of aminoglycosides that remain bound to the ribosome decoding center during several elongation cycles. Notably, the three proposed mechanisms are not mutually exclusive but could act synergistically. The absence of detectable error propagation during translation by the error-prone ribosome indicates that the proposed error-propagation mechanism depends on the presence of antibiotics which leads to the incorporation of consecutive misincorporations. Importantly, mutations that make the ribosomes error-prone do not interfere with the selection mechanism proposed by Green and colleagues (Zaher and Green, 2010b).

Further indications for the sources of multiple errors come from the analysis of the misincorporation pattern of E306D-Y310H peptide, in which the first miscoding event (E → D substitution) is followed by the correct incorporation of S, E, and V (Figure 38), followed by a Y → H substitution. Because there are multiple isoacceptor tRNAs that can deliver S and V (6 and 3 isoacceptors, respectively), we cannot exclude that the correct amino acid is delivered by a an isoacceptor that is near-cognate to the given codon However, the correct incorporation of E, which has only one isoacceptor, must definitely be the result of a cognate tRNA, which should terminate the P-site-induced error-prone decoding. Thus, we suggest that consecutive miscoding events are most likely introduced by aminoglycosides. In this case, the propagation efficiency should depend on the balance between the speed of elongation and the dissociation rate constant of the respective aminoglycoside. Over several elongation cycles after the initial misincorporation event, aminoglycosides should dissociate and the error propagation effect should drop dramatically approaching the low level given by the stochastic occurrence of the single errors. However, for the quantified consecutive misincorporation events, the error-propagation efficiencies are rather constant, between 3 and 10 % (Figure 40) and almost independent of the EF-Tu source, antibiotic concentration and the distance in the sequence.

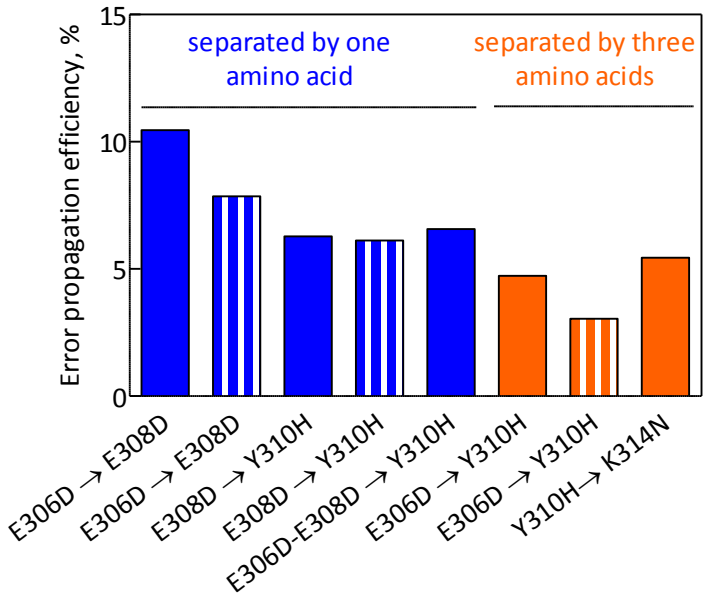

Figure 40. Frequencies of multiple consecutive errors. EF-Tu purified from K12 chromosomal-tag cells grown in 8 µM streptomycin (filled bars) or from wild type cells grown in 4 µM str (striped bars).

Assuming an elongation rate of 10 amino acids per second (Young and Bremer, 1976), this implies that to induce several consecutive errors, Str has to be stabily bound to the ribosome for at least 0.5 seconds. Due to the absence of kinetic data for the dissociation rate constants of aminoglycosides from the ribosome, the plausibility of this hypothesis is hard to evaluate. Notably, the error propagation efficiencies of E308D → Y310H and E306D-E308D → Y310H (Figure 40) are identical and thus the consecutive introduction of misincorporations is not additive or cumulative, and is consistent with a model in which the second misincorporation solely depends on the presence of the antibiotic.

Notably, all multiple-substituted variants of the target peptide FESEVYILSK we tried to enrich were successfully detected in Str treated samples. When the contribution of the consecutive misincorporations relative to the single substitutions is inspected for individual residues (e.g., E306D, Figure 41, A) it becomes clear that a significant part of the errors is involved in multiple errors patches (>15 %). This number is likely to be an underestimation because only a very small subset of all possible error combination has been taken into consideration in our experiments (Figure 41, B). The proposed mechanism implies that aminoglycosides whose binding to the ribosome lasts longer should induce a more persisting miscoding effect and a richer repertoire of multiple errors.

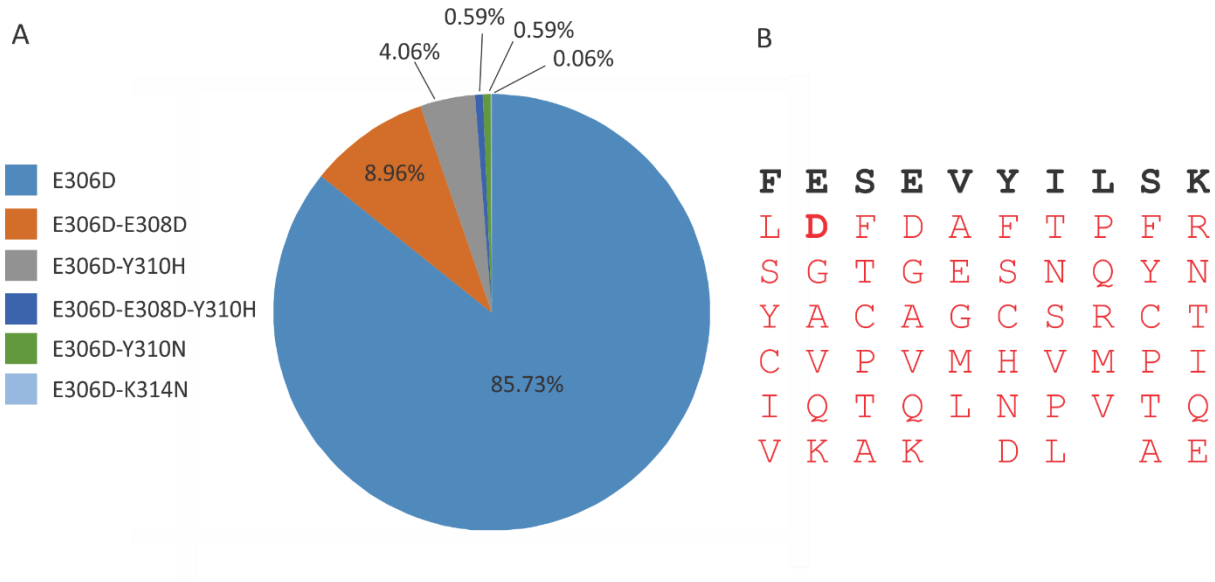

Figure 41. Significance of complex miscoding patterns. A) Relative contribution of consecutive misincorporation as quantified for the E306D peptide in EF-Tu with chromosomal tag from K12 cells grown in the presence of 8 µM Str. B) All possible near-cognate replacements for the model peptide and the possible combinatorial expansion of consecutive misincorporation events.

The qualitative contribution of error patches to protein structure can be very severe. Sequential misincorporations are most likely far more detrimental to the functional and structural integrity of proteins than single substitutions. The structural destabilization by multiple mutations may increase exponentially with the number of misincorporations. Membrane insertion of proteins that have a single incorrect amino acid can already have a dramatic impact on the integrity of the membrane. This is demonstrated by the importance of positively charged residues in membrane-spanning polytopic proteins, which are well tolerated when facing the cytoplasm, but are avoided in transmembrane regions. Their correct distribution constitute the major determinant in protein topology (von Heijne, 1989) and substitutions affecting these residues are likely to cause structural problems and incorrect folding. Proteins with two or more replacements, as it happens upon aminoglycosides treatment, can have even more severe effects.

In summary, the preferential aminoglycoside-mediated induction of certain types of misincorporations, e.g., E → D (Kramer and Farabaugh, 2007) (Figure 32, B), in combination with the discovered error propagation mechanism will most likely lead to complex misincorporation patterns and ultimately to error hotspots in protein sequences. Such error hotspots, in combination with the varying tolerance towards mutations in different proteins or parts of proteins, may explain why only a small subset of proteins is overrepresented in streptomycin-induced aggregates and inclusion bodies (Ruan et al., 2008). It is not yet clear to which extent multiple misincorporations contribute to the bactericidal efficacy of AGs in prokaryotes or to the oto- and nephrotoxicity in human cells. If the error propagation would occur in human mitochondria as well, this might be relevant for the

aminoglycoside-based treatment of genetic disorders. While the curative effect is based on the readthrough of accidentally introduced stop codons, complex misincorporation pattern are not intended and may be responsible for parts of the side effects. Thus, a better molecular understanding of the underlying mechanisms of error-propagation effects might help to uncouple the induction of single substitutions and error-propagation events.

Our findings on the mechanism of aminoglycosides-mediated bactericidal effects can be incorporated into the existing model for the aminoglycoside bactericidal mechanism (Davis, 1987). During aminoglycoside treatment, only a small amount of the antibiotic can initially enter the cell, where it interacts with ribosomes reducing their translational fidelity and inducing miscoding. When erroneous and potentially unfolded proteins are inserted in the membrane, this causes the formation of channels and favors membrane damage enhancing the intake of more aminoglycoside into the cell. When erroneous protein begin to appear, the ribosome induces multiple sequential miscoding events, which stimulates termination of the synthesis of erroneous proteins and triggers their release (Zaher and Green, 2009). Truncated proteins can be toxic and their membrane insertion can cause abnormal depolarization (Hurwitz et al., 1981) and change membrane potential and permeability (Bryan and Kwan, 1983; Taber et al., 1987). Erroneous and truncated proteins synergistically affect the membrane promoting an increased influx of aminoglycosides which inevitably leads to a positive feedback loop in which more aminoglycoside will enter the cell and more errors will be made until , the integrity of the membrane is destroyed and the cell dies. It has been observed that Str treatment causes an increased demand for polyamines, and the induction of a polyamine transport system can be utilized in a competitive manner by Str (Holtje, 1979) facilitating even more the entrance of the antibiotic into the cell. The relationship between incorrect protein synthesis and membrane damage is thus a key element in the aminoglycosides-induced miscoding. The insertion of erroneous proteins in the cellular membrane may also generate hydroxyl radical and oxidative stress, ultimately damaging nucleic acids and proteins (Dwyer et al., 2014; Kohanski et al., 2008), although the latter notion has been recently challenged (Keren et al., 2013; Liu and Imlay, 2013).

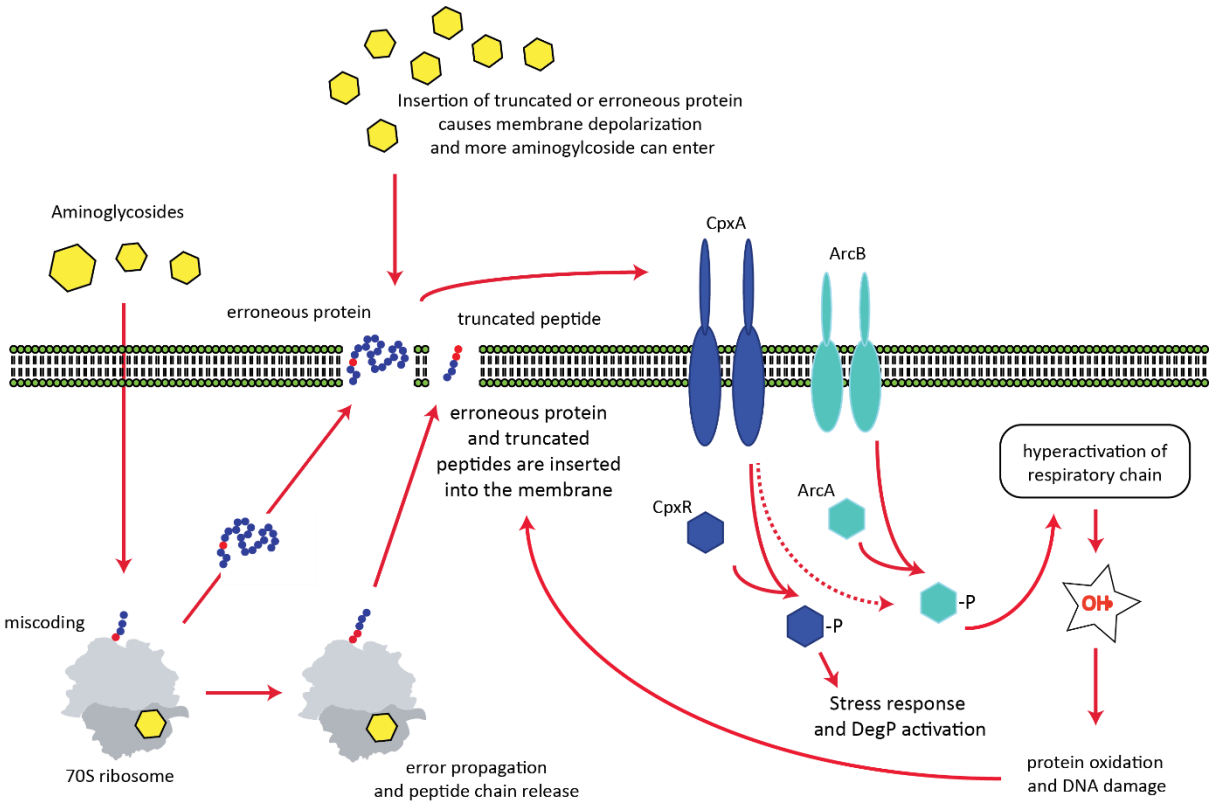

Figure 42. Proposed mechanism of aminoglycosides activity. A small amount of aminoglycoside enters the cell and interacts with ribosomes reducing the fidelity of translation and inducing miscoding. Erroneous proteins are produced and the ribosomes promote consecutive errors incorporation and stimulate translation termination and peptide release. When erroneous and/or truncated proteins are inserted into the membrane they trigger the phosphorylation of members of two-component regulatory systems such as CpxA and ArcB, which in turn activate their corresponding regulatory proteins CpxR and ArcA, respectively. CpxR regulates the expression of stress-response protein e.g., DegP. ArcA regulates genes involved in the respiratory chain, leading to its hyperactivation, culminating in the generation of hydroxyl radicals which damage nucleic acids and proteins. Figure adapted from (Kohanski et al., 2007; Kohanski et al., 2008).

3.7 Aminoglycosides effect investigation and future perspectives

The present work demonstrated that our developed experimental approach constitutes a robust and reliable tool for the investigation of amino acid misincorporation *in vivo*. When applied to the study of aminoglyocosides, our study revealed that the increased frequency of some errors during the treatment can be seen as a fingerprint characterizing each antibiotic. However, the results obtained so far are resistricted to a limited set of peptides and only 8 substitutions have been taken into consideration (Figure 33, B). As part of the future perspectives, the pool of substitutions analyzed will be extended to provide a more comprehensive overview on the aminoglycosides charachteristics. The charachterization of aminoglycosides effect could also be extended to a broader analysis of the cellular response by systematically monitoring the expression of, not only IbpA and IbpB chaperones (Figure 33), but also of proteins part of the SOS response for DNA damage e.g., RecA and LexA or protein involved in the respiratory chain (Kohanski et al., 2007) which might shed some light on whether or

not the oxidative stress and the consequent nucleic acid damage are involved in the aminoglycosides killing mechanism.

Our data indicate that the induction of error patches may play an important role in the mechanism of aminoglycosides-mediated cell death. In the future work, consecutive errors which were never reported in literature so far, but which already showed promising initial results with Apr, Tob and Par (Figure 35), will be studied in the presence of other antibiotics, and other model peptides will be taken into consideration. These combined results could lead to a deeper understanding of the mechanisms of action of aminoglycosides. In addition, because aminoglycosides toxicity has been often associated with their interaction with mitochondrial ribosomes, the flexibility and sensitivity of our method could be employed to investigate single errors and more complex error patterns in eukaryotic systems. This could have a potential medical impact, for example in the selection of the lowest-toxicity aminoglycosides for the palliative treatment of genetic diseases (Bukowy-Bieryllo et al., 2016; Ho et al., 2013; Malik et al., 2010a; Malik et al., 2010b) or to perform more focused treatments, tailored to the type of miscoding event to induced.

4. MATERIALS AND METHODS

Table 6. List of equipments

Device	Supplier
Allegra X-22R centrifuge	Beckmann Coulter
Amicon Ultra-4 30K cut-off	Merck Millipore
Avanti J-26 XP centrifuge	Beckmann Coulter
Avanti J-30I centrifuge	Beckmann Coulter
Acclaim PepMapRSLC 15 cm, 75 µm inner diameter, 3 µm particle size	Thermo Fisher Scientific
ÄKTA FPLC	GE Healthcare
Benchtop centrifuge 5415R	Eppendorf
Biostat B-plus 5 l fermenter	Sartorius
Digital sonifier cell distruptor W-250D	Branson
Dounce tissue grinder	Wheaton
Easy nLCII chromatography system	Thermo Fisher Scientific
Electrophoresis power supply	PeqLab
Emulsiflex C-3 homogenizer	Avestin
HighTrap Q HP anion exchange column	GE Healthcare
Hiload 26/60 Superdex 75 size-exclusion chromatography	GE Healthcare
Innova 44 incubator shaker	New Brunswick
Intelli-mixer	ELMI Ltd.
JA30.1 rotor	Beckmann Coulter
JLA-8.1000 rotor	Beckmann Coulter
LiChrospher WP300 RP-18 (5µm)	Merck Millipore
Low retention 1.5 ml tubes	Eppendorf
Low retention 0.5 ml tubes	Eppendorf
Nanodrop 2000	Peqlab
Optima XPN centrifuge	Beckmann Coulter
pH-indicator strips pH 6.5-10.0	Merck Millipore
Pierce BCA Protein Assay Kit	Thermo Fisher Scientific
Polyolefin foil for microplates	HJ-Bioanalytik GmbH
Polypropylene 96-well microplates	VWR
Protino Ni-IDA 2000 Packed Columns	Macherey-Nagel
Q-Exactive hybrid mass spectrometer	Thermo Fisher Scientific
Q-Exactive Plus hybrid mass spectrometer	Thermo Fisher Scientific
Reprosil-Pur 120 C18 3 µm column	Dr Maisch
SDS-PAGE electrophoresis chamber	Bio-Rad
SpeedVac vacuum concentrator SPD121P	Thermo Fischer Scientific
Spin-X centrifuge tube filter 0.45µm cellulose acetate	Corning Inc.
Superdex Peptide 10/300 GL	GE Healthcare

SX4250 rotor	Beckmann Coulter
Thermomixer comfort	Eppendorf
Thermostatic oven	Memmert
TSQ Quantiva triple quadrupole mass spectrometer	Thermo Fisher Scientific
TSQ Vantage triple quadrupole mass spectrometer	Thermo Fisher Scientific
Ultimate 3000RSLC	Thermo Fisher Scientific
Ultrasonic cleaner	VWR
Vivaspin 20 centrifugal concentrator	Sartorius
Vortex Genie 2	Scientific Industries
50.2Ti rotor	Beckmann Coulter

Table 7. List of softwares

Software	**Provider**
DNA Star Lasergene	DNASTAR, Inc
GraphPad Prism 5.0	GraphPad Software
Pymol 1.5	Schrödinger
Skyline 3.5	MacCoss Lab Software
Xcalibur 2.2	Thermo Fischer Scientific
Adobe Illustrator CS5	Adobe Systems
CorelDRAW X7	Corel

4.1 Chemicals

All reactions are performed in low-retention reaction cups (Eppendorf). If not indicated elsewhere, the chemicals are purchased from Merck Millipore or Sigma Aldrich. The chemicals used for chromatographic separation are of HPLC grade. Water, acetonitrile, methanol and formic acid used for mass spectrometric analysis are of HPLC/MS grade and purchased from Fischer Scientific. Custom-synthetized isotopically-labeled peptides (5 µM) are obtained from Thermo Fisher Scientific (highly quantified Ultimate grade peptides with concentration precision ±5 % and QuantPro grade peptides with concentration precision ±25 %) or JPT Peptide Technologies (Berlin, Germany) (highly-quantified peptides SpikeTides_TQL or non-quantified SpikeTides_L grade peptides). All peptides used are listed in the appendix of this thesis (Table 15 and 16). Pierce Retention Time Calibration mix (PRTC) used to regularly assess the performances of chromatographic system and mass spectrometer is from Thermo Fisher Scientific.

Table 8. List of buffers

Buffer	Composition
LB medium	10 g/L tryptone, 10g/L NaCl, 5g/L yeast extract
LB agar	10 g/L tryptone, 10g/L NaCl, 5g/L yeast extract, 15g/L agar
TB medium	12 g/L tryptone, 24 g/L yeast extract, 4 ml/L glycerol, 17 mM KH_2PO_4, 72 mM K_2HPO_4
Buffer A	50mM HEPES pH 7.5, 50 mM KCL, 10 mM $MgCl_2$, 5mM 2-mercaptoethanol, Complete Protease inhibitor 1 tablet/50 ml (Roche Diagnostics, Mannheim), DNase
Buffer B	B-PER reagent (Thermo Scientific), 200mM KCl, 3mM $MgCl_2$, Complete Protease inhibitor 1 tablet/50 ml (Roche Diagnostics, Mannheim), 30 µM GDP, 5mM 2-mercaptoethanol, DNase
Buffer C	8 M Urea, 25 mM Hepes pH 7.5, 200 mM KCl, 10 mM $MgCl_2$, 5 mM 2-mercaptoethanol
Buffer D	25 mM HEPES pH 7.5, 200 mM KCl, 3mM $MgCl_2$, 30 µM GDP
Buffer E	Buffer D + 500mM KCl
Buffer F	Buffer D + 200 mM Imidazole
Buffer G	Buffer C + 400 mM KCl
Buffer H	Buffer C + 150 mM Imidazole
$TAKM_7$	50 mM Tris-HCl pH 7.5, 70 mM NH_4Cl, 30 mM KCl, 7mM $MgCl_2$
Staking gel SDS-PAGE	4.8 % AA:Bis (29:1), 0.125 M Tris-HCl pH 6.8, 0.1 % SDS
Resolving gel SDS-PAGE	16 % AA:Bis (29:1), 0.3 M Tris-HCl pH 8.8, 0.1 % SDS
Coomassie Blue staining solution	0.1 % Coomassie brilliant blue, 50 % ethanol, 10 % acetic acid
Destaining solution	20 % ethanol, 10 % acetic acid
Laemmli SDS loading buffer 4X	40 % glycerol, 240 mM Tris-HCl pH 6.8, 8 % SDS, 0.04 % bromophenol blue, 5 % 2-mercaptoethanol
SDS running buffer 10X	250 mM Tris base, 1.92 M glycine, 1 % SDS (to be diluted 10 times to obtain SDS running buffer 1X)
TBS buffer	50 mM Tris-HCl pH 7.5, 150 mM NaCl
High salt TBS buffer	TBS buffer + 500 mM NaCl

Table 9. List of plasmids

Vector	Purpose	Supplier	Resistance	Tag
pET24a	Overexpressed his-tag EF-Tu (*tufA*)	Merck Millipore	Kan	C-terminal Hisx6
pET21a	Overexpressed his-tag EF-Tu (*tufA*) and sumo constructs	Novagen	Amp	C-terminal Hisx6
pSUMO	Sumo-tag constructs		Kan	Hisx6
pET21-flag	C-terminus-flag EF-Tu (*tufA*)	In-house produced from pET21	Kan	Flag (DYKDDDDK)

Table 10. List of bacterial strains

***E. coli* strain**	**Purpose**	**Supplier**
BL21 (DE3)	EF-Tu (*tufA*) overexpression	Merck Millipore
TOP10	Plasmid replication	Novagen
MRE-600 (ATCC29417)	Wild type EF-Tu	UAB school of medicine
MG1655 (K-12)	Wild type EF-Tu	Leibniz Institute DSMZ
W3110 (K-12)	EF-Tu chromosomal tag (*tufA*)	
E. coli UD 131 (Xac rpsD12)	Error prone (ram)	These strains have been kindly provided by Dr. Hani Zaher (Deptartment of Biology, Washington University in St. Louis, MO, USA)
E. coli US157 (Xac rspL141 zcg-174::Tn10)	Error restricted (hyperaccurate)	
E. coli (Xac ara D[lacproAB] gyrA rpoB argEamber)	Wild type EF-Tu for comparison with hyperaccurate and error prone strain	

4.2 Primers

Primers are designed using the SeqBuilder software (DNASTAR) and purchased from IBA Life Sciences or Eurofins MWG Operon. Forward and reverse primers (F and R, respectively) are listed.

Table 11. List of primers for EF-Tu mutants

Primers used for EF-Tu *in-situ* directed mutagenesis	
Mutation to introduce	**Sequence 5´-3´**
R45H	**F** CCTACGGCGGTGCTGCTCATGCATTCGACCAGATCG
	R CGATCTGGTCGAATGCATGAGCAGCACCGCCGTAGG
R59H	**F** CGCGCCGGAAGAAAAAGCTCATGGTATCACCATCAACACTTC
	R GAAGTGTTGATGGTGATACCATGAGCTTTTTCTTCCGGCGCG
R172H	**F** GACGACACTCCGATCGTTCATGGTTCTGCTCTGAAAGC
	R CGCTTTCAGAGCAGAACCATGAACGATCGGAGTGTCGTC
R231S	**F** GTGGTACCGTTGTTACCGGTAGTGTAGAACGCGGTATCATC
	R GATGATACCGCGTTCTACACTACCGGTAACAACGGTACCAC
R231G	**F** GTGGTACCGTTGTTACCGGTGGTGTAGAACGCGGTATCATC
	R GATGATACCGCGTTCTACACCACCGGTAACAACGGTACCAC
R231C	**F** GTACCGTTGTTACCGGTTGTGTAGAACGCGGTATCATC
	R GATGATACCGCGTTCTACACAACCGGTAACAACGGTAC
R231H	**F** GTACCGTTGTTACCGGTCATGTAGAACGCGGTATCATC
	R GATGATACCGCGTTCTACATGACCGGTAACAACGGTAC
R231P	**F** GTGGTACCGTTGTTACCGGTCCGGTAGAACGCGGTATCATC
	R GATGATACCGCGTTCTACCGGACCGGTAACAACGGTACCAC
R231L	**F** GTGGTACCGTTGTTACCGGTCTGGTAGAACGCGGTATCATC
	R GATGATACCGCGTTCTACCAGACCGGTAACAACGGTACCAC
R231A	**F** GTGGTACCGTTGTTACCGGTGCTGTAGAACGCGGTATCATC
	R GATGATACCGCGTTCTACAGCACCGGTAACAACGGTACCAC

R231D	**F** GTGGTACCGTTGTTACCGGTGATGTAGAACGCGGTATCATC
	R GATGATACCGCGTTCTACATCACCGGTAACAACGGTACCAC
R231E	**F** GTGGTACCGTTGTTACCGGTGAAGTAGAACGCGGTATCATC
	R GATGATACCGCGTTCTACTTCACCGGTAACAACGGTACCAC
R231F	**F** GTGGTACCGTTGTTACCGGTTTTGTAGAACGCGGTATCATC
	R GATGATACCGCGTTCTACAAAACCGGTAACAACGGTACCAC
R231Y	**F** GTGGTACCGTTGTTACCGGTTATGTAGAACGCGGTATCATC
	R GATGATACCGCGTTCTACATAACCGGTAACAACGGTACCAC
R231Q	**F** GTACCGTTGTTACCGGTCAAGTAGAACGCGGTATCATC
	R GATGATACCGCGTTCTACTTGACCGGTAACAACGGTAC
R231T	**F** GTGGTACCGTTGTTACCGGTACCGTAGAACGCGGTATCATC
	R GATGATACCGCGTTCTACGGTACCGGTAACAACGGTACCAC
R231V	**F** GTGGTACCGTTGTTACCGGTGTTGTAGAACGCGGTATCATC
	R GATGATACCGCGTTCTACAACACCGGTAACAACGGTACCAC
R234H	**F** CAACTTTGATGATACCATGTTCTACACGACCGG
	R CCGGTCGTGTAGAACATGGTATCATCAAAGTTG
K249Q	**F** GGTAGACTTCTGAGTCTCTTGGATACCAACGATTTCAAC
	R GTTGAAATCGTTGGTATCCAAGAGACTCAGAAGTCTACC
K249E	**F** GGTAGACTTCTGAGTCTCTTCGATACCAACGATTTCAAC
	R GTTGAAATCGTTGGTATCGAAGAGACTCAGAAGTCTACC
K249T	**F** GGTAGACTTCTGAGTCTCTGTGATACCAACGATTTCAAC
	R GTTGAAATCGTTGGTATCACAGAGACTCAGAAGTCTACC
K249R	**F** GAAATCGTTGGTATCCGTGAGACTCAGAAGTCTAC
	R GTAGACTTCTGAGTCTCACGGATACCAACGATTTC
K249I	**F** GAAATCGTTGGTATCATCGAGACTCAGAAGTCTAC
	R GTAGACTTCTGAGTCTCGATGATACCAACGATTTC
K249N	**F** GTTGGTGAAGAAGTTGAAATCGTTGGTATCAACGAGACTCAGAAGT CTACCTGTACTGGCGTTG
	R CAACGCCAGTACAGGTAGACTTCTGAGTCTCGTTGATACCAACGA TTTCAACTTCTTCACCAAC
R270H	**F** CAAACTGCTGGACGAAGGCCATGCTGGTGAGAACGTAGGTG
	R CACCTACGTTCTCACCAGCATGGCCTTCGTCCAGCAGTTTG
R280H	**F** CGTAGGTGTTCTGCTGCATGGTATCAAACGTGAAGAAATCG
	R CGATTTCTTCACGTTTGATACCATGCAGCAGAACACCTAC
R284H	**F** CGTTCGATTTCTTCATGTTTGATACCAC
	R GTGGTATCAAACATGAAGAAATCGAACG
K314Q	**F** GAAGTGTACATTCTGTCCCAAGATGAAGGCGGCCGTCATAC
	R GTATGACGGCCGCCTTCATCTTGGGACAGAATGTACACTTC
K314E	**F** CTTTGAAGAACGGAGTATGACGGCCGCCTTCATCTTCGGACAGAAT GTACACTTCAGATTCGAACTTG
	R CAAGTTCGAATCTGAAGTGTACATTCTGTCCGAAGATGAAG

	GCGGCCGTCATACTCCGTTCTTCAAAG
K314T	**F** GTATGACGGCCGCCTTCATCTGTGGACAGAATGTACACTTC
	R GAAGTGTACATTCTGTCCACAGATGAAGGCGGCCGTCATAC
K314R	**F** GACGGCCGCCTTCATCACGGGACAGAATGTACAC
	R GTGTACATTCTGTCCCGTGATGAAGGCGGCCGTC
K314I	**F** GACGGCCGCCTTCATCGATGGACAGAATGTACAC
	R GTGTACATTCTGTCCATCGATGAAGGCGGCCGTC
K314N	**F** GAAGAACGGAGTATGACGGCCGCCTTCATCGTTGGACAGAAT GTACACTTCAGATTCGAAC
	R GAAGAACGGAGTATGACGGCCGCCTTCATCGTTGGACAGA ATGTACACTTCAGATTCGAAC
R319H	**F** CCAAAGATGAAGGCGGCCATCATACTCCGTTCTTCAAAGGC
	R GCCTTTGAAGAACGGAGTATGATGGCCGCCTTCATCTTTGG
R328H	**F** CGTTCTTCAAAGGCTACCATCCGCAGTTCTACTTCCG
	R CGGAAGTAGAACTGCGGATGGTAGCCTTTGAAGAACG
R378H	**F** GCCAACGGTACGGCCGCCTTCATGGATTGCGAAACGCAGACCG
	R CGGTCTGCGTTTCGCAATCCATGAAGGCGGCCGTACCGTTGGC
R382H	**F** CAATCCGTGAAGGCGGCCATACCGTTGGCGCGGGCGTTG
	R CAACGCCCGCGCCAACGGTATGGCCGCCTTCACGGATTG

Table 12. List of primers for SUMO-constructs

Primers used to obtain SUMO-constructs	
Construct	**Sequence 5´-3´**
pet21a linearization	**F** GATCCGGCTGCTAACAAAGCCCGAAAGG
	R ATGTATATCTCCTTCTTAAAGTTAAACAAAATTATTTC
pSUMO-FESEVYILSK	**F** CACACCAAGTTCGAATCTGAAGTGTACATTCTGTCCAAAGATGAAGGC GATCCGGCTGCTAACAAAGCCCG
	R ACCACCAATCTGTTCTCTGTGAGCCTC
SUMO-FESEVYILSK insertion	**F** CTTTAAGAAGGAGATATACATATGGGTCATCACCATCATCACCATGGTTCG
	R CGGGCTTTGTTAGCAGCCGGATCCTAGCCTTCATCTTTGGACAGAATGTAC
SUMO-H378H short	**F** TGAGATCCGGCTGCTAACAAAGCCCG
	R GCCAACGGTACGGCCGCCTTCACGGATTGCGAAACGCAGACCGCCTT CATCTTTGGACAGAATG
SUMO-H378H long	**F** TAGGATCCGGCTGCTAACAAAGCCCGAAAGG
	R TTTTGCTACAACGCCCGCGCCAACGGTACGGCCGCCTTCACGGATT GCGAAACGCAGACCGTCGTCCATCGCGATCGGGTGGCCTTCATCTTT GGACAGAATGTAC
SUMO-R319H	**F** TAGGATCCGGCTGCTAACAAAGCCCGAAAGG

	R ACGGTAGCCTTTGAAGAACGGAGTATGACGGCCGCCTTCATCTTTG GACAGGCCTTCATCTTTGGACAGAATGTAC
SUMO-R231H	**F** TAGGATCCGGCTGCTAACAAAGCCCGAAAGG
	R GATGATACCGCGTTCTACACGACCGGTAACAACGGTACCACGACCG GAGCCTTCATCTTTGGACAGAATG
SUMO-R280H	**F** TAGGATCCGGCTGCTAACAAAGCCCGAAAGG
	R GATTTCTTCACGTTTGATACCACGCAGCAGAACACCTACGTTCTC ACCAGCACGGCCTTCGCCTTCATCTTTGGACAGAATG
SUMO-R382H	**F** TAGGATCCGGCTGCTAACAAAGCCCGAAAGG
	R GCCCAGAACTTTTGCTACAACGCCCGCGCCAACGGTACGGCCGC CTTCACGGATTGCGCCTTCATCTTTGGACAGAATGTAC
SUMO-R328H	**F** TAGGATCCGGCTGCTAACAAAGCCCGAAAGG
	R GTCAGTAGTACGGAAGTAGAACTGCGGACGGTAGCCTTTGAAGA AGCCTTCATCTTTGGACAGAATGTAC

Table 13. List of primers for chromosomal tag insertion

Primers for chromosomal tag insertion	
Construct	**Sequence 5´-3´**
His-tag insertion on chromosomal *tufA* gene (his-tag nucleotide sequence is underlined).	**F** CCGTACCGTTGGCGCGGGCGTTGTTGCTAAAGTTCTGGGC CACCACCACCACCACCACTAGAATTAACCCTCACTAAAGGGCG
	R GGGCGCCGAAGCGCCCTTTTCAATTCAAAACTAATTAACGTGTAA TAATACGACTCACTATAGGGCTC

4.3 EF-Tu constructs

4.3.1 Site-directed mutagenesis for generation of EF-Tu mutants

Site-directed mutagenesis has been performed in PCR tubes using Phusion High-fidelity DNA polymerase (New England Biolabs) following the protocol suggested by the supplier. The plasmid pET21 containing the *tufA* gene coding for EF-Tu is amplified by polymerase chain reaction (PCR) (Saiki et al., 1985) using the Quick Change kit (Agilent) and a set of forward and reverse primer specific for the mutation of choice (Table 11). Parental plasmid is digested with DpnI enzyme and the PCR product is used to transform TOP10 chemically competent *E. coli* cells (Invitrogen). Clones containing the plasmid are selected for resistance to Kan. The plasmid is extracted using plasmid miniprep kit (Macherey-Nagel). Mutation insertion is verified by plasmid sequencing performed by SeqLab (Göttingen, Germany). The constructs expressing the EF-Tu mutants have been kindly provided by Christina Kothe.

4.3.2 Generation of constructs containing a Sumo protein fused with an EF-Tu peptide epitope

In order to dissect the impact of the sequence context and cellular protease activity on the measured error frequency from selected EF-Tu epitopes are cloned in a pSUMO vector together with a quantifier peptide (FESEVYILSK) for their quantification. The quantifier peptide for EF-Tu is cloned into a linearized pSUMO vector, amplified and the vector ultimately ligated with T4 DNA ligase enzyme. The sumo tag and the nucleotide stretch for the cognate peptide are amplified by PCR using primers containing homologous region to pET21a vector (Table 12). The product is introduced into a linearized pET21a vector and ligated using In-Fusion HD cloning kit (Clontech Laboratories, USA) as described in the manufacturer's protocol. EF-Tu peptides for which the error frequency had to be assessed in the SUMO construct are chosen based on experimental data and their nucleotide sequence is introduced into the pET21a-SUMO-FESEVYILSK construct by PCR using the primers indicated in the table 12. SUMO constructs have been obtained by Christina Kothe.

4.3.3 C-terminal his-tag insertion into the EF-Tu gene

Insertion of His-tag on the K12 strain W3110 and of the Kan resistance cassette is performed using the Gene deletion kit (Gene Bridges) as described in the manual and was performed by Christina Kothe. The primers used are listed in Table 13.

4.3.4 Generation of flag EF-Tu

The pET21a plasmid encoding for EF-Tu protein with the C-terminus octameric flag DYKDDDDK was generated by Sarah Lambrecht.

4.4 Cell cultures

4.4.1 Cell transformation

BL21 (DE3) *E. coli* competent cells are thawed on ice for 10 min and gently mixed with 100 ng of plasmid DNA. After 10 min on ice, transformation is induced by incubating cells at 42°C for 1-2 min before transferring them back on ice. After 3 minutes, 500 µl LB medium are added and cells are allowed to recovery at 37°C for 1hr with gentle agitation using a thermomixer. After the incubation, 100 µl are plated on an LB agar plates supplemented with the antibiotic of choice and stored overnight in a thermostatic oven.

4.4.2 Cell growth

A saturated LB culture is used to inoculate fresh LB medium. For *E.coli* K12 chromosomal tag, the overnight preinoculum is performed in LB medium supplemented with 50 µg/ml Kan. *E. coli* K12 chromosomal tag, MG1655, *rpsD*, *spsL*, and their parental wild type strains are grown in an incubator

shaker at 37°C and 200 rpm to ~1 OD_{600}. *E.coli* BL21 (DE3) cells for EF-Tu mutants and pSUMO-constructs overexpression are grown in LB medium supplemented with 50 µg/ml Kan (Serva Electrophoresis GmbH). Induction is started at 0.7-0.8 OD_{600} and performed by incubating cells with with 1 mM IPTG for 2 hrs. Alternatively, *E. coli* BL21 (DE3) for His-tagged EF-Tu are grown in TB medium in a 5 L fermenter and induced at the beginning of exponential phase with 1mM IPTG for 3 hrs. To test the effects of aminoglycoside antibiotics on *E. coli* K12 chromosomal tag MG1655 cells are grown in LB without antibiotics. At 0.3 OD_{600}, the antibiotic of interest is added and cells are incubated for 120 min. In the negative control cell culture, no antibiotic is added and after reaching 0.3 OD_{600}, cells are grown for 120 min. Cells are harvested by centrifugation in a refrigerated centrifuge at 5000 rpm (JLA-8.1000 rotor).

4.4.3 Cell lysis

E. coli MRE-600 are used for the purification of wild type EF-Tu. Cells are resuspended and lysed in buffer A using the Emulsiflex C3 homogenizer after manual homogenization in a Dounce tissue grinder. Cell debris are removed by centrifugation for 30 min at 25000 rpm (JA30.1 rotor) and the lysate is cleared by 30 min ultracentrifugation at 50000 rpm (50.2Ti rotor). Cells for EF-Tu purification under native conditions are solubilized in buffer B or buffer C (for purification under native or denaturing conditions, respectively) and sonicated 1 min by 10 s shots at 30 % amplitude followed by 5 s of rest using a sonifier cell disruptor.

4.5 PURexpress system for the *in-vitro* translation of flag EF-Tu

The EF-Tu carrying the flag DYKDDDDK is translated *in vitro* to assess the error frequency in a protease-free environment. For this purpose the commercial kit PURexpress system (New England BioLabs) is used as described in the manufacturer´s manual and by others (Tuckey et al., 2014).

4.6 Purification of EF-Tu protein

EF-Tu purified from different sources was used for the investigation and quantification of misincorporations.

4.6.1 Purification under native conditions

His-tag EF-Tu is purified using Protino Ni-TED 2000 packed columns. After initial column equilibration with 4 volumes buffer D, the cleared lysate is loaded onto the column and eluted by gravity. Column is washed with 6 volumes of high salt buffer E and re-equilibrated with 4 volumes of buffer D. Protein is finally eluted with 3 volumes of elution buffer F and concentrated using Amicon Ultra-4 with a 30

KDa cut-off. Buffer is exchanged with $TAKM_7$ before the protein is shock frozen in liquid nitrogen and stored at -80°C. EF-Tu from MRE600 and ram strains was purified as described elsewhere (Rodnina et al., 1995b).

4.6.2 Purification under denaturing conditions

A Protiono Ni-TED 2000 column is equilibrated with 4 column volumes of buffer C before the lysate is loaded on the column by gravity flow. The column is then washed with 8 volumes of buffer G and finally re-equilibrated in 6 volumes of buffer C. Protein is eluted with 4 volumes of elution buffer H, concentrated and rebuffered in 3 M Urea and 0.1 M ammonium hydrogencarbonate by centrifugation at 4000 rpm in Vivaspin concentrators MWCO 30000 in a refrigerated benchtop centrifuge.

4.6.3 Purification of FLAG-EF-Tu

In-vitro translated FLAG-EF-Tu is purified from components of the PURexpress *in-vitro* translation kit, using anti-flag M2 magnetic beads (Sigma Aldrich). For each PURExpress kit tube, 40 µl of beads slurry are used (corresponding to 20 µl packed gel volume, as stated in the technical bulleting of the product). The whole procedure from EF-Tu binding to its elution is carried out at 4°C while tubes are rotated in an Intelli-mixer rotating device. Beads are washed to remove the storage buffer and mixed with the sample and TBS to a final volume of 1 ml. After 2 hrs incubation, the beads are separated from the supernatant with the help of a magnet and washed with high-salt TBS buffer to remove unspecific binders. After each washing step the protein content in the buffer is measured photometrically and the washing procedure is repeated until the absorbance difference between the wash solution aspirated from the beads and the wash solution blank is <0.05 . At this point the washing buffer is eliminated and EF-Tu can be eluted from the beads.

4.6.3.1 Elution of FLAG-EF-Tu with 3X flag peptides

Competitive elution with 3X FLAG peptides (Sigma Aldrich) showed to be the most efficient method to detach EF-Tu protein from the beads. They are synthetic peptide of 23 amino acid residue. The Asp-Tyr-Lys-Xaa-Xaa-Asp motif is repeated three times in the peptide and eight amino acids at the C-terminus make up the classic FLAG sequence (Asp-Tyr-Lys-Asp-Asp-Asp-Asp-Lys). An excess of 3X FLAG peptides is added and beads are incubated with 5 gel packed volumes of 150 ng/µl flag peptides for 15 min for two times. Buffer is picked up and concentrated using 500 µl Amicon Ultra 10 KDa cut-off before being loaded on a 16 % PAGE-SDS for analysis and further in-gel digestion (Figure 43).

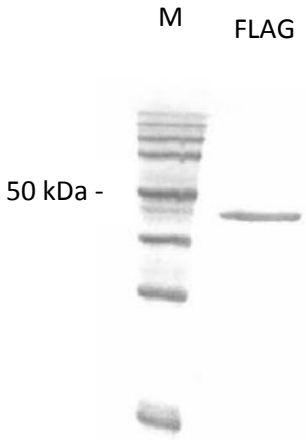

Figure 43. Purification of FLAG EF-Tu. Purified EF-Tu protein is run together with Perfect Protein Marker 15-150 kDa (M) on a 16 % PAGE-SDS.

4.7 SDS-PAGE electrophoresis

Purified EF-Tu is quantified using a Pierce BCA protein assay kit (Thermo Scientific) as described in the manual and its purity is assessed by SDS-PAGE electrophoresis essentially performed as described in (Laemmli, 1970). Bands molecular weights are identified by comparison with Perfect Protein Marker 10-150 kDa (Novagen) or SeeBlue Plus2 Pre-Stained Protein Standard (Thermo Fisher Scientific). Stacking gel solution is prepared using Acrylamide:Bisacrylamide (29:1) (Serva Electrophoresis GmbH) to a final concentration of 4.8 %. Resolving gel solution is prepared to a final Acrylamide:Bisacrylamide (29:1) concentration of 16 %. Gel polymerizatzion is started by the addition of 1:100 (v/v) 10 % APS (Calbiochem) and 1:1000 (v/v) TEMED. Gels are run for 1 hr at 180 V before being stained in Coomassie Blue solution and finally destained in destaining solution.

4.8 Acetone precipitation of proteins

EF-Tu (3000 - 30000 pmol) purified under native-conditions is precipitated overnight with 5 volumes of ice-cold acetone at -20°C. Precipitated protein is collected by centrifugation at 12000 rpm for 30 min in a refrigerated benchtop centrifuge and washed with 300 µl of ice-cold ethanol 80 %. The sample is centrifuged again to pellet the protein and remove the ethanol supernatant and the pellet is dried for 10 min.

4.9 EF-Tu trypsination

4.9.1 In-solution proteolysis of EF-Tu purified under native conditions

Unless stated otherwise, the whole proteolysis procedure is carried out in a Thermomixer comfort (Eppendorf) at 600 rpm. Dried protein pellet is resuspended in 20 µl of RapiGest 1 % (Waters) in 25 mM NH_4HCO_3 and incubated for 10 min at 37°C. Disulfide bonds are reduced by adding 20 µl 50 mM

DTT (in 25 mM NH_4HCO_3) in a two-steps incubation at 60°C for 10 min and at 37°C for 20 min. Alkylation of thiols was achieved adding 20 µl of IAA (in 25 mM NH_4HCO_3) and incubating the sample at 37°C for 30 min in the dark. Rapigest in the sample is diluted to 0.1 % by the addition of 25 mM NH_4HCO_3. Trypsin 1 µg/µl (Promega) dissolved in 25 mM NH_4HCO_3 is added to the sample (final concentration 0.01 µg/µl) and EF-Tu is proteolyzed overnight at 37°C.

4.9.2 In-solution proteolysis of EF-Tu purified in denaturing conditions

Protein is reduced in 1/10 vol 50 mM DTT and incubated 50 min at 65°C in a thermomixer. Cysteines are alkylated in 1/10 vol 100 mM IAA for 30 min at 30°C in the dark. The protein is finally digested overnight in trypsin (Promega) at 37°C (1:100 protease to protein ratio).

4.10 Sample preparation for the characterization of aminoglycosides effects

The induction of stress response and error incorporation caused by aminoglycosides was investigated in MG1655 *E. coli* cells grown at increasing concentration of Kan, Gen, Tob, Neo, Par, Rib, Nea, Apr, Hyg B, Str and Spc. Cells (1 OD_{600}) are collected 2 min at 13000 rpm on a benchtop centrifuge and the LB medium is removed. The pellet is resuspended in 100 µl RNase-free water and 50 µl 4x Laemmli buffer (Biorad) and incubated for 5 min at 95°C. After the incubation, the samples are cooled down to room temperature and mixed with 50 µl of a buffer containing 8 M Urea/Tris buffer pH 7.5. Samples are centrifuges 5 min at 13000 rpm in a benchtop centrifuge to remove any small particles before being separated by electrophoresis.

To analyze the stress response, 15 µl of lysate are separated on a 16 % SDS-PAGE at 185 V until all proteins are in the separation gel. In one lane 5 µl of Perfect Protein Marker 10-150 KDa (Merck) are loaded (Figure 44). The gel is then stained in Coomassie Blue solution for 20 min and destained. The lysate's bands are vertically cut with a scalpel, further reduced into smaller pieces and stored in 1.5 ml Eppendorf tube at -20°C.

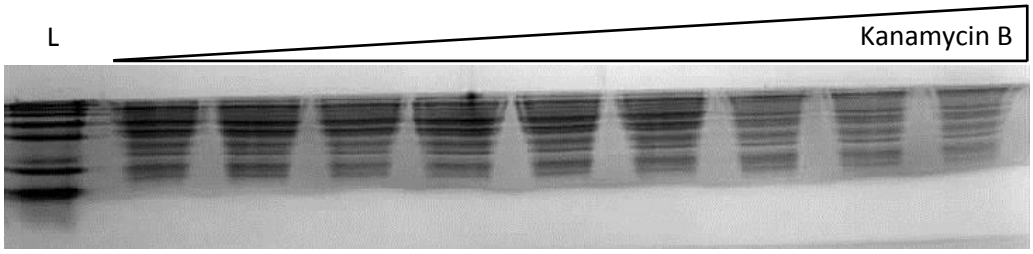

Figure 44. Proteins separation in *E.coli* lysate for proteome change analysis. The lysate of *E.coli* MG1655 cells grown at increasing concentrations of antibiotic (in the example, Kanamycin B 0.25, 0.5, 1, 2, 4, 8, 16, 32, 64, 128 µM) is loaded on the gel. SeeBlue Plus marker is loaded in the first lane L.

To investigate the induction of errors in EF-Tu, 15 µl of lysare are separated on a precasted Mini-PROTEAN TGX Gel (BioRad) 20 min at 200 V. In one lane 5 µl of the SeeBlue Plus marker (Thermo Scientific) are loaded (Figure 45). The gel is stained and destained as already described and the EF-Tu band identified by comparison with the marker, excised with a scalpel and crushed into smaller pieces.

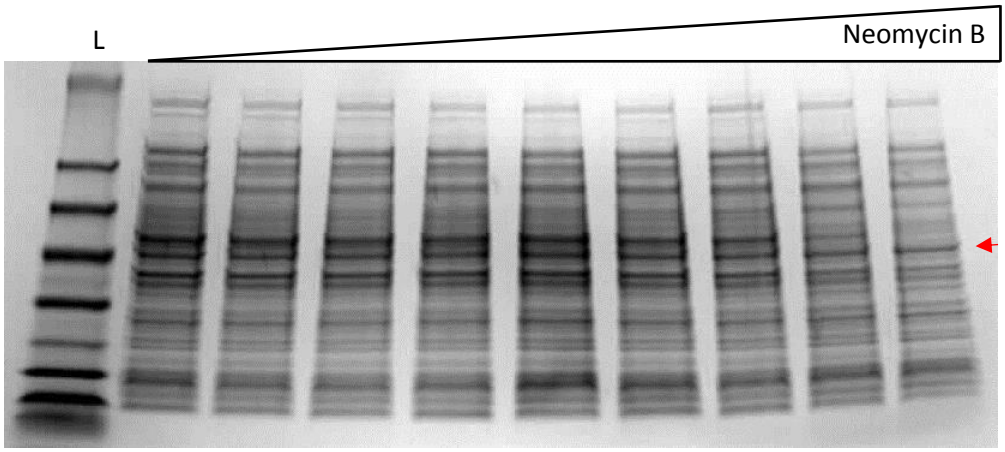

Figure 45. Lysate separation for the quantification of misincorporations in EF-Tu. The lysate of *E.coli* MG1655 cells grown at increasing concentration of antibiotic (in the example, Neomycin B 0.25, 0.5, 1, 2, 4, 8, 16, 32, 64, 128 µM) is loaded on the gel. EF-Tu is indicated by the red arrow. Seeblue Plus marker is loaded in the first lane L.

4.10.1 In-gel proteolysis of EF-Tu, pSUMO-constructs, and *E.coli* lysate

Gel pieces containing the proteins of interest are digested as described by (Shevchenko et al., 2006). Digested peptides are then mixed with heavy-labeled reference peptides before the SRM analysis. For the list of all peptides used, refer to Appendix (Section B).

4.11 Peptides

4.11.1 Selection of proteotypic peptides in EF-Tu

Proteotypic peptides for mass spectrometric absolute quantification are selected from existing mass spectrometry data obtained by data-dependent aquistition (DDA) analysis (from Dr. Ingo Wohlgemuth). In general, only tryptic peptides between 6 and 20 residues are taken into

consideration. The sequence is checked in order to exclude peptides containing highly reactive amino acids (e.g., methionine, tryptophan) or missed cleavage (adjacent KK). Peptides sequence is also checked in BLAST to be unique for the protein target in the case of peptides used for protein quantification (proteotypic (Mallick et al., 2007)) or to exclude a second source in the *E. coli* proteome in the case of peptide used for erroneous peptides enrichment.

4.11.2 Proteolysis of Spike-Tides_TQL

The highly-quantified Spike-Tides_TQL peptides are purchased from JPT (Berlin) and have to be digested prior to mass spectrometric analysis to remove the tag used by the producer for their quantification. The tag is removed by trypsin digestion (1:100) for 5 hrs at 37°C performed as indicated by the producer.

4.11.3 LC-MS/MS method development for peptides detection

The open source program Skyline version 3.5 (MacLean et al., 2010b) is used for the SRM method set up and results analysis (MacLean et al., 2010b). For each peptide of the SRM method, the predominant charge state of the precusor is experimentally assessed and 3 - 5 transitions per peptide are chosen (Lange et al., 2008).

All peptides used in this study are separated on an Easy nLCII Nano LC or Ultimate 3000RSLC system using an in-house packed columns (14 cm length, 50 µm inner diameter, packed with Reprosil-Pur 120 C18 3 µm material) at 50°C or Acclaim PepMapRSLC (15 cm length, 75 µm inner diameter, 2µm RP18 material). Peptides are eluted in a 45 min linear gradient from 5 % ACN/ 0.1 % FA to 50 % ACN/ 0.1 % FA at 0.300 µl/min flow. Q1 and Q3 are set to unit resolution 0.7 full width at half maximum (FWHM) except for non-cognate peptides analysis where it is set at 0.5 . A spray voltage of 1800 V (TSQ Vantage) and 2100 V (TSQ Quantiva) is used with a heated ion transfer tube setting of 270°C (TSQ Vantage) and 325°C (TSQ Quantiva), respectively. The declustering voltage is kept at 10 V (TSQ Vantage) and a Chromfilter setting of 4 (TSQ Vantage) or 3 (TSQ Quantiva). Collision energies are optimized as decribed elsewhere (Maclean et al., 2010a). Scheduled transitions are recorded in a 5 min window and a cycle time of 3 s (TSQ Vantage) or 1 s (TSQ Quantiva) is applied, typically resulting in a dwell time of 100-200 ms per transition.

For data analyisis, raw files are imported into Skyline software that automatically calculates the area under each transition peak to yield the light/heavy ratio for each peptide. To achieve high identification reliability, only peptides with a dot-product (rdotp) close to 1 are considered. The light/heavy ratio of each peptide is ultimately used to calculate the error frequency.

4.11.4 Peptides stability assessment by LC-MS/MS

In order to ensure that the determined peptide concentrations of misincorporation-containing peptides correctly represent their error frequency in the cell, we validated our quantifications in a model system in which these peptides occur at known 1:1 stoichiometry. Misincorporations whose quantification was validated were introduced as point mutations in EF-Tu. EF-Tu mutants were purified and in-gel digested as described previously. Cognate AQUA peptides 1 - 4 are mixed 1:1 with the AQUA peptide containing the amino acid substitution from the mutant under analysis. The AQUA mix is spiked in the sample in a buffer containing 5 % ACN/ 0.1 % FA. 300 fmol of AQUA peptides (Thermo Scientific) and endogenous EF-Tu peptides are separated on an Ultimate 3000RSLC system (Thermo Fisher Scientific) and analyzed in triplicate on a TSQ Quantiva (Thermo Scientific) mass spectrometer in SRM mode (see below for details). Raw files are analyzed using Skyline software and the ratio L/H determined.

4.12 Quantification of EF-Tu for multidimensional enrichment of misincorporation-containing peptides

Absolute quantification of digested EF-Tu is performed by mass spectrometric analysis. The final volume of tryptic digest is determined. 2 µl of the digestion are diluted 1:20 in 5 % ACN/ 0.5 % FA and mixed with varying ratios of cognate AQUA Peptides 1 - 4. The ratio of endogenous/AQUA peptides is determined by SRM (see below for details) analysis performed on TSQ Vantage or TSQ Quantiva (Thermo Scientific) mass spectrometer in triplicate. The ratios calculated for each peptide are averaged and used to determine the amount of digested EF-Tu.

4.12.1 Multidimensional chromatographic enrichment of misincorporation-containing peptides

The tryptic digest is spiked with substoichiometric amounts of AQUA peptides containing the misincorporations of interest (AQUA: proteolyzed EF-Tu; 1:10000). Normally 10 - 15 misincorporation-containing peptides are quantified in a single enrichment. Before the enrichment procedure, Rapigest is degraded by incubating the sample at acidic pH for 30 min at 37°C and its hydrolytic by-products removed by centrifugation. To remove any particles, the supernatant is further filtered using Costar Spin-X Centrifuge Tube Filter 0.45 µm Cellulose Acetate and lyophilized in a SpeedVac vacuum concentrator. Peptides are dissolved in 200 µl 20 % ACN/ 0.1 % FA and separated by size-exclusion chromatography on a Superdex Peptide 10/300 GL column in an isocratic HPLC run (20% ACN/ 0.1 % FA; 0.8 ml/min flow, fraction size 0.4 ml) as a first chromatographic dimension. From each fraction, an aliquot is taken and diluted 1:5 in 0.1 % FA to dilute the final concentration of ACN and analyzed by SRM on TSQ Quantiva mass spectrometer. Depending on the peptides´ distribution, 1 - 3 fractions are

pooled and lyophilized. Pooled peptides are redissolved in 10 mM ammonium acetate in 2 % ACN and separated by reversed phase chromatography at neutral pH in the second dimension (Immler et al., 2006) using a LiChrospher WP300 RP-18 (5 µm) column. Peptides are eluted with a 2 - 82 % ACN gradient in 10 mM ammonium acetate in 45 min run and 0.8 ml/min flow; fraction size 0.8 ml. The elution time for each peptide is established in an independent chromatographic run performed with AQUA peptides only, by screening each fraction by SRM analysis. According to this, respective fractions from the second dimension are selected, lyophilized and resuspended in 50 µl 5 % ACN/ 0.1 % FA for final SRM quantification. For the separation of misincorporation-containing peptides which are similar to their respective cognate one (Table 5), a third step of reversed phase chromatography at acidic pH is performed using the same LiChrospher WP300 RP-18 (5 µm) column used for the separation at neutral pH. Peptides are eluted with a 0 - 65 % ACN gradient in 0.1 % TFA, 10 mM ammonium acetate in 65 min run and 0.8 ml/min flow; fraction size 0.8 ml.

4.13 Validation and quantification of misincorporation-containing peptides

The enriched peptides are separated on nanoflow chromatography system and detected by SRM analysis as described before (Material and metod, 4.11.3).

The identity of enriched peptides is further verified by targeted SIM (tSIM) and parallel reaction monitoring (PRM) on a QExactive mass spectrometer. Peptides are separated by a 58 minute linear reversed phase gradients from 5 % ACN /0.1 % FA to 50 % acetonitrile/ 0.1 % FA on in-house packed columns (28 cm length, packed with Reprosil 1.9 µm C18 material) at 60°C. Eluted peptides are sprayed by an ESI-source set at 2400 V and capillary temperature 275°C in a Q-Exactive Plus mass spectrometer and t-SIM method is set at microscan 1, resolution 70000, ACG target $5e^4$, maximum it 70 ms and scan range 150 to 2000 *m/z* and a 3.0 *m/*z isolation window. PRM method is set at microscan 1, resolution of 35000, AGC target $1e^6$ and maximum IT 300 ms and an isolation windows of 0.4 *m/z* and inclusion list on. Raw files are analyzed using Skyline software. MS1 and MS/MS filtering settings are set at a 60000 *m/z* and 35000 *m/z* resolving power respectively.

4.14 Quantification of error in-gel digested EF-Tu and SUMO-constructs

In-gel digested EF-Tu is lyophilized and resuspended in 50 µl 5% ACN/ 0.1 % by sonication. The sample is centrifuged 10 min at 13000 rpm using a benchtop centrifuge. An aliquot is then taken and mixed with AQUA peptides for the amino acid substitutions to quantify and analyzed by SRM.

4.15 Quantification of stress response proteins in *E. coli* lysate

In-gel digested EF-Tu is lyophilized and resuspended in 50 µl 5 % ACN/ 0.1 % by sonication. For each protein to quantify i.e., EF-Tu, RpoH, S10, IbpA and IbpB 2 - 3 AQUA peptides are spiked in and the sample is analyzed by SRM. For a list of peptides used refer to Appendix (Section B).

4.16 Quadrupole performance assessment

30 fmol of PRTC mix (Thermo Fisher Scientific) are routinely used to check the performances in terms of signal intensity and chromatographic separation of the TSQ Quantiva mass spectrometer and Ultimate 3000RSLC chromatographic system (Figure 46).

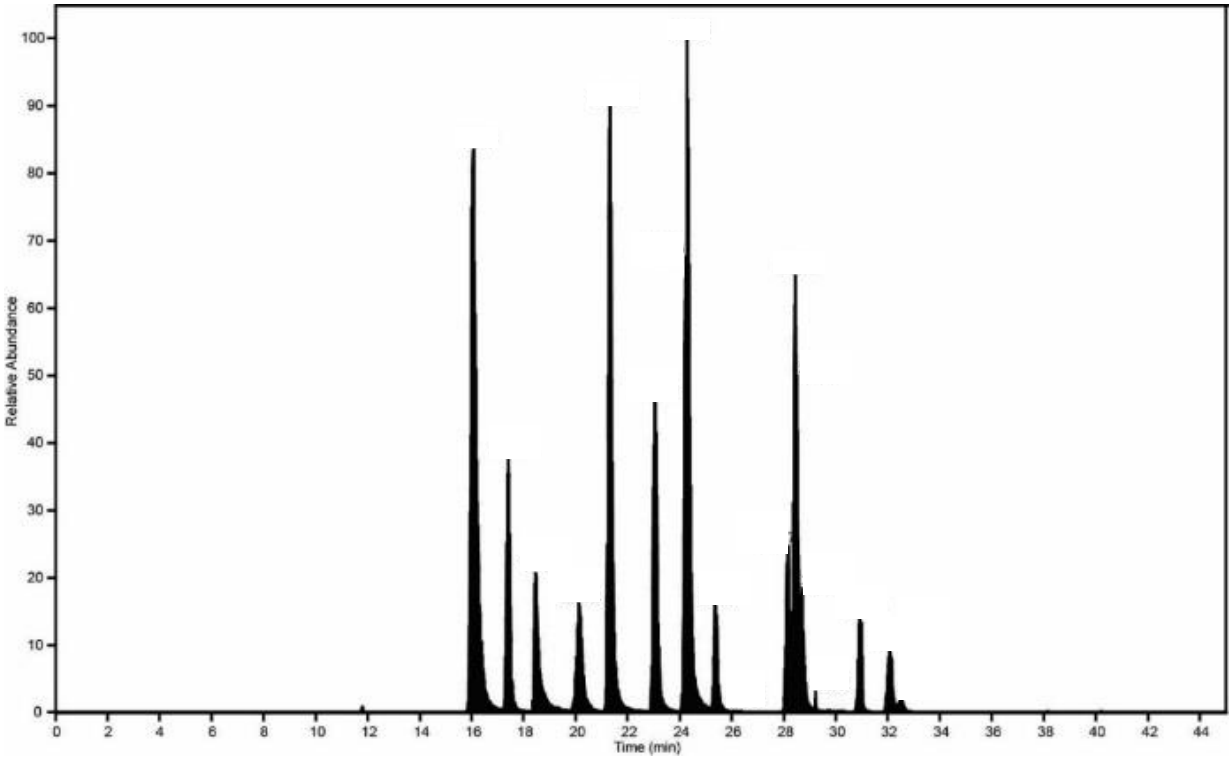

Figure 46. Pierce retention time mix (30 fmol) injected in TSQ Quantiva. Peptides are separated on the base of their hydrophobicit

5. REFERENCES

Abbatiello, S.E., Mani, D.R., Keshishian, H., and Carr, S.A. (2010). Automated detection of inaccurate and imprecise transitions in peptide quantification by multiple reaction monitoring mass spectrometry. Clinical chemistry *56*, 291-305.

Abel, K., Yoder, M.D., Hilgenfeld, R., and Jurnak, F. (1996). An alpha to beta conformational switch in EF-Tu. Structure *4*, 1153-1159.

Akashi, H. (1994). Synonymous codon usage in Drosophila melanogaster: natural selection and translational accuracy. Genetics *136*, 927-935.

Anderson, P., Davies, J., and Davis, B.D. (1967). Effect of spectinomycin on polypeptide synthesis in extracts of Escherichia coli. Journal of molecular biology *29*, 203-215.

Andrews, K.J., and Hegeman, G.D. (1976). Selective disadvantage of non-functional protein synthesis in Escherichia coli. Journal of molecular evolution *8*, 317-328.

Ang, C.S., and Nice, E.C. (2010). Targeted in-gel MRM: a hypothesis driven approach for colorectal cancer biomarker discovery in human feces. Journal of proteome research *9*, 4346-4355.

Aqvist, J., and Kamerlin, S.C. (2015). Exceptionally large entropy contributions enable the high rates of GTP hydrolysis on the ribosome. Scientific reports *5*, 15817.

Arai, K., Clark, B.F., Duffy, L., Jones, M.D., Kaziro, Y., Laursen, R.A., L'Italien, J., Miller, D.L., Nagarkatti, S., Nakamura, S*., et al.* (1980). Primary structure of elongation factor Tu from Escherichia coli. Proceedings of the National Academy of Sciences of the United States of America *77*, 1326-1330.

Archetti, M. (2006). Genetic robustness and selection at the protein level for synonymous codons. Journal of evolutionary biology *19*, 353-365.

Atkins, J.F., Weiss, R.B., Thompson, S., and Gesteland, R.F. (1991). Towards a genetic dissection of the basis of triplet decoding, and its natural subversion: programmed reading frame shifts and hops. Annu Rev Genet *25*, 201-228.

Bantscheff, M., and Kuster, B. (2012). Quantitative mass spectrometry in proteomics. Analytical and bioanalytical chemistry *404*, 937-938.

Belenky, P., Ye, J.D., Porter, C.B., Cohen, N.R., Lobritz, M.A., Ferrante, T., Jain, S., Korry, B.J., Schwarz, E.G., Walker, G.C*., et al.* (2015). Bactericidal Antibiotics Induce Toxic Metabolic Perturbations that Lead to Cellular Damage. Cell Rep *13*, 968-980.

Bentley, W.E., Mirjalili, N., Andersen, D.C., Davis, R.H., and Kompala, D.S. (1990). Plasmid-encoded protein: the principal factor in the "metabolic burden" associated with recombinant bacteria. Biotechnology and bioengineering *35*, 668-681.

Bhattacharjee, S., Deb, J., Dattachaudhuri, A., Tapadar, S.R., Dhua, A., Mukherjee, T., and Ghosh, P. (2012). Unilateral lung hypoplasia: a rare cause of unilateral opaque hemithorax in chest X-ray in a young boy. Indian journal of medical sciences *66*, 192-196.

Bilgin, N., Richter, A.A., Ehrenberg, M., Dahlberg, A.E., and Kurland, C.G. (1990). Ribosomal RNA and protein mutants resistant to spectinomycin. The EMBO journal *9*, 735-739.

Bjork, G.R., Durand, J.M., Hagervall, T.G., Leipuviene, R., Lundgren, H.K., Nilsson, K., Chen, P., Qian, Q., and Urbonavicius, J. (1999). Transfer RNA modification: influence on translational frameshifting and metabolism. FEBS letters *452*, 47-51.

Bloom, J.D., Silberg, J.J., Wilke, C.O., Drummond, D.A., Adami, C., and Arnold, F.H. (2005). Thermodynamic prediction of protein neutrality. Proceedings of the National Academy of Sciences of the United States of America *102*, 606-611.

Bogdanow, B., Zauber, H., and Selbach, M. (2016). Systematic Errors in Peptide and Protein Identification and Quantification by Modified Peptides. Molecular & cellular proteomics : MCP *15*, 2791-2801.

Boon, K., Vijgenboom, E., Madsen, L.V., Talens, A., Kraal, B., and Bosch, L. (1992). Isolation and functional analysis of histidine-tagged elongation factor Tu. European journal of biochemistry *210*, 177-183.

Borovinskaya, M.A., Pai, R.D., Zhang, W., Schuwirth, B.S., Holton, J.M., Hirokawa, G., Kaji, H., Kaji, A., and Cate, J.H. (2007a). Structural basis for aminoglycoside inhibition of bacterial ribosome recycling. Nature structural & molecular biology *14*, 727-732.

Borovinskaya, M.A., Shoji, S., Fredrick, K., and Cate, J.H. (2008). Structural basis for hygromycin B inhibition of protein biosynthesis. RNA *14*, 1590-1599.

Borovinskaya, M.A., Shoji, S., Holton, J.M., Fredrick, K., and Cate, J.H. (2007b). A steric block in translation caused by the antibiotic spectinomycin. ACS chemical biology *2*, 545-552.

Bouadloun, F., Donner, D., and Kurland, C.G. (1983). Codon-specific missense errors in vivo. The EMBO journal *2*, 1351-1356.

Bratulic, S., Gerber, F., and Wagner, A. (2015). Mistranslation drives the evolution of robustness in TEM-1 beta-lactamase. Proceedings of the National Academy of Sciences of the United States of America *112*, 12758-12763.

Bremer, H., and Dennis, P.P. (2008). Modulation of Chemical Composition and Other Parameters of the Cell at Different Exponential Growth Rates. EcoSal Plus *3*.

Brodersen, D.E., Clemons, W.M., Jr., Carter, A.P., Morgan-Warren, R.J., Wimberly, B.T., and Ramakrishnan, V. (2000). The structural basis for the action of the antibiotics tetracycline, pactamycin, and hygromycin B on the 30S ribosomal subunit. Cell *103*, 1143-1154.

Brownridge, P., and Beynon, R.J. (2011). The importance of the digest: proteolysis and absolute quantification in proteomics. Methods *54*, 351-360.

Bryan, L.E., and Kwan, S. (1983). Roles of ribosomal binding, membrane potential, and electron transport in bacterial uptake of streptomycin and gentamicin. Antimicrobial agents and chemotherapy *23*, 835-845.

Bukowy-Bieryllo, Z., Dabrowski, M., Witt, M., and Zietkiewicz, E. (2016). Aminoglycoside-stimulated readthrough of premature termination codons in selected genes involved in primary ciliary dyskinesia. RNA biology *13*, 1041-1050.

Cabanas, M.J., Vazquez, D., and Modolell, J. (1978). Inhibition of ribosomal translocation by aminoglycoside antibiotics. Biochemical and biophysical research communications *83*, 991-997.

Caglayan, M., and Bilgin, N. (2012). Temperature dependence of accuracy of DNA polymerase I from Geobacillus anatolicus. Biochimie *94*, 1968-1973.

Carter, A.P., Clemons, W.M., Brodersen, D.E., Morgan-Warren, R.J., Wimberly, B.T., and Ramakrishnan, V. (2000). Functional insights from the structure of the 30S ribosomal subunit and its interactions with antibiotics. Nature *407*, 340-348.

Chen, G., Liu, H., Wang, X., and Li, Z. (2010). In vitro methylation by methanol: proteomic screening and prevalence investigation. Analytica chimica acta *661*, 67-75.

Chick, J.M., Kolippakkam, D., Nusinow, D.P., Zhai, B., Rad, R., Huttlin, E.L., and Gygi, S.P. (2015). A mass-tolerant database search identifies a large proportion of unassigned spectra in shotgun proteomics as modified peptides. Nature biotechnology *33*, 743-749.

Cox, J., and Mann, M. (2008). MaxQuant enables high peptide identification rates, individualized p.p.b.-range mass accuracies and proteome-wide protein quantification. Nature biotechnology *26*, 1367-1372.

Cox, J., Neuhauser, N., Michalski, A., Scheltema, R.A., Olsen, J.V., and Mann, M. (2011). Andromeda: a peptide search engine integrated into the MaxQuant environment. Journal of proteome research *10*, 1794-1805.

Creasy, D.M., and Cottrell, J.S. (2002). Error tolerant searching of uninterpreted tandem mass spectrometry data. Proteomics *2*, 1426-1434.

Crick, F.H. (1966). Codon--anticodon pairing: the wobble hypothesis. Journal of molecular biology *19*, 548-555.

Crick, F.H., Barnett, L., Brenner, S., and Watts-Tobin, R.J. (1961). General nature of the genetic code for proteins. Nature *192*, 1227-1232.

Curran, J.F., and Yarus, M. (1986). Base substitutions in the tRNA anticodon arm do not degrade the accuracy of reading frame maintenance. Proceedings of the National Academy of Sciences of the United States of America *83*, 6538-6542.

Cvetesic, N., Semanjski, M., Soufi, B., Krug, K., Gruic-Sovulj, I., and Macek, B. (2016). Proteome-wide measurement of non-canonical bacterial mistranslation by quantitative mass spectrometry of protein modifications. Scientific reports *6*, 28631.

Danese, P.N., Snyder, W.B., Cosma, C.L., Davis, L.J., and Silhavy, T.J. (1995). The Cpx two-component signal transduction pathway of Escherichia coli regulates transcription of the gene specifying the stress-inducible periplasmic protease, DegP. Genes & development *9*, 387-398.

Davies, J., Anderson, P., and Davis, B.D. (1965a). Inhibition of protein synthesis by spectinomycin. Science *149*, 1096-1098.

Davies, J., Gilbert, W., and Gorini, L. (1964). Streptomycin, Suppression, and the Code. Proceedings of the National Academy of Sciences of the United States of America *51*, 883-890.

Davies, J., Gorini, L., and Davis, B.D. (1965b). Misreading of RNA codewords induced by aminoglycoside antibiotics. Molecular pharmacology *1*, 93-106.

Davis, B.D. (1987). Mechanism of bactericidal action of aminoglycosides. Microbiological reviews *51*, 341-350.

Davis, B.D., Chen, L.L., and Tai, P.C. (1986). Misread protein creates membrane channels: an essential step in the bactericidal action of aminoglycosides. Proceedings of the National Academy of Sciences of the United States of America *83*, 6164-6168.

Demeshkina, N., Jenner, L., Westhof, E., Yusupov, M., and Yusupova, G. (2012). A new understanding of the decoding principle on the ribosome. Nature *484*, 256-259.

Demeshkina, N., Jenner, L., Westhof, E., Yusupov, M., and Yusupova, G. (2013). New structural insights into the decoding mechanism: translation infidelity via a G.U pair with Watson-Crick geometry. FEBS Lett *587*, 1848-1857.

Demirci, H., Murphy, F.t., Murphy, E., Gregory, S.T., Dahlberg, A.E., and Jogl, G. (2013a). A structural basis for streptomycin-induced misreading of the genetic code. Nature communications *4*, 1355.

Demirci, H., Wang, L., Murphy, F.V.t., Murphy, E.L., Carr, J.F., Blanchard, S.C., Jogl, G., Dahlberg, A.E., and Gregory, S.T. (2013b). The central role of protein S12 in organizing the structure of the decoding site of the ribosome. RNA *19*, 1791-1801.

Dennis, P.P., Ehrenberg, M., and Bremer, H. (2004). Control of rRNA synthesis in Escherichia coli: a systems biology approach. Microbiology and molecular biology reviews : MMBR *68*, 639-668.

Domon, B., and Aebersold, R. (2010). Options and considerations when selecting a quantitative proteomics strategy. Nature biotechnology *28*, 710-721.

Dong, J., Iuchi, S., Kwan, H.S., Lu, Z., and Lin, E.C. (1993). The deduced amino-acid sequence of the cloned cpxR gene suggests the protein is the cognate regulator for the membrane sensor, CpxA, in a two-component signal transduction system of Escherichia coli. Gene *136*, 227-230.

Drummond, D.A., and Wilke, C.O. (2009). The evolutionary consequences of erroneous protein synthesis. Nature reviews Genetics *10*, 715-724.

Dukan, S., Farewell, A., Ballesteros, M., Taddei, F., Radman, M., and Nystrom, T. (2000). Protein oxidation in response to increased transcriptional or translational errors. Proceedings of the National Academy of Sciences of the United States of America *97*, 5746-5749.

Dvorak, P., Chrast, L., Nikel, P.I., Fedr, R., Soucek, K., Sedlackova, M., Chaloupkova, R., de Lorenzo, V., Prokop, Z., and Damborsky, J. (2015). Exacerbation of substrate toxicity by IPTG in Escherichia coli BL21(DE3) carrying a synthetic metabolic pathway. Microbial cell factories *14*, 201.

Dwyer, D.J., Belenky, P.A., Yang, J.H., MacDonald, I.C., Martell, J.D., Takahashi, N., Chan, C.T., Lobritz, M.A., Braff, D., Schwarz, E.G*., et al.* (2014). Antibiotics induce redox-related physiological alterations as part of their lethality. Proceedings of the National Academy of Sciences of the United States of America *111*, E2100-2109.

Dwyer, D.J., Camacho, D.M., Kohanski, M.A., Callura, J.M., and Collins, J.J. (2012). Antibiotic-induced bacterial cell death exhibits physiological and biochemical hallmarks of apoptosis. Molecular cell *46*, 561-572.

Edelmann, P., and Gallant, J. (1977). Mistranslation in E. coli. Cell *10*, 131-137.

Ellis, N., and Gallant, J. (1982). An estimate of the global error frequency in translation. Molecular & general genetics : MGG *188*, 169-172.

Eng, J.K., McCormack, A.L., and Yates, J.R. (1994). An approach to correlate tandem mass spectral data of peptides with amino acid sequences in a protein database. Journal of the American Society for Mass Spectrometry *5*, 976-989.

Erickson, J.W., Vaughn, V., Walter, W.A., Neidhardt, F.C., and Gross, C.A. (1987). Regulation of the promoters and transcripts of rpoH, the Escherichia coli heat shock regulatory gene. Genes & development *1*, 419-432.

Eustice, D.C., and Wilhelm, J.M. (1984a). Fidelity of the eukaryotic codon-anticodon interaction: interference by aminoglycoside antibiotics. Biochemistry *23*, 1462-1467.

Eustice, D.C., and Wilhelm, J.M. (1984b). Mechanisms of action of aminoglycoside antibiotics in eucaryotic protein synthesis. Antimicrobial agents and chemotherapy *26*, 53-60.

Ezraty, B., Vergnes, A., Banzhaf, M., Duverger, Y., Huguenot, A., Brochado, A.R., Su, S.Y., Espinosa, L., Loiseau, L., Py, B.*, et al.* (2013). Fe-S cluster biosynthesis controls uptake of aminoglycosides in a ROS-less death pathway. Science *340*, 1583-1587.

Feldman, M.B., Terry, D.S., Altman, R.B., and Blanchard, S.C. (2010). Aminoglycoside activity observed on single pre-translocation ribosome complexes. Nature chemical biology *6*, 244.

Fersht, A.R. (1977). Editing mechanisms in protein synthesis. Rejection of valine by the isoleucyl-tRNA synthetase. Biochemistry *16*, 1025-1030.

Fischel-Ghodsian, N. (2005). Genetic factors in aminoglycoside toxicity. Pharmacogenomics *6*, 27-36.

Fischer, N., Neumann, P., Konevega, A.L., Bock, L.V., Ficner, R., Rodnina, M.V., and Stark, H. (2015). Structure of the E. coli ribosome-EF-Tu complex at <3 A resolution by Cs-corrected cryo-EM. Nature *520*, 567-570.

Fodor, S., and Zhang, Z. (2006). Rearrangement of terminal amino acid residues in peptides by protease-catalyzed intramolecular transpeptidation. Analytical biochemistry *356*, 282-290.

Fosso, M.Y., Zhu, H., Green, K.D., Garneau-Tsodikova, S., and Fredrick, K. (2015). Tobramycin Variants with Enhanced Ribosome-Targeting Activity. Chembiochem : a European journal of chemical biology *16*, 1565-1570.

Foti, J.J., Devadoss, B., Winkler, J.A., Collins, J.J., and Walker, G.C. (2012). Oxidation of the guanine nucleotide pool underlies cell death by bactericidal antibiotics. Science *336*, 315-319.

Francois, B., Russell, R.J., Murray, J.B., Aboul-ela, F., Masquida, B., Vicens, Q., and Westhof, E. (2005). Crystal structures of complexes between aminoglycosides and decoding A site oligonucleotides: role of the number of rings and positive charges in the specific binding leading to miscoding. Nucleic acids research *33*, 5677-5690.

Frank, A., and Pevzner, P. (2005). PepNovo: de novo peptide sequencing via probabilistic network modeling. Analytical chemistry *77*, 964-973.

Frank, J., and Agrawal, R.K. (2000). A ratchet-like inter-subunit reorganization of the ribosome during translocation. Nature *406*, 318-322.

Freistroffer, D.V., Kwiatkowski, M., Buckingham, R.H., and Ehrenberg, M. (2000). The accuracy of codon recognition by polypeptide release factors. Proc Natl Acad Sci U S A *97*, 2046-2051.

Frewen, B.E., Merrihew, G.E., Wu, C.C., Noble, W.S., and MacCoss, M.J. (2006). Analysis of peptide MS/MS spectra from large-scale proteomics experiments using spectrum libraries. Analytical chemistry *78*, 5678-5684.

Furano, A.V. (1975). Content of elongation factor Tu in Escherichia coli. Proceedings of the National Academy of Sciences of the United States of America *72*, 4780-4784.

Gallien, S., Duriez, E., Crone, C., Kellmann, M., Moehring, T., and Domon, B. (2012). Targeted proteomic quantification on quadrupole-orbitrap mass spectrometer. Molecular & cellular proteomics : MCP *11*, 1709-1723.

Gallien, S., Duriez, E., Demeure, K., and Domon, B. (2013). Selectivity of LC-MS/MS analysis: implication for proteomics experiments. Journal of proteomics *81*, 148-158.

Gerber, S.A., Rush, J., Stemman, O., Kirschner, M.W., and Gygi, S.P. (2003). Absolute quantification of proteins and phosphoproteins from cell lysates by tandem MS. Proceedings of the National Academy of Sciences of the United States of America *100*, 6940-6945.

Gidalevitz, T., Ben-Zvi, A., Ho, K.H., Brignull, H.R., and Morimoto, R.I. (2006). Progressive disruption of cellular protein folding in models of polyglutamine diseases. Science *311*, 1471-1474.

Gill, R.T., Valdes, J.J., and Bentley, W.E. (2000). A comparative study of global stress gene regulation in response to overexpression of recombinant proteins in Escherichia coli. Metabolic engineering *2*, 178-189.

Gillet, L.C., Navarro, P., Tate, S., Rost, H., Selevsek, N., Reiter, L., Bonner, R., and Aebersold, R. (2012). Targeted data extraction of the MS/MS spectra generated by data-independent acquisition: a new concept for consistent and accurate proteome analysis. Molecular & cellular proteomics : MCP *11*, O111 016717.

Gonzalez, A., Jimenez, A., Vazquez, D., Davies, J.E., and Schindler, D. (1978). Studies on the mode of action of hygromycin B, an inhibitor of translocation in eukaryotes. Biochimica et biophysica acta *521*, 459-469.

Gromadski, K.B., Daviter, T., and Rodnina, M.V. (2006). A uniform response to mismatches in codon-anticodon complexes ensures ribosomal fidelity. Molecular cell *21*, 369-377.

Gromadski, K.B., and Rodnina, M.V. (2004a). Kinetic determinants of high-fidelity tRNA discrimination on the ribosome. Molecular cell *13*, 191-200.

Gromadski, K.B., and Rodnina, M.V. (2004b). Streptomycin interferes with conformational coupling between codon recognition and GTPase activation on the ribosome. Nature structural & molecular biology *11*, 316-322.

Grosjean, H.J., de Henau, S., and Crothers, D.M. (1978). On the physical basis for ambiguity in genetic coding interactions. Proceedings of the National Academy of Sciences of the United States of America *75*, 610-614.

Gualerzi, C.O., Brandi, L., Fabbretti, A., Pon, C.L. (2013). Antibiotics: Targets, Mechanisms and Resistance.

Gualerzi, C.O.F., A.; Brandi, L.; Milon, Pohl.; Pon, Cynthia L. (2010). Role of the Initiation Factors in mRNA Start Site Selection and fMet-tRNA recruitment by Bacterial Ribosome. Israel Journal of Biochemistry *50*.

Guo, H.H., Choe, J., and Loeb, L.A. (2004). Protein tolerance to random amino acid change. Proceedings of the National Academy of Sciences of the United States of America *101*, 9205-9210.

Haft, R.J., Keating, D.H., Schwaegler, T., Schwalbach, M.S., Vinokur, J., Tremaine, M., Peters, J.M., Kotlajich, M.V., Pohlmann, E.L., Ong, I.M.*, et al.* (2014). Correcting direct effects of ethanol on translation and transcription machinery confers ethanol tolerance in bacteria. Proceedings of the National Academy of Sciences of the United States of America *111*, E2576-2585.

Hancock, R.E. (1981). Aminoglycoside uptake and mode of action-with special reference to streptomycin and gentamicin. II. Effects of aminoglycosides on cells. The Journal of antimicrobial chemotherapy *8*, 429-445.

Hart-Smith, G., Yagoub, D., Tay, A.P., Pickford, R., and Wilkins, M.R. (2016). Large Scale Mass Spectrometry-based Identifications of Enzyme-mediated Protein Methylation Are Subject to High False Discovery Rates. Molecular & cellular proteomics : MCP *15*, 989-1006.

Ho, C.S., Lam, C.W., Chan, M.H., Cheung, R.C., Law, L.K., Lit, L.C., Ng, K.F., Suen, M.W., and Tai, H.L. (2003). Electrospray ionisation mass spectrometry: principles and clinical applications. The Clinical biochemist Reviews / Australian Association of Clinical Biochemists *24*, 3-12.

Ho, G., Reichardt, J., and Christodoulou, J. (2013). In vitro read-through of phenylalanine hydroxylase (PAH) nonsense mutations using aminoglycosides: a potential therapy for phenylketonuria. Journal of inherited metabolic disease *36*, 955-959.

Holtje, J.V. (1978). Streptomycin uptake via an inducible polyamine transport system in Escherichia coli. European journal of biochemistry *86*, 345-351.

Holtje, J.V. (1979). Induction of streptomycin uptake in resistant strains of Escherichia coli. Antimicrobial agents and chemotherapy *15*, 177-181.

Hong, S., Harris, K.A., Fanning, K.D., Sarachan, K.L., Frohlich, K.M., and Agris, P.F. (2015). Evidence That Antibiotics Bind to Human Mitochondrial Ribosomal RNA Has Implications for Aminoglycoside Toxicity. The Journal of biological chemistry *290*, 19273-19286.

Hopfield, J.J., Yamane, T., Yue, V., and Coutts, S.M. (1976). Direct experimental evidence for kinetic proofreading in amino acylation of tRNAIle. Proceedings of the National Academy of Sciences of the United States of America *73*, 1164-1168.

Hu, Q., Noll, R.J., Li, H., Makarov, A., Hardman, M., and Graham Cooks, R. (2005). The Orbitrap: a new mass spectrometer. Journal of mass spectrometry : JMS *40*, 430-443.

Huang, J., Brieba, L.G., and Sousa, R. (2000). Misincorporation by wild-type and mutant T7 RNA polymerases: identification of interactions that reduce misincorporation rates by stabilizing the catalytically incompetent open conformation. Biochemistry *39*, 11571-11580.

Hurwitz, C., Braun, C.B., and Rosano, C.L. (1981). Role of ribosome recycling in uptake of dihydrostreptomycin by sensitive and resistant Escherichia coli. Biochim Biophys Acta *652*, 168-176.

Ibba, M., and Soll, D. (2000). Aminoacyl-tRNA synthesis. Annual review of biochemistry *69*, 617-650.

Ikemura, T. (1985). Codon usage and tRNA content in unicellular and multicellular organisms. Molecular biology and evolution *2*, 13-34.

Immler, D., Greven, S., and Reinemer, P. (2006). Targeted proteomics in biomarker validation: detection and quantification of proteins using a multi-dimensional peptide separation strategy. Proteomics *6*, 2947-2958.

Isaac, D.D., Pinkner, J.S., Hultgren, S.J., and Silhavy, T.J. (2005). The extracytoplasmic adaptor protein CpxP is degraded with substrate by DegP. Proceedings of the National Academy of Sciences of the United States of America *102*, 17775-17779.

Ito, K., Uno, M., and Nakamura, Y. (2000). A tripeptide 'anticodon' deciphers stop codons in messenger RNA. Nature *403*, 680-684.

Iuchi, S., Furlong, D., and Lin, E.C. (1989). Differentiation of arcA, arcB, and cpxA mutant phenotypes of Escherichia coli by sex pilus formation and enzyme regulation. Journal of bacteriology *171*, 2889-2893.

Jakubowski, H., and Goldman, E. (1992). Editing of errors in selection of amino acids for protein synthesis. Microbiological reviews *56*, 412-429.

Javid, B., Sorrentino, F., Toosky, M., Zheng, W., Pinkham, J.T., Jain, N., Pan, M., Deighan, P., and Rubin, E.J. (2014). Mycobacterial mistranslation is necessary and sufficient for rifampicin phenotypic resistance. Proceedings of the National Academy of Sciences of the United States of America *111*, 1132-1137.

Jawetz, E., Gunnison, J.B., and Speck, R.S. (1951). Antibiotic synergism and antagonism. The New England journal of medicine *245*, 966-968.

Jorgensen, F., and Kurland, C.G. (1990). Processivity errors of gene expression in Escherichia coli. J Mol Biol *215*, 511-521.

Jung, S.Y., Li, Y., Wang, Y., Chen, Y., Zhao, Y., and Qin, J. (2008). Complications in the assignment of 14 and 28 Da mass shift detected by mass spectrometry as in vivo methylation from endogenous proteins. Analytical chemistry *80*, 1721-1729.

Kafri, M., Metzl-Raz, E., Jona, G., and Barkai, N. (2016). The Cost of Protein Production. Cell reports *14*, 22-31.

Keren, I., Wu, Y., Inocencio, J., Mulcahy, L.R., and Lewis, K. (2013). Killing by bactericidal antibiotics does not depend on reactive oxygen species. Science *339*, 1213-1216.

Kimsey, I.J., Petzold, K., Sathyamoorthy, B., Stein, Z.W., and Al-Hashimi, H.M. (2015). Visualizing transient Watson-Crick-like mispairs in DNA and RNA duplexes. Nature *519*, 315-320.

Kjeldgaard, M., and Nyborg, J. (1992). Refined structure of elongation factor EF-Tu from Escherichia coli. Journal of molecular biology *223*, 721-742.

Kohanski, M.A., Dwyer, D.J., Hayete, B., Lawrence, C.A., and Collins, J.J. (2007). A common mechanism of cellular death induced by bactericidal antibiotics. Cell *130*, 797-810.

Kohanski, M.A., Dwyer, D.J., Wierzbowski, J., Cottarel, G., and Collins, J.J. (2008). Mistranslation of membrane proteins and two-component system activation trigger antibiotic-mediated cell death. Cell *135*, 679-690.

Kramer, E.B., and Farabaugh, P.J. (2007). The frequency of translational misreading errors in E. coli is largely determined by tRNA competition. RNA *13*, 87-96.

Kramer, E.B., Vallabhaneni, H., Mayer, L.M., and Farabaugh, P.J. (2010). A comprehensive analysis of translational missense errors in the yeast Saccharomyces cerevisiae. RNA *16*, 1797-1808.

Kuczynska-Wisnik, D., Laskowska, E., and Taylor, A. (2001). Transcription of the ibpB heat-shock gene is under control of sigma(32)- and sigma(54)-promoters, a third regulon of heat-shock response. Biochemical and biophysical research communications *284*, 57-64.

Kunkel, T.A. (2004). DNA replication fidelity. The Journal of biological chemistry *279*, 16895-16898.

Kunkel, T.A., and Bebenek, K. (2000). DNA replication fidelity. Annual review of biochemistry *69*, 497-529.

Kurland, C.G. (1992). Translational accuracy and the fitness of bacteria. Annual review of genetics *26*, 29-50.

Kurland, C.G., Rigler, R., Ehrenberg, M., and Blomberg, C. (1975). Allosteric mechanism for codon-dependent tRNA selection on ribosomes. Proceedings of the National Academy of Sciences of the United States of America *72*, 4248-4251.

Laemmli, U.K. (1970). Cleavage of structural proteins during the assembly of the head of bacteriophage T4. Nature *227*, 680-685.

Lange, V., Picotti, P., Domon, B., and Aebersold, R. (2008). Selected reaction monitoring for quantitative proteomics: a tutorial. Molecular systems biology *4*, 222.

Laskowska, E., Wawrzynow, A., and Taylor, A. (1996). IbpA and IbpB, the new heat-shock proteins, bind to endogenous Escherichia coli proteins aggregated intracellularly by heat shock. Biochimie *78*, 117-122.

Lee, J.W., Beebe, K., Nangle, L.A., Jang, J., Longo-Guess, C.M., Cook, S.A., Davisson, M.T., Sundberg, J.P., Schimmel, P., and Ackerman, S.L. (2006). Editing-defective tRNA synthetase causes protein misfolding and neurodegeneration. Nature *443*, 50-55.

Lee, Y., Zhou, T., Tartaglia, G.G., Vendruscolo, M., and Wilke, C.O. (2010). Translationally optimal codons associate with aggregation-prone sites in proteins. Proteomics *10*, 4163-4171.

Li, L., Boniecki, M.T., Jaffe, J.D., Imai, B.S., Yau, P.M., Luthey-Schulten, Z.A., and Martinis, S.A. (2011). Naturally occurring aminoacyl-tRNA synthetases editing-domain mutations that cause mistranslation in Mycoplasma parasites. Proceedings of the National Academy of Sciences of the United States of America *108*, 9378-9383.

Liao, H., Wu, J., Kuhn, E., Chin, W., Chang, B., Jones, M.D., O'Neil, S., Clauser, K.R., Karl, J., Hasler, F.*, et al.* (2004). Use of mass spectrometry to identify protein biomarkers of disease severity in the synovial fluid and serum of patients with rheumatoid arthritis. Arthritis and rheumatism *50*, 3792-3803.

Lin, D., Tabb, D.L., and Yates, J.R., 3rd (2003). Large-scale protein identification using mass spectrometry. Biochimica et biophysica acta *1646*, 1-10.

Lindahl, L., Jaskunas, S.R., Dennis, P.P., and Nomura, M. (1975). Cluster of genes in Escherichia coli for ribosomal proteins, ribosomal RNA, and RNA polymerase subunits. Proceedings of the National Academy of Sciences of the United States of America *72*, 2743-2747.

Ling, J., Cho, C., Guo, L.T., Aerni, H.R., Rinehart, J., and Soll, D. (2012). Protein aggregation caused by aminoglycoside action is prevented by a hydrogen peroxide scavenger. Molecular cell *48*, 713-722.

Ling, J., and Soll, D. (2010). Severe oxidative stress induces protein mistranslation through impairment of an aminoacyl-tRNA synthetase editing site. Proceedings of the National Academy of Sciences of the United States of America *107*, 4028-4033.

Liu, Y., and Imlay, J.A. (2013). Cell death from antibiotics without the involvement of reactive oxygen species. Science *339*, 1210-1213.

Loftfield, R.B., and Vanderjagt, D. (1972). The frequency of errors in protein biosynthesis. The Biochemical journal *128*, 1353-1356.

Ma, B., Zhang, K., Hendrie, C., Liang, C., Li, M., Doherty-Kirby, A., and Lajoie, G. (2003). PEAKS: powerful software for peptide de novo sequencing by tandem mass spectrometry. Rapid communications in mass spectrometry : RCM *17*, 2337-2342.

Maclean, B., Tomazela, D.M., Abbatiello, S.E., Zhang, S., Whiteaker, J.R., Paulovich, A.G., Carr, S.A., and Maccoss, M.J. (2010a). Effect of collision energy optimization on the measurement of peptides by selected reaction monitoring (SRM) mass spectrometry. Analytical chemistry *82*, 10116-10124.

MacLean, B., Tomazela, D.M., Shulman, N., Chambers, M., Finney, G.L., Frewen, B., Kern, R., Tabb, D.L., Liebler, D.C., and MacCoss, M.J. (2010b). Skyline: an open source document editor for creating and analyzing targeted proteomics experiments. Bioinformatics *26*, 966-968.

Malik, V., Rodino-Klapac, L.R., Viollet, L., and Mendell, J.R. (2010a). Aminoglycoside-induced mutation suppression (stop codon readthrough) as a therapeutic strategy for Duchenne muscular dystrophy. Therapeutic advances in neurological disorders *3*, 379-389.

Malik, V., Rodino-Klapac, L.R., Viollet, L., Wall, C., King, W., Al-Dahhak, R., Lewis, S., Shilling, C.J., Kota, J., Serrano-Munuera, C.*, et al.* (2010b). Gentamicin-induced readthrough of stop codons in Duchenne muscular dystrophy. Annals of neurology *67*, 771-780.

Mallick, P., Schirle, M., Chen, S.S., Flory, M.R., Lee, H., Martin, D., Ranish, J., Raught, B., Schmitt, R., Werner, T.*, et al.* (2007). Computational prediction of proteotypic peptides for quantitative proteomics. Nature biotechnology *25*, 125-131.

Manickam, N., Nag, N., Abbasi, A., Patel, K., and Farabaugh, P.J. (2014). Studies of translational misreading in vivo show that the ribosome very efficiently discriminates against most potential errors. RNA *20*, 9-15.

Mann, M., and Wilm, M. (1994). Error-tolerant identification of peptides in sequence databases by peptide sequence tags. Analytical chemistry *66*, 4390-4399.

Manning, M.C., Chou, D.K., Murphy, B.M., Payne, R.W., and Katayama, D.S. (2010). Stability of protein pharmaceuticals: an update. Pharmaceutical research *27*, 544-575.

Matt, T., Ng, C.L., Lang, K., Sha, S.H., Akbergenov, R., Shcherbakov, D., Meyer, M., Duscha, S., Xie, J., Dubbaka, S.R.*, et al.* (2012). Dissociation of antibacterial activity and aminoglycoside ototoxicity in the 4-monosubstituted 2-deoxystreptamine apramycin. Proceedings of the National Academy of Sciences of the United States of America *109*, 10984-10989.

McGaha, S.M., and Champney, W.S. (2007). Hygromycin B inhibition of protein synthesis and ribosome biogenesis in Escherichia coli. Antimicrobial agents and chemotherapy *51*, 591-596.

Meng, F., Cargile, B.J., Patrie, S.M., Johnson, J.R., McLoughlin, S.M., and Kelleher, N.L. (2002). Processing complex mixtures of intact proteins for direct analysis by mass spectrometry. Analytical chemistry *74*, 2923-2929.

Meyerovich, M., Mamou, G., and Ben-Yehuda, S. (2010). Visualizing high error levels during gene expression in living bacterial cells. Proceedings of the National Academy of Sciences of the United States of America *107*, 11543-11548.

Michalski, A., Cox, J., and Mann, M. (2011). More than 100,000 detectable peptide species elute in single shotgun proteomics runs but the majority is inaccessible to data-dependent LC-MS/MS. Journal of proteome research *10*, 1785-1793.

Milon, P., and Rodnina, M.V. (2012). Kinetic control of translation initiation in bacteria. Critical reviews in biochemistry and molecular biology *47*, 334-348.

Miroux, B., and Walker, J.E. (1996). Over-production of proteins in Escherichia coli: mutant hosts that allow synthesis of some membrane proteins and globular proteins at high levels. Journal of molecular biology *260*, 289-298.

Misumi, M., Nishimura, T., Komai, T., and Tanaka, N. (1978). Interaction of kanamycin and related antibiotics with the large subunit of ribosomes and the inhibition of translocation. Biochemical and biophysical research communications *84*, 358-365.

Moazed, D., and Noller, H.F. (1987). Interaction of antibiotics with functional sites in 16S ribosomal RNA. Nature *327*, 389-394.

Muhlhausen, S., Findeisen, P., Plessmann, U., Urlaub, H., and Kollmar, M. (2016). A novel nuclear genetic code alteration in yeasts and the evolution of codon reassignment in eukaryotes. Genome research *26*, 945-955.

Muramatsu, R., Misawa, S., and Hayashi, H. (2003). Finding of an isoleucine derivative of a recombinant protein for pharmaceutical use. Journal of pharmaceutical and biomedical analysis *31*, 979-987.

Netzer, N., Goodenbour, J.M., David, A., Dittmar, K.A., Jones, R.B., Schneider, J.R., Boone, D., Eves, E.M., Rosner, M.R., Gibbs, J.S.*, et al.* (2009). Innate immune and chemically triggered oxidative stress modifies translational fidelity. Nature *462*, 522-526.

Ogle, J.M., Brodersen, D.E., Clemons, W.M., Jr., Tarry, M.J., Carter, A.P., and Ramakrishnan, V. (2001). Recognition of cognate transfer RNA by the 30S ribosomal subunit. Science *292*, 897-902.

Ogle, J.M., Carter, A.P., and Ramakrishnan, V. (2003). Insights into the decoding mechanism from recent ribosome structures. Trends in biochemical sciences *28*, 259-266.

Ogle, J.M., Murphy, F.V., Tarry, M.J., and Ramakrishnan, V. (2002). Selection of tRNA by the ribosome requires a transition from an open to a closed form. Cell *111*, 721-732.

Ong, S.E., and Mann, M. (2005). Mass spectrometry-based proteomics turns quantitative. Nature chemical biology *1*, 252-262.

Pape, T., Wintermeyer, W., and Rodnina, M. (1999). Induced fit in initial selection and proofreading of aminoacyl-tRNA on the ribosome. The EMBO journal *18*, 3800-3807.

Pape, T., Wintermeyer, W., and Rodnina, M.V. (1998). Complete kinetic mechanism of elongation factor Tu-dependent binding of aminoacyl-tRNA to the A site of the E. coli ribosome. The EMBO journal *17*, 7490-7497.

Pape, T., Wintermeyer, W., and Rodnina, M.V. (2000). Conformational switch in the decoding region of 16S rRNA during aminoacyl-tRNA selection on the ribosome. Nature structural biology *7*, 104-107.

Parker, J. (1989). Errors and alternatives in reading the universal genetic code. Microbiological reviews *53*, 273-298.

Parker, J., Johnston, T.C., and Borgia, P.T. (1980). Mistranslation in cells infected with the bacteriophage MS2: direct evidence of Lys for Asn substitution. Molecular & general genetics : MGG *180*, 275-281.

Parker, J., Johnston, T.C., Borgia, P.T., Holtz, G., Remaut, E., and Fiers, W. (1983). Codon usage and mistranslation. In vivo basal level misreading of the MS2 coat protein message. The Journal of biological chemistry *258*, 10007-10012.

Perkins, D.N., Pappin, D.J., Creasy, D.M., and Cottrell, J.S. (1999). Probability-based protein identification by searching sequence databases using mass spectrometry data. Electrophoresis *20*, 3551-3567.

Perzynski, S., Cannon, M., Cundliffe, E., Chahwala, S.B., and Davies, J. (1979). Effects of apramycin, a novel aminoglycoside antibiotic on bacterial protein synthesis. European journal of biochemistry / FEBS *99*, 623-628.

Peske, F., Rodnina, M.V., and Wintermeyer, W. (2005). Sequence of steps in ribosome recycling as defined by kinetic analysis. Molecular cell *18*, 403-412.

Peske, F., Savelsbergh, A., Katunin, V.I., Rodnina, M.V., and Wintermeyer, W. (2004). Conformational changes of the small ribosomal subunit during elongation factor G-dependent tRNA-mRNA translocation. Journal of molecular biology *343*, 1183-1194.

Peterson, A.C., Russell, J.D., Bailey, D.J., Westphall, M.S., and Coon, J.J. (2012). Parallel reaction monitoring for high resolution and high mass accuracy quantitative, targeted proteomics. Molecular & cellular proteomics : MCP *11*, 1475-1488.

Picotti, P., and Aebersold, R. (2012). Selected reaction monitoring-based proteomics: workflows, potential, pitfalls and future directions. Nature methods *9*, 555-566.

Picotti, P., Aebersold, R., and Domon, B. (2007). The implications of proteolytic background for shotgun proteomics. Molecular & cellular proteomics : MCP *6*, 1589-1598.

Pogliano, J., Lynch, A.S., Belin, D., Lin, E.C., and Beckwith, J. (1997). Regulation of Escherichia coli cell envelope proteins involved in protein folding and degradation by the Cpx two-component system. Genes & development *11*, 1169-1182.

Ram Prasad, B., and Warshel, A. (2011). Prechemistry versus preorganization in DNA replication fidelity. Proteins *79*, 2900-2919.

Ramu, H., Vazquez-Laslop, N., Klepacki, D., Dai, Q., Piccirilli, J., Micura, R., and Mankin, A.S. (2011). Nascent peptide in the ribosome exit tunnel affects functional properties of the A-site of the peptidyl transferase center. Molecular cell *41*, 321-330.

Ranjan, N., and Rodnina, M.V. (2016). tRNA wobble modifications and protein homeostasis. Translation (Austin) *4*, e1143076.

Reha-Krantz, L.J. (2010). DNA polymerase proofreading: Multiple roles maintain genome stability. Biochimica et biophysica acta *1804*, 1049-1063.

Ribas de Pouplana, L., Santos, M.A., Zhu, J.H., Farabaugh, P.J., and Javid, B. (2014). Protein mistranslation: friend or foe? Trends in biochemical sciences *39*, 355-362.

Rodnina, M.V., Fricke, R., Kuhn, L., and Wintermeyer, W. (1995a). Codon-dependent conformational change of elongation factor Tu preceding GTP hydrolysis on the ribosome. The EMBO journal *14*, 2613-2619.

Rodnina, M.V., Pape, T., Fricke, R., and Wintermeyer, W. (1995b). Elongation factor Tu, a GTPase triggered by codon recognition on the ribosome: mechanism and GTP consumption. Biochemistry and cell biology = Biochimie et biologie cellulaire *73*, 1221-1227.

Rodnina, M.V., and Wintermeyer, W. (1995). GTP consumption of elongation factor Tu during translation of heteropolymeric mRNAs. Proceedings of the National Academy of Sciences of the United States of America *92*, 1945-1949.

Rodnina, M.V., and Wintermeyer, W. (2001a). Fidelity of aminoacyl-tRNA selection on the ribosome: kinetic and structural mechanisms. Annual review of biochemistry *70*, 415-435.

Rodnina, M.V., and Wintermeyer, W. (2001b). Ribosome fidelity: tRNA discrimination, proofreading and induced fit. Trends in biochemical sciences *26*, 124-130.

Roepstorff, P., and Fohlman, J. (1984). Proposal for a common nomenclature for sequence ions in mass spectra of peptides. Biomedical mass spectrometry *11*, 601.

Ronson, C.W., Nixon, B.T., and Ausubel, F.M. (1987). Conserved domains in bacterial regulatory proteins that respond to environmental stimuli. Cell *49*, 579-581.

Rosset, R., and Gorini, L. (1969). A ribosomal ambiguity mutation. Journal of molecular biology *39*, 95-112.

Rozov, A., Demeshkina, N., Westhof, E., Yusupov, M., and Yusupova, G. (2015). Structural insights into the translational infidelity mechanism. Nature communications *6*, 7251.

Rozov, A., Demeshkina, N., Westhof, E., Yusupov, M., and Yusupova, G. (2016). New Structural Insights into Translational Miscoding. Trends in biochemical sciences.

Ruan, B., Palioura, S., Sabina, J., Marvin-Guy, L., Kochhar, S., Larossa, R.A., and Soll, D. (2008). Quality control despite mistranslation caused by an ambiguous genetic code. Proceedings of the National Academy of Sciences of the United States of America *105*, 16502-16507.

Russell, J.B., and Cook, G.M. (1995). Energetics of bacterial growth: balance of anabolic and catabolic reactions. Microbiological reviews *59*, 48-62.

Ruusala, T., Andersson, D., Ehrenberg, M., and Kurland, C.G. (1984). Hyper-accurate ribosomes inhibit growth. The EMBO journal *3*, 2575-2580.

Ruusala, T., Ehrenberg, M., and Kurland, C.G. (1982). Is there proofreading during polypeptide synthesis? The EMBO journal *1*, 741-745.

Saiki, R.K., Scharf, S., Faloona, F., Mullis, K.B., Horn, G.T., Erlich, H.A., and Arnheim, N. (1985). Enzymatic amplification of beta-globin genomic sequences and restriction site analysis for diagnosis of sickle cell anemia. Science *230*, 1350-1354.

Sandhu, C., Hewel, J.A., Badis, G., Talukder, S., Liu, J., Hughes, T.R., and Emili, A. (2008). Evaluation of data-dependent versus targeted shotgun proteomic approaches for monitoring transcription factor expression in breast cancer. Journal of proteome research *7*, 1529-1541.

Schaaper, R.M. (1993). Base selection, proofreading, and mismatch repair during DNA replication in Escherichia coli. The Journal of biological chemistry *268*, 23762-23765.

Schaefer, H., Chamrad, D.C., Marcus, K., Reidegeld, K.A., Bluggel, M., and Meyer, H.E. (2005). Tryptic transpeptidation products observed in proteome analysis by liquid chromatography-tandem mass spectrometry. Proteomics *5*, 846-852.

Scheunemann, A.E., Graham, W.D., Vendeix, F.A., and Agris, P.F. (2010). Binding of aminoglycoside antibiotics to helix 69 of 23S rRNA. Nucleic acids research *38*, 3094-3105.

Schmeing, T.M., and Ramakrishnan, V. (2009). What recent ribosome structures have revealed about the mechanism of translation. Nature *461*, 1234-1242.

Schmidt, A., Kochanowski, K., Vedelaar, S., Ahrne, E., Volkmer, B., Callipo, L., Knoops, K., Bauer, M., Aebersold, R., and Heinemann, M. (2016). The quantitative and condition-dependent Escherichia coli proteome. Nature biotechnology *34*, 104-110.

Scorer, C.A., Carrier, M.J., and Rosenberger, R.F. (1991). Amino acid misincorporation during high-level expression of mouse epidermal growth factor in Escherichia coli. Nucleic acids research *19*, 3511-3516.

Scott, M., Gunderson, C.W., Mateescu, E.M., Zhang, Z., and Hwa, T. (2010). Interdependence of cell growth and gene expression: origins and consequences. Science *330*, 1099-1102.

Sherman, J., McKay, M.J., Ashman, K., and Molloy, M.P. (2009). How specific is my SRM?: The issue of precursor and product ion redundancy. Proteomics *9*, 1120-1123.

Sherwood, C.A., Eastham, A., Lee, L.W., Risler, J., Vitek, O., and Martin, D.B. (2009). Correlation between y-type ions observed in ion trap and triple quadrupole mass spectrometers. Journal of proteome research *8*, 4243-4251.

Shevchenko, A., Tomas, H., Havlis, J., Olsen, J.V., and Mann, M. (2006). In-gel digestion for mass spectrometric characterization of proteins and proteomes. Nature protocols *1*, 2856-2860.

Shi, T., Su, D., Liu, T., Tang, K., Camp, D.G., 2nd, Qian, W.J., and Smith, R.D. (2012). Advancing the sensitivity of selected reaction monitoring-based targeted quantitative proteomics. Proteomics *12*, 1074-1092.

Shilov, I.V., Seymour, S.L., Patel, A.A., Loboda, A., Tang, W.H., Keating, S.P., Hunter, C.L., Nuwaysir, L.M., and Schaeffer, D.A. (2007). The Paragon Algorithm, a next generation search engine that uses sequence temperature values and feature probabilities to identify peptides from tandem mass spectra. Molecular & cellular proteomics : MCP *6*, 1638-1655.

Shine, J., and Dalgarno, L. (1974). The 3'-terminal sequence of Escherichia coli 16S ribosomal RNA: complementarity to nonsense triplets and ribosome binding sites. Proceedings of the National Academy of Sciences of the United States of America *71*, 1342-1346.

Shuford, C.M., Sederoff, R.R., Chiang, V.L., and Muddiman, D.C. (2012). Peptide production and decay rates affect the quantitative accuracy of protein cleavage isotope dilution mass spectrometry (PC-IDMS). Molecular & cellular proteomics : MCP *11*, 814-823.

Sin, C., Chiarugi, D., and Valleriani, A. (2016). Quantitative assessment of ribosome drop-off in E. coli. Nucleic Acids Res *44*, 2528-2537.

Soll, D. (1990). The accuracy of aminoacylation--ensuring the fidelity of the genetic code. Experientia *46*, 1089-1096.

Stahl-Zeng, J., Lange, V., Ossola, R., Eckhardt, K., Krek, W., Aebersold, R., and Domon, B. (2007). High sensitivity detection of plasma proteins by multiple reaction monitoring of N-glycosites. Molecular & cellular proteomics : MCP *6*, 1809-1817.

Stansfield, I., Jones, K.M., Herbert, P., Lewendon, A., Shaw, W.V., and Tuite, M.F. (1998). Missense translation errors in Saccharomyces cerevisiae. Journal of molecular biology *282*, 13-24.

Steitz, T.A., and Moore, P.B. (2003). RNA, the first macromolecular catalyst: the ribosome is a ribozyme. Trends in biochemical sciences *28*, 411-418.

Sumpton, D., and Bienvenut, W. (2009). Coomassie stains: are they really mass spectrometry compatible? Rapid communications in mass spectrometry : RCM *23*, 1525-1529.

Surinova, S., Schiess, R., Huttenhain, R., Cerciello, F., Wollscheid, B., and Aebersold, R. (2011). On the development of plasma protein biomarkers. Journal of proteome research *10*, 5-16.

Sydow, J.F., and Cramer, P. (2009). RNA polymerase fidelity and transcriptional proofreading. Current opinion in structural biology *19*, 732-739.

Sydow, J.F., Lipsmeier, F., Larraillet, V., Hilger, M., Mautz, B., Molhoj, M., Kuentzer, J., Klostermann, S., Schoch, J., Voelger, H.R*., et al.* (2014). Structure-based prediction of asparagine and aspartate degradation sites in antibody variable regions. PloS one *9*, e100736.

Taber, H.W., Mueller, J.P., Miller, P.F., and Arrow, A.S. (1987). Bacterial uptake of aminoglycoside antibiotics. Microbiological reviews *51*, 439-457.

Tanaka, N., Sashikata, K., and Umezawa, H. (1967). Antibiotic-sensitivity of ribosomes from kanamycin-resistant E. coli. The Journal of antibiotics *20*, 115-119.

Tawfik, D.S. (2014). Accuracy-rate tradeoffs: how do enzymes meet demands of selectivity and catalytic efficiency? Curr Opin Chem Biol *21*, 73-80.

Taylor, G. (1964). Disintegration of Water Drops in an Electric Field. Proceedings of the Royal Society of London A: Mathematical, Physical and Engineering Sciences *280*, 383-397.

Thompson, R.C., and Stone, P.J. (1977). Proofreading of the codon-anticodon interaction on ribosomes. Proceedings of the National Academy of Sciences *74*, 198-202.

Toth, M.J., Murgola, E.J., and Schimmel, P. (1988). Evidence for a unique first position codon-anticodon mismatch in vivo. Journal of molecular biology *201*, 451-454.

Traverse, C.C., and Ochman, H. (2016). Conserved rates and patterns of transcription errors across bacterial growth states and lifestyles. Proceedings of the National Academy of Sciences of the United States of America *113*, 3311-3316.

Tsai, A., Uemura, S., Johansson, M., Puglisi, E.V., Marshall, R.A., Aitken, C.E., Korlach, J., Ehrenberg, M., and Puglisi, J.D. (2013). The impact of aminoglycosides on the dynamics of translation elongation. Cell reports *3*, 497-508.

Tuckey, C., Asahara, H., Zhou, Y., and Chong, S. (2014). Protein synthesis using a reconstituted cell-free system. Current protocols in molecular biology / edited by Frederick M Ausubel [et al] *108*, 16 31 11-22.

Valledor, L., Castillejo, M.A., Lenz, C., Rodriguez, R., Canal, M.J., and Jorrin, J. (2008). Proteomic analysis of Pinus radiata needles: 2-DE map and protein identification by LC/MS/MS and substitution-tolerant database searching. Journal of proteome research *7*, 2616-2631.

Van Noort, J.M., Kraal, B., Sinjorgo, K.M., Persoon, N.L., Johanns, E.S., and Bosch, L. (1986). Methylation in vivo of elongation factor EF-Tu at lysine-56 decreases the rate of tRNA-dependent GTP hydrolysis. European journal of biochemistry / FEBS *160*, 557-561.

Vermulst, M., Denney, A.S., Lang, M.J., Hung, C.W., Moore, S., Moseley, M.A., Thompson, J.W., Madden, V., Gauer, J., Wolfe, K.J.*, et al.* (2015). Transcription errors induce proteotoxic stress and shorten cellular lifespan. Nature communications *6*, 8065.

Vicens, Q., and Westhof, E. (2002). Crystal structure of a complex between the aminoglycoside tobramycin and an oligonucleotide containing the ribosomal decoding a site. Chemistry & biology *9*, 747-755.

von Heijne, G. (1989). Control of topology and mode of assembly of a polytopic membrane protein by positively charged residues. Nature *341*, 456-458.

Wagner, G.R., and Hirschey, M.D. (2014). Nonenzymatic protein acylation as a carbon stress regulated by sirtuin deacylases. Molecular cell *54*, 5-16.

Walton, J.R. (1978). Apramycin, a new aminocyclitol antibiotic. I. In vitro microbiological studies. The Journal of antimicrobial chemotherapy *4*, 309-313.

Wang, H., Xiao, Y., Fu, L., Zhao, H., Zhang, Y., Wan, X., Qin, Y., Huang, Y., Gao, H., and Li, X. (2010). High-level expression and purification of soluble recombinant FGF21 protein by SUMO fusion in Escherichia coli. BMC biotechnology *10*, 14.

Wang, L., Pulk, A., Wasserman, M.R., Feldman, M.B., Altman, R.B., Cate, J.H., and Blanchard, S.C. (2012). Allosteric control of the ribosome by small-molecule antibiotics. Nat Struct Mol Biol *19*, 957-963.

Wasserman, M.R., Pulk, A., Zhou, Z., Altman, R.B., Zinder, J.C., Green, K.D., Garneau-Tsodikova, S., Cate, J.H., and Blanchard, S.C. (2015). Chemically related 4,5-linked aminoglycoside antibiotics drive subunit rotation in opposite directions. Nat Commun *6*, 7896.

Weinert, B.T., Iesmantavicius, V., Wagner, S.A., Scholz, C., Gummesson, B., Beli, P., Nystrom, T., and Choudhary, C. (2013). Acetyl-phosphate is a critical determinant of lysine acetylation in E. coli. Molecular cell *51*, 265-272.

Westhof, E., Yusupov, M., and Yusupova, G. (2014). Recognition of Watson-Crick base pairs: constraints and limits due to geometric selection and tautomerism. F1000prime reports *6*, 19.

Wickner, S., Maurizi, M.R., and Gottesman, S. (1999). Posttranslational quality control: folding, refolding, and degrading proteins. Science *286*, 1888-1893.

Wiegand, I., Hilpert, K., and Hancock, R.E. (2008). Agar and broth dilution methods to determine the minimal inhibitory concentration (MIC) of antimicrobial substances. Nature protocols *3*, 163-175.

Woese, C.R. (1965). On the evolution of the genetic code. Proceedings of the National Academy of Sciences of the United States of America *54*, 1546-1552.

Wohlgemuth, I., Pohl, C., and Rodnina, M.V. (2010). Optimization of speed and accuracy of decoding in translation. The EMBO journal *29*, 3701-3709.

Worboys, J.D., Sinclair, J., Yuan, Y., and Jorgensen, C. (2014). Systematic evaluation of quantotypic peptides for targeted analysis of the human kinome. Nature methods *11*, 1041-1044.

Wright, G.D. (1999). Aminoglycoside-modifying enzymes. Current opinion in microbiology *2*, 499-503.

Wu, X., Held, K., Zheng, C., Staudinger, B.J., Chavez, J.D., Weisbrod, C.R., Eng, J.K., Singh, P.K., Manoil, C., and Bruce, J.E. (2015). Dynamic Proteome Response of Pseudomonas aeruginosa to Tobramycin Antibiotic Treatment. Molecular & cellular proteomics : MCP *14*, 2126-2137.

Yates, J.R., 3rd (2004). Mass spectral analysis in proteomics. Annual review of biophysics and biomolecular structure *33*, 297-316.

Yikilmaz, E., Chapman, S.J., Schrader, J.M., and Uhlenbeck, O.C. (2014). The interface between Escherichia coli elongation factor Tu and aminoacyl-tRNA. Biochemistry *53*, 5710-5720.

Young, R., and Bremer, H. (1976). Polypeptide-chain-elongation rate in Escherichia coli B/r as a function of growth rate. The Biochemical journal *160*, 185-194.

Yu, X.C., Borisov, O.V., Alvarez, M., Michels, D.A., Wang, Y.J., and Ling, V. (2009). Identification of codon-specific serine to asparagine mistranslation in recombinant monoclonal antibodies by high-resolution mass spectrometry. Analytical chemistry *81*, 9282-9290.

Zaborske, J.M., DuMont, V.L., Wallace, E.W., Pan, T., Aquadro, C.F., and Drummond, D.A. (2014). A nutrient-driven tRNA modification alters translational fidelity and genome-wide protein coding across an animal genus. PLoS biology *12*, e1002015.

Zaher, H.S., and Green, R. (2009). Quality control by the ribosome following peptide bond formation. Nature *457*, 161-166.

Zaher, H.S., and Green, R. (2010a). Hyperaccurate and error-prone ribosomes exploit distinct mechanisms during tRNA selection. Molecular cell *39*, 110-120.

Zaher, H.S., and Green, R. (2010b). Kinetic basis for global loss of fidelity arising from mismatches in the P-site codon:anticodon helix. RNA *16*, 1980-1989.

Zaher, H.S., and Green, R. (2011). A primary role for release factor 3 in quality control during translation elongation in Escherichia coli. Cell *147*, 396-408.

Zhang, J., Ieong, K.W., Johansson, M., and Ehrenberg, M. (2015). Accuracy of initial codon selection by aminoacyl-tRNAs on the mRNA-programmed bacterial ribosome. Proceedings of the National Academy of Sciences of the United States of America *112*, 9602-9607.

Zhang, J., Ieong, K.W., Mellenius, H., and Ehrenberg, M. (2016). Proofreading neutralizes potential error hotspots in genetic code translation by transfer RNAs. RNA *22*, 896-904.

Zhang, Z. (2009). Large-scale identification and quantification of covalent modifications in therapeutic proteins. Analytical chemistry *81*, 8354-8364.

Zhang, Z., Shah, B., and Bondarenko, P.V. (2013). G/U and certain wobble position mismatches as possible main causes of amino acid misincorporations. Biochemistry *52*, 8165-8176.

Zhou, J., Lancaster, L., Donohue, J.P., and Noller, H.F. (2014). How the ribosome hands the A-site tRNA to the P site during EF-G-catalyzed translocation. Science *345*, 1188-1191.

Zhou, T., Weems, M., and Wilke, C.O. (2009). Translationally optimal codons associate with structurally sensitive sites in proteins. Molecular biology and evolution *26*, 1571-1580.

6. APPENDIX

6.1 Section A. EF-Tu genes sequence

The sequence of *tufA* and *tufB* genes from the various strain used in this projects are reported together with the translated sequence of EF-Tu.

```
                     10        20        30        40        50        60        70        80
                     ....|....|....|....|....|....|....|....|....|....|....|....|....|....|
BL21-TufA            GTGTCTAAAGAAAAATTTGAACGTACAAAACCGCACGTTAACGTTGGTACTATCGGCCACGTTGACCACGGTAAAACTAC
BL21-TufB-(over)     A------------G----------------------------C----------------------T--------A--
W3110-TufA-(chrom)   --------------------------------------------------------------------------------
W3110-TufB           A------------G----------------------------C----------------------T--------A--
MRE600-TufA-(wt)     --------------------------------------------------------------------------------
MRE600-TufB-(wt)     A------------G----------------------------C----------------------T--------A--
                      M  S  K  E  K  F  E  R  T  K  P  H  V  N  V  G  T  I  G  H  V  D  H  G  K  T  T

                             90       100       110       120       130       140       150       160
                     ....|....|....|....|....|....|....|....|....|....|....|....|....|....|....|....|
BL21-TufA            TCTGACCGCTGCAATCACCACCGTACTGGCTAAAACCTACGGCGGTGCTGCTCGTGCATTCGACCAGATCGATAACGCGC
BL21-TufB-(over)     G-----------------T-----------------------------------C------------------------
W3110-TufA-(chrom)   --------------------------------------------------------------------------------
W3110-TufB           G-----------------T-----------------------------------C------------------------
MRE600-TufA-(wt)     --------------------------------------------------------------------------------
MRE600-TufB-(wt)     G-----------------T-----------------------------------C------------------------
                       L  T  A  A  I  T  T  V  L  A  K  T  Y  G  G  A  A  R  A  F  D  Q  I  D  N  A

                           170       180       190       200       210       220       230       240
                     ....|....|....|....|....|....|....|....|....|....|....|....|....|....|....|....|
BL21-TufA            CGGAAGAAAAAGCTCGTGGTATCACCATCAACACTTCTCACGTTGAATATGACACCCCGACCCGTCACTACGCACACGTA
BL21-TufB-(over)     ------------------------------------------------C-------------------------------
W3110-TufA-(chrom)   ------------------------------------------------C-------------------------------
W3110-TufB           ------------------------------------------------C-------------------------------
MRE600-TufA-(wt)     --------------------------------------------------------------------------------
MRE600-TufB-(wt)     ------------------------------------------------C-------------------------------
                     P  E  E  K  A  R  G  I  T  I  N  T  S  H  V  E  Y  D  T  P  T  R  H  Y  A  H  V

                           250       260       270       280       290       300       310       320
                     ....|....|....|....|....|....|....|....|....|....|....|....|....|....|....|....|
BL21-TufA            GACTGCCCGGGGCACGCCGACTATGTTAAAAACATGATCACTGGTGCTGCTCAGATGGACGGCGCGATCCTGGTAGTTGC
BL21-TufB-(over)     ----------------------------------------C---------------------------------------
W3110-TufA-(chrom)   ----------------------------------------C---------------------------------------
W3110-TufB           ----------------------------------------C--------G------------------------------
MRE600-TufA-(wt)     ----------------------------------------C---------------------------------------
MRE600-TufB-(wt)     ----------------------------------------C---------------------------------------
                      D  C  P  G  H  A  D  Y  V  K  N  M  I  T  G  A  A  Q  M  D  G  A  I  L  V  V  A

                           330       340       350       360       370       380       390       400
                     ....|....|....|....|....|....|....|....|....|....|....|....|....|....|....|....|
BL21-TufA            TGCGACTGACGGCCCGATGCCGCAGACTCGTGAGCACATCCTGCTGGGTCGTCAGGTAGGCGTTCCGTACATCATCGTGT
BL21-TufB-(over)     --------------------------------------------------------------------------------
W3110-TufA-(chrom)   --------------------------------------------------------------------------------
W3110-TufB           --------------------------------------------------------------------------------
MRE600-TufA-(wt)     --------------------------------------------------------------------------------
MRE600-TufB-(wt)     --------------------------------------------------------------------------------
                       A  T  D  G  P  M  P  Q  T  R  E  H  I  L  L  G  R  Q  V  G  V  P  Y  I  I  V

                           410       420       430       440       450       460       470       480
                     ....|....|....|....|....|....|....|....|....|....|....|....|....|....|....|....|
BL21-TufA            TCCTGAACAAATGCGACATGGTTGATGACGAAGAGCTGCTGGAACTGGTTGAAATGGAAGTTCGTGAACTTCTGTCTCAG
BL21-TufB-(over)     --------------------------------------------------------------------------------
W3110-TufA-(chrom)   --------------------------------------------------------------------------------
W3110-TufB           --------------------------------------------------------------------------------
MRE600-TufA-(wt)     --------------------------------------------------------------------------------
MRE600-TufB-(wt)     --------------------------------------------------------------------------------
                     F  L  N  K  C  D  M  V  D  D  E  E  L  L  E  L  V  E  M  E  V  R  E  L  L  S  Q
```

```
                       490       500       510       520       530       540       550       560
                  ....|....|....|....|....|....|....|....|....|....|....|....|....|....|....|....|
BL21-TufA         TACGACTTCCCGGGCGACGACACTCCGATCGTTCGTGGTTCTGCTCTGAAAGCGCTGGAAGGCGACGCAGAGTGGGAAGC
BL21-TufB-(over)  --T-----------------------------------------------------------------------------
W3110-TufA-(chrom) -----------------------------------------------------------------------------
W3110-TufB        -----------------------------------------------------------------------------
MRE600-TufA-(wt)  -----T-----------------------------------------------------------------G-----------
MRE600-TufB-(wt)  --T-----------------------------------------------------------------------------
                   Y  D  F  P  G  D  D  T  P  I  V  R  G  S  A  L  K  A  L  E  G  D  A  E  W  E  A

                       570       580       590       600       610       620       630       640
                  ....|....|....|....|....|....|....|....|....|....|....|....|....|....|....|....|
BL21-TufA         GAAAATCCTGGAACTGGCTGGCTTCCTGGATTCTTACATTCCGGAACCAGAGCGTGCGATTGACAAGCCGTTCCTGCTGC
BL21-TufB-(over)  -----------------------------------------------------------------------------
W3110-TufA-(chrom) ----------------------------------T----------------------------------------
W3110-TufB        -----------------------------------------------------------------------------
MRE600-TufA-(wt)  -----------------------------------------------------------------------------
MRE600-TufB-(wt)  -----------------------------------------------------------------------------
                    K  I  L  E  L  A  G  F  L  D  S  Y  I  P  E  P  E  R  A  I  D  K  P  F  L  L

                       650       660       670       680       690       700       710       720
                  ....|....|....|....|....|....|....|....|....|....|....|....|....|....|....|....|
BL21-TufA         CGATCGAAGACGTATTCTCCATCTCCGGTCGTGGTACCGTTGTTACCGGTCGTGTAGAACGCGGTATCATCAAAGTTGGT
BL21-TufB-(over)  -----------------------------------------------------------------------------
W3110-TufA-(chrom) -----------------------------------------------------------------------------
W3110-TufB        -----------------------------------------------------------------------------
MRE600-TufA-(wt)  -----------------------------------------------------------------------------
MRE600-TufB-(wt)  -----------------------------------------------------------------------------
                   P  I  E  D  V  F  S  I  S  G  R  G  T  V  V  T  G  R  V  E  R  G  I  I  K  V  G

                       730       740       750       760       770       780       790       800
                  ....|....|....|....|....|....|....|....|....|....|....|....|....|....|....|....|
BL21-TufA         GAAGAAGTTGAAATCGTTGGTATCAAAGAGACTCAGAAGTCTACCTGTACTGGCGTTGAAATGTTCCGCAAACTGCTGGA
BL21-TufB-(over)  -----------------------------------------------------------------------------
W3110-TufA-(chrom) -----------------------------------------------------------------------------
W3110-TufB        -----------------------------------------------------------------------------
MRE600-TufA-(wt)  -----------------------------------------------------------------------------
MRE600-TufB-(wt)  -----------------------------------------------------------------------------
                    E  E  V  E  I  V  G  I  K  E  T  Q  K  S  T  C  T  G  V  E  M  F  R  K  L  L  D

                       810       820       830       840       850       860       870       880
                  ....|....|....|....|....|....|....|....|....|....|....|....|....|....|....|....|
BL21-TufA         CGAAGGCCGTGCTGGTGAGAACGTAGGTGTTCTGCTGCGTGGTATCAAACGTGAAGAAATCGAACGTGGTCAGGTACTGG
BL21-TufB-(over)  -----------------------------------------------------------------------------
W3110-TufA-(chrom) -----------------------------------------------------------------------------
W3110-TufB        -----------------------------------------------------------------------------
MRE600-TufA-(wt)  ------T----------------------------------------------------------------------------
MRE600-TufB-(wt)  ----------------------A-----------------------------------------------------------
                    E  G  R  A  G  E  N  I  G  V  L  L  R  G  I  K  R  E  E  I  E  R  G  Q  V  L

                       890       900       910       920       930       940       950       960
                  ....|....|....|....|....|....|....|....|....|....|....|....|....|....|....|....|
BL21-TufA         CTAAGCCGGGCACCATCAAGCCGCACACCAAGTTCGAATCTGAAGTGTACATTCTGTCCAAAGATGAAGGCGGCCGTCAT
BL21-TufB-(over)  -----------------------------------------------------------------------------T------
W3110-TufA-(chrom) -----------------------------------------------------------------------------
W3110-TufB        -----------------------------------------------------------------------------
MRE600-TufA-(wt)  -----------------------------------------------------------------------------
MRE600-TufB-(wt)  -----------------------------------------------------------------------------
                   A  K  P  G  T  I  K  P  H  T  K  F  E  S  E  V  Y  I  L  S  K  D  E  G  G  R  H

                       970       980       990       1000      1010      1020      1030      1040
                  ....|....|....|....|....|....|....|....|....|....|....|....|....|....|....|....|
BL21-TufA         ACTCCGTTCTTCAAAGGCTACCGTCCGCAGTTCTACTTCCGTACTACTGACGTGACTGGTACCATCGAACTGCCGGAAGG
BL21-TufB-(over)  -----------------------------------------------------------------------------
W3110-TufA-(chrom) -----------------------------------------------------------------------------
W3110-TufB        -----------------------------------------------------------------------------
MRE600-TufA-(wt)  ------------------------------------------------------------C--------------------
MRE600-TufB-(wt)  -----------------------------------------------------------------------------
                   T  P  F  F  K  G  Y  R  P  Q  F  Y  F  R  T  T  D  V  T  G  T  I  E  L  P  E  G
```

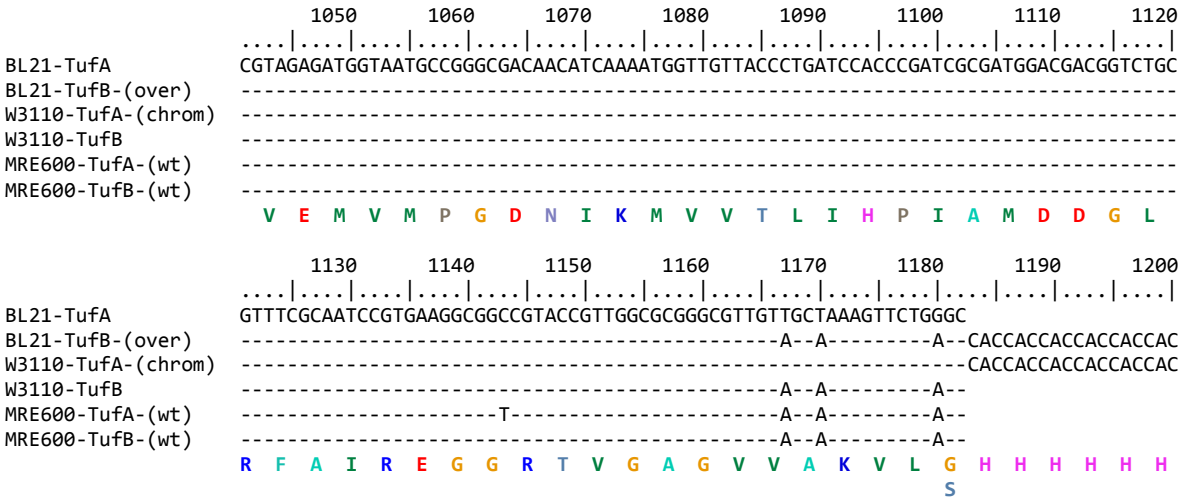
1050 1060 1070 1080 1090 1100 1110 1120
BL21-TufA CGTAGAGATGGTAATGCCGGGCGACAACATCAAAATGGTTGTTACCCTGATCCACCCGATCGCGATGGACGACGGTCTGC
BL21-TufB-(over)
W3110-TufA-(chrom)
W3110-TufB
MRE600-TufA-(wt)
MRE600-TufB-(wt)
V E M V M P G D N I K M V V T L I H P I A M D D G L
1130 1140 1150 1160 1170 1180 1190 1200
BL21-TufA GTTTCGCAATCCGTGAAGGCGGCCGTACCGTTGGCGCGGGCGTTGTTGCTAAAGTTCTGGGC
BL21-TufB-(over) A--A---------A--CACCACCACCACCACCAC
W3110-TufA-(chrom) CACCACCACCACCACCAC
W3110-TufB A--A---------A--
MRE600-TufA-(wt) T A--A---------A--
MRE600-TufB-(wt) A--A---------A--
R F A I R E G G R T V G A G V V A K V L G H H H H H H
S

6.2 Section B. SRM optimized parameters

The optimized SRM parameters for heavy-labeled and endogenous peptides used during enrichment workflow are listed. For each peptide, the precursor mass and the fragment mass are indicated (Q1 and Q3 columns). The transitions used during the SRM scan (fragment) and the optimized collision energies (CE) are also indicated.

	Peptide	Q1	Q3	Fragment	CE
R45H	TYGGAAHAFDQIDNAPEEK light	678.64483	915.44180	y8	24.1
		678.64483	802.35774	y7	24.1
		678.64483	687.33080	y6	23.1
		678.64483	502.25075	y4	27.1
	TYGGAAHAFDQIDNAPEEK* heavy	681.31623	923.45600	y8	24.1
		681.31623	810.37194	y7	24.1
		681.31623	695.34499	y6	23.1
		681.31623	510.26495	y4	27.1
R59H	AHGITINTSHVEYDTPTR light	671.33258	980.46835	y8	25.8
		671.33258	881.39994	y7	27.8
		671.33258	752.35734	y6	25.8
		671.33258	373.21939	y3	27.8
	AHGITINTSHVEYDTPTR* heavy	674.66867	990.47662	y8	25.8
		674.66867	891.40821	y7	27.8
		674.66867	762.36561	y6	25.8
		674.66867	383.22766	y3	27.8
R172H	ELLSQYDFPGDDTPIVHGSALK light	801.40066	1406.72742	y14	29.7
		801.40066	1022.59931	y10	30.7
		801.40066	921.55163	y9	30.7
	ELLSQYDFPGDDTPIVHGSALK* heavy	804.07206	1414.74162	y14	29.7
		804.07206	1030.61351	y10	30.7
		804.07206	929.56583	y9	30.7
R231S	GTVVTGSVER light	502.77219	747.39954	y7	17
		502.77219	648.33113	y6	17
		502.77219	547.28345	y5	15
	GTVVTGSVER* heavy	507.77632	757.40781	y7	17
		507.77632	658.33940	y6	17
		507.77632	557.29172	y5	15
R231G	GTVVTGGVER light	487.76691	717.38898	y7	16.5
		487.76691	618.32057	y6	18.5
		487.76691	517.27289	y5	15.5
	GTVVTGGVER * heavy	492.77104	727.39725	y7	16.5
		492.77104	628.32883	y6	18.5
		492.77104	527.28116	y5	15.5

	Peptide	Q1	Q3	Fragment	CE
R231C	GTVVTGC[+57.0]VER light	539.27150	721.32975	y6	18.1
		539.27150	620.28207	y5	17.1
		539.27150	563.26061	y4	17.1
	GTVVTGC[+57.0]VER* heavy	544.27563	731.33802	y6	18.1
		544.27563	630.29034	y5	17.1
		544.27563	573.26888	y4	17.1
R231H	GTVVTGHVER light	527.78563	698.35801	y6	20.7
		527.78563	597.31033	y5	21.7
		527.78563	540.28887	y4	21.7
		527.78563	880.45231	b9	20.7
	GTVVTGHVER* heavy	532.78976	708.36628	y6	20.7
		532.78976	607.31860	y5	21.7
		532.78976	550.29714	y4	21.7
		532.78976	880.45231	b9	20.7
R231P	GTVVTGPVER light	507.78256	757.42028	y7	16.1
		507.78256	658.35187	y6	16.1
		507.78256	557.30419	y5	14.1
		507.78256	500.28272	y4	16.1
	GTVVTGPVER* heavy	512.78669	767.42855	y7	16.1
		512.78669	668.36013	y6	16.1
		512.78669	567.31246	y5	14.1
		512.78669	510.29099	y4	16.1
R231L	GTVVTGLVER light	515.79821	674.38317	y6	16.4
		515.79821	573.33549	y5	17.4
		515.79821	516.31402	y4	16.4
		515.79821	628.36645	b7	14.4
	GTVVTGLVER * heavy	520.80234	684.39143	y6	16.4
		520.80234	583.34376	y5	17.4
		520.80234	526.32229	y4	16.4
		520.80234	628.36645	b7	14.4
R231Q	GTVVTGQVER light	523.28546	403.22996	y3	18.6
		523.28546	531.28854	y4	15.6
		523.28546	588.31000	y5	16.6
		523.28546	689.35768	y6	17.6
		523.28546	788.42609	y7	18.6
	GTVVTGQVER* heavy	528.28960	413.23823	y3	18.6
		528.28960	541.29681	y4	15.6
		528.28960	598.31827	y5	16.6
		528.28960	699.36595	y6	17.6
		528.28960	798.43436	y7	18.6
R231E	GTVVTGEVER light	523.77747	532.27255	y4	16.6
		523.77747	589.29402	y5	15.6
		523.77747	644.32498	b7	13.6
		523.77747	690.34169	y6	17.6
		523.77747	743.39340	b8	13.6

	GTVVTGEVER* heavy	528.78161	542.28082	y4	16.6
		528.78161	599.30229	y5	15.6
		528.78161	644.32498	b7	13.6
		528.78161	700.34996	y6	17.6
		528.78161	743.39340	b8	13.6
R231D	GTVVTGDVER light	516.76965	518.25690	y4	15.4
		516.76965	575.27837	y5	16.4
		516.76965	676.32604	y6	17.4
	GTVVTGDVER* heavy	521.77378	528.26517	y4	15.4
		521.77378	585.28664	y5	16.4
		521.77378	686.33431	y6	17.4
R231A	GTVVTGAVER light	494.77473	531.28854	y5	15.7
		494.77473	632.33622	y6	15.7
		494.77473	731.40463	y7	16.7
	GTVVTGAVER*heavy	499.77887	541.29681	y5	15.7
		499.77887	642.34448	y6	15.7
		499.77887	741.41290	y7	16.7
R231V	GTVVTGVVER light	508.79038	515.28239	b6	14.2
		508.79038	559.31984	y5	15.2
		508.79038	614.35080	b7	13.2
		508.79038	660.36752	y6	16.2
		508.79038	759.43593	y7	17.2
	GTVVTGVVER*heavy	513.79452	515.28239	b6	14.2
		513.79452	569.32811	y5	15.2
		513.79452	614.35080	b7	13.2
		513.79452	670.37578	y6	16.2
		513.79452	769.44420	y7	17.2
R231Y	GTVVTGYVER light	540.78784	566.29329	y4	17.1
		540.78784	623.31475	y5	17.1
		540.78784	678.34572	b7	14.1
		540.78784	724.36243	y6	17.1
		540.78784	777.41413	b8	14.1
	GTVVTGYVER*heavy	545.79197	576.30156	y4	17.1
		545.79197	633.32302	y5	17.1
		545.79197	678.34572	b7	14.1
		545.79197	734.37070	y6	17.1
		545.79197	777.41413	b8	14.1
R231F	GTVVTGFVER light	532.79038	550.29837	y4	16.9
		532.79038	607.31984	y5	16.9
		532.79038	662.35080	b7	13.9
	GTVVTGFVER* heavy	537.79452	560.30664	y4	16.9
		537.79452	617.32811	y5	16.9
		537.79452	662.35080	b7	13.9
R231T	GTVVTGTVER light	509.78001	515.28239	b6	13.2
		509.78001	561.29910	y5	15.2
		509.78001	662.34678	y6	17.2

		509.78001	761.41519	y7	17.2
	GTVVTGTVER* heavy	514.78415	515.28239	b6	13.2
		514.78415	571.30737	y5	15.2
		514.78415	672.35505	y6	17.2
		514.78415	771.42346	y7	17.2
R234H	VEHGIIK light	398.23980	696.40390	y6	14.9
		398.23980	567.36131	y5	15.9
		398.23980	430.30240	y4	17.9
		398.23980	536.28272	b5	17.9
		398.23980	649.36679	b6	14.9
	VEHGIIK* heavy	402.24690	704.41810	y6	14.9
		402.24690	575.37551	y5	15.9
		402.24690	438.31660	y4	17.9
		402.24690	536.28272	b5	17.9
		402.24690	649.36679	b6	14.9
K249R	VGEEVEIVGIR light	600.33515	914.53056	y8	20.9
		600.33515	785.48797	y7	20.9
		600.33515	686.41955	y6	18.9
		600.33515	643.29335	b6	17.9
		600.33515	756.37741	b7	17.9
	VGEEVEIVGIR* heavy	605.33929	924.53883	y8	20.9
		605.33929	795.49623	y7	20.9
		605.33929	696.42782	y6	18.9
		605.33929	643.29335	b6	17.9
		605.33929	756.37741	b7	17.9
K249N	VGEEVEIVGINETQK light	822.42797	1130.60518	y10	27.6
		822.42797	1001.56259	y9	27.6
		822.42797	888.47852	y8	26.6
		822.42797	855.44583	b8	22.6
	VGEEVEIVGINETQK* heavy	826.43507	1138.61938	y10	27.6
		826.43507	1009.57679	y9	27.6
		826.43507	896.49272	y8	26.6
		826.43507	855.44583	b8	22.6
K249Q double	VGEEVEIVGIQETQK light	829.43579	1144.62083	y10	28.8
		829.43579	1015.57824	y9	28.8
		829.43579	902.49417	y8	30.8
		829.43579	855.44583	b8	22.8
	VGEEVEIVGIQETQK* heavy	836.95147	1159.65219	y10	28.8
		836.95147	1030.60960	y9	28.8
		836.95147	917.52554	y8	30.8
		836.95147	855.44583	b8	22.8
K249Q single	VGEEVEIVGIQETQK light	829.43579	1144.62083	y10	30.8
		829.43579	1015.57824	y9	28.8
		829.43579	902.49417	y8	30.8
		829.43579	855.44583	b8	23.8
	VGEEVEIVGIQETQK* heavy	833.44289	1152.63503	y10	30.8

		833.44289	1023.59244	y9	28.8
		833.44289	910.50837	y8	30.8
		833.44289	855.44583	b8	23.8
K249T single	VGEEVEIVGITETQK light	815.93034	1117.60993	y10	29.4
		815.93034	988.56734	y9	28.4
		815.93034	875.48327	y8	26.4
		815.93034	855.44583	b8	23.4
	VGEEVEIVGITETQK* heavy	819.93744	1125.62413	y10	29.4
		819.93744	996.58154	y9	28.4
		819.93744	883.49747	y8	26.4
		819.93744	855.44583	b8	23.4
K249E single	VGEEVEIVGIEETQK light	829.92780	1145.60485	y10	28.8
		829.92780	1016.56225	y9	27.8
		829.92780	903.47819	y8	26.8
		829.92780	855.44583	b8	23.8
	VGEEVEIVGIEETQK* heavy	833.93490	1153.61904	y10	28.8
		833.93490	1024.57645	y9	27.8
		833.93490	911.49239	y8	26.8
		833.93490	855.44583	b8	23.8
R270H	LLDEGHAGENVGVLLR light	564.64069	899.53089	y8	19.7
		564.64069	770.48830	y7	20.7
		564.64069	656.44537	y6	19.7
		564.64069	665.32532	b6	19.7
	LLDEGHAGENVGVLLR* heavy	567.97678	909.53916	y8	19.7
		567.97678	780.49657	y7	20.7
		567.97678	666.45364	y6	19.7
		567.97678	665.32532	b6	19.7
R280H	AGENVGVLLHGIK light	653.87752	836.53525	y8	24.5
		653.87752	779.51379	y7	23.5
		653.87752	680.44537	y6	23.5
		653.87752	990.53671	b10	24.5
	AGENVGVLLHGIK* heavy	657.88462	844.54945	y8	24.5
		657.88462	787.52798	y7	23.5
		657.88462	688.45957	y6	23.5
		657.88462	990.53671	b10	24.5
R284H	HEEIER light	406.69849	675.33080	y5	18.1
		406.69849	546.28820	y4	18.1
		406.69849	417.24561	y3	16.1
		406.69849	638.27803	b5	14.1
	HEEIER* heavy	411.70263	685.33906	y5	18.1
		411.70263	556.29647	y4	18.1
		411.70263	427.25388	y3	16.1
		411.70263	638.27803	b5	14.1
F305L	LESEVYILSK light	590.82663	347.228896	y3	25.6
		590.82663	460.31296	y4	19.6
		590.82663	623.376289	y5	16.6

		590.82663	722.444703	y6	17.6
		590.82663	938.519324	y8	15.6
	LESEVYILSK* heavy	594.83373	355.243095	y3	25.6
		594.83373	468.327159	y4	19.6
		594.83373	631.390488	y5	16.6
		594.83373	730.458902	y6	17.6
		594.83373	946.533523	y8	15.6
E306D	FDSEVYILSK light	600.81098	234.144832	y2	19.9
		600.81098	347.228896	y3	21.9
		600.81098	350.134661	b3	16.9
		600.81098	460.31296	y4	19.9
		600.81098	623.376289	y5	15.9
		600.81098	722.444703	y6	18.9
		600.81098	851.487296	y7	17.9
		600.81098	938.519324	y8	17.9
	FDSEVYILSK* heavy	604.81808	263.102633	y2	17.9
		604.81808	350.134661	y3	16.9
		604.81808	355.243095	b3	21.9
		604.81808	468.327159	y4	19.9
		604.81808	631.390488	y5	15.9
		604.81808	730.458902	y6	18.9
		604.81808	859.501495	y7	17.9
		604.81808	946.533523	y8	17.9
E308D	FESDVYILSK light	600.81098	347.228896	y3	23.9
		600.81098	460.31296	y4	21.9
		600.81098	623.376289	y5	17.9
		600.81098	722.444703	y6	16.9
		600.81098	837.471646	y7	16.9
		600.81098	924.503674	y8	16.9
	FESDVYILSK* heavy	604.81808	355.243095	y3	23.9
		604.81808	468.327159	y4	21.9
		604.81808	631.390488	y5	17.9
		604.81808	730.458902	y6	16.9
		604.81808	845.485845	y7	16.9
		604.81808	932.517873	y8	16.9
Y310H	FESEVHILSK light	594.81660	347.228896	y3	25.7
		594.81660	460.31296	y4	25.7
		594.81660	696.440286	y6	21.7
		594.81660	825.482879	y7	23.7
		594.81660	842.404294	b7	20.7
		594.81660	912.514908	y8	18.7
	FESEVHILSK* heavy	598.82370	355.243095	y3	25.7
		598.82370	468.327159	y4	25.7
		598.82370	704.454485	y6	21.7
		598.82370	833.497078	y7	23.7
		598.82370	842.404294	b7	20.7

		598.82370	920.529107	y8	18.7
Y310N	FESEVNILSK light	583.30860	889.498923	y8	16.4
		583.30860	802.466895	y7	15.4
		583.30860	673.424302	y6	16.4
		583.30860	574.355888	y5	17.4
		583.30860	460.31296	y4	20.4
		583.30860	347.228896	y3	22.4
		583.30860	234.144832	y2	17.4
	FESEVNILSK* heavy	587.31570	897.513122	y8	16.4
		587.31570	810.481094	y7	15.4
		587.31570	681.438501	y6	16.4
		587.31570	582.370087	y5	17.4
		587.31570	468.327159	y4	20.4
		587.31570	355.243095	y3	22.4
		587.31570	242.159031	y2	17.4
K314Q	FESEVYILSQDEGGR light	576.94069	861.40609	y8	20.2
		576.94069	748.32202	y7	19.2
		576.94069	661.28999	y6	19.2
		576.94069	592.26132	b5	20.2
		576.94069	755.32465	b6	19.2
	FESEVYILSQDEGGR* heavy	580.27678	871.41435	y8	20.2
		580.27678	758.33029	y7	19.2
		580.27678	671.29826	y6	19.2
		580.27678	592.26132	b5	20.2
		580.27678	755.32465	b6	19.2
K314T	FESEVYILSTDEGGR light	567.93706	834.39519	y8	18.9
		567.93706	721.31112	y7	18.9
		567.93706	634.27909	y6	18.9
		567.93706	592.26132	b5	18.9
	FESEVYILSTDEGGR* heavy	571.27315	844.40346	y8	18.9
		571.27315	731.31939	y7	18.9
		571.27315	644.28736	y6	18.9
		571.27315	592.26132	b5	18.9
K314N	FESEVYILSNDEGGR light	572.26881	847.39044	y8	19
		572.26881	734.30637	y7	19
		572.26881	647.27434	y6	20
		572.26881	592.26132	b5	19
		572.26881	755.32465	b6	20
	FESEVYILSNDEGGR* heavy	575.60490	857.39870	y8	19
		575.60490	744.31464	y7	19
		575.60490	657.28261	y6	20
		575.60490	592.26132	b5	19
		575.60490	755.32465	b6	20
K314E	FESEVYILSEDEGGR light	577.26870	862.39010	y8	19.2
		577.26870	749.30604	y7	19.2
		577.26870	662.27401	y6	19.2

		577.26870	592.26132	b5	19.2
		577.26870	755.32465	b6	19.2
	FESEVYILSEDEGGR* heavy	580.60479	872.39837	y8	19.2
		580.60479	759.31431	y7	19.2
		580.60479	672.28228	y6	19.2
		580.60479	592.26132	b5	19.2
		580.60479	755.32465	b6	19.2
K314R	FESEVYILSR light	621.82188	879.49344	y7	20.6
		621.82188	750.45085	y6	23.6
		621.82188	651.38244	y5	21.6
		621.82188	755.32465	b6	16.6
		621.82188	868.40871	b7	16.6
	FESEVYILSR* heavy	626.82601	889.50171	y7	20.6
		626.82601	760.45912	y6	23.6
		626.82601	661.39071	y5	21.6
		626.82601	755.32465	b6	16.6
		626.82601	868.40871	b7	16.6
R319H	DEGGHHTPFFK light	424.53164	639.35007	y5	16.4
		424.53164	538.30240	y4	16.4
		424.53164	441.24963	y3	20.4
		424.53164	734.28524	b7	14.4
	DEGGHHTPFFK* heavy	427.20304	647.36427	y5	16.4
		427.20304	546.31660	y4	16.4
		427.20304	449.26383	y3	20.4
		427.20304	734.28524	b7	14.4
R328H	GYHPQFYFR light	607.79072	857.43045	y6	23.1
		607.79072	760.37769	y5	25.1
		607.79072	632.31911	y4	25.1
		607.79072	358.15098	b3	21.1
	GYHPQFYFR* heavy	612.79485	867.43872	y6	23.1
		612.79485	770.38596	y5	25.1
		612.79485	642.32738	y4	25.1
		612.79485	358.15098	b3	21.1
R378H	FAIHEGGR light	443.73013	739.38456	y7	18.2
		443.73013	668.34745	y6	19.2
		443.73013	555.26338	y5	18.2
		443.73013	469.25578	b4	16.2
	FAIHEGGR* heavy	448.73426	749.39283	y7	18.2
		448.73426	678.35572	y6	19.2
		448.73426	565.27165	y5	18.2
		448.73426	469.25578	b4	16.2
R382H	EGGHTVGAGVVAK light	394.54729	544.34532	y6	12.3
		394.54729	473.30821	y5	13.3
		394.54729	416.28675	y4	13.3
		394.54729	482.19939	b5	14.3
	EGGHTVGAGVVAK* heavy	397.21869	552.35952	y6	12.3

		397.21869	481.32241	y5	13.3
		397.21869	424.30094	y4	13.3
		397.21869	482.19939	b5	14.3
E308D-Y310H	FESDVHILSK light	587.80877	234.144832	y2	20.5
		587.80877	364.150312	b3	21.5
		587.80877	597.371872	y5	21.5
		587.80877	811.467229	y7	22.5
		587.80877	898.499258	y8	19.5
	FESDVHILSK* heavy	591.81587	242.159031	y2	20.5
		591.81587	364.150312	b3	21.5
		591.81587	605.386071	y5	21.5
		591.81587	819.481428	y7	22.5
		591.81587	906.513457	y8	19.5
E306D-Y310H	FDSEVHILSK light	587.80877	234.144832	y2	21.5
		587.80877	597.371872	y5	20.5
		587.80877	696.440286	y6	19.5
		587.80877	825.482879	y7	19.5
		587.80877	912.514908	y8	19.5
	FDSEVHILSK* heavy	591.81587	242.159031	y2	21.5
		591.81587	605.386071	y5	20.5
		591.81587	704.454485	y6	19.5
		591.81587	833.497078	y7	19.5
		591.81587	920.529107	y8	19.5
E306D-E308D	FDSDVYILSK light	593.80315	347.228896	y3	22.7
		593.80315	460.31296	y4	16.7
		593.80315	623.376289	y5	17.7
		593.80315	722.444703	y6	16.7
		593.80315	837.471646	y7	18.7
		593.80315	924.503674	y8	16.7
	FDSDVYILSK* heavy	597.81025	355.243095	y3	22.7
		597.81025	468.327159	y4	16.7
		597.81025	631.390488	y5	17.7
		597.81025	730.458902	y6	16.7
		597.81025	845.485845	y7	18.7
		597.81025	932.517873	y8	16.7
E308D-Y310N	FESDVNILSK light	576.30078	1004.525866	y9	19.2
		576.30078	875.483273	y8	18.2
		576.30078	788.451245	y7	18.2
		576.30078	673.424302	y6	20.2
		576.30078	574.355888	y5	19.2
		576.30078	460.31296	y4	24.2
		576.30078	347.228896	y3	24.2
		576.30078	578.245669	b5	16.2
	FESDVNILSK* heavy	580.30788	1012.540065	y9	19.2
		580.30788	883.497472	y8	18.2
		580.30788	796.465444	y7	18.2

		580.30788	681.438501	y6	20.2
		580.30788	582.370087	y5	19.2
		580.30788	468.327159	y4	24.2
		580.30788	355.243095	y3	24.2
		580.30788	578.245669	b5	16.2
E306D-Y310N	FDSEVNILSK light	576.30078	1004.525866	y9	20.2
		576.30078	889.498923	y8	18.2
		576.30078	802.466895	y7	18.2
		576.30078	673.424302	y6	18.2
		576.30078	574.355888	y5	17.2
		576.30078	460.31296	y4	21.2
		576.30078	347.228896	y3	22.2
		576.30078	578.245669	b5	15.2
	FDSEVNILSK* heavy	580.30788	1012.540065	y9	20.2
		580.30788	897.513122	y8	18.2
		580.30788	810.481094	y7	18.2
		580.30788	681.438501	y6	18.2
		580.30788	582.370087	y5	17.2
		580.30788	468.327159	y4	21.2
		580.30788	355.243095	y3	22.2
		580.30788	578.245669	b5	15.2
E306D-E308D-Y310H	FDSDVHILSK light	387.536389	811.467229	y7	14
		387.536389	696.440286	y6	15
		387.536389	597.371872	y5	15
		387.536389	460.31296	y4	15
		387.536389	347.228896	y3	17
		387.536389	234.144832	y2	19
		387.536389	465.161605	b4	13
	FDSDVHILSK* heavy	390.207789	819.481428	y7	14
		390.207789	704.454485	y6	15
		390.207789	605.386071	y5	15
		390.207789	468.327159	y4	15
		390.207789	355.243095	y3	17
		390.207789	242.159031	y2	19
		390.207789	465.161605	b4	13
cognate 1	ELLSQYDFPGDDTPIVR light	982.98364	1394.65867	y12	29.4
		982.98364	1231.59534	y11	32.4
		982.98364	1116.56840	y10	34.4
		982.98364	969.49999	y9	34.4
		982.98364	484.32419	y4	33.4
	ELLSQYDFPGDDTPIVR* heavy	987.98777	1404.66694	y12	29.4
		987.98777	1241.60361	y11	32.4
		987.98777	1126.57667	y10	34.4
		987.98777	979.50826	y9	34.4
		987.98777	494.33246	y4	33.4
cognate 2	VGEEVEIVGIK light	586.33208	886.52441	y8	20.5

		586.33208	757.48182	y7	20.5
		586.33208	658.41340	y6	19.5
		586.33208	643.29335	b6	16.5
	VGEEVEIVGIK* heavy	590.33918	894.53861	y8	20.5
		590.33918	765.49602	y7	20.5
		590.33918	666.42760	y6	19.5
		590.33918	643.29335	b6	16.5
cognate 3	FESEVYILSK light	607.81880	851.48730	y7	21.1
		607.81880	722.44470	y6	18.1
		607.81880	623.37629	y5	19.1
		607.81880	755.32465	b6	16.1
	FESEVYILSK* heavy	611.82590	859.50150	y7	21.1
		611.82590	730.45890	y6	18.1
		611.82590	631.39049	y5	19.1
		611.82590	755.32465	b6	16.1
cognate 4	TVGAGVVAK light	401.24508	544.34532	y6	15.9
		401.24508	473.30821	y5	14.9
		401.24508	416.28675	y4	18.9
		401.24508	485.27182	b6	10.9
	TVGAGVVAK* heavy	405.25218	552.35952	y6	15.9
		405.25218	481.32241	y5	14.9
		405.25218	424.30094	y4	18.9
		405.25218	485.27182	b6	10.9
IbpB 1	ITLALAGFR light	481.295102	848.498864	y8	17.3
		481.295102	747.451185	y7	15.3
		481.295102	634.367121	y6	16.3
		481.295102	563.330007	y5	15.3
		481.295102	583.381374	b6	12.3
	ITLALAGFR* heavy	486.299236	858.507133	y8	17.3
		486.299236	757.459454	y7	15.3
		486.299236	644.37539	y6	16.3
		486.299236	573.338276	y5	15.3
		486.299236	583.381374	b6	12.3
IbpB 2	QEDLEIQLEGTR light	715.85972	1173.610993	y10	24.4
		715.85972	1058.58405	y9	26.4
		715.85972	945.499986	y8	25.4
		715.85972	816.457393	y7	26.4
		715.85972	728.346111	b6	20.4
	QEDLEIQLEGTR* heavy	720.863854	1183.619262	y10	24.4
		720.863854	1068.592319	y9	26.4
		720.863854	955.508255	y8	25.4
		720.863854	826.465662	y7	26.4
		720.863854	728.346111	b6	20.4
IbpB 3	NEPEPIAAQR light	562.788369	881.483942	y8	16.8
		562.788369	784.431178	y7	21.8
		562.788369	655.388585	y6	21.8

		562.788369	558.335821	y5	14.8
		562.788369	445.251757	y4	24.8
		562.788369	374.214643	y3	23.8
	NEPEPIAAQR* heavy	567.792504	891.492211	y8	16.8
		567.792504	794.439447	y7	21.8
		567.792504	665.396854	y6	21.8
		567.792504	568.34409	y5	14.8
		567.792504	455.260026	y4	24.8
		567.792504	384.222912	y3	23.8
rpoH 1	AEIHEYVLR light	565.303655	929.520327	y7	20.9
		565.303655	816.436263	y6	21.9
		565.303655	679.377351	y5	23.9
		565.303655	580.272552	y4	17.9
	AEIHEYVLR* heavy	570.30779	939.528596	y7	20.9
		570.30779	826.444532	y6	21.9
		570.30779	689.38562	y5	23.9
		570.30779	580.272552	y4	17.9
rpoH 2	LHYHGDLEAAK light	418.547288	840.421007	y8	17.2
		418.547288	703.362095	y7	13.2
		418.547288	646.340632	y6	15.2
		418.547288	531.313689	y5	14.2
		418.547288	723.320899	b6	16.2
	LHYHGDLEAAK* heavy	421.218688	848.435206	y8	17.2
		421.218688	711.376294	y7	13.2
		421.218688	654.354831	y6	15.2
		421.218688	539.327888	y5	14.2
		421.218688	723.320899	b6	16.2
rpoH 3	TLILSHLR light	476.800551	851.546148	y7	19.2
		476.800551	738.462084	y6	17.2
		476.800551	625.37802	y5	18.2
		476.800551	512.293956	y4	19.2
	TLILSHLR* heavy	481.804686	861.554417	y7	19.2
		481.804686	748.470353	y6	17.2
		481.804686	635.386289	y5	18.2
		481.804686	522.302225	y4	19.2
L10 1	AAAFEGELIPASQIDR light	844.43613	1198.64263	y11	31.2
		844.43613	1012.57857	y9	30.2
		844.43613	899.49451	y8	27.2
		844.43613	786.41044	y7	27.2
		844.43613	618.32057	y5	24.2
		844.43613	403.22996	y3	24.2
		844.43613	902.46181	b9	23.2
	AAAFEGELIPASQIDR* heavy	849.44026	1208.65090	y11	31.2
		849.44026	1022.58684	y9	30.2
		849.44026	909.50278	y8	27.2
		849.44026	796.41871	y7	27.2

		849.44026	628.32883	y5	24.2
		849.44026	413.23823	y3	24.2
		849.44026	902.46181	b9	23.2
L10 2	LATLPTYEEAIAR light	724.39320	1049.52620	y9	22.6
		724.39320	952.47344	y8	29.6
		724.39320	851.42576	y7	27.6
		724.39320	430.27724	y4	29.6
	LATLPTYEEAIAR* heavy	729.39733	1059.53447	y9	22.6
		729.39733	962.48171	y8	29.6
		729.39733	861.43403	y7	27.6
		729.39733	440.28551	y4	29.6
L10 3	GALSAVVADSR light	523.28546	804.42101	y8	16.6
		523.28546	717.38898	y7	18.6
		523.28546	646.35187	y6	15.6
		523.28546	547.28345	y5	14.6
		523.28546	448.21504	y4	14.6
		523.28546	262.15098	y2	23.6
	GALSAVVADSR* heavy	528.28960	814.42928	y8	16.6
		528.28960	727.39725	y7	18.6
		528.28960	656.36013	y6	15.6
		528.28960	557.29172	y5	14.6
		528.28960	458.22331	y4	14.6
		528.28960	272.15925	y2	23.6
IbpA 1	SAIGFDR light	383.19813	678.35695	y6	15.4
		383.19813	607.31984	y5	11.4
		383.19813	494.23577	y4	13.4
		383.19813	437.21431	y3	13.4
	SAIGFDR* heavy	388.20226	688.36522	y6	15.4
		388.20226	617.32811	y5	11.4
		388.20226	504.24404	y4	13.4
		388.20226	447.22258	y3	13.4
IbpA 2	TYLYQGIAER light	607.31422	949.51016	y8	19.1
		607.31422	836.42609	y7	20.1
		607.31422	673.36276	y6	19.1
		607.31422	545.30419	y5	20.1
		607.31422	488.28272	y4	19.1
		607.31422	375.19866	y3	19.1
	TYLYQGIAER* heavy	612.31835	959.51843	y8	19.1
		612.31835	846.43436	y7	20.1
		612.31835	683.37103	y6	19.1
		612.31835	555.31246	y5	20.1
		612.31835	498.29099	y4	19.1
		612.31835	385.20693	y3	19.1
IbpA 3	NFDLSPLYR light	562.79038	863.46214	y7	16.8
		562.79038	748.43520	y3	15.8
		562.79038	635.35114	y5	15.8

	562.79038	548.31911	y4	17.8
	562.79038	262.11862	b2	14.8
	562.79038	377.14556	b3	15.8
NFDLSPLYR* heavy	567.79452	873.47041	y7	16.8
	567.79452	758.44347	y3	15.8
	567.79452	645.35941	y5	15.8
	567.79452	558.32738	y4	17.8
	567.79452	262.11862	b2	14.8
	567.79452	377.14556	b3	15.8

6.3 Section C. validation of near-cognate amino acid substitutions

The position of the substituted amino acid (red) is shown in the context of EF-Tu structure. The identity of the error-containing peptide is validated at MS1 (B) and MS/MS (C) level and precursor and fragment ions spectra are compared with the fragmentation patter predicted for the peptide (D). For the K249R peptide the MS1 spectrum is replaced by the tSIM and PRM signals. The validation of the quantification is performed by comparing the stoichiometry of erroneous peptide with respect to four cognate EF-Tu peptides (E), as described in Results and Materials and Method. The SRM trace used for the determination of error frequency is shown (F). To confirm the absence of contamination by the light peptide, the heavy-labeled peptides are analysed by mass spectrometry and the signals for both light and heavy are recorded (G). The monitored transitions are indicated.

R45H: lak.TYGGAAHAFDQIDNAPEEK.arg

A

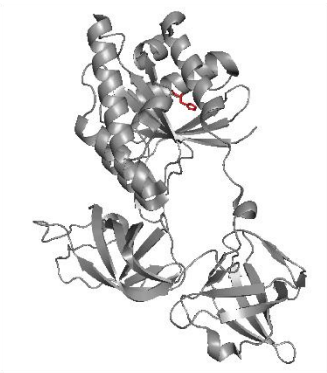

B

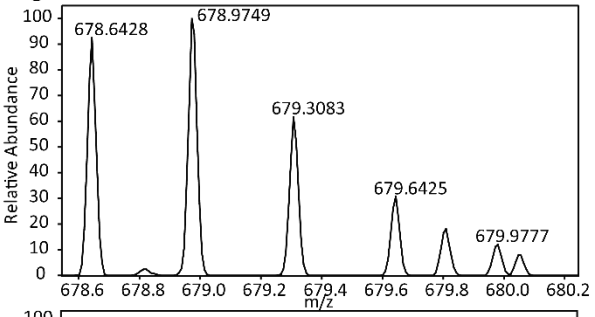

C

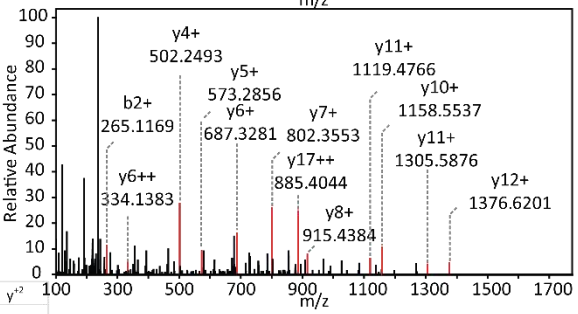

D

MH^{+1}	MH^{+2}	MH^{+3}
2033.9199	1017.4636	**678.6448**

b	b^{+2}				y	y^{+2}
-	-	1	T	19	-	-
265.1183	-	2	Y	18	1932.8722	966.9398
322.1397	-	3	G	17	1769.8089	885.4081
379.1612	-	4	G	16	1712.7875	856.8974
450.1983	-	5	A	15	1655.7660	828.3866
521.2354	-	6	A	14	1584.7289	792.8681
658.2944	329.6508	7	H	13	1513.6918	757.3495
729.3315	365.1694	8	A	12	1376.6329	688.8201
876.3999	438.7036	9	F	11	1305.5957	653.3015
991.4268	496.2170	10	D	10	1158.5273	579.7673
1119.4854	560.2463	11	Q	9	1043.5004	522.2538
1232.5695	616.7884	12	I	8	**915.4418**	458.2245
1347.5964	674.3018	13	D	7	**802.3577**	401.6825
1461.6393	731.3233	14	N	6	**687.3308**	344.1690
1532.6764	766.8419	15	A	5	573.2879	287.1476
1629.7292	815.3682	16	P	4	**502.2508**	251.6290
1758.7718	879.8895	17	E	3	405.1980	203.1026
1887.8144	944.4108	18	E	2	276.1554	138.5813
-	-	19	K	1	147.1128	74.0600

E

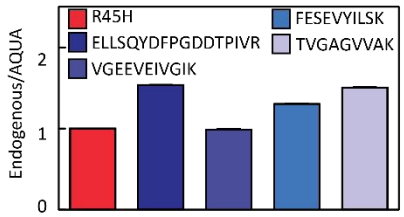

F

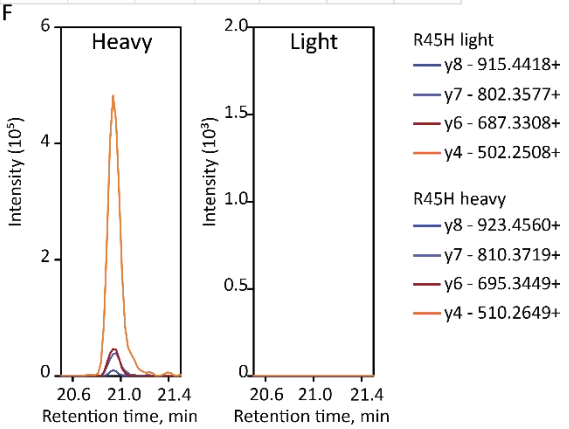

G

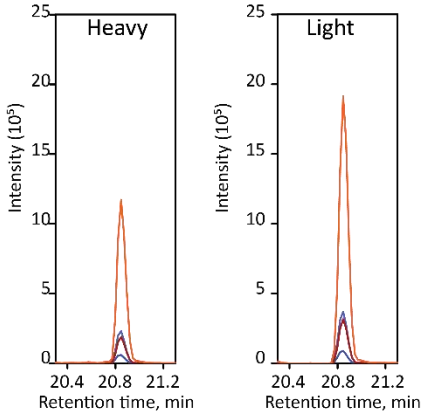

R59H: eek.AHGITINTSHVEYDTPTR.hya

A

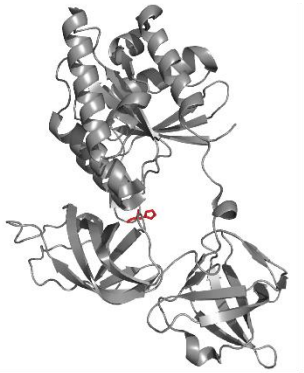

B

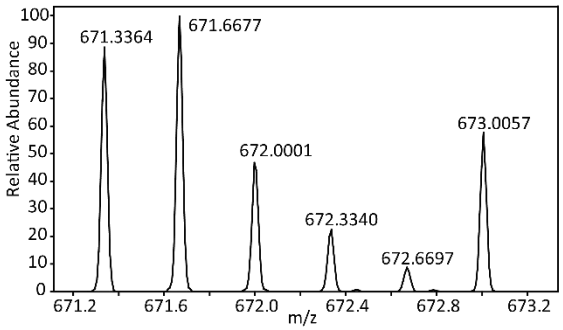

C

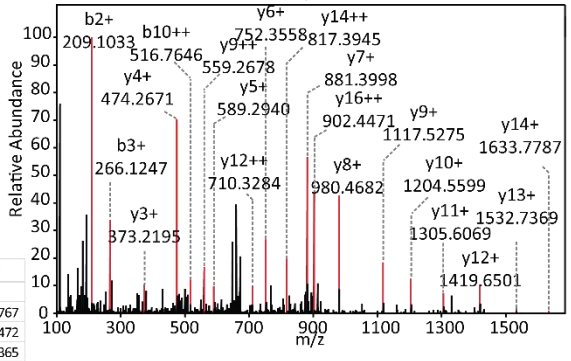

D

	MH^{+1}	MH^{+2}	MH^{+3}			
	2011.9832	1006.4952	**671.3326**			
b	b^{+2}				y	y^{+2}
-	-	1	A	18	-	-
209.1033	105.0553	2	H	17	1940.9641	970.9767
266.1248	133.5660	3	G	16	1803.8872	902.4472
379.2088	190.1081	4	I	15	1746.8657	873.9365
480.2565	240.6319	5	T	14	1633.7816	817.3945
593.3406	297.1739	6	I	13	1532.7340	766.8706
707.3835	354.1954	7	N	12	1419.6499	710.3286
808.4312	404.7192	8	T	11	1305.6070	653.3071
895.4632	448.2352	9	S	10	1204.5593	602.7833
1032.5221	516.7647	10	H	9	1117.5273	559.2673
1131.5905	566.2989	11	V	8	**980.4684**	490.7378
1260.6331	630.8202	12	E	7	**881.3999**	441.2036
1423.6965	712.3519	13	Y	6	**752.3575**	376.6823
1538.7234	796.8653	14	D	5	589.2940	295.1506
1639.7711	820.3892	15	T	4	474.2671	237.6372
1736.8238	868.9156	16	P	3	**373.2194**	187.1133
1837.8715	919.4392	17	T	2	276.1666	138.5870
-	-	18	R	1	175.1190	88.0631

E

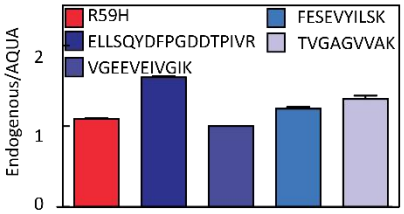

F

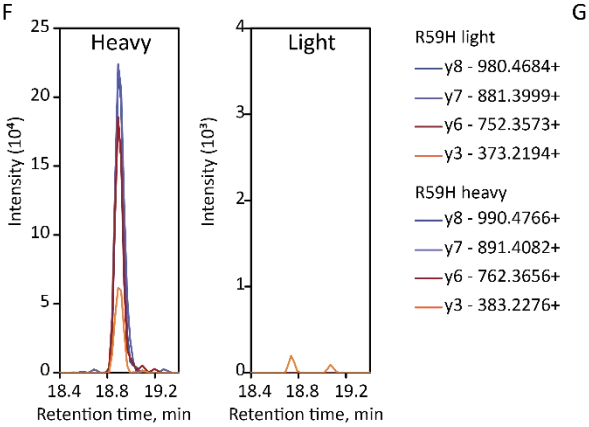

G

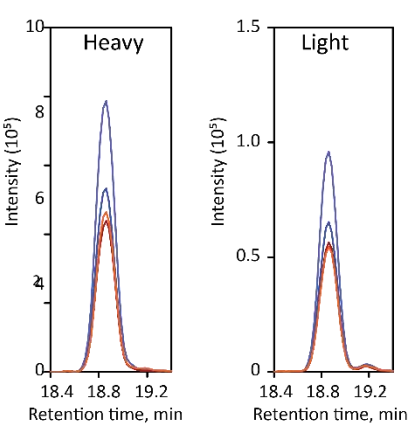

R172H: evr.ELLSQYDFPGDDTPIVHGSALK.ale

A

B

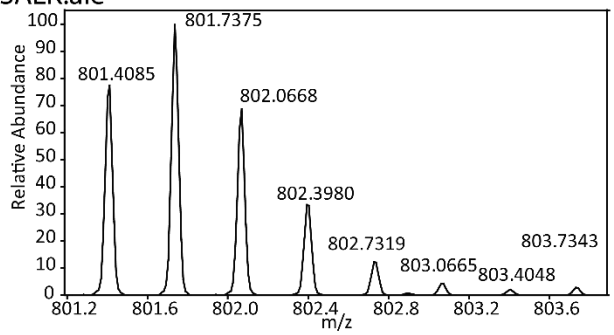

C

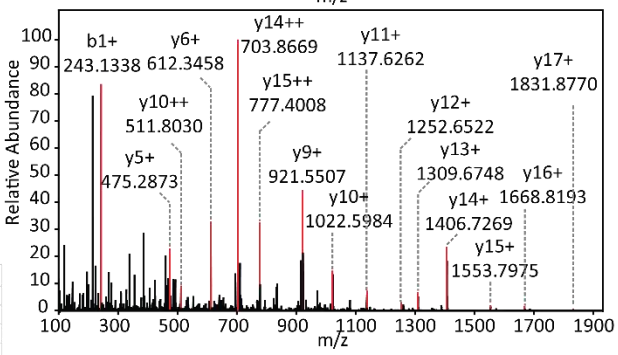

D

	MH+1	MH+2	MH+3			
	2402.187	1201.597	801.401			
b	b+2				y	y+2
-	-	1	E	22	-	-
243.1339	-	2	L	21	2273.1448	1137.0761
356.2180	-	3	L	20	2160.0608	1080.5340
443.2500	-	4	S	19	2046.9767	1023.9920
571.3086	-	5	Q	18	1959.9447	980.7460
734.3719	-	6	Y	17	1831.8861	916.4467
849.3989	-	7	D	16	1668.8228	834.9150
996.4673	-	8	F	15	1553.7958	777.4016
1093.5201	-	9	P	14	1406.7274	703.8673
1150.5415	-	10	G	13	1309.6747	655.3410
1265.5685	-	11	D	12	1252.6532	626.8302
1380.5954	-	12	D	11	1137.6262	569.3168
1481.6431	-	13	T	10	1022.5993	511.8033
1578.6958	-	14	P	9	921.5516	461.2795
1691.7799	-	15	I	8	824.4989	412.7531
1790.8483	-	16	V	7	711.4148	356.2110
1927.9072	964.4573	17	H	6	612.3464	306.6768
1984.9287	992.9680	18	G	5	475.2878	238.1474
2071.9607	1036.4840	19	S	4	418.2660	209.6366
2142.9978	1072.0026	20	A	3	331.2340	166.1206
2256.0819	1128.5446	21	L	2	260.1969	130.6021
-	-	22	K	1	147.1128	74.0600

E

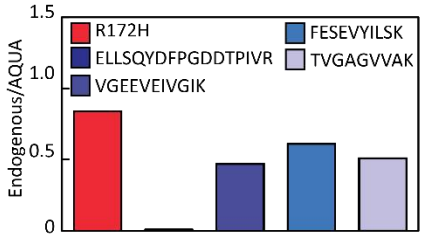

F

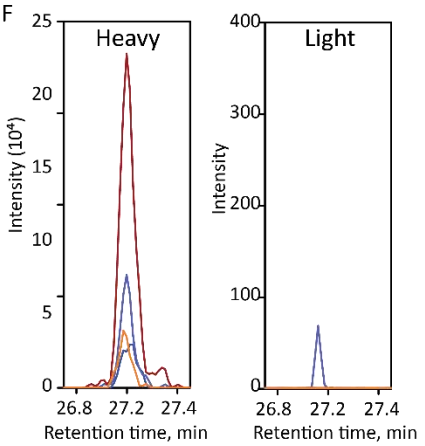

G

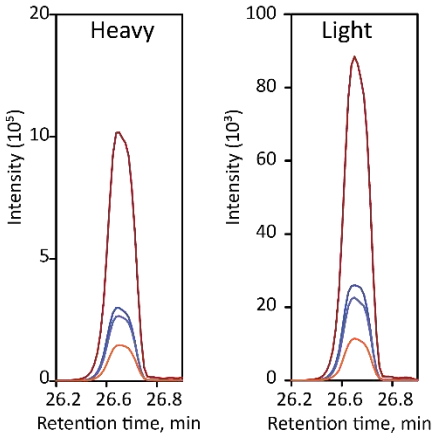

R231S: sgr.GTVVTGSVER.gii

A

B

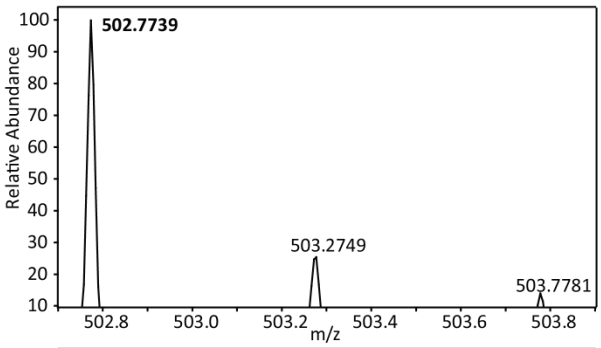

C

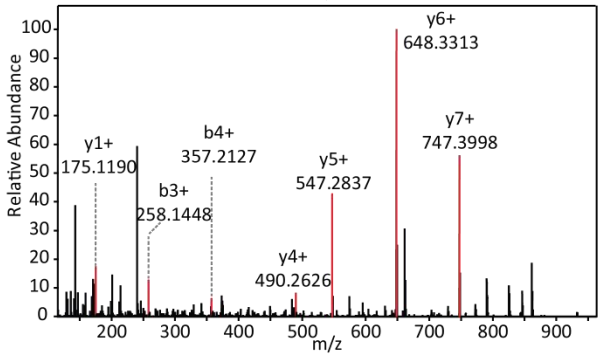

D

	MH^{+1}	MH^{+2}	MH^{+3}
	1004.5371	**502.7722**	335.5172

b				y	y^{+2}
-	1	G	10	-	-
159.0764	2	T	9	947.5156	474.2615
258.1448	3	V	8	846.4680	423.7376
357.2132	4	V	7	**747.3995**	374.2034
458.2609	5	T	6	**648.3311**	324.6692
515.2824	6	G	5	**547.2835**	274.1451
602.3144	7	S	4	**490.2620**	245.6346
701.3828	8	V	3	403.2300	202.1186
830.4254	9	E	2	304.1615	152.5844
-	10	R	1	**175.1190**	88.0631

E

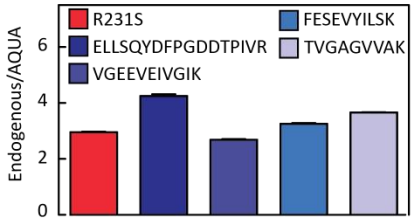

F

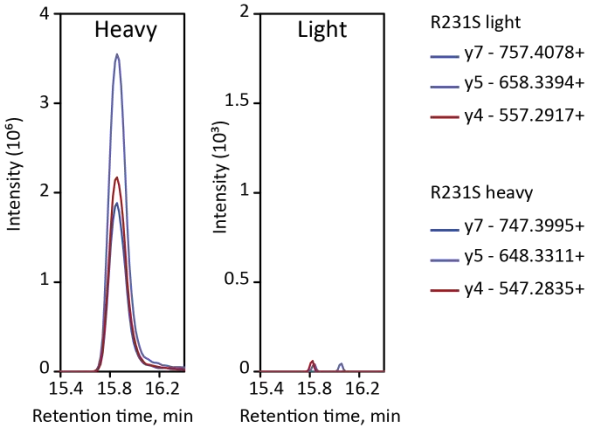

G

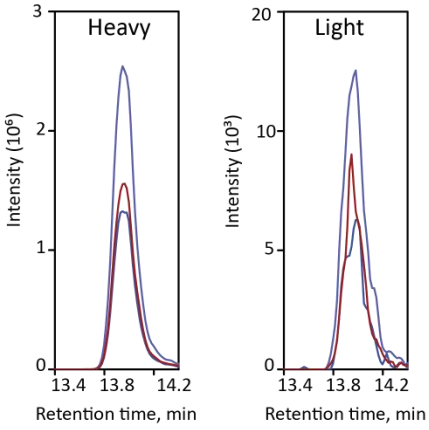

R231G: sgr.GTVVTGGVER.gii

A

B

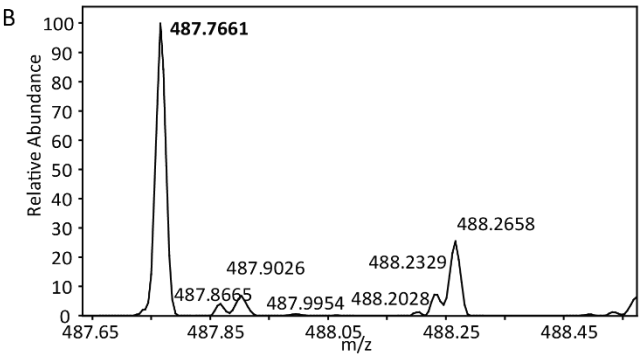

C

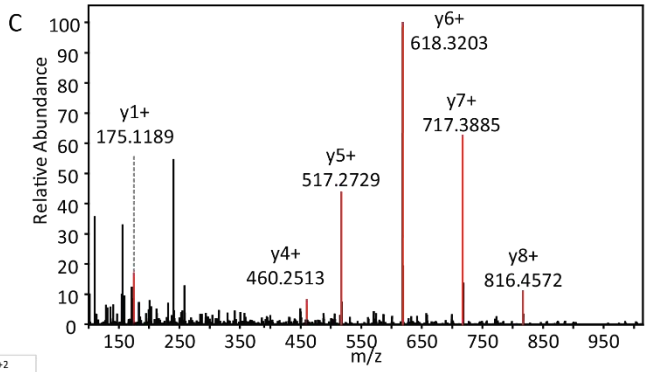

D

MH^{+1}	MH^{+2}	MH^{+3}
974.5265	**487.7669**	325.5137

b				y	y^{+2}
-	1	G	10	-	-
159.0764	2	T	9	917.5051	459.2562
258.1448	3	V	8	**816.4574**	409.7323
357.2132	4	V	7	**717.3890**	359.1981
458.2609	5	T	6	**618.3206**	309.6639
515.2824	6	G	5	**517.2729**	259.1401
572.0337	7	G	4	**460.2514**	230.6293
671.3723	8	V	3	403.2300	202.1186
800.4149	9	E	2	304.1615	152.5844
-	10	R	1	**175.1190**	88.0631

E

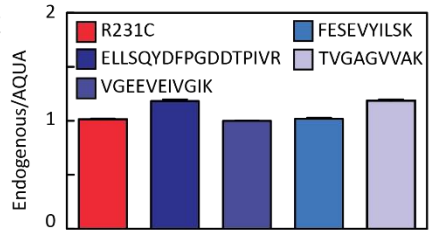

F

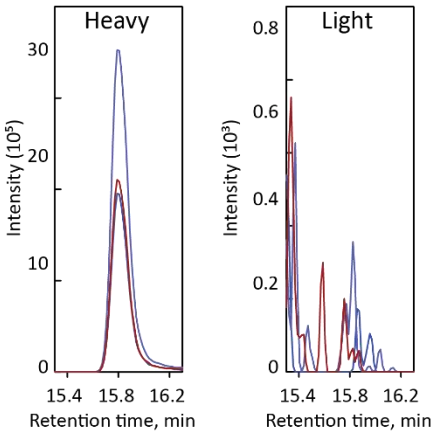

G

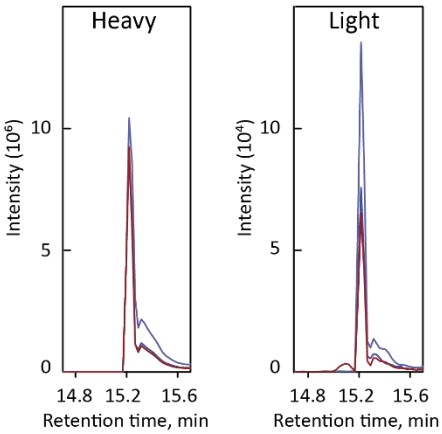

R231C: sgr.GTVVTGCVER.gii

A

B

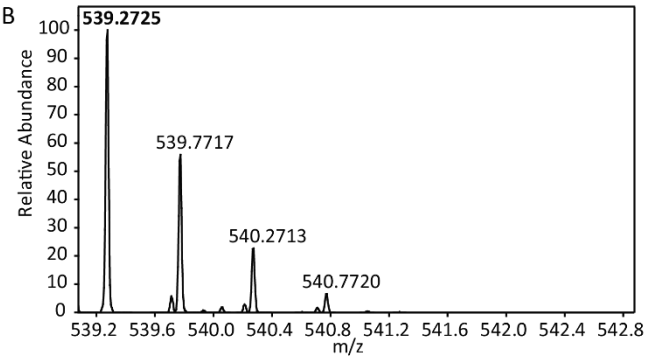

C

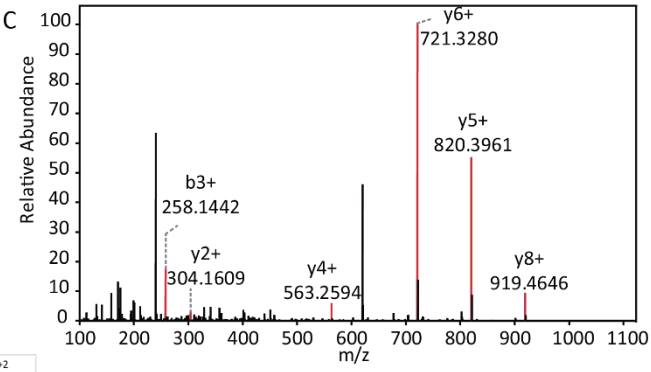

D

	MH^{+1}	MH^{+2}	MH^{+3}		
	1077.5357	**539.6236**	359.8501		
b				y	y^{+2}
-	1	G	10	-	-
159.0764	2	T	9	1020.5143	510.7608
258.1448	3	V	8	**919.4666**	460.2369
357.2132	4	V	7	**820.3892**	410.7027
458.2609	5	T	6	**721.3297**	361.1685
515.2824	6	G	5	620.2821	310.6447
675.3130	7	C	4	**563.2606**	282.1339
774.3815	8	V	3	**403.2300**	202.1186
903.4240	9	E	2	**304.1615**	152.5844
-	10	R	1	175.1190	88.0631

E

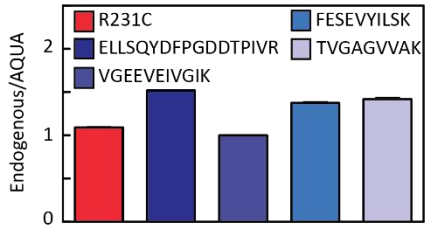

F

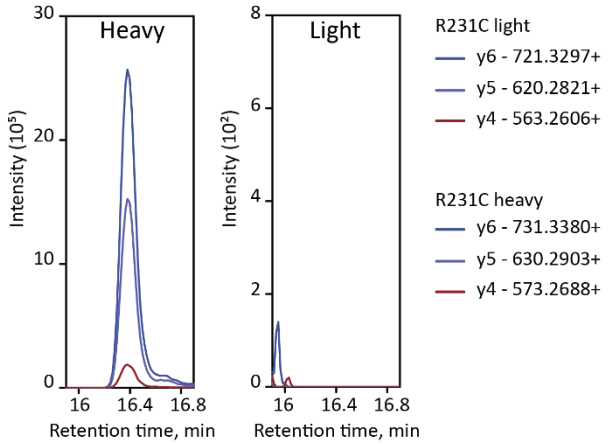

G

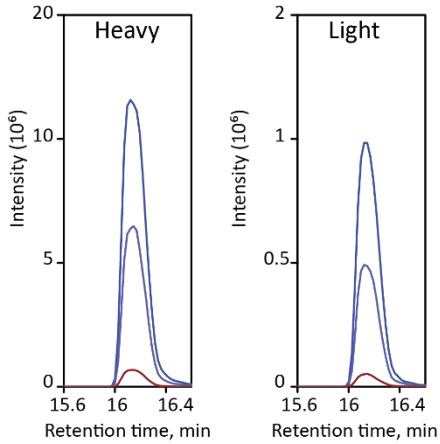

R231H: sgr.GTVVTGHVER.gii

A

B

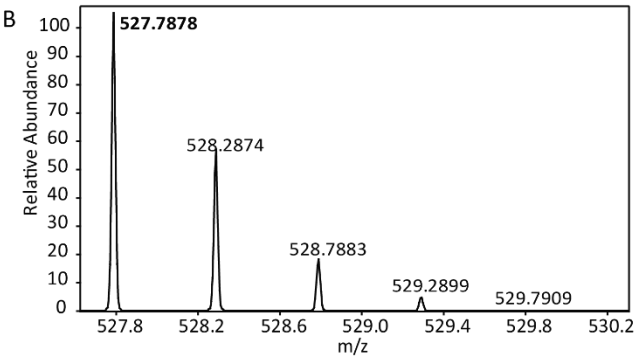

C

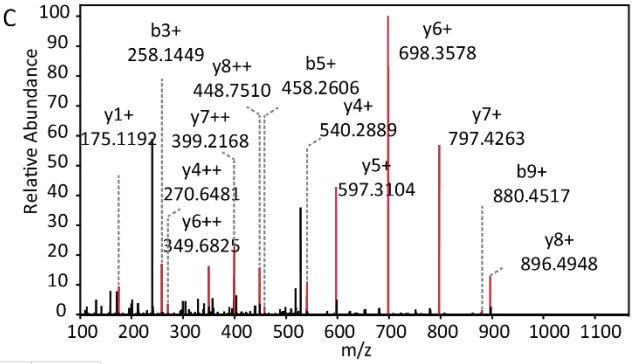

D

	MH^{+1}	MH^{+2}	MH^{+3}
	1045.5640	**527.7856**	352.1928

b	b^{+2}				y	y^{+2}
-	-	1	G	10	-	-
159.0764	-	2	T	9	977.5425	499.2749
258.1448	-	3	V	8	**896.4948**	**448.7511**
357.2132	-	4	V	7	**797.4264**	**399.2169**
458.2609	-	5	T	6	**698.3580**	**349.6826**
515.2824	-	6	G	5	**597.3103**	299.1588
652.3431	326.6743	7	H	4	**540.2889**	**270.6481**
751.4097	376.2085	8	V	3	403.2300	202.1186
880.4523	440.7298	9	E	2	304.1615	152.5844
-	-	10	R	1	**175.1190**	88.0631

E

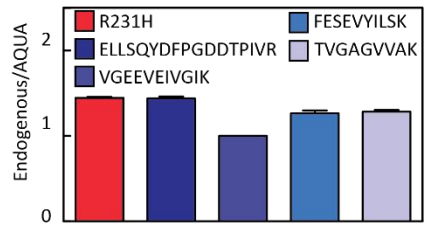

F

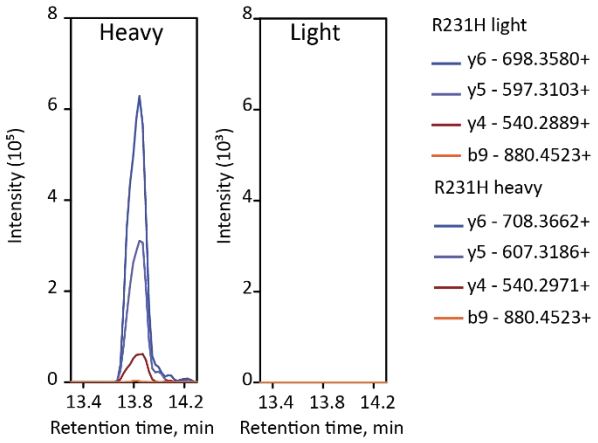

G

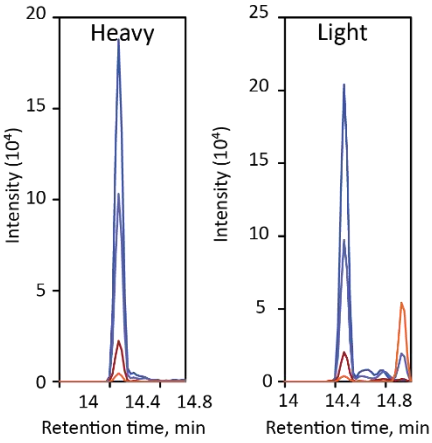

R231P: sgr.GTVVTGPVER.gii

A

B

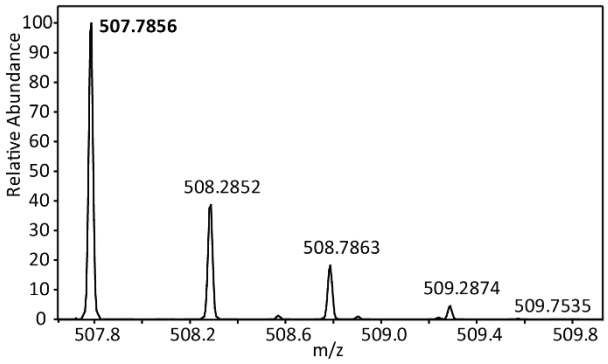

C

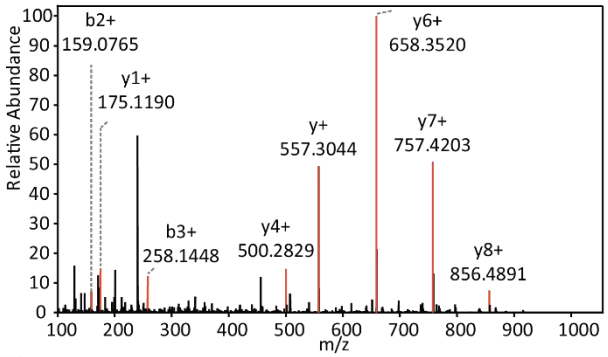

D

MH^{+1}	MH^{+2}	MH^{+3}
1014.5578	**507.7826**	338.8575

b				y	y^{+2}
-	1	G	10	-	-
159.0764	2	T	9	957.5364	479.2718
258.1448	3	V	8	**856.4887**	428.7480
357.2132	4	V	7	**757.4203**	379.2138
458.2609	5	T	6	**658.3519**	329.6796
515.2824	6	G	5	**557.3042**	279.1557
612.3352	7	P	4	**500.2827**	250.6450
711.4036	8	V	3	403.2300	202.1186
840.4462	9	E	2	304.1615	152.5844
-	10	R	1	**175.1190**	88.0631

E

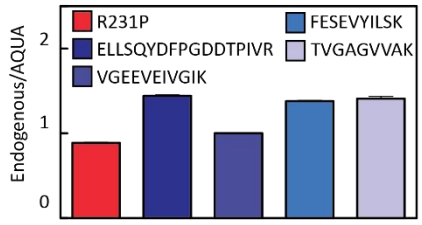

F

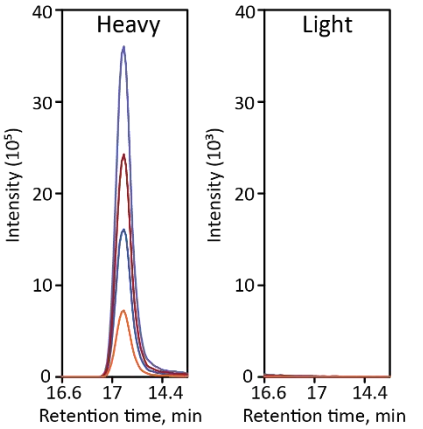

G

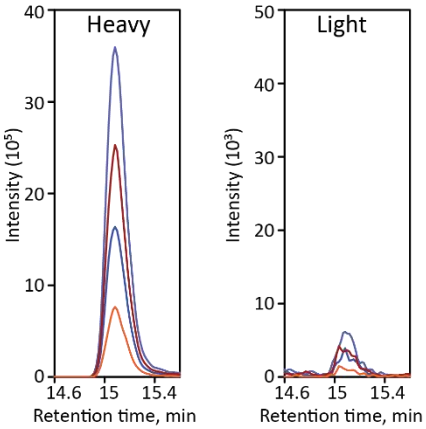

R231L: sgr.GTVVTGLVER.gii

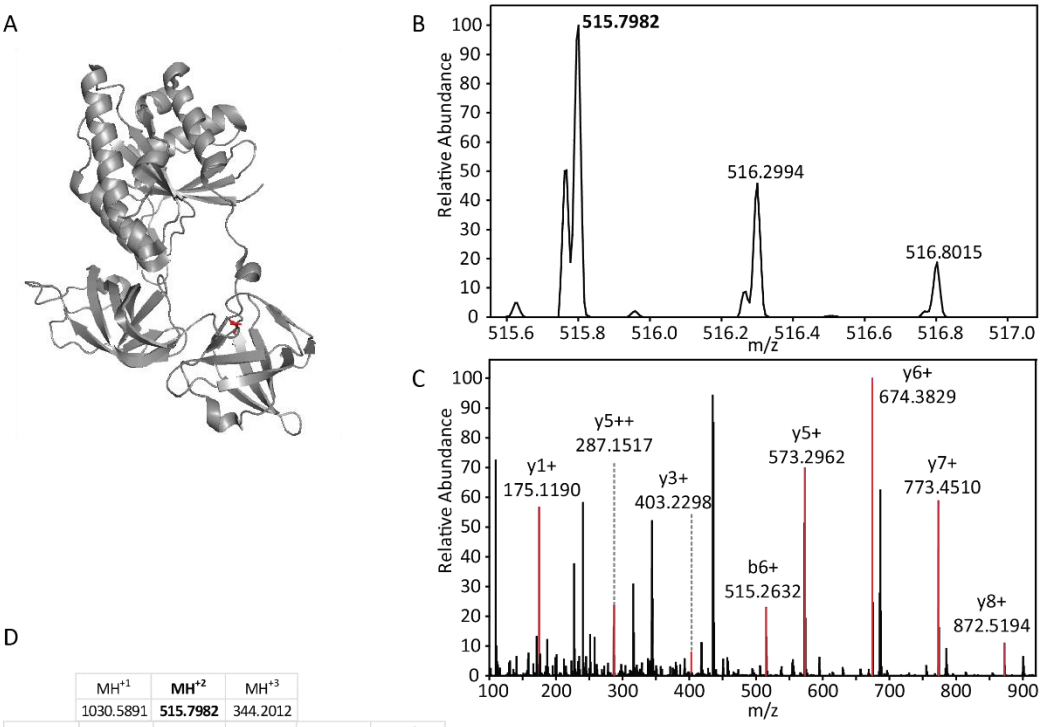

D

	MH^{+1}	MH^{+2}	MH^{+3}		
	1030.5891	**515.7982**	344.2012		
b				y	y^{+2}
-	1	G	10	-	-
159.0764	2	T	9	973.5677	487.2875
258.1448	3	V	8	**872.5200**	436.7636
357.2132	4	V	7	**773.4516**	387.2294
458.2609	5	T	6	**674.3832**	337.6952
515.2824	6	G	5	**573.3355**	**287.1714**
628.3665	7	L	4	516.3140	258.6606
727.4349	8	V	3	**403.2300**	202.1186
856.4775	9	E	2	304.1615	152.5844
-	10	R	1	**175.1190**	88.0631

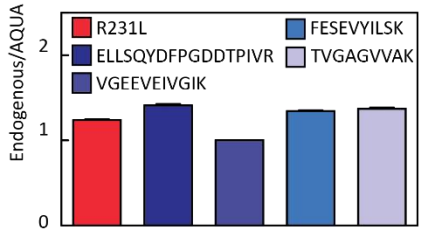

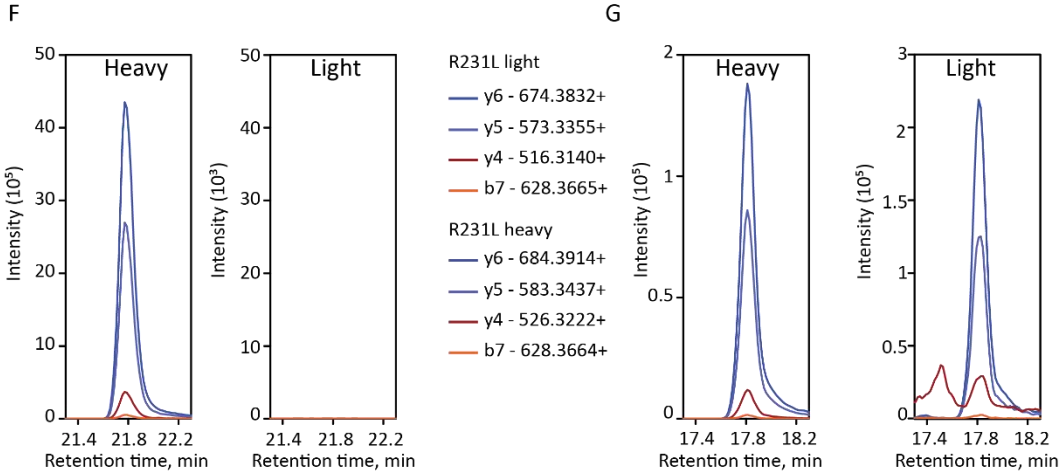

R234H: tgr.VEHGIIK.vge

A

B

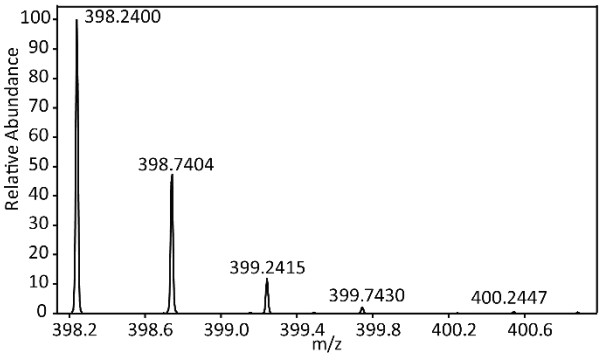

C

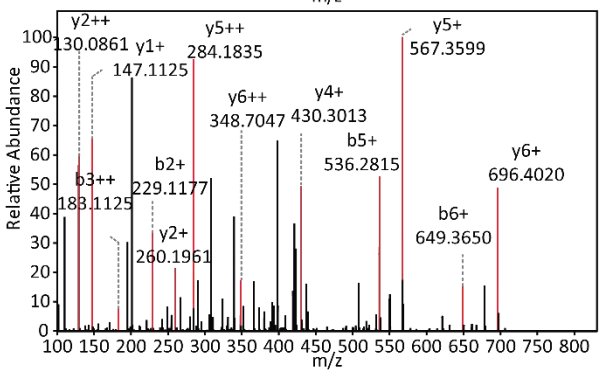

D

	MH^{+1}	MH^{+2}	MH^{+3}			
	795.4723	398.2398	265.829			
b	b^{+2}				y	y^{+2}
-	-	1	V	7	-	-
219.1183	-	2	E	6	696.4093	348.7056
266.1772	183.5922	3	H	5	567.3613	284.1843
423.1987	212.1030	4	G	4	430.3024	215.6548
536.2827	268.6450	5	I	3	373.2809	187.1441
649.3668	325.1870	6	I	2	260.1969	130.6021
-		7	K	1	147.1128	74.0600

E

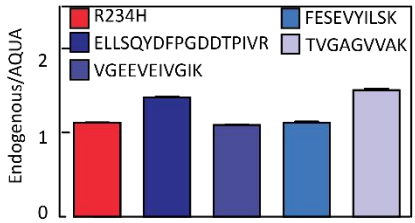

F

G

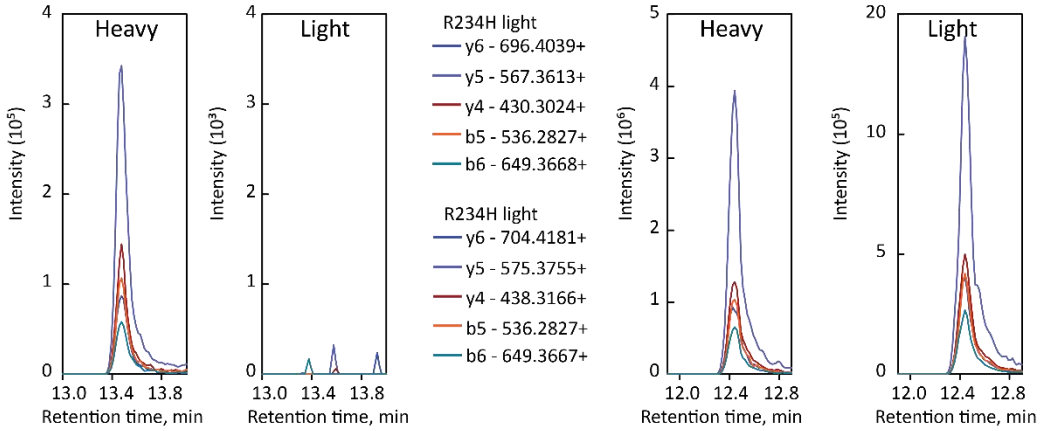

K249Q: iik.VGEEVEIVGIQETQK.stc

A

B

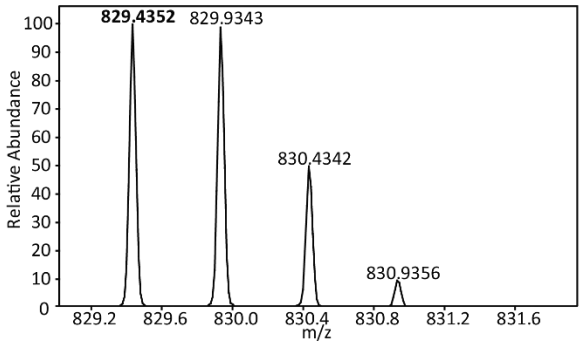

C

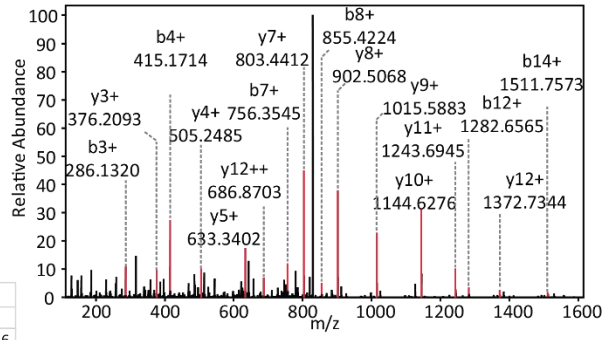

D

MH^{+1}	MH^{+2}	MH^{+3}
1657.8643	**829.4358**	553.2930

b				y	y^{+2}
-	1	V	15	-	-
157.0972	2	G	14	1558.7959	779.9016
286.1397	3	E	13	1501.7744	751.3909
415.1823	4	E	12	**1372.7318**	**686.8696**
514.2508	5	V	11	**1243.6892**	622.3483
643.2933	6	E	10	**1144.6208**	572.8141
756.3774	7	I	9	**1015.5782**	508.2928
855.4458	8	V	8	**902.4942**	451.7507
912.4673	9	G	7	**803.4258**	402.2165
1025.5514	10	I	6	746.4043	373.7058
1153.6099	11	Q	5	**633.3202**	317.1638
1282.6525	12	E	4	**505.2617**	253.1345
1383.7002	13	T	3	**376.2191**	188.6132
1511.7588	14	Q	2	275.1714	138.0893
-	15	K	1	147.1128	74.0600

E

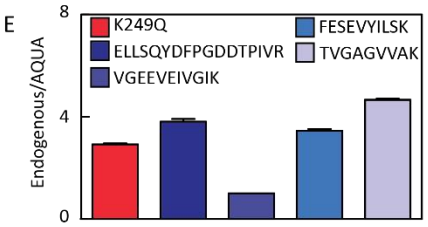

F

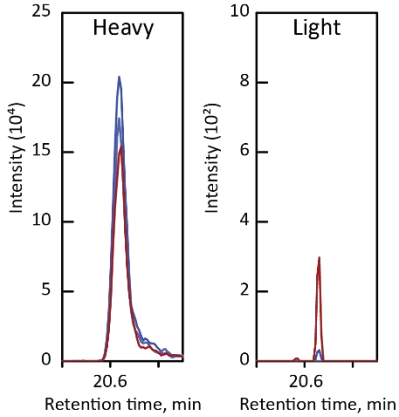

K249Q double
y10 - 1159.6522
y9 - 1030.6096
b8 - 855.4458
K249Q light
y10 - 1144.6208
y9 - 1015.5782
y8 - 855.4458

G

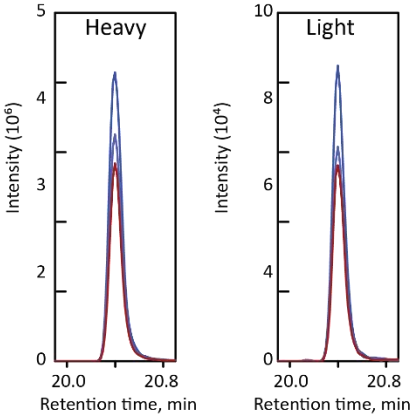

K249E: iik.VGEEVEIVGIEETQK.stc

A

B

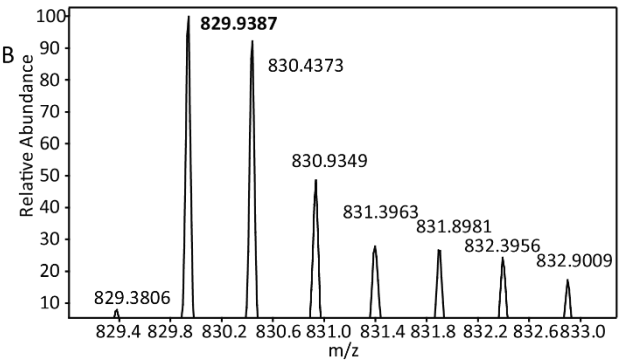

C

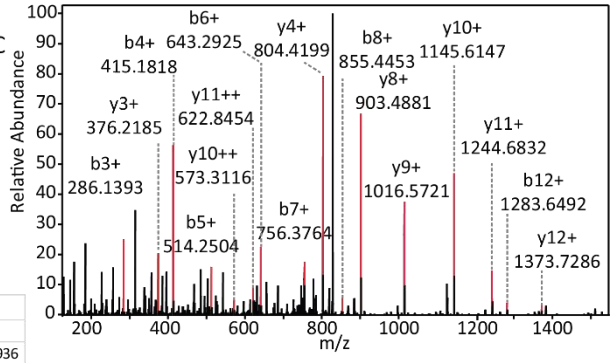

D

	MH^{+1}	MH^{+2}	MH^{+3}
	1658.8483	**829.9278**	553.6210

b				y	y^{+2}
-	1	V	15	-	-
157.0972	2	G	14	1559.7799	780.3936
286.1397	3	E	13	1502.7584	751.8829
415.1823	4	E	12	**1373.7159**	687.3616
514.2508	5	V	11	**1244.6733**	**622.8403**
643.2933	6	E	10	**1145.6048**	**573.3061**
756.3774	7	I	9	**1016.5623**	508.7848
855.4458	8	V	8	**903.4782**	452.2427
912.4673	9	G	7	**804.4098**	402.7085
1025.5514	10	I	6	747.3883	374.1978
1154.5939	11	E	5	**634.6042**	317.6558
1283.6365	12	E	4	505.2617	253.1345
1384.6842	13	T	3	**376.2191**	188.6132
1512.7428	14	Q	2	275.1714	138.0893
-	15	K	1	147.1128	74.0600

E

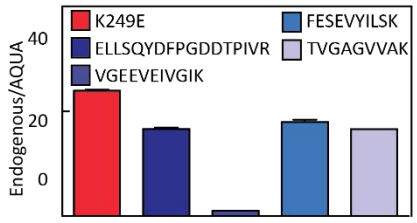

F

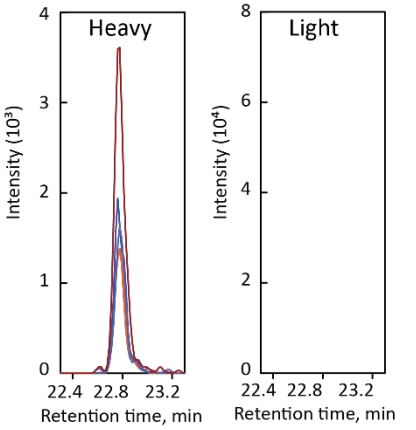

G

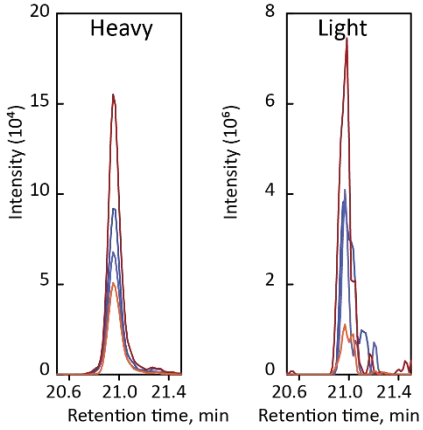

K249T: iik.VGEEVEIVGITETQK.stc

A

B

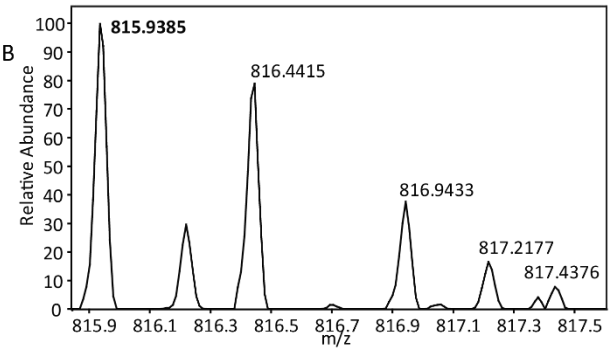

C

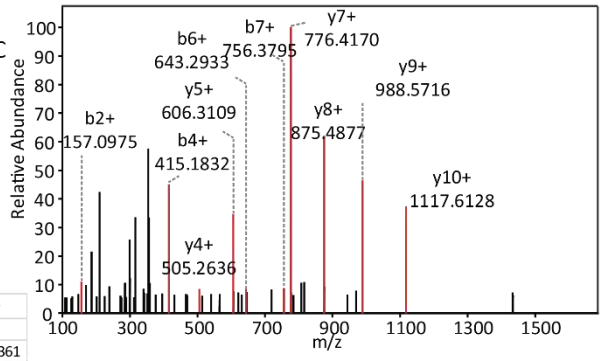

D

MH^{+1}	MH^{+2}	MH^{+3}
1630.8534	**815.9303**	544.2893

b				y	y^{+2}
-	1	V	15	-	-
157.0972	2	G	14	1531.7850	766.9361
286.1397	3	E	13	1474.7635	737.8854
415.1823	4	E	12	1345.7209	673.3641
514.2508	5	V	11	1216.6783	608.8428
643.2933	6	E	10	**1117.6099**	559.3086
756.3774	7	I	9	**988.5673**	494.7873
855.4458	8	V	8	**875.4833**	438.2453
912.4673	9	G	7	**776.4149**	388.7111
1025.5514	10	I	6	719.3934	360.2003
1126.599	11	T	5	**606.3093**	303.6583
1255.6416	12	E	4	**505.2617**	253.1345
1356.6893	13	T	3	376.2191	188.6132
1484.7479	14	Q	2	275.1714	138.0893
-	15	K	1	147.1128	74.0600

E

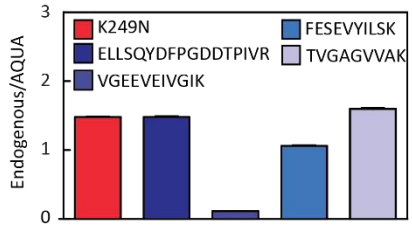

F

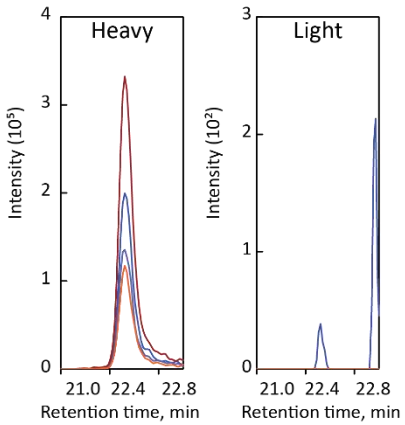

K249T light
- y10 - 1117.6099+
- y9 - 988.5673+
- y8 - 875.4833+
- b8 - 855.4458+

K249T heavy
- y10 - 1125.6241+
- y9 - 996.5815+
- y8 - 883.4975+
- b8 - 855.4975+

G

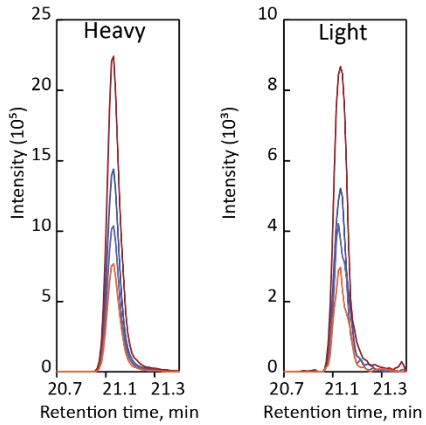

K249R: iik.VGEEVEIVGIR.etq

A

B

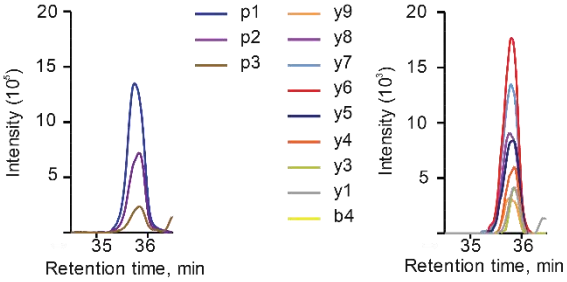

C

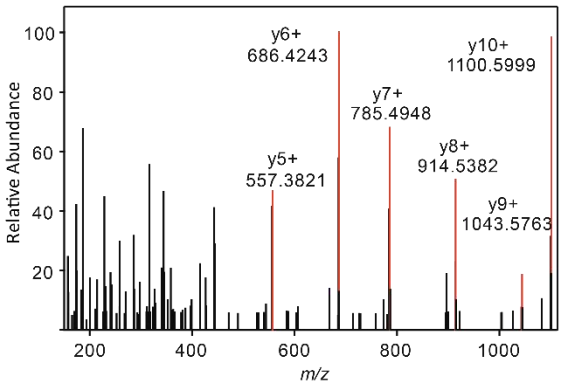

D

	MH+1	MH+2	MH+3		
	1199.663	600.3352	400.5592		
b				y	y+2
-	1	V	11	-	-
157.0972	2	G	10	1100.5946	550.8009
286.1397	3	E	9	1043.5732	522.2902
415.1823	4	E	8	914.5306	457.7689
514.2508	5	V	7	785.4880	393.2476
643.2933	6	E	6	686.4196	343.7134
756.3774	7	I	5	557.3770	279.1921
855.4458	8	V	4	444.2929	222.6501
912.4673	9	G	3	345.2245	173.1159
1025.5514	10	I	2	288.2030	144.6051
-	11	R	1	175.1190	88.0631

E

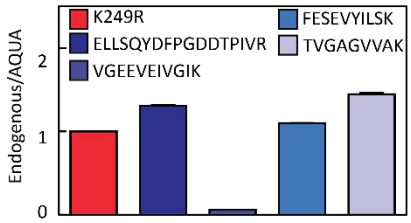

F

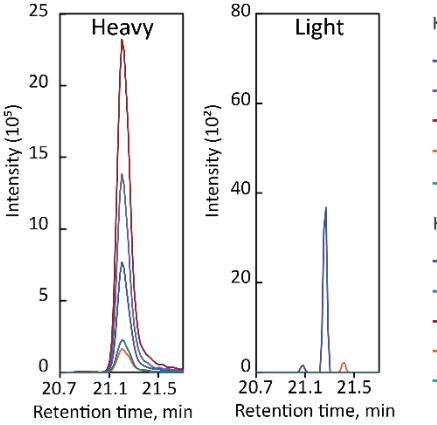

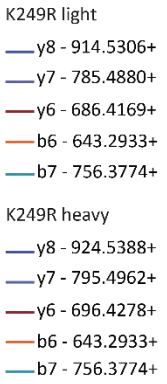

G

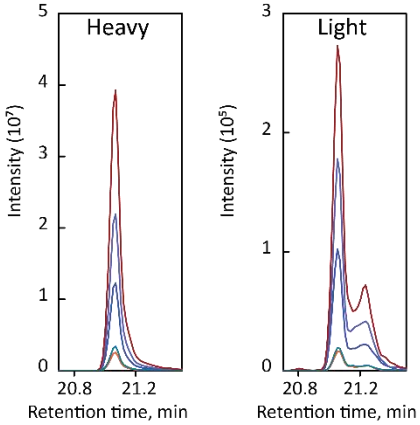

K249N: iik.VGEEVEIVGINETQK.stc

A

B

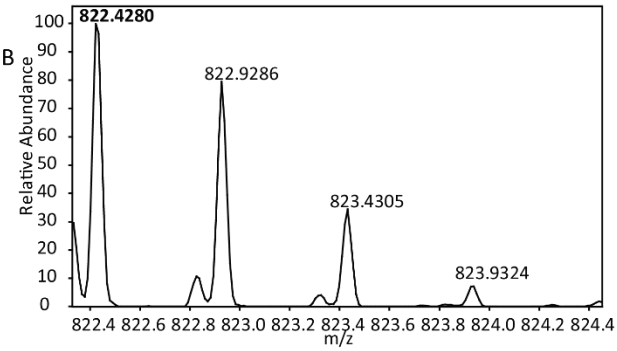

C

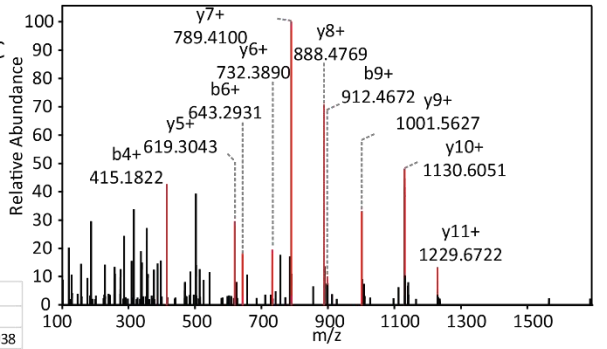

D

MH^{+1}	MH^{+2}	MH^{+3}
1643.8487	**822.428**	548.6211

b				y	y^{+2}
-	1	V	15	-	-
157.0972	2	G	14	1544.7802	772.8938
286.1397	3	E	13	1487.7588	744.3830
415.1823	4	E	12	1358.7162	679.8617
514.2508	5	V	11	**1229.6736**	615.3404
643.2933	6	E	10	**1130.6052**	565.8062
756.3774	7	I	9	**1001.5626**	501.2849
855.4458	8	V	8	**888.4785**	444.7429
912.4673	9	G	7	**789.4101**	395.2087
1025.5514	10	I	6	**732.3886**	366.6980
1139.5943	11	N	5	**619.3046**	310.1559
1268.6369	12	E	4	505.2617	253.1345
1369.6846	13	T	3	376.2191	188.6132
1497.7431	14	Q	2	275.1714	138.0893
-	15	K	1	147.1128	74.0600

E

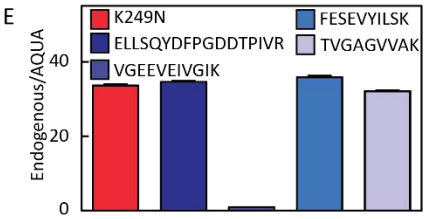

F

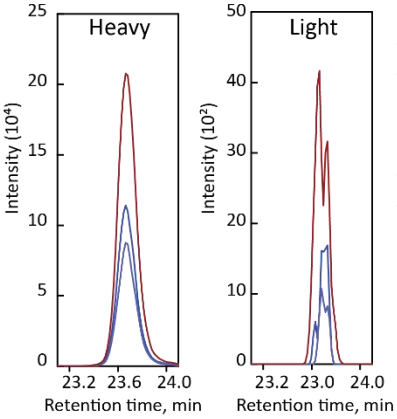

K249N heavy
y10 - 1138.6194+
y9 - 1009.5768
y8 - 896.4927+

K249N light
y10 - 1130.6052+
y9 - 1001.5626
y8 - 888.4785+

G

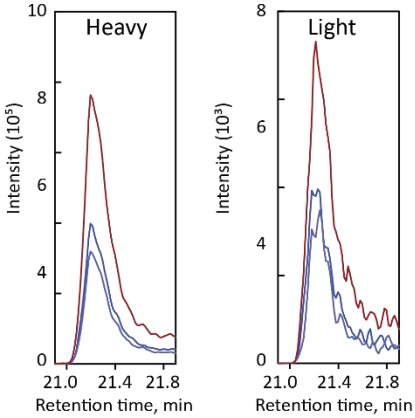

R270H: frk.LLDEGHAGENVGVLLR.gik

A

B

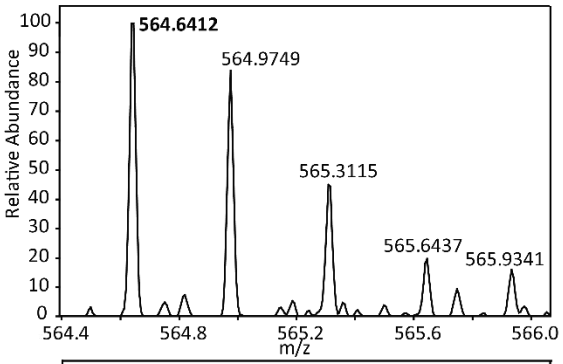

C

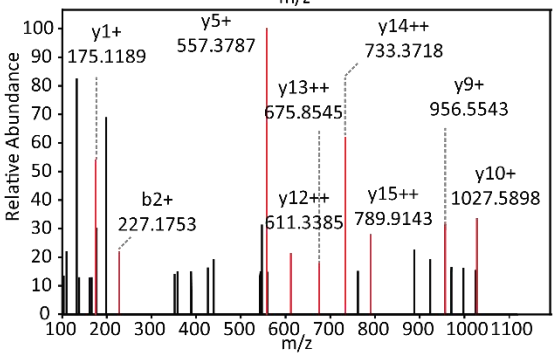

D

		MH+1	MH+2	MH+3		
		1691.9075	864.4574	**564.6407**		
b	b+2				y	y+2
-	-	1	L	16	-	-
227.1754	-	2	L	15	1578.8234	789.9154
342.2023	-	3	D	14	1465.7394	733.3733
471.2449	-	4	E	13	1350.7124	657.8599
528.2664	-	5	G	12	1221.6698	611.3386
665.3253	333.1663	6	H	11	1164.6484	582.8278
736.3624	368.6849	7	A	10	1027.5895	514.2984
793.3839	397.1956	8	G	9	956.5524	478.7798
922.4565	461.7169	9	E	8	899.5309	450.2961
1036.4964	518.7383	10	N	7	770.4883	385.7478
1135.5378	568.2726	11	V	6	656.4454	328.7263
1192.5593	596.7833	12	G	5	557.3770	297.1921
1291.6277	646.3175	13	V	4	500.3555	250.6814
1404.7118	702.8595	14	L	3	401.2871	201.1472
1517.7958	759.4016	15	L	2	288.2030	144.6051
-	-	16	R	1	175.1190	88.0631

E

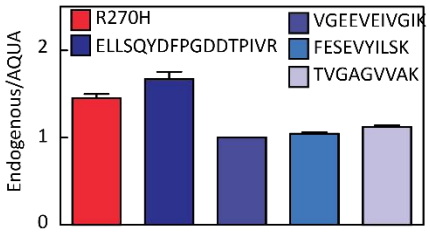

F

G

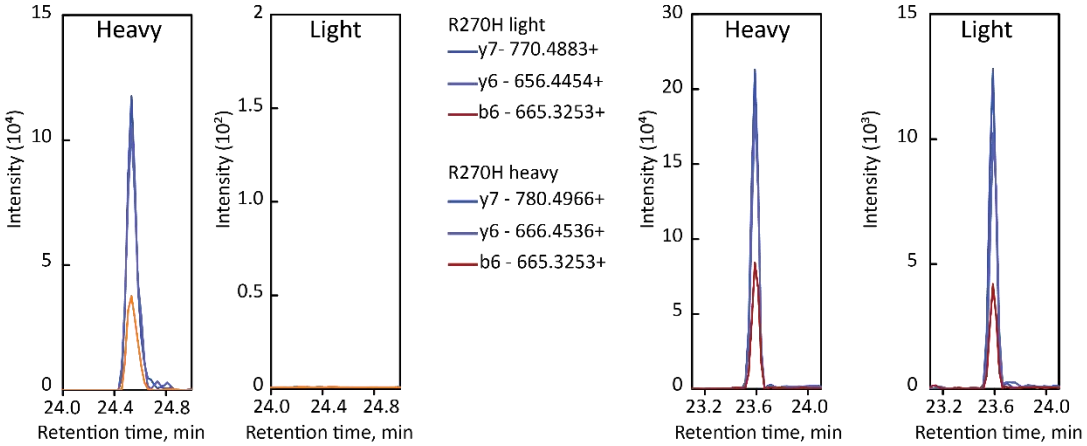

R280H: EGR.AGENVGVLLHGIK.REE

A

B

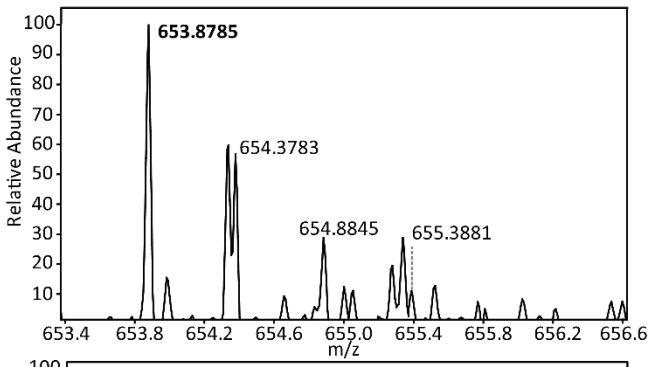

C

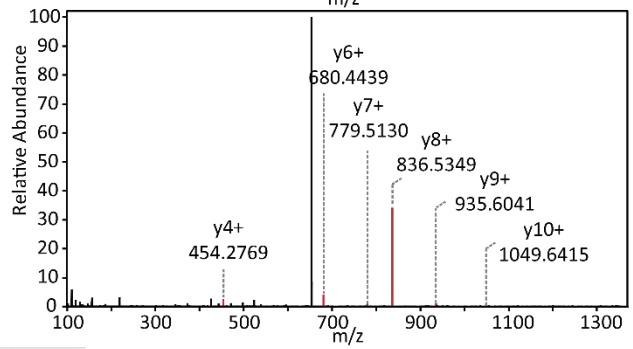

D

	MH^{+1}	MH^{+2}	MH^{+3}
	1306.7478	**653.8775**	436.2541

b	b^{+2}				y	y^{+2}
-	-	1	A	13	-	-
129.0659	-	2	G	12	1235.7106	618.3590
258.1084	-	3	E	11	1178.6892	589.8482
372.1514	-	4	N	10	1049.6466	525.3269
471.2198	-	5	V	9	935.6037	468.3055
528.2413	-	6	G	8	836.5352	418.7713
627.3097	-	7	V	7	779.5138	390.2605
740.3937	-	8	L	6	680.4454	340.7263
853.4778	-	9	L	5	567.3613	284.1843
990.5367	495.7720	10	H	4	454.2772	227.6423
1047.5582	524.2827	11	G	3	317.2183	159.1128
1160.6422	580.8248	12	I	2	260.1969	130.6021
-	-	13	K	1	147.1128	74.0600

E

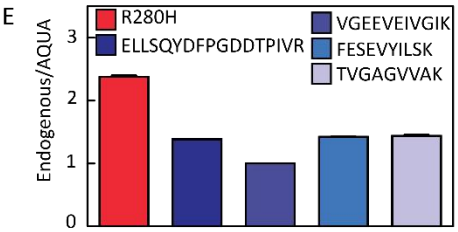

F

G

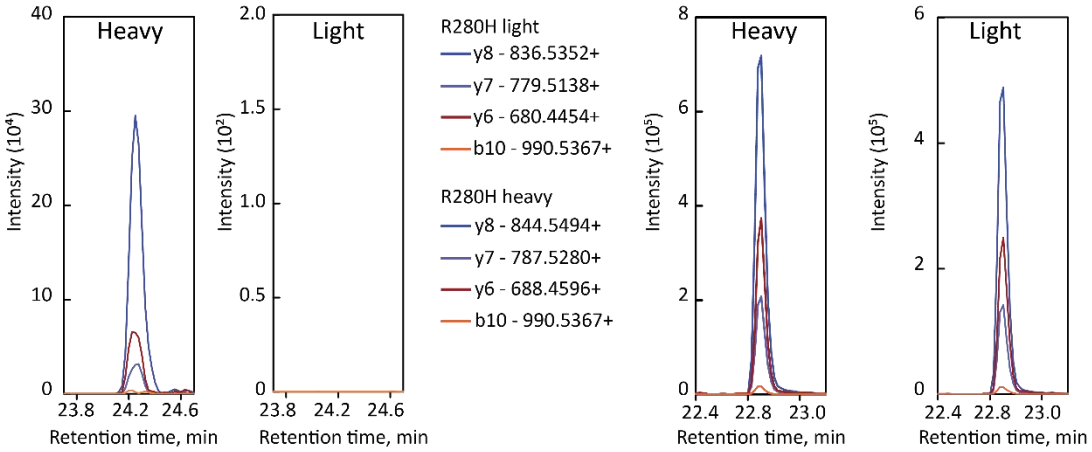

R284H: lak.HEEIER.arg

A

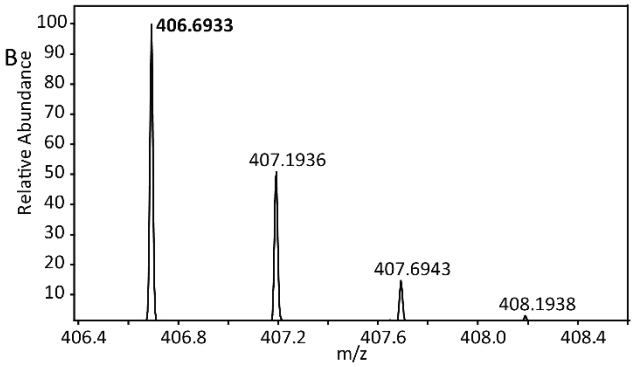

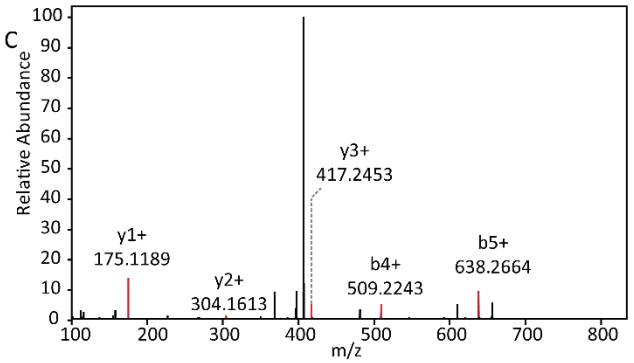

D

	MH^{+1}	MH^{+2}	MH^{+3}			
	812.3897	406.6985	271.4681			
b	b^{+2}				y	y^{+2}
-	-	1	H	6	-	-
267.1088	134.0580	2	E	5	675.3308	338.1690
396.1514	198.5793	3	E	4	546.2882	273.6477
509.2354	255.1214	4	I	3	417.2456	209.1264
638.2780	319.6427	5	E	2	304.1615	152.5844
-	-	6	R	1	175.1190	88.0631

E

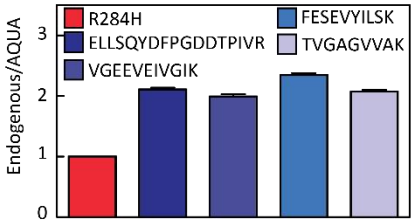

F

G

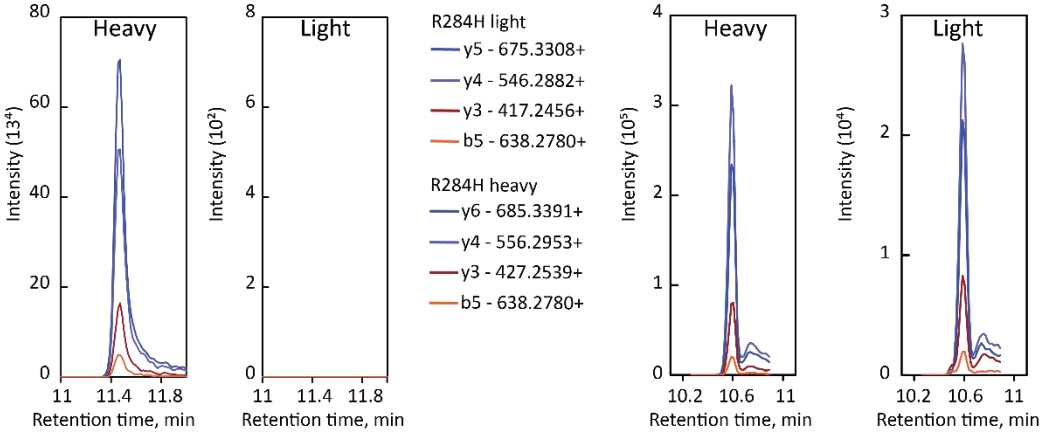

K314Q: htk.FESEVYILSQDEGGR.deg

A

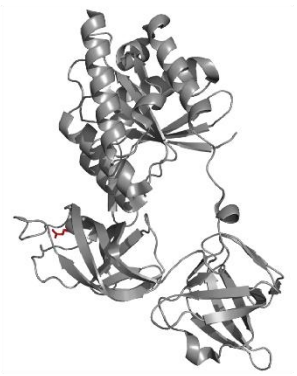

B

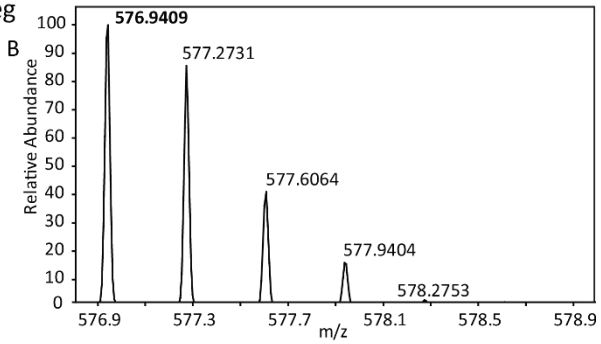

C

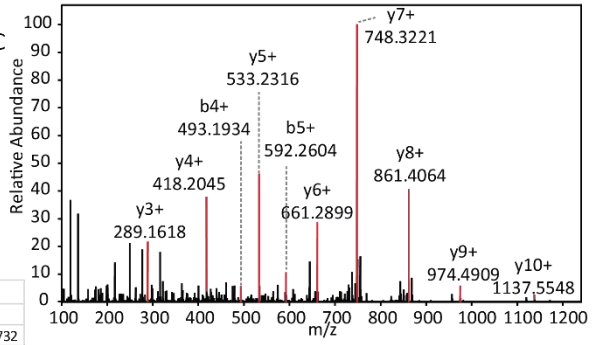

D

	MH^{+1}	MH^{+2}	MH^{+3}
	1728.8075	864.9074	**576.9407**

b				y	y^{+2}
-	1	F	15	-	-
277.1183	2	E	14	1581.7391	791.3732
364.1503	3	S	13	1452.6965	726.8519
493.1929	4	E	12	1365.6645	683.3359
592.2613	5	V	11	1236.6219	618.8146
755.3246	6	Y	10	**1137.5535**	569.2804
868.4087	7	I	9	**974.4901**	487.7487
981.4928	8	L	8	**861.4061**	431.2067
1068.5248	9	S	7	**748.3220**	374.6646
1196.5834	10	Q	6	**661.2900**	331.1486
1311.6103	11	D	5	**533.2314**	267.1193
1440.6529	12	E	4	**418.2045**	209.6059
1497.6744	13	G	3	**289.1619**	145.0846
1554.6958	14	G	2	232.1404	116.5738
-	15	R	1	175.1190	88.0631

E

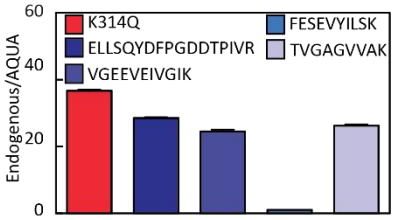

F

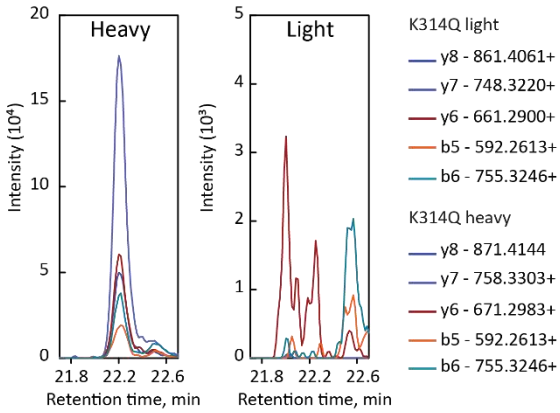

G

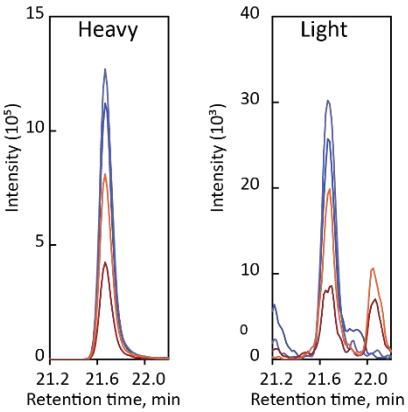

K314T: htk.FESEVYILSTDEGGR.deg

A

B

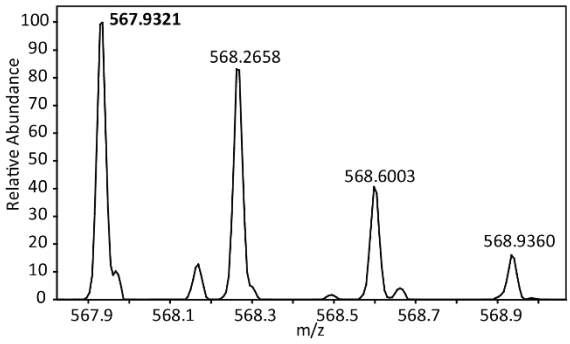

C

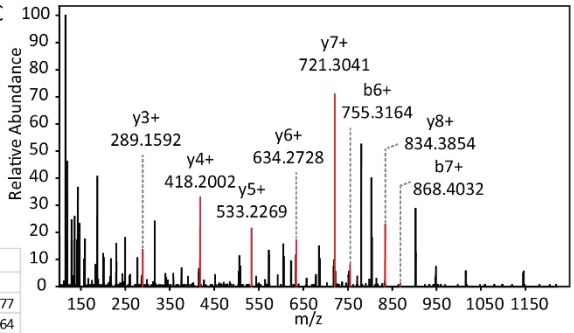

D

MH^{+1}	MH^{+2}	MH^{+3}
1701.7966	851.4019	**567.9371**

b				y	y^{+2}
-	1	F	15	-	-
277.1183	2	E	14	1554.7282	777.8677
364.1503	3	S	13	1425.6856	713.3464
493.1929	4	E	12	1338.6536	669.8304
592.2613	5	V	11	1209.6110	605.3091
755.3246	6	Y	10	1110.5426	555.7749
868.4087	7	I	9	947.4793	474.2433
981.4928	8	L	8	**834.3952**	417.7012
1068.5248	9	S	7	**721.3111**	361.1592
1169.5725	10	T	6	**634.2791**	317.6432
1284.5994	11	D	5	**533.2314**	267.1193
1413.642	12	E	4	**418.2045**	209.6059
1470.6635	13	G	3	**289.1619**	145.0846
1527.6849	14	G	2	232.1404	116.5738
-	15	R	1	175.1190	88.0631

F

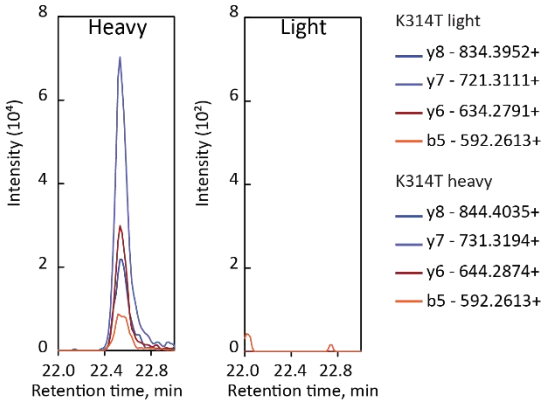

G

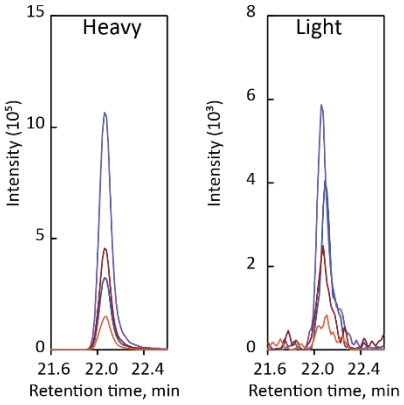

K314E: htk.FESEVYILSEDEGGR.deg

A

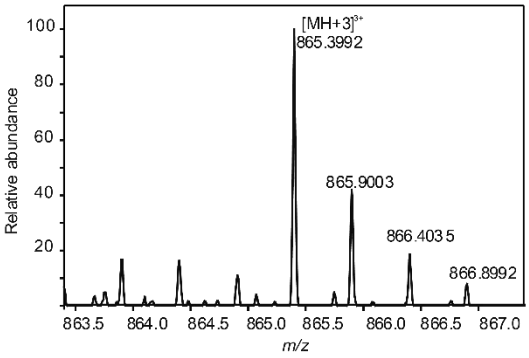

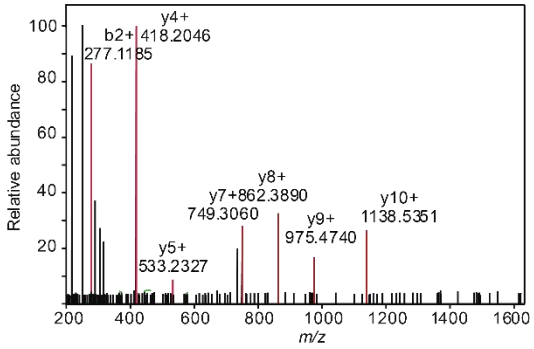

D

MH^{+1}	MH^{+2}	MH^{+3}
1729.7915	865.3994	577.2687

b				y	y^{+2}
-	1	F	15	-	-
277.1183	2	E	14	1582.7231	791.8652
364.1503	3	S	13	1453.6805	727.3439
493.1929	4	E	12	1366.6485	683.8279
592.2613	5	V	11	1237.6059	619.3066
755.3246	6	Y	10	1138.5375	569.7724
868.4087	7	I	9	975.4742	488.2407
981.4928	8	L	8	862.3901	431.6987
1068.5248	9	S	7	749.3060	375.1567
1197.5674	10	E	6	662.2740	331.6406
1312.5943	11	D	5	533.2314	267.1193
1441.6369	12	E	4	418.2045	209.6059
1498.6584	13	G	3	289.1619	145.0846
1555.6799	14	G	2	232.1404	116.5738
-	15	R	1	175.1190	88.0631

E

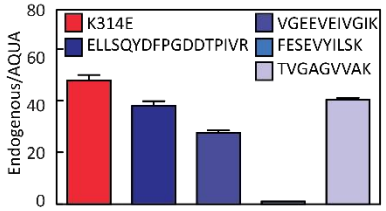

F

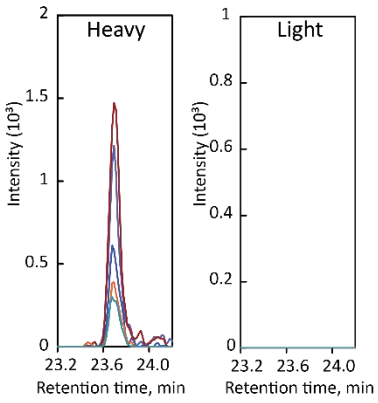

G

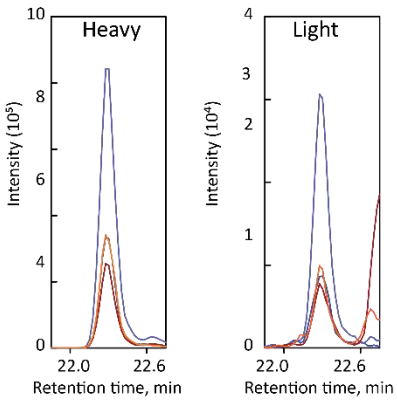

K314R: htk.FESEVYILSRDEGGR.deg

A

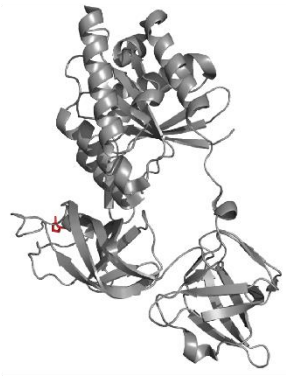

B

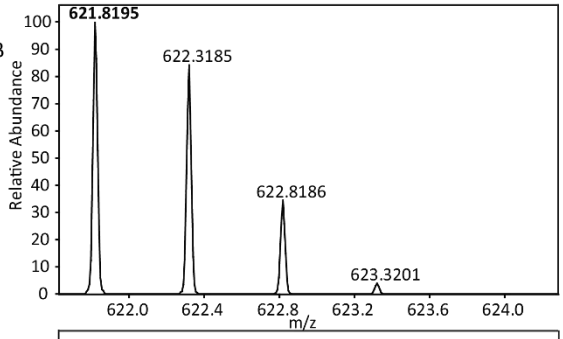

C

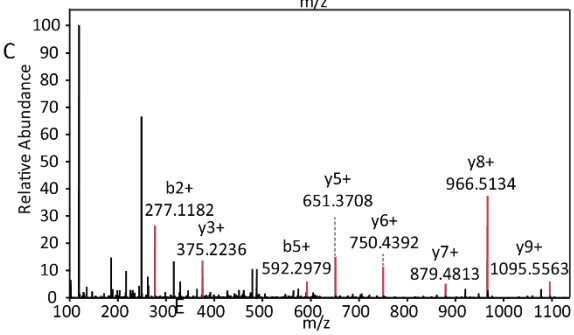

D

MH+1	MH+2	MH+3
1242.6365	**621.8219**	414.8837

b				y	y+2
-	1	F	10	-	-
277.1183	2	E	9	**1095.5681**	548.2877
364.1503	3	S	8	**966.5255**	483.7664
493.1929	4	E	7	**879.4934**	440.2504
592.2613	5	V	6	**750.4509**	375.7291
755.3246	6	Y	5	**651.3824**	326.1949
868.4087	7	I	4	488.3191	244.6632
981.4928	8	L	3	**375.2350**	188.1212
1068.5248	9	S	2	262.1510	131.5791
-	10	R	1	175.1190	88.0631

G

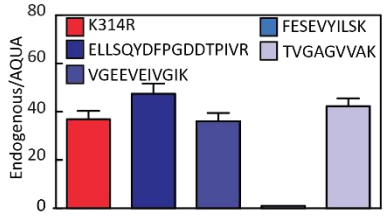

F

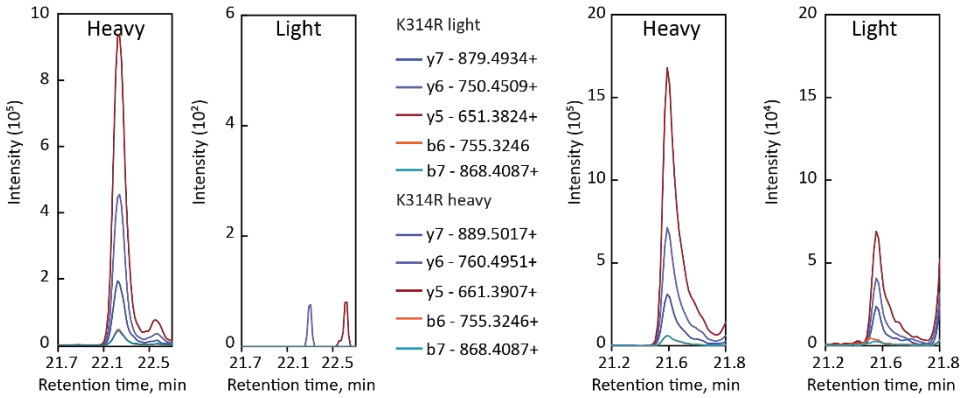

K314N: htk.FESEVYILSNDEGGR.deg

A

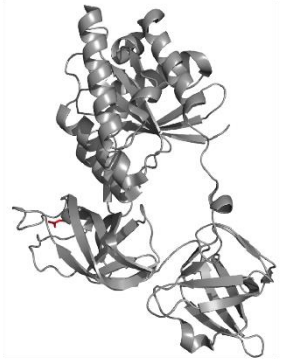

B

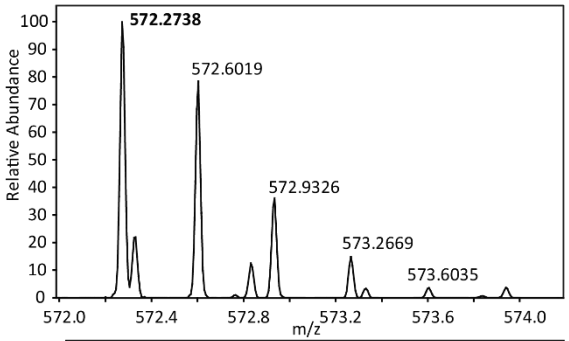

C

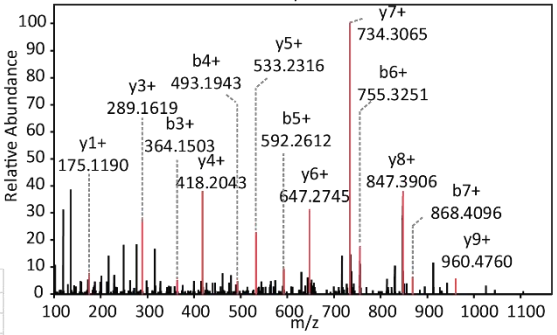

D

MH^{+1}	MH^{+2}	MH^{+3}
1714.7919	857.8996	**572.2688**

b				y	y^{+2}
-	1	F	15	-	-
277.1183	2	E	14	1567.7235	784.3654
364.1503	3	S	13	1438.6809	719.8441
493.1929	4	E	12	1351.6488	676.3281
592.2613	5	V	11	1222.6062	611.8068
755.3246	6	Y	10	1123.5378	562.2726
868.4087	7	I	9	**960.4745**	480.7409
981.4928	8	L	8	**847.3904**	424.1989
1068.5248	9	S	7	**734.3064**	367.6568
1182.5677	10	N	6	**647.2743**	324.1408
1297.5947	11	D	5	**533.2314**	267.1193
1426.6373	12	E	4	**418.2045**	209.6059
1483.6587	13	G	3	**289.1619**	145.0846
1540.6802	14	G	2	232.1404	116.5738
-	15	R	1	**175.1190**	88.0631

E

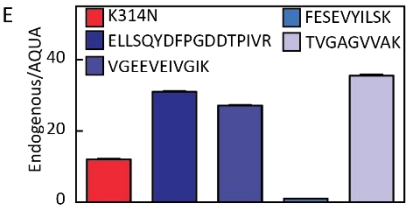

F

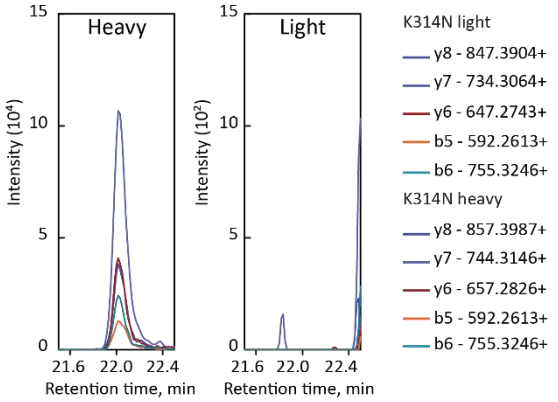

G

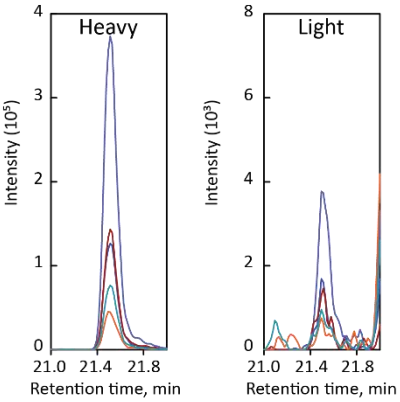

R319H: LSK.DEGGHHTPFFK.GYR

A

B

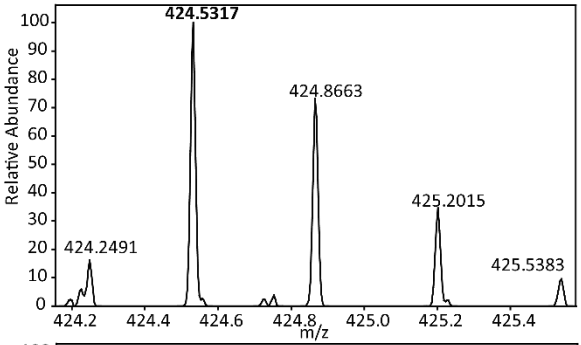

C

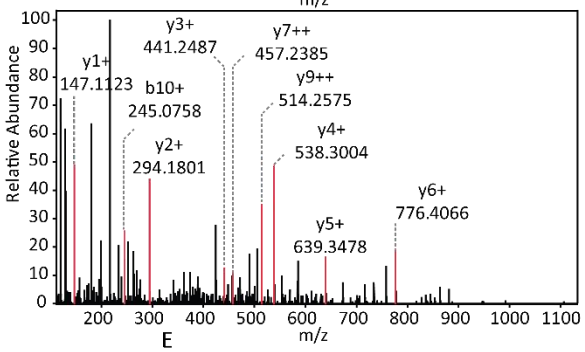

D

	MH^{+1}	MH^{+2}	MH^{+3}			
	1270.5804	636.2938	**424.5316**			
b	b^{+2}				y	y^{+2}
-	-	1	D	11	-	-
245.0768	-	2	E	10	1156.5534	578.7803
302.0983	-	3	G	9	1027.5108	514.2591
359.1197	-	4	G	8	970.4894	485.7483
469.1787	248.5930	5	H	7	913.4679	457.2376
633.2376	317.1224	6	H	6	776.4090	388.7081
734.2852	367.6463	7	T	5	**639.3501**	320.1787
831.3380	416.1726	8	P	4	**538.3024**	269.6548
978.4064	489.7068	9	F	3	**441.2496**	221.1285
1125.4748	563.2411	10	F	2	294.1812	147.5942
-	-	11	K	1	147.1128	74.0600

E

F

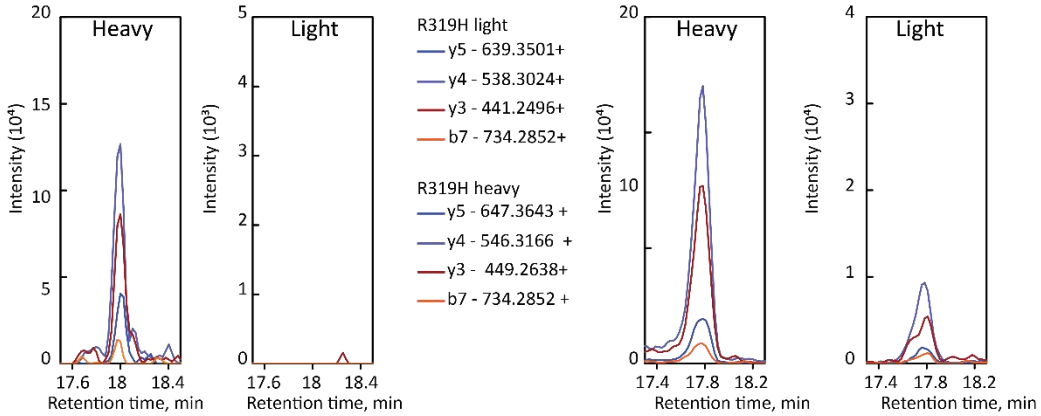

G

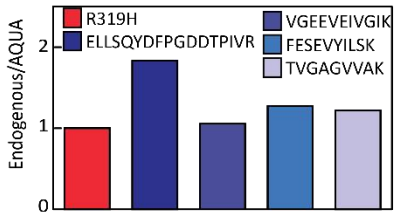

R328H: FFK.GYHPQFYFR.TTD

A

B

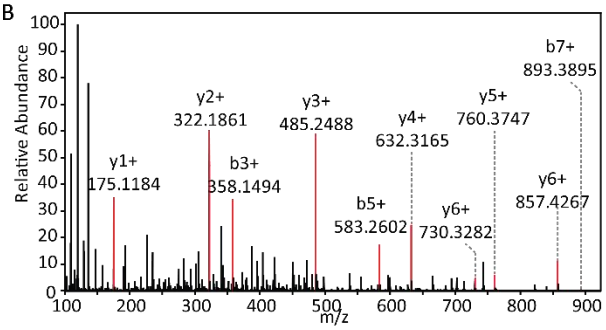

C

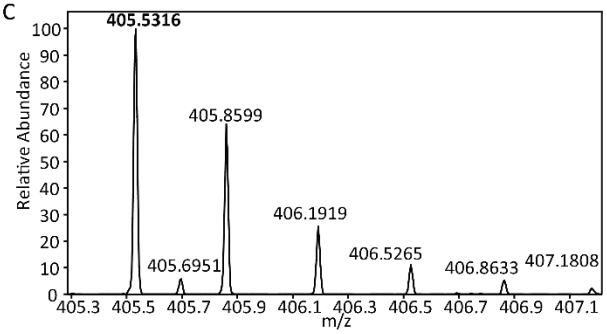

D

	MH^{+1}	MH^{+2}	MH^{+3}			
	1214.5742	607.7907	**405.5296**			
b	b^{+2}				y	y^{+2}
-	-	1	G	9	-	-
221.0921	-	2	Y	8	1157.5527	579.2800
358.1510	179.5791	3	H	7	994.4894	497.7483
455.2037	228.1055	4	P	6	857.4304	429.2189
593.2623	292.1348	5	Q	5	760.3777	380.6925
730.3307	356.6690	6	F	4	632.3191	316.6632
893.3941	447.2007	7	Y	3	485.2507	243.1290
1040.4625	520.7349	8	F	2	322.1874	161.5973
-	-	9	R	1	175.1190	88.0631

E

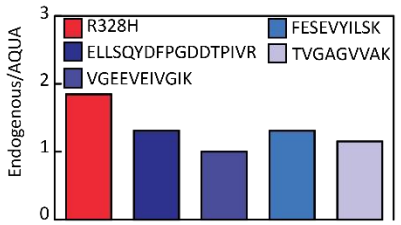

F

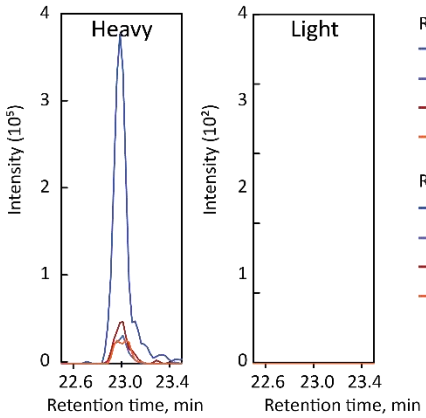

G

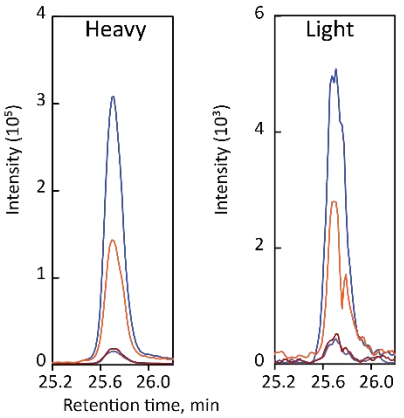

R378H: GLR.FAIHEGGR.TVG

A

B

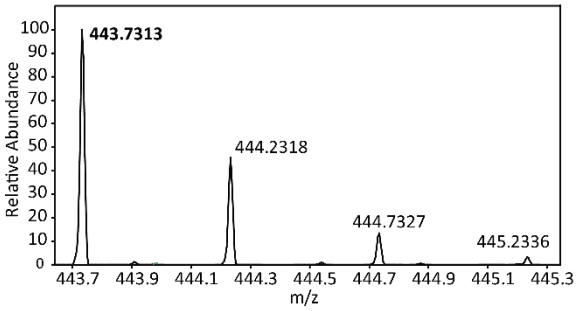

C

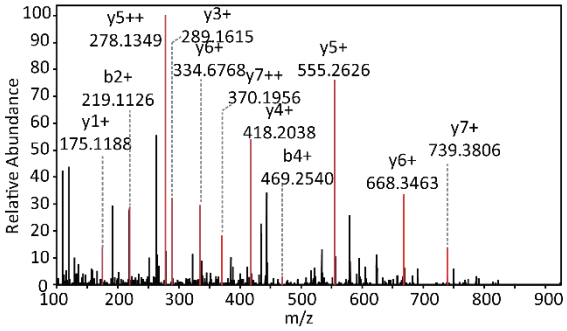

D

	MH^{+1}	MH^{+2}	MH^{+3}			
	886.453	**443.7301**	296.1558			
b	b^{+2}				y	y^{+2}
-	-	1	F	8	-	-
219.1128	-	2	A	7	**739.3846**	370.1959
332.1969	-	3	I	6	**668.3474**	334.6774
469.2558	235.1315	4	H	5	**555.2634**	278.1353
598.2984	299.6528	5	E	4	418.2045	209.6059
655.3198	328.1636	6	G	3	289.1619	145.0846
712.3413	356.6743	7	G	2	232.1404	116.5738
-	-	8	R	1	175.1190	88.0631

E

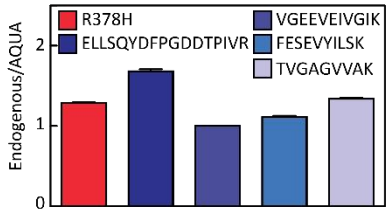

F

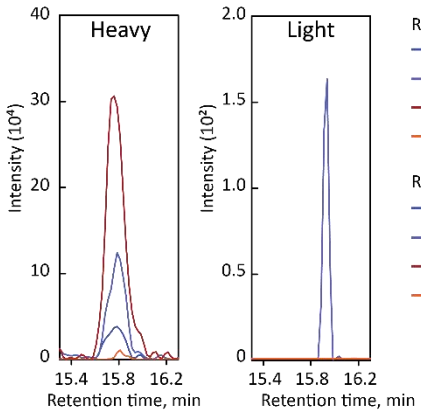

G

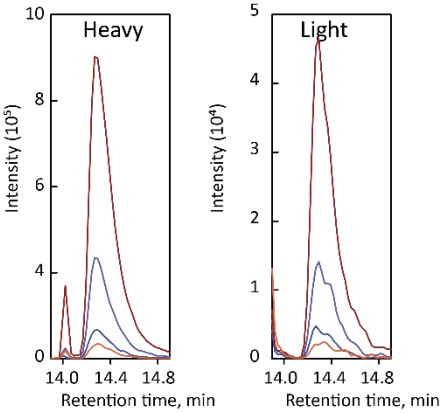

R382H: air.EGGHTVGAGVVAK.ylg

A

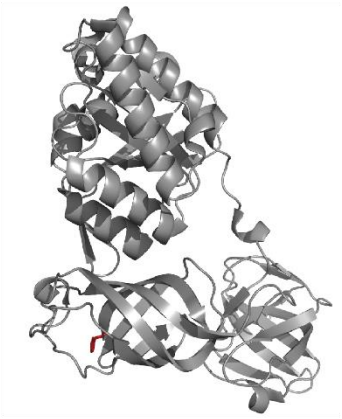

B

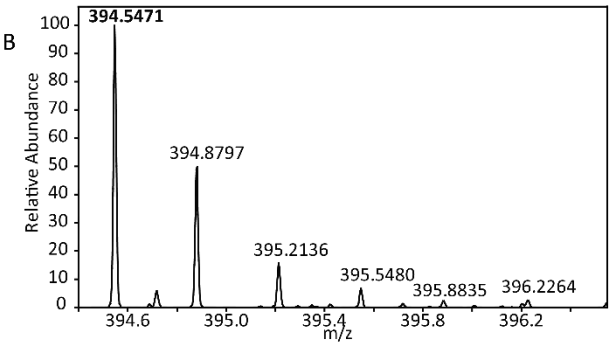

C

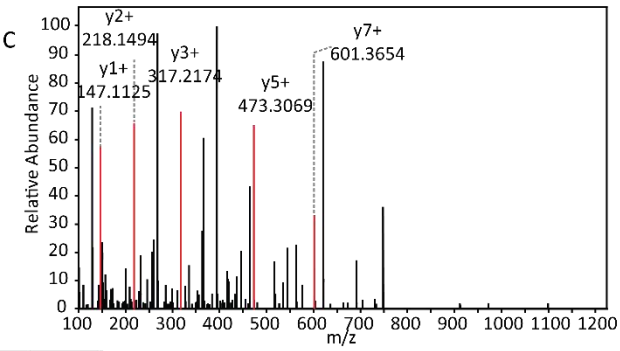

D

	MH^{+1}	MH^{+2}	MH^{+3}			
	1181.6273	591.3173	**394.5473**			
b	b^{+2}				y	y^{+2}
-	-	1	E	13	-	-
187.0713	-	2	G	12	1052.5847	526.7960
244.0928	-	3	G	11	995.5633	498.2853
381.1517	191.0795	4	H	10	938.5418	469.7745
482.1994	241.6033	5	T	9	801.4829	401.2451
581.2678	291.1375	6	V	8	700.4352	350.7212
638.2893	319.6483	7	G	7	601.3668	301.1870
709.3264	355.1668	8	A	6	544.3453	272.6763
766.3478	383.6776	9	G	5	473.3082	237.1577
865.4163	433.2118	10	V	4	416.2867	208.6470
964.4847	482.7460	11	V	3	317.2183	159.1128
1035.5218	518.2645	12	A	2	218.1499	109.5786
-	-	13	K	1	147.1128	74.0600

E

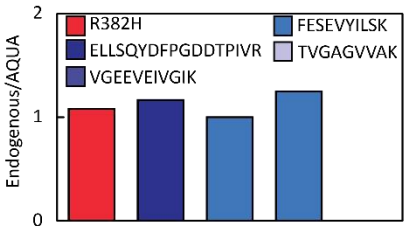

F

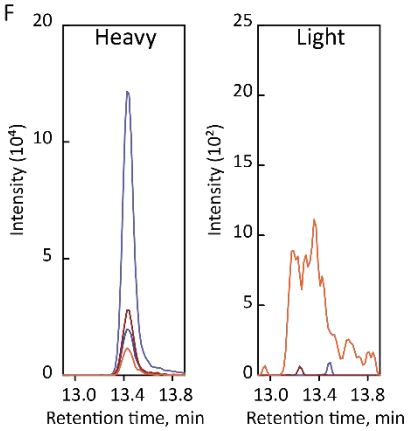

G

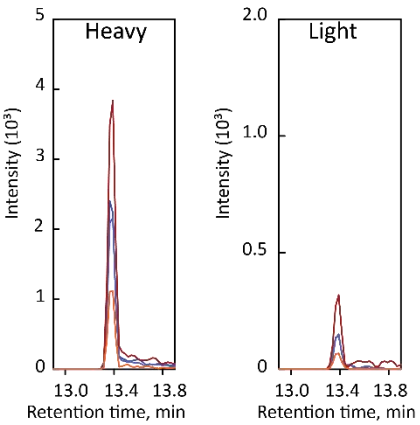

6.4 Section D. validation of non-cognate amino acid substitutions

The position of the substituted amino acid (red) is shown in the context of EF-Tu structure. The identity of the error-containing peptide is validated by PRM analysis (B). The predicted fragmentation pattern for the peptide is shown in (C). The validation of the quantification is performed by comparing the stoichiometry of erroneous peptide with respect to four cognate EF-Tu peptides (D), as described in Results and Materials and Method. The SRM trace used for the determination of error frequency is shown (E). To confirm the absence of contamination by the light peptide, the heavy-labeled peptides are analysed by mass spectrometry and the signals for both light and heavy are recorded (F). The monitored transitions are indicated.

R231A: sgr.GTVVTGAVER.gii

A

B

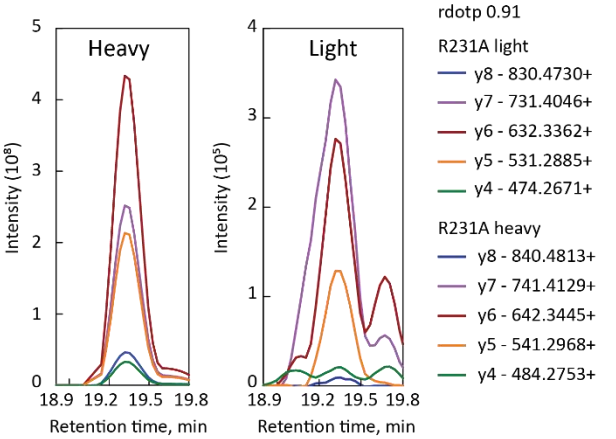

C

	MH+1	MH+2	MH+3		
	988.5422	494.7747	330.1856		
b				y	y+2
-	1	G	10	-	-
159.0764	2	T	9	931.5207	466.2640
258.1448	3	V	8	830.4730	415.7402
357.2132	4	V	7	731.4046	366.2060
458.2609	5	T	6	632.3362	316.6717
515.2824	6	G	5	531.2885	266.1479
586.3195	7	A	4	474.2671	237.6372
685.3879	8	V	3	403.2300	202.1186
814.4305	9	E	2	304.1615	152.5844
-	10	R	1	175.1190	88.0631

D

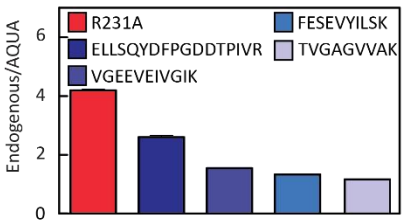

E

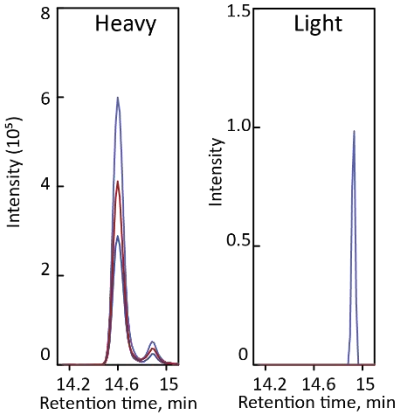

F

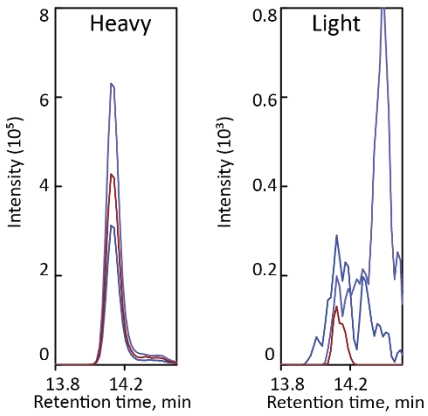

R231D: sgr.GTVVTGDVER.gii

A

B

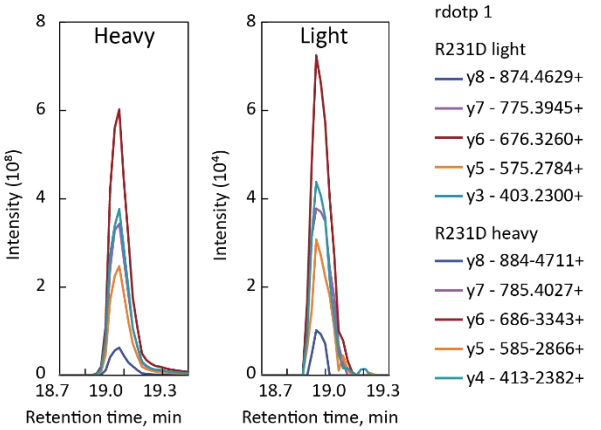

C

	MH+1	MH+2	MH+3		
	1032.532	516.7696	344.8489		
b				y	y+2
-	1	G	10	-	-
159.0764	2	T	9	975.5106	488.2589
258.1448	3	V	8	874.4629	437.7351
357.2132	4	V	7	775.9345	388.2009
458.2609	5	T	6	676.3260	339.6667
515.2824	6	G	5	575.2784	288.1428
630.3093	7	D	4	518.2569	259.6321
729.3777	8	V	3	403.2300	202.1186
858.4203	9	E	2	304.1615	152.5844
-	10	R	1	175.1190	88.0631

D

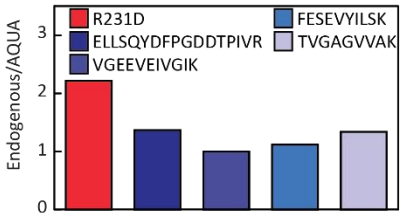

E

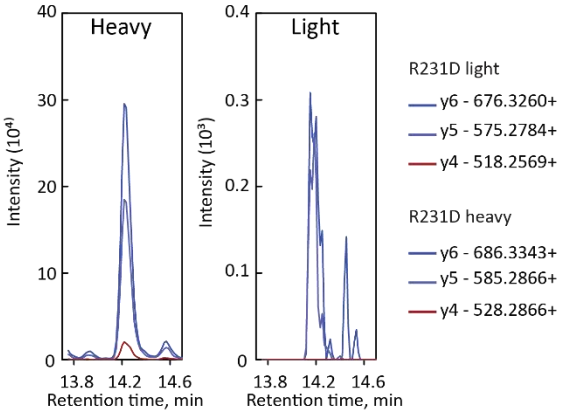

F

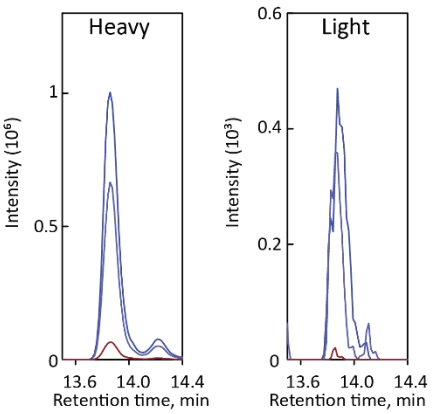

R231E: sgr.GTVVTGEVER.gii

A

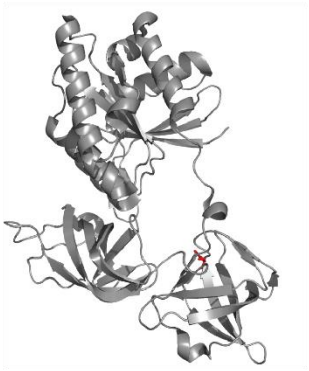

B

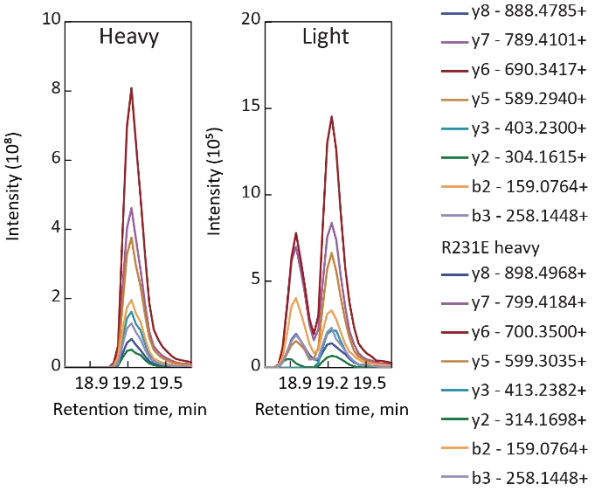

C

	MH+1	MH+2	MH+3		
	1046.16	523.7775	349.5207		
b				y	y+2
-	1	G	10	-	-
159.0764	2	T	9	989.5262	495.2667
258.1448	3	V	8	888.4785	444.7429
357.2132	4	V	7	789.4101	395.2087
458.2609	5	T	6	690.3417	345.6745
515.2824	6	G	5	589.2940	295.1506
644.3250	7	E	4	532.2726	266.6399
743.3934	8	V	3	403.2300	202.1186
872.4360	9	E	2	304.1615	152.5844
-	10	R	1	175.1190	88.0631

D

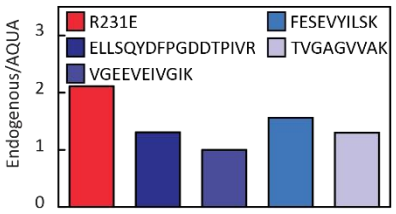

E

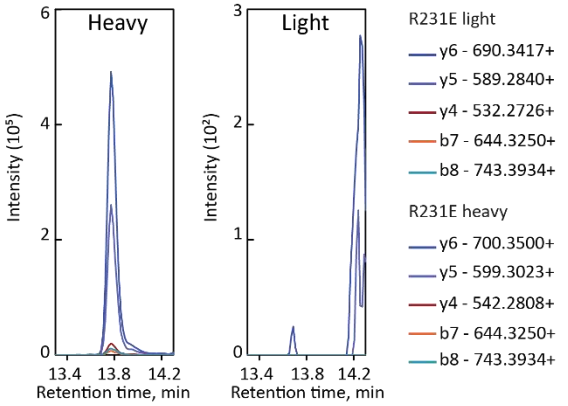

F

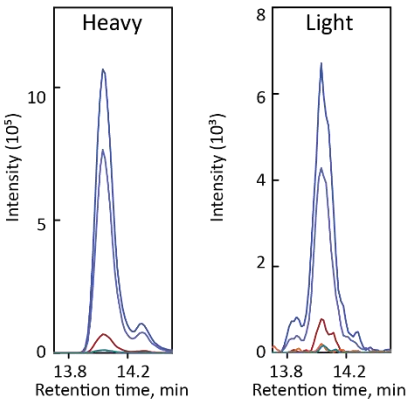

R231F: sgr.GTVVTGFVER.gii

A

B

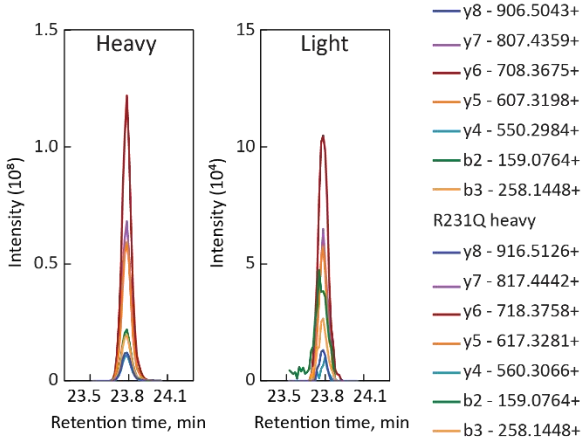

C

	MH+1	MH+2	MH+3		
	1064.5735	532.7904	355.5293		
b				y	y+2
-	1	G	10	-	-
159.0764	2	T	9	1007.5520	504.2796
258.1448	3	V	8	906.5043	453.7558
357.2132	4	V	7	807.4359	404.2216
458.2609	5	T	6	708.3675	354.6874
515.2824	6	G	5	607.3198	304.1636
662.3508	7	F	4	550.2984	257.6528
761.4192	8	V	3	403.2300	202.1186
890.4618	9	E	2	304.1615	152.5844
-	10	R	1	175.1190	88.0631

D

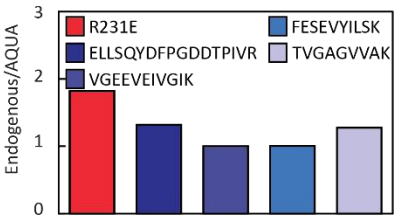

E

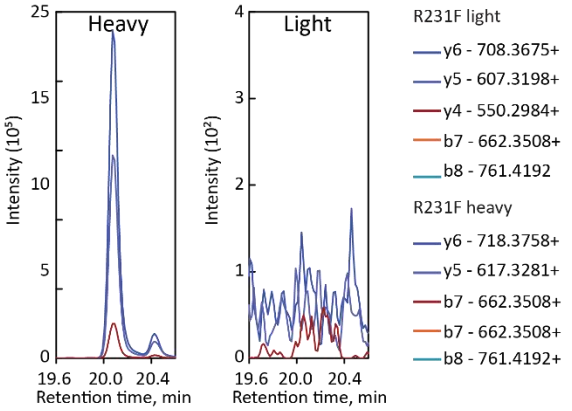

F

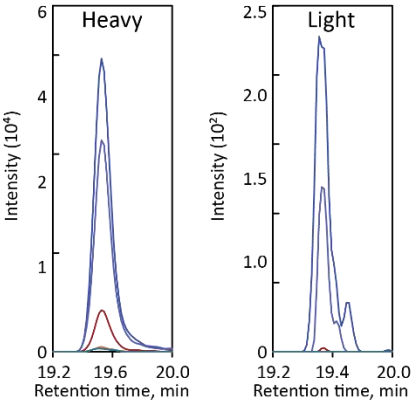

R231Y: sgr.GTVVTGYVER.gii

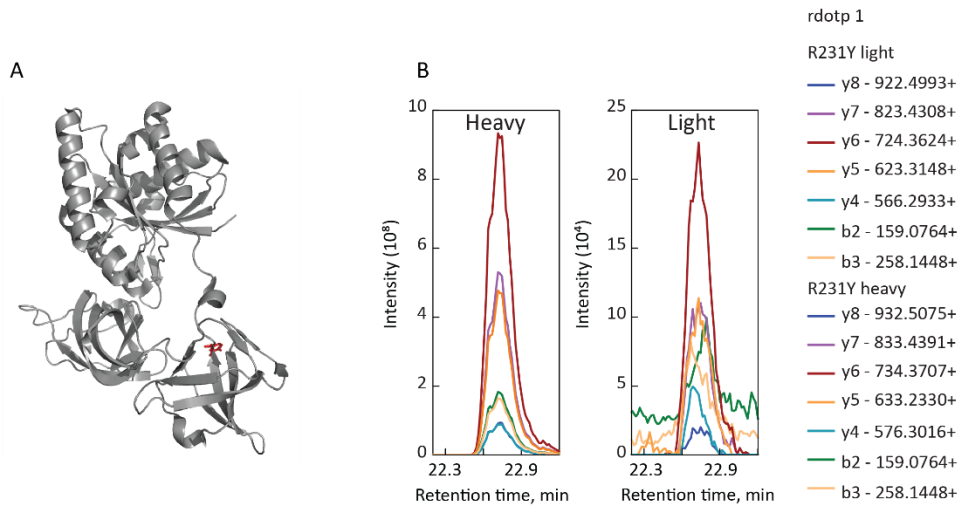

C

	MH+1	MH+2	MH+3		
	1080.5684	540.7878	360.861		
b				y	y+2
-	1	G	10	-	-
159.0764	2	T	9	1023.5469	512.2771
258.1448	3	V	8	922.4993	461.7533
357.2132	4	V	7	823.4308	412.2191
458.2609	5	T	6	724.3624	362.6849
515.2824	6	G	5	623.3148	312.1610
678.3457	7	Y	4	566.2933	283.6503
777.4141	8	V	3	403.2300	202.1186
906.4567	9	E	2	304.1615	152.5844
-	10	R	1	175.1190	88.0631

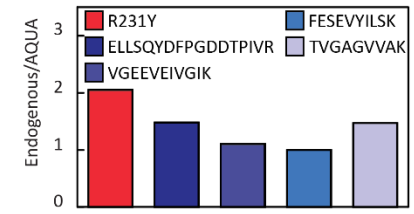

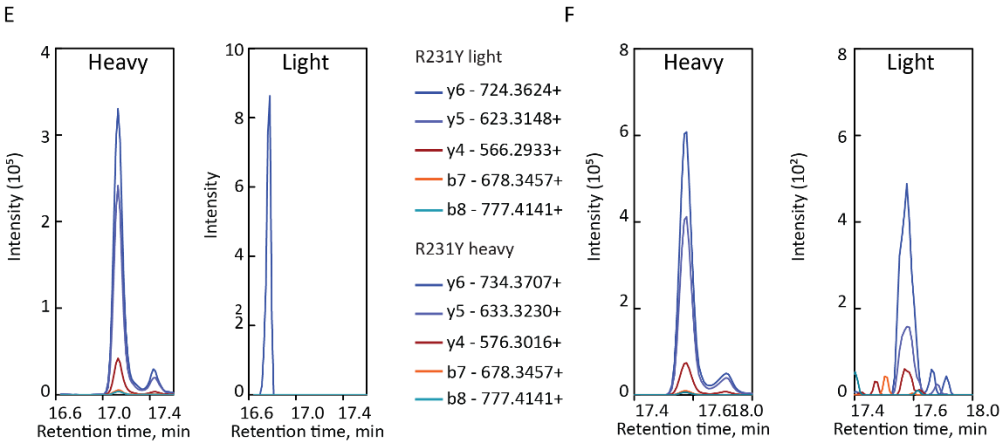

R231Q: sgr.GTVVTGQVER.gii

A

B

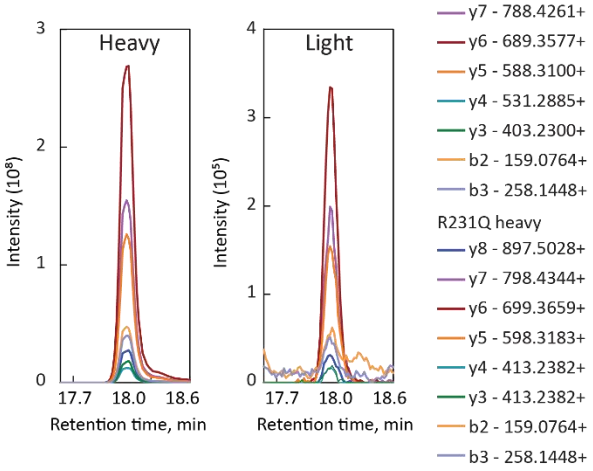

C

	MH+1	MH+2	MH+3		
	1045.5636	523.2855	349.1927		
b				y	y+2
-	1	G	10	-	-
159.0764	2	T	9	988.4522	494.7747
258.1448	3	V	8	887.4945	444.2509
357.2132	4	V	7	788.4261	394.7167
458.2609	5	T	6	689.3577	345.1825
515.2824	6	G	5	588.3100	294.6586
643.3410	7	Q	4	531.2885	266.1479
742.4094	8	V	3	403.2300	202.1186
871.4520	9	E	2	304.1615	152.5844
-	10	R	1	175.1190	88.0631

D

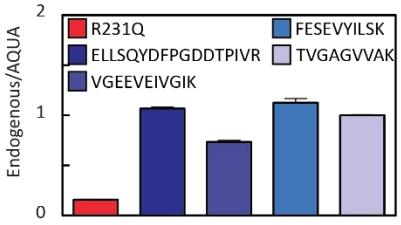

E

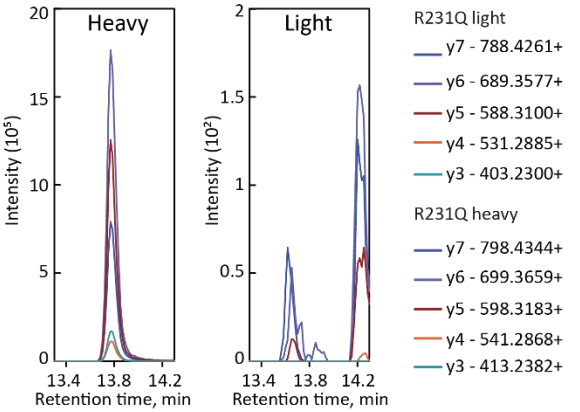

F

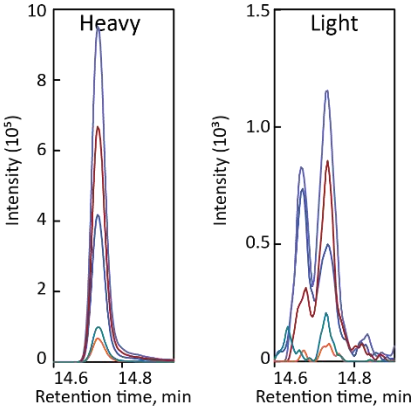

R231T: sgr.GTVVTGTVER.gii

A

B

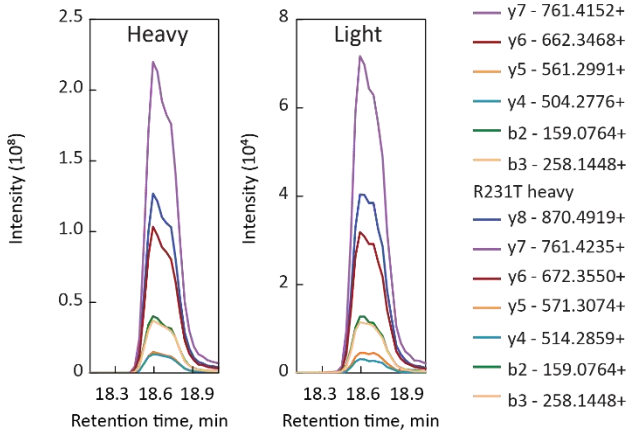

C

	MH+1	MH+2	MH+3		
	1018.5527	509.78	340.1891		
b				y	y+2
-	1	G	10	-	-
159.0764	2	T	9	961.5313	481.2693
258.1448	3	V	8	860.4836	430.7454
357.2132	4	V	7	761.4152	381.2112
458.2609	5	T	6	662.3468	331.6770
515.2824	6	G	5	561.2991	281.1532
616.3301	7	T	4	504.2776	525.6425
715.3985	8	V	3	403.2300	202.1186
844.4411	9	E	2	304.1615	152.5844
-	10	R	1	175.1190	88.0631

D

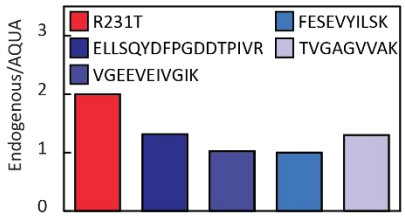

E

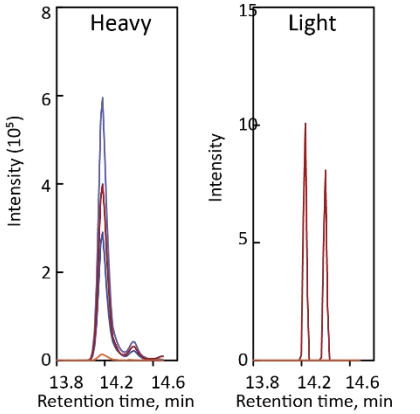

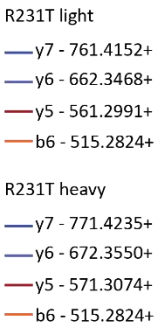

E

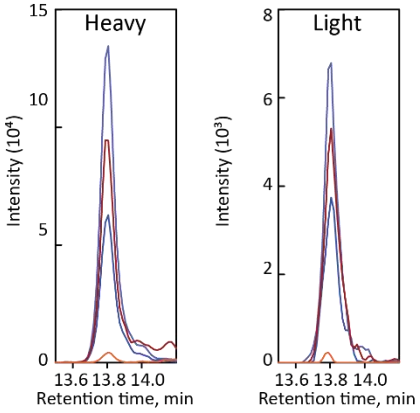

R231V: sgr.GTVVTGVVER.gii

A

B

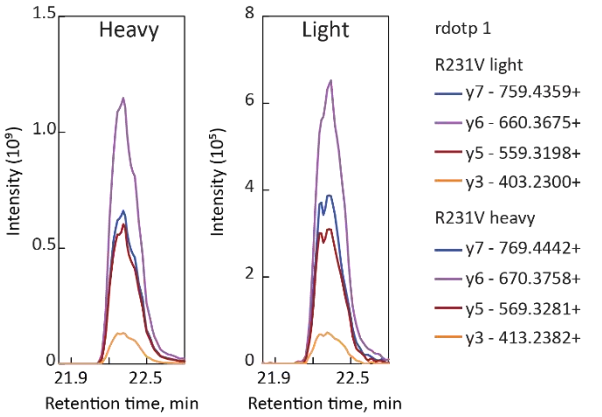

C

	MH+1	MH+2	MH+3		
	1016.5735	508.7904	339.5293		
b				y	y+2
-	1	G	10	-	-
159.0764	2	T	9	959.5520	480.2796
258.1448	3	V	8	858.5043	429.7558
357.2132	4	V	7	759.4359	380.2216
458.2609	5	T	6	660.3675	330.6874
515.2824	6	G	5	559.3198	280.1636
614.2508	7	V	4	502.2984	251.6528
713.4192	8	V	3	403.2300	202.1186
842.4618	9	E	2	304.1615	152.5844
-	10	R	1	175.1190	88.0631

D

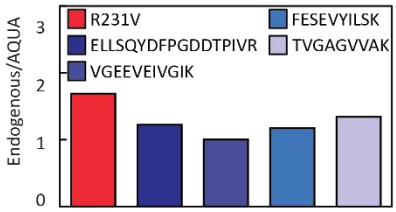

E

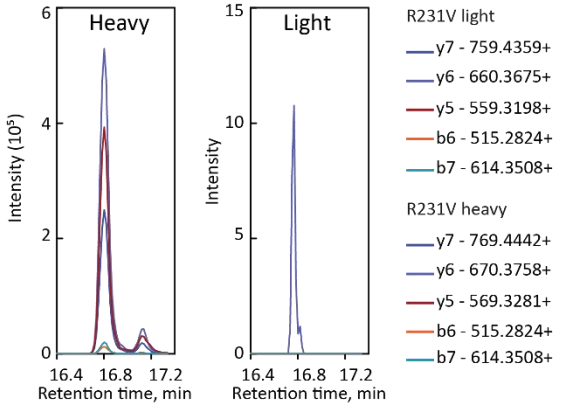

F

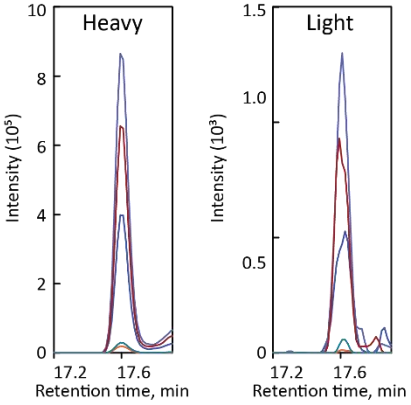

6.5 Section E. SRM signals of peptides for multiple errors investigation

The SRM signal of enriched heavy-labeled and endogenous peptides is shown (left). To confirm the absence of contamination by the light peptide, the heavy-labeled peptides are analysed by mass spectrometry and the signals for both light and heavy are recorded (right). The monitored transitions are indicated.

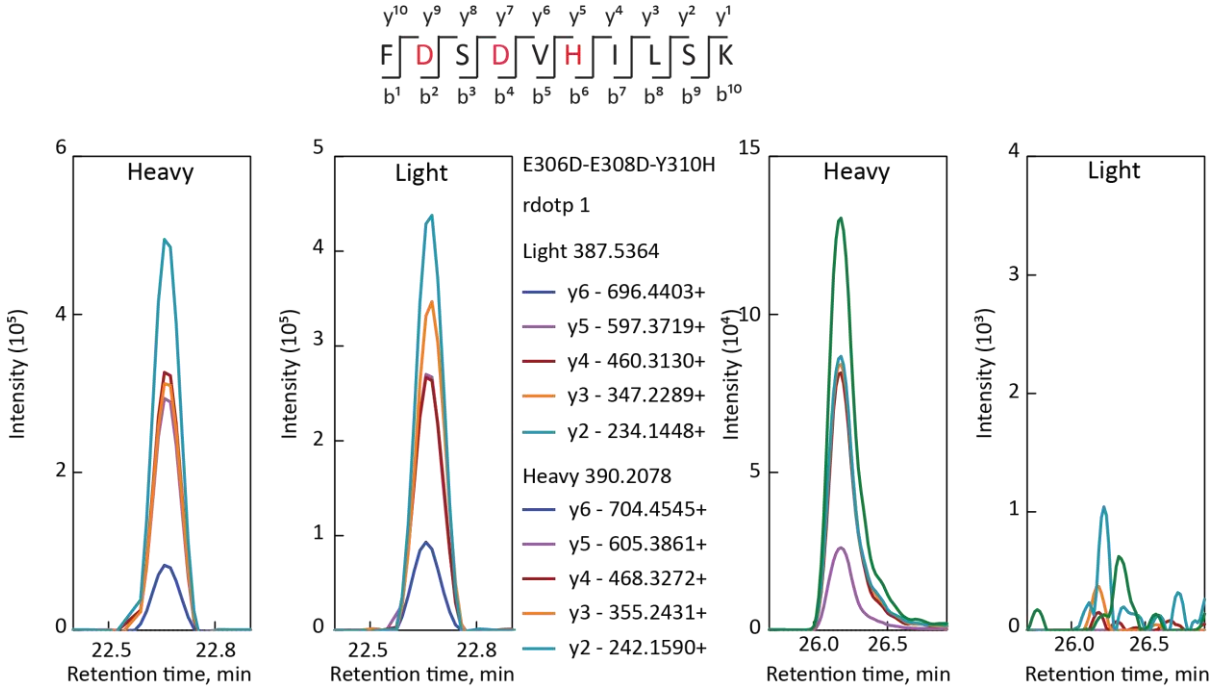

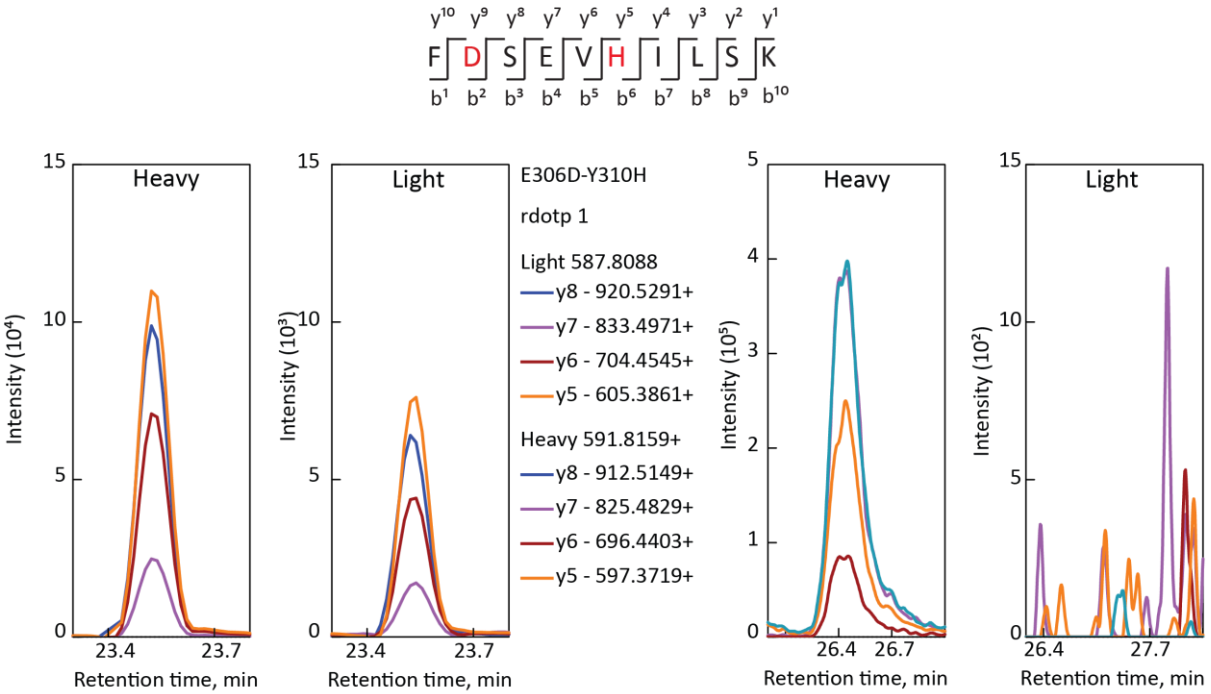
y10 y9 y8 y7 y6 y5 y4 y3 y2 y1
F D S E V H I L S K
b1 b2 b3 b4 b5 b6 b7 b8 b9 b10
Heavy
Light
E306D-Y310H
rdotp 1
Light 587.8088
y8 - 920.5291+
y7 - 833.4971+
y6 - 704.4545+
y5 - 605.3861+
Heavy 591.8159+
y8 - 912.5149+
y7 - 825.4829+
y6 - 696.4403+
y5 - 597.3719+
Intensity (10⁴)
Intensity (10³)
Intensity (10⁵)
Intensity (10²)
Retention time, min

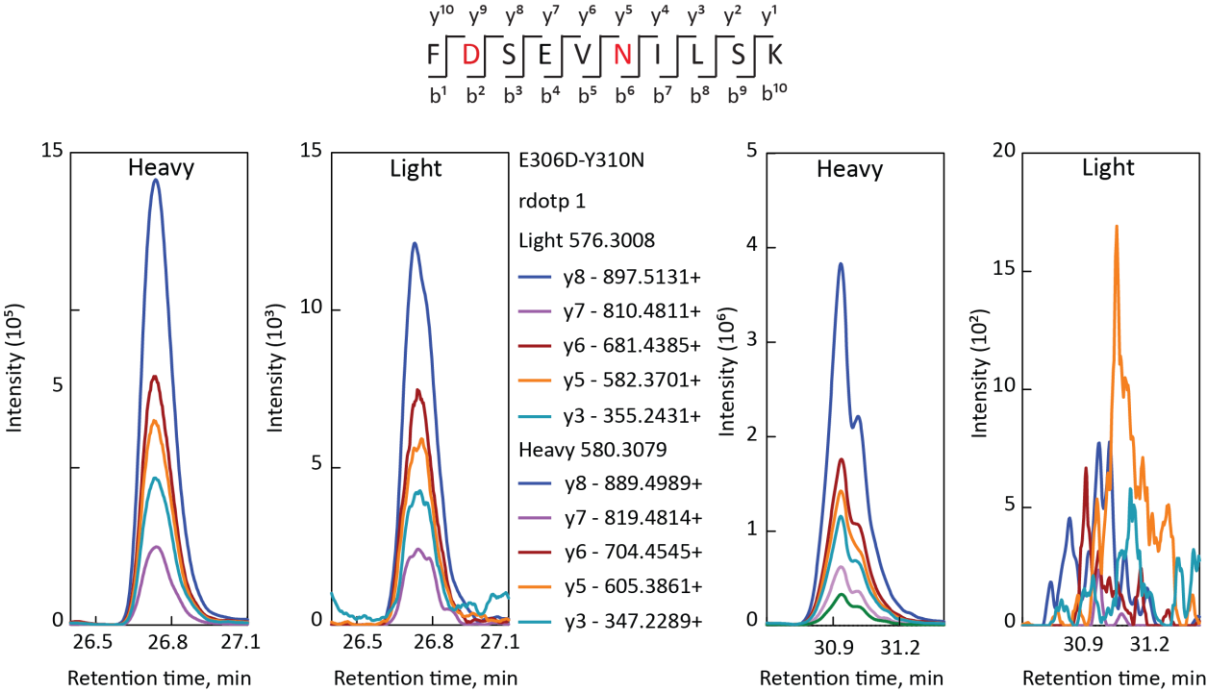
y10 y9 y8 y7 y6 y5 y4 y3 y2 y1
F D S E V N I L S K
b1 b2 b3 b4 b5 b6 b7 b8 b9 b10
Heavy
Light
E306D-Y310N
rdotp 1
Light 576.3008
y8 - 897.5131+
y7 - 810.4811+
y6 - 681.4385+
y5 - 582.3701+
y3 - 355.2431+
Heavy 580.3079
y8 - 889.4989+
y7 - 819.4814+
y6 - 704.4545+
y5 - 605.3861+
y3 - 347.2289+
Intensity (10⁵)
Intensity (10³)
Intensity (10⁶)
Intensity (10²)
Retention time, min

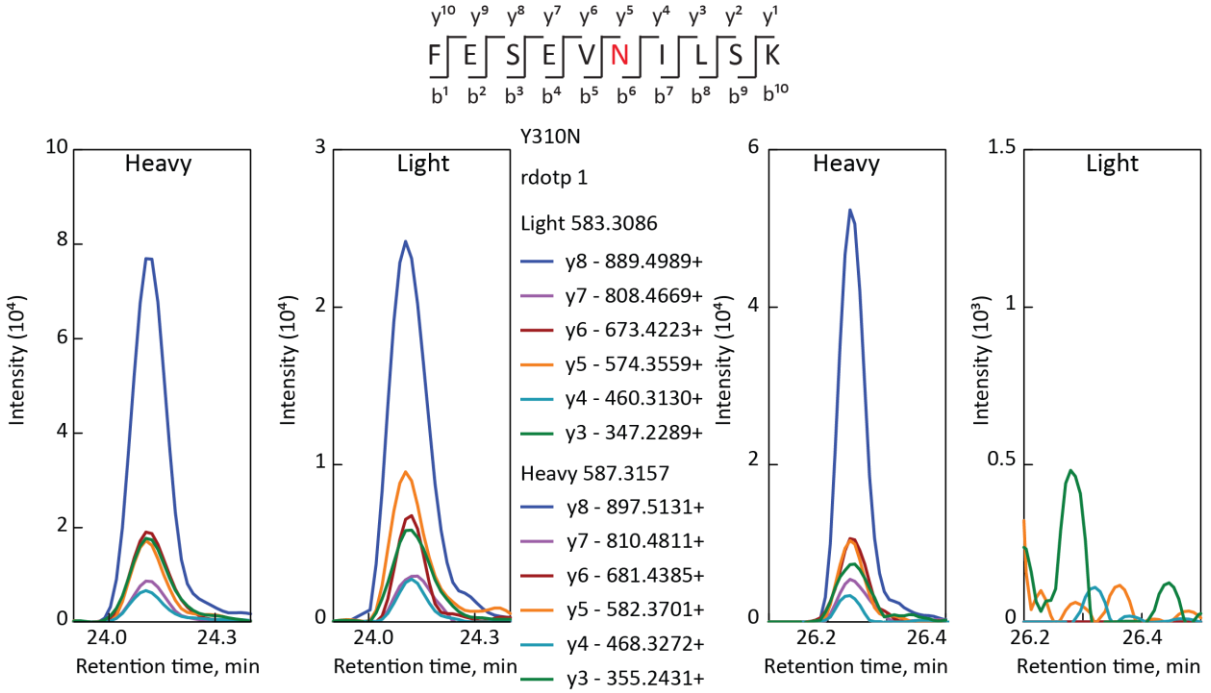
y10 y9 y8 y7 y6 y5 y4 y3 y2 y1
F E S E V N I L S K
b1 b2 b3 b4 b5 b6 b7 b8 b9 b10
Heavy
Light
Heavy
Light
Intensity (10^4)
Intensity (10^4)
Intensity (10^4)
Intensity (10^3)
Retention time, min
Retention time, min
Retention time, min
Retention time, min
Y310N
rdotp 1
Light 583.3086
y8 - 889.4989+
y7 - 808.4669+
y6 - 673.4223+
y5 - 574.3559+
y4 - 460.3130+
y3 - 347.2289+
Heavy 587.3157
y8 - 897.5131+
y7 - 810.4811+
y6 - 681.4385+
y5 - 582.3701+
y4 - 468.3272+
y3 - 355.2431+

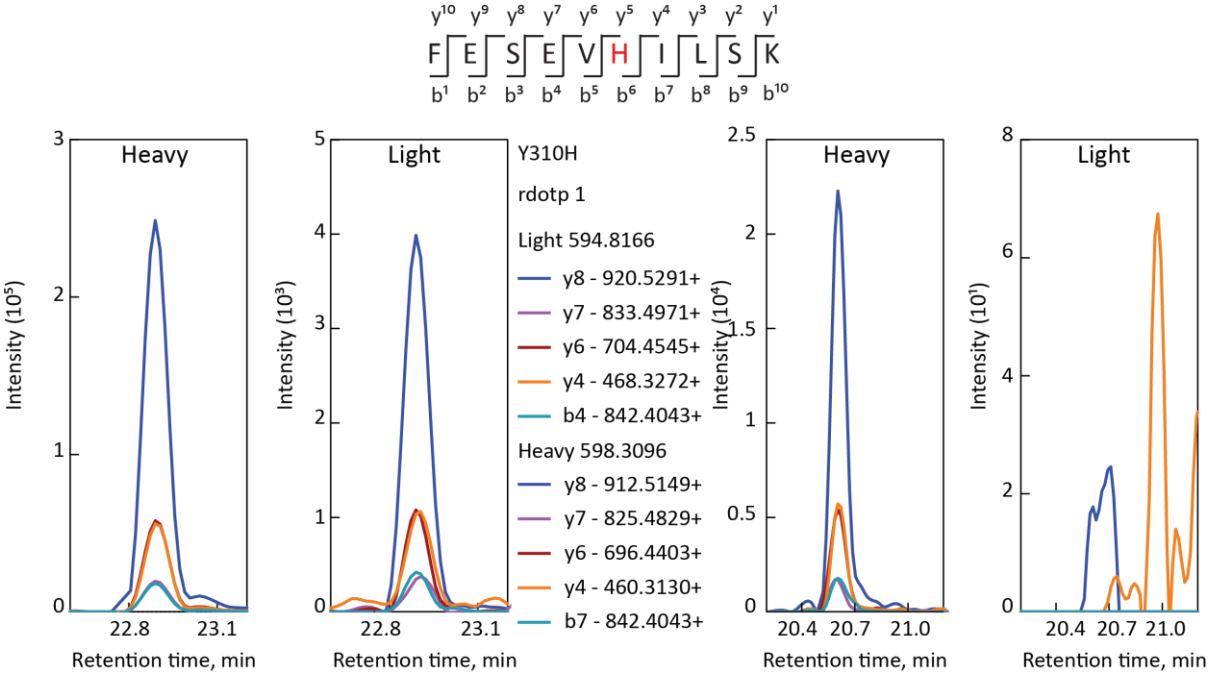
y10 y9 y8 y7 y6 y5 y4 y3 y2 y1
F E S E V H I L S K
b1 b2 b3 b4 b5 b6 b7 b8 b9 b10
Heavy
Light
Heavy
Light
Intensity (10^5)
Intensity (10^3)
Intensity (10^4)
Intensity (10^1)
Retention time, min
Retention time, min
Retention time, min
Retention time, min
Y310H
rdotp 1
Light 594.8166
y8 - 920.5291+
y7 - 833.4971+
y6 - 704.4545+
y4 - 468.3272+
b4 - 842.4043+
Heavy 598.3096
y8 - 912.5149+
y7 - 825.4829+
y6 - 696.4403+
y4 - 460.3130+
b7 - 842.4043+

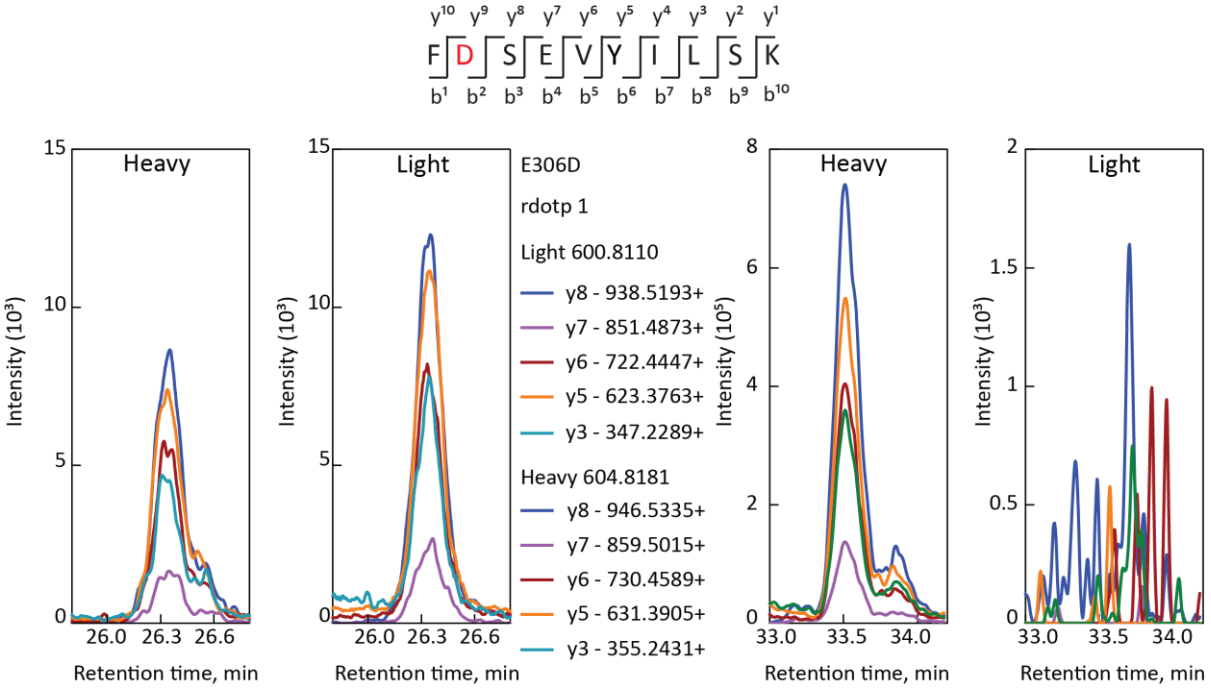
y10 y9 y8 y7 y6 y5 y4 y3 y2 y1
F D S E V Y I L S K
b1 b2 b3 b4 b5 b6 b7 b8 b9 b10
Heavy
Light
E306D
rdotp 1
Light 600.8110
y8 - 938.5193+
y7 - 851.4873+
y6 - 722.4447+
y5 - 623.3763+
y3 - 347.2289+
Heavy 604.8181
y8 - 946.5335+
y7 - 859.5015+
y6 - 730.4589+
y5 - 631.3905+
y3 - 355.2431+
Intensity (10³)
Intensity (10⁵)
Retention time, min

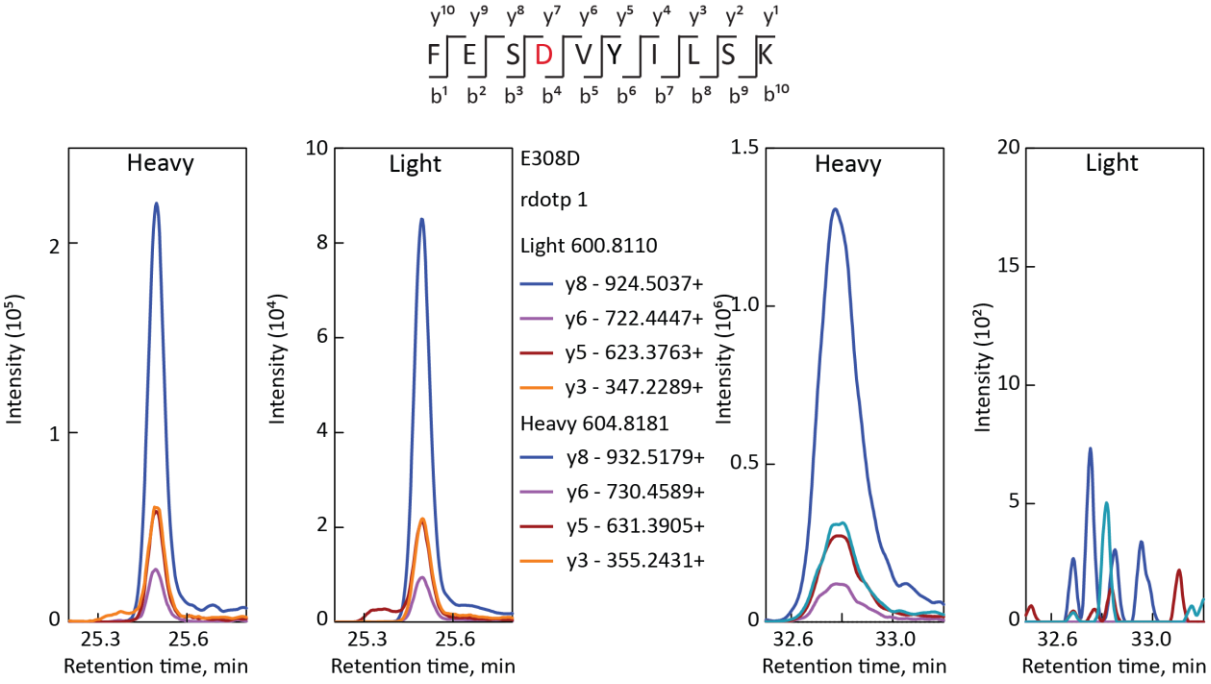
y10 y9 y8 y7 y6 y5 y4 y3 y2 y1
F E S D V Y I L S K
b1 b2 b3 b4 b5 b6 b7 b8 b9 b10
Heavy
Light
E308D
rdotp 1
Light 600.8110
y8 - 924.5037+
y6 - 722.4447+
y5 - 623.3763+
y3 - 347.2289+
Heavy 604.8181
y8 - 932.5179+
y6 - 730.4589+
y5 - 631.3905+
y3 - 355.2431+
Intensity (10⁵)
Intensity (10⁴)
Intensity (10⁶)
Intensity (10²)
Retention time, min

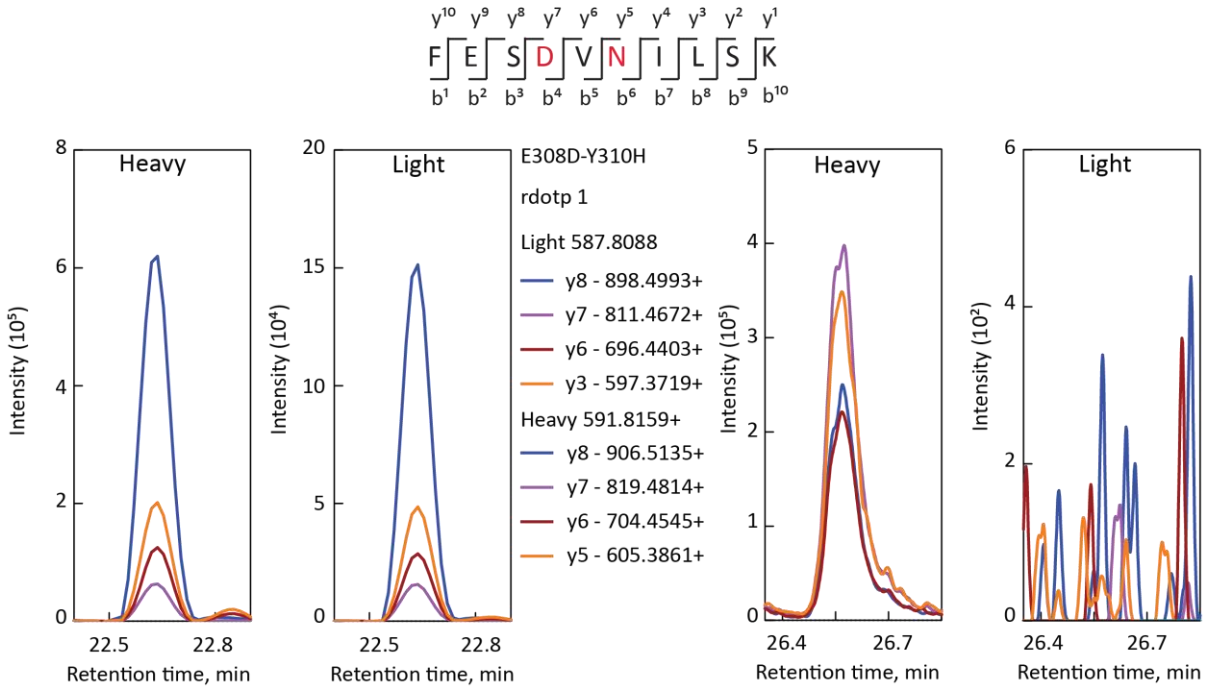
y10 y9 y8 y7 y6 y5 y4 y3 y2 y1
F E S D V N I L S K
b1 b2 b3 b4 b5 b6 b7 b8 b9 b10
Heavy
Light
Intensity (10^5)
Intensity (10^4)
Intensity (10^2)
Retention time, min
E308D-Y310H
rdotp 1
Light 587.8088
y8 - 898.4993+
y7 - 811.4672+
y6 - 696.4403+
y3 - 597.3719+
Heavy 591.8159+
y8 - 906.5135+
y7 - 819.4814+
y6 - 704.4545+
y5 - 605.3861+

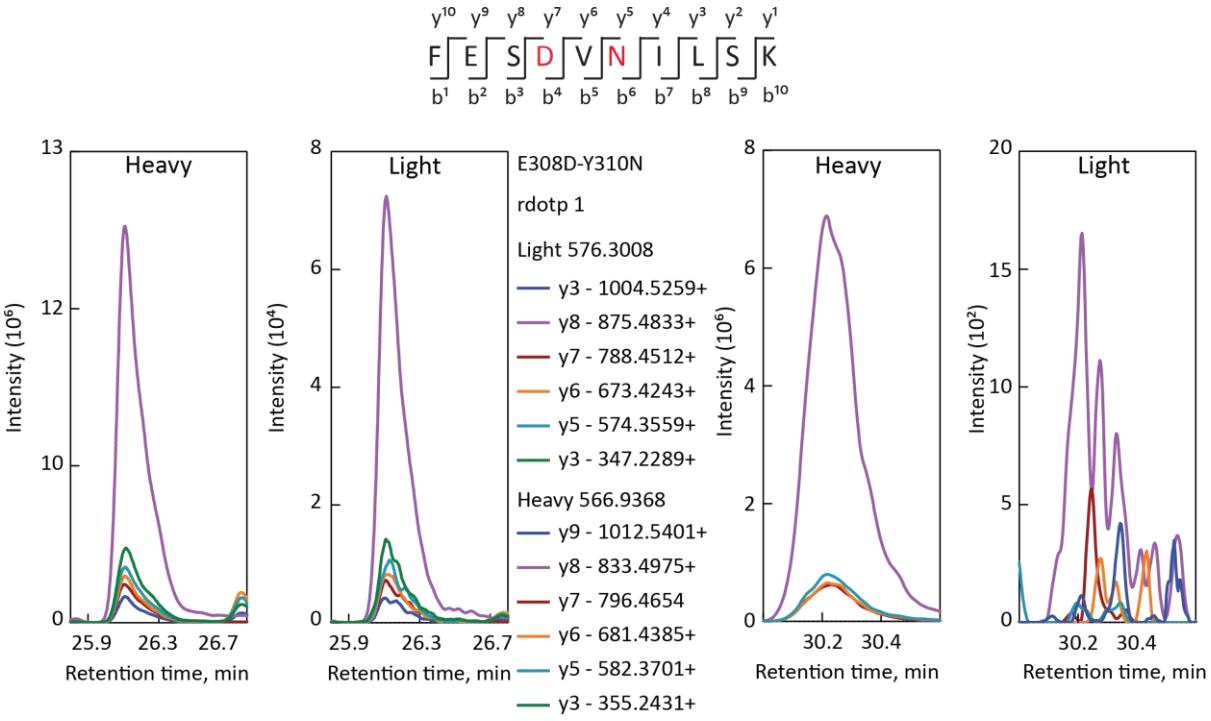
y10 y9 y8 y7 y6 y5 y4 y3 y2 y1
F E S D V N I L S K
b1 b2 b3 b4 b5 b6 b7 b8 b9 b10
Heavy
Light
Intensity (10^6)
Intensity (10^4)
Intensity (10^2)
Retention time, min
E308D-Y310N
rdotp 1
Light 576.3008
y3 - 1004.5259+
y8 - 875.4833+
y7 - 788.4512+
y6 - 673.4243+
y5 - 574.3559+
y3 - 347.2289+
Heavy 566.9368
y9 - 1012.5401+
y8 - 833.4975+
y7 - 796.4654
y6 - 681.4385+
y5 - 582.3701+
y3 - 355.2431+

6.6 List of tables

6.7 List of figures

6.8 List of abbreviations

Abbreviation	Description
ACN	Acetonitrile
Amp	Ampicillin
APS	Ammonium Persulfate
CID	Collision energy induced dissociation
DDA	Data-dependent acquisition
DTT	Dithiothreitol
FA	Formic acid
Gen	Gentamicin
GS	Ground state
Hyg	Hygromycin
HPLC	High performance liquid chromatrography
IAA	Iodoacetamide
Kan	Kanamycin
kDa	Kilo Dalton
LC	Liquid chromatography
MS	Mass spectrometry
Nea	Neamine
Neo	Neomycin
PAGE	Polyacrylamide gel electrophoresis
Par	Paromomycin
PRM	Parallel reaction monitoring
PRTC mix	Pierce retention time calibration mix
Rib	Ribostamycin
RP	Reversed phase
SDS	Sodium Dodecyl Sulfate
SIM	Selected ion monitoring chromatogram
Spc	Spectinomycin
SRM	Selected reaction monitoring
Str	Streptomycin
TEMED	Tetramethylethylenediamine
Tob	Tobramycin
TS	Transition state
XIC	Extracted ion chromatogram

7. ACKNOWLEDGMENTS

Here I am at the end of this long journey that has been my PhD. Four years in this amazing place have passed by so quickly that I could bearely realize it. Among all the people I have met, some deserve a special acknowledgments. First of all Marina and Henning, for giving me the chance to work in their laboratories. I will never forget the feeling I got the first day I stepped in their labs. A special thanks to Prof. Rehling, who is part of my Advisory Board since the very beginning, and to Prof. Stark, Prof. Ficner and Prof. Bohnsack for joining it in this last step which precedes the defense. Thanks to all the wonderful colleagues I found. I would mention them all but I am sure they already know how much I liked working with them.

And then a huge acknowledgment is reserved to those people that filled these four years with good moments and smiles. Ale, Mario, Roby, Bianca, Gianmarco for being like a family to me. The all great friends I found at the Institute: Benny, Dima, Theo, Ole, Tahaere, Irena, Michi, Aki, Neva, Heena, Sandra, Namit, Christina and Karine. Among these great guys I also found a great supervisor. Thank you Ingo for all your support.

And finally, thanks to my family, for their constant and precious support. And to my loving husband, for standing by my side. Always.